UNIVERSITY OF CALIFORNIA

Los Angeles

Data-driven approaches to fast voltammetry for neurochemical detection

A dissertation submitted in partial satisfaction of the

requirements for the degree Doctor of Philosophy

in Chemistry

by

Cameron Shane Movassaghi

2024

ABSTRACT OF THE DISSERTATION

Data-driven approaches to fast voltammetry for neurochemical detection

by

Cameron Shane Movassaghi

Doctor of Philosophy in Chemistry

University of California, Los Angeles, 2024

Professor Anne M. Andrews, Chair

My research develops tools to enable understanding of how information is encoded in chemical messengers (neurotransmitters; *e.g.,* serotonin, dopamine) in the brain by measuring them in real-time, in awake, behaving mice models. A molecular scale understanding of complex behavior and brain (dys)function would enable better treatments for neuropsychiatric disorders such as anxiety and depression (which affect 50% of families worldwide). A major challenge is the lack of analytical techniques that can detect multiple neurotransmitters simultaneously, across physiologically and behaviorally relevant time scales (ms, min, h). To date, the most suitable technique is voltammetry, which applies a specific voltage waveform to a micron-sized brain-implantable sensor. However, voltammetry is limited by the number of analytes and timescales that can be achieved for *in vivo* monitoring, impeding an understanding of how our brains encode information across neurotransmitters in a coordinated manner.

My graduate work involves developing a new voltammetry technique that combines novel voltammetry waveforms with machine learning. The technique is called rapid pulse voltammetry with partial least squares regression (RPV-PLSR), which utilizes a new type of pulse waveform and data analysis approach. Using RPV-PLSR, we published a proof-of-concept study to monitor serotonin and dopamine at both basal and stimulated levels, simultaneously, and compared these results to conventional approaches. We showed the utility of faradaic and non-faradaic current responses to build robust statistical models. The unique electrochemical signals present in pulse, rather than sweep, waveforms provide valuable chemical information in the background current that other methods do not generate.

However, the design of RPV waveforms (and voltammetry waveforms in general) is an arduous and inefficient process. To address this challenge, I developed a machine learning-guided approach for systematic design of novel-yet-optimal voltammetry waveforms using Bayesian optimization. Here, I identified optimal serotonin detection RPV waveforms under various physiologically relevant conditions.

Lastly, the custom waveforms and data analysis procedures used for RPV required the development of several open-source software solutions for user-friendly acquisition, analysis, storage, and sharing of voltammetry data at scale, which are reported herein. I outline how future extensions of fast voltammetry and machine learning can address domain generalizability (*i.e.,* the 'beaker-to-brain' issue), and how the techniques developed herein will broaden the scope of multi-analyte electroanalytical method development.

The dissertation of Cameron Shane Movassaghi is approved.

Chong Liu

Joseph Ambrose Loo

Aaron S. Meyer

Anne M. Andrews, Committee Chair

University of California, Los Angeles

2024

For my Dad

Table of Contents

List of Figures

List of Tables

Acknowledgements

Science is a team sport, and I am grateful for the best teammates I could ask for. To Callie- my best friend, dearest confidant and cheerleader, and now wife, thank you for your unconditional love and support. To my Dad- thank you for instilling in me the value of education, pursuit of knowledge, and the importance of dreaming. To the rest of my family and friends, thank you for always making me feel close to home regardless of the miles between us.

I would like to recognize the impact of my teachers, professors, colleagues, and mentors. First, I would like to thank my advisor, Professor Anne M. Andrews, for the guidance, motivation, opportunities, and confidence you provided me with throughout graduate school. Thank you to all the Andrews lab members past and present, with specific appreciation to Katie, Merel, Sara, Noelle, and our many talented undergraduate researchers. The laughs and friendship made science all the sweeter. To my collaborators and committee members, Professors Miguel Alcañiz, Aaron Meyer, Joe Loo, and Chong Liu – thank you for your willingness to share and teach as if I were a student in your own group.

To those that impacted me prior to graduate school, too many to list here in entirety, thank you for the impact you had on me professionally and personally, no matter how small the interactions may have seemed at the time. A specific thank you to Tony, Courtney, Michael, Deepak, Dominic, and Todd for the experiences and letters of recommendation that led me to study chemistry and pursue graduate school in the first place.

To all, I look forward as we keep exploring the world together and calling the adventure science. Here is to many more adventures together.

Vita

I received my Bachelor of Science in Chemistry, with a minor in Entrepreneurship, from the University of North Carolina at Chapel Hill in 2016. During my undergraduate studies, I performed undergraduate research in total synthesis under the supervision of Professor Michael T. Crimmins. In the summers of 2014 and 2015, I was an intern for HyperBranch Medical Technology, Inc., in Durham, NC.

After graduation, I completed an Oak Ridge Institute for Science and Education fellowship at the Centers for Disease Control and Prevention in Atlanta, GA from 2016-2019. Here, I implemented and developed several targeted metabolomics methods using liquid chromatography-mass spectrometry, resulting in various presentations, publications, and a research award. This experience solidified my desire to pursue graduate school.

In 2019, I joined the laboratory of Professor Anne M. Andrews at the University of California, Los Angeles (UCLA) as a Doctor of Philosophy student in Analytical Chemistry. During this time, I received support from the National Science Foundation Graduate Research Fellowship and UCLA Dissertation Year Fellowship. This thesis details the work, both published and unpublished, that I completed during my graduate studies. I presented this work at various conferences, both local, national, and international.

Chapter 1

Machine learning applications in brain neurotransmitter monitoring by fast voltammetry: A critical review

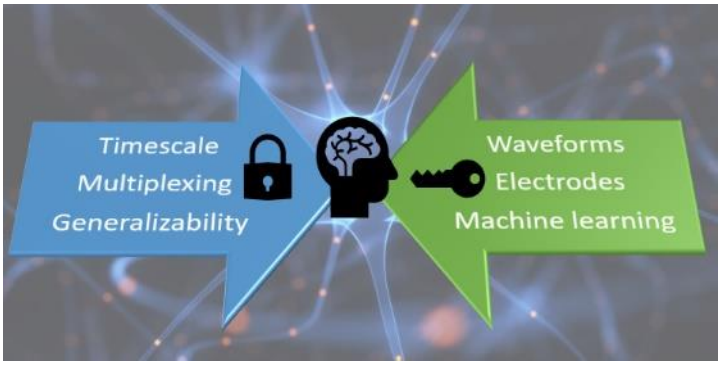

Part of the information in this chapter is in preparation for submission and has been adapted here.

Authors: **Movassaghi, C.S.**; Andrews, A.M.

1.1 ABSTRACT

Chemical neuroscience wields the tools to uncover the molecular mysteries of the brain. Sensors with tailored materials properties can be fabricated at neural scales. The latest instrumentation is capable of measurements exceeding the rates of neurochemical release. Modern machine learning models are approaching parameterization near the number of synaptic connections in the brain. Fast voltammetry has remained a neuro-analytical workhorse technique for nearly half a century but has been transformed in many aspects by these advances in hardware and software. Here, we review the past, present, and future uses of fast voltammetry with machine learning to quantitate neurochemical dynamics in brains of behaving animal subjects. We focus on the advances that machine learning offers to conventional problems in fast voltammetry. We identify current challenges and limitations for *in vivo* studies and outline several routes for future development.

1.2 OUTLINE

1.1 Abstract

1.2 Outline

1.3 Introduction
- 1.3.1 Why detect neurotransmitters using fast voltammetry?
- 1.3.2 What is machine learning and why use it?
- 1.3.3 Structuring voltammetry data
- 1.3.4 Information contained within voltammetry data
- 1.3.5 Approaches to model training, validation, and testing
  - 1.3.5.1 *Training sets*
  - 1.3.5.2 *Validation & test sets*

1.4 Linear Methods
- 1.4.1 Dimensionality reduction
  - *1.4.1.1 Choosing components*
  - *1.4.1.2 Qα validation*
- 1.4.2 Regularization
- 1.4.3 Feature engineering
- 1.4.4 Extensions of linear models

1.5 Non-linear Methods
- 1.5.1 Kernel & tree-based approaches

1.6 Deep Learning
- 1.6.1 Are big data required?

1.7 Data Fusion, Devices & Auxiliary Uses

1.8 Transfer Learning
- 1.8.1 *In vitro* multi-electrode models
- 1.8.2 Best subset selection
- 1.8.3 Uses of *in vivo* data for model training and selection

1.9 Interpretability

1.10 Progress, Challenges & Future Directions

1.11 References

1.3 INTRODUCTION

Machine learning is primed to revolutionize the electrochemical sciences.[1] The allure of machine learning is the automated ability to perform quantitative predictions from complex datasets across domains. One of the most complex datasets and domains known is the chemical dynamics of the awake, behaving brain. To study brain molecular messengers at relevant temporal, spatial, and chemical resolution, a group of electroanalytical techniques encompassed by fast voltammetry has emerged to identify and quantitate neurochemicals.[2-6] Fast voltammetry utilizes waveforms with scan rates on the order of hundreds of V/s, sequences of pulses with each pulse on the order of milliseconds, or their combination. Several key challenges in fast voltammetry have hindered its full potential to explore the molecular diversity in the brain and unlock the chemical connectome.[7,8]

This review discusses the challenges of performing fast voltammetry measurements in the brain and explores different data analysis landscapes attempting to address these challenges. We only briefly mention slow-scan, non-voltammetric, or non-brain recording techniques. Instead, our discussions are tailored towards *in vivo* neurochemical monitoring in the brains of behaving subjects (mainly mice, rats, and humans). The key benefit of the techniques covered is the ability to correlate real-time neurochemical dynamics with behavioral processes.[9,10] A molecular-scale understanding of chemical neurotransmission will advance our understanding of the brain from its circuitry to pathology and pharmacology.[7]

Recent reviews on fast neurochemical voltammetry have focused on specific neurotransmitters,[11] electrode materials,[12-14] and waveforms.[13,15] Broader topics such as *in vivo* monitoring techniques[10,16] or machine learning in fundamental electrochemistry[17,18] or various types of electrochemical/bio-sensors have also been reviewed.[19-22] However, few reports focus

on advances in machine learning for neuro-analytical voltammetry, which has heavily impacted experimental designs, analyses and interpretations of voltammetry data in recent years. Accordingly, we provide a critical review of how machine learning is shaping the future of fast voltammetry, one of the most historic and utilized methods to study brain chemicals in real-time. We identify gaps and trends in literature and outline several forward-looking paths for neuroscientists and electrochemists alike to draw inspiration. A specific focus is given to analogous fields undergoing complementary development such as chemometrics, spectroscopy, and electrochemistry *writ large*. Thus, this review should interest domain experts across these areas.

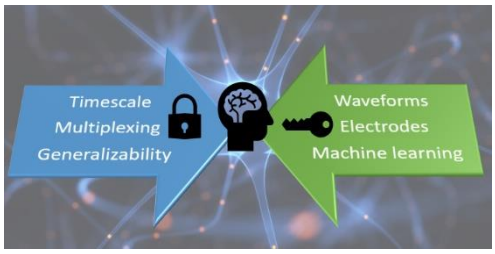

Figure 1.1. Grand challenges & solutions in fast voltammetry.

1.3.1 Why detect neurotransmitters using fast voltammetry?

Compared to alternative techniques (*e.g.,* microdialysis, genetically encoded sensors, biosensors), fast voltammetry offers an attractive combination of physiologically relevant sensitivity, and spatiotemporal and chemical resolution.[10] These figures of merit can be tuned using waveform parameters, electrode material and coating choices, and data analysis procedures (**Fig. 1.1**).[11,15,23-27] Still, a single technique for detecting multiple neurochemicals in the brain simultaneously, across recording locations, timescales, and behavioral states has remained elusive.[7,8,28-30] Fast voltammetry is limited to electroactive analytes and by measurement duration (*i.e.,* recording timescales of seconds to minutes rather than hours to days), challenges in multi-analyte detection (multiplexing), and failures in calibrating electrodes *in vitro* for *in vivo* studies (generalizability). Given the growing volumes of data being collected, the need to perform

quantification in complex deployment environments, and the ever-expanding panel of neurochemicals, materials, and waveforms in use, machine learning is poised to unlock the full power of fast voltammetry (**Fig. 1.1**).

1.3.2 What is machine learning and why use it?

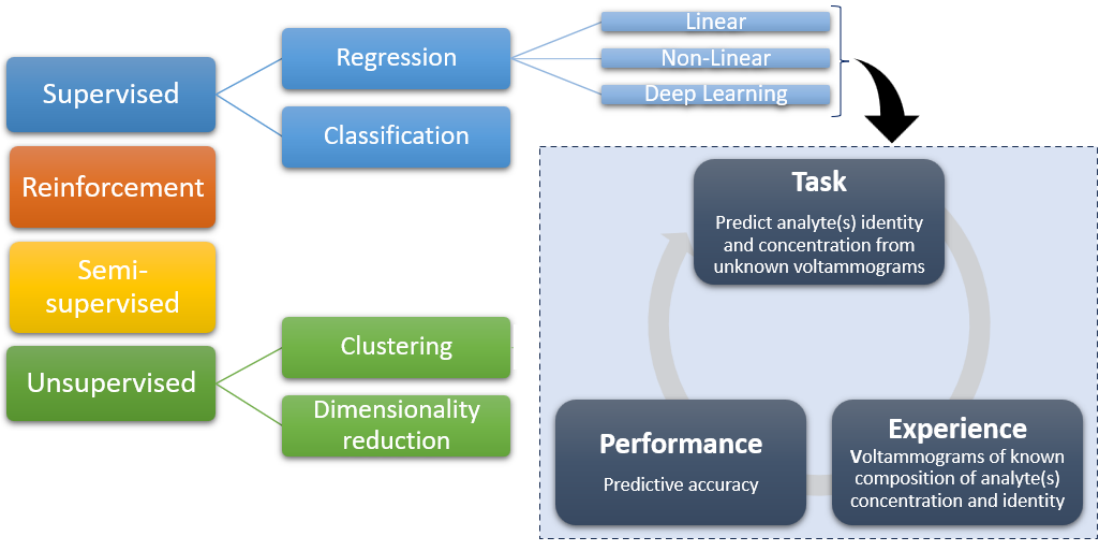

Figure 1.2. Approaches to machine learning in fast voltammetry.

Machine learning is when a *"computer program is said to learn from experience E with respect to some class of tasks T, and performance measure P, if its performance at tasks in T, as measured by P, improves with experience E"*.[31] Analogous terms such as statistical learning, data analysis, artificial intelligence, and chemometrics are used interchangeably with machine learning. Full treatment of the models and algorithms discussed herein are referenced as needed.

Machine learning is broadly delineated into unsupervised (which utilizes unlabeled data), supervised (labeled data), semi-supervised (labeled and unlabeled data), and reinforcement (feedback loop) learning (**Fig. 1.2**). We focus on supervised learning because the task is to predict unknown *in vivo* concentrations from known concentration samples used for *in vitro*

training data for a given panel of neurochemicals. We briefly mention approaches for classification (*i.e.,* does a voltammogram contain dopamine or not) but maintain that the most powerful applications of machine learning and fast voltammetry in terms of discovering new biology will result from the exploration of quantitative changes in multiple neurotransmitters and not solely their individual qualitative presence.

Some of the earliest work on voltammetry and machine learning dating back to the 1970s utilized classification and/or clustering approaches.[32,33] Since the advent of computers to control chemical instrumentation, machine learning has been pursued to increase the resolving power of overlapping voltammetric signals. Prior to the use of machine learning, conventional voltammetric discrimination of analytes in aqueous (*i.e.,* physiological) solution was thought to be limited to < 15 compounds (even under ideal conditions and generous solvent windows).[34] Monitoring more than one neurotransmitter simultaneously using voltammetry was a noteworthy feat. Today, monitoring multi-analyte mixtures is becoming commonplace with unparalleled accuracy, sensitivity, and selectivity.[35-37]

1.3.3 Structuring voltammetry data.

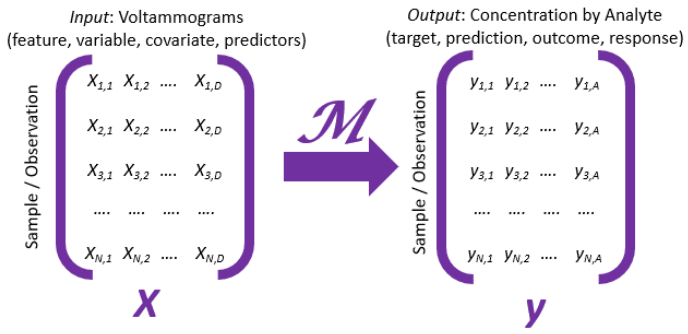

Figure 1.3. Format of vectorized voltammetry data as input (X) and output (y) to train on or predict from a model (M).

Voltammetry input data **X** can be structured in a tabular format with design matrices N x D, where N is a single sample (*e.g.,* voltammogram) and D is a feature (*e.g.,* sampled data point within a

voltammogram) (**Fig. 1.3**). In fast voltammetry, data points are often collected on the microsecond timescale (kHz to MHz sampling frequencies; $D > 1000$). This sampling is repeated for each waveform cycle, ~10 Hz in most cases, resulting in $D >> N$ (*e.g.,* "wide" data rather than "big" data[38]).

In the simplest case, all data are obtained using a single electrode in a single experiment, and inference is performed for the same electrode (*i.e.,* 'within electrode'). However, as discussed below, data from multiple electrodes can be combined, and inference may or may not be performed on data from the same electrode ('across electrodes' or 'out-of-probe'; ***Section 1.8.1***). The model used to perform inference (M) is trained on and outputs predictions as a matrix **y** of shape N x A, where A is the number of analytes (*i.e.,* if only predicting dopamine, only one column is output). Each row in **y** corresponds to the known or predicted analyte(s) and concentration(s) of each voltammogram in **X**. When the voltammograms in **X** are ordered sequentially across time, the resulting predictions in **y** yield a plot of concentration *vs*. time, which is useful for visualizing *in vivo* dynamics and correlating changes with known stimuli.

1.3.4 Information contained within voltammetry data.

Voltammetry data consist of three main experimental variables: the voltage sequence applied at the electrode surface (the waveform), the resulting measured electrode current (the voltammogram), and the time (between waveform cycles and sampled data points). Voltammograms provide information on physiochemical and material properties such as analyte concentration, diffusion, and adsorption, electron transfer kinetics, impedance, and capacitance. Fundamental electrochemical theory and formulae are available to describe these relationships,[39]

and research is being done to parameterize these relationships and incorporate electrochemistry and physics into machine learning models.[40-42]

Prior to the use of machine learning, manual analyses of voltammograms involved identifying characteristic peak positions and shapes. However, pattern matching or extending known theory can be difficult at high scan rates and under the non-ideal experimental conditions encountered in fast voltammetry. As an alternative, automated analysis approaches for identifying neurochemical voltammogram patterns have been employed for analytes such as adenosine and dopamine.[43-46] However, these are rule-based approaches rather than models with learnable parameters. Instead, machine learning in fast voltammetry focuses on modeling empirical relationships inherent in the evoked current as a function of quantity of the analyte(s) present. These relationships are learned from experimental training data.

1.3.5 Approaches to model training, validation, and testing

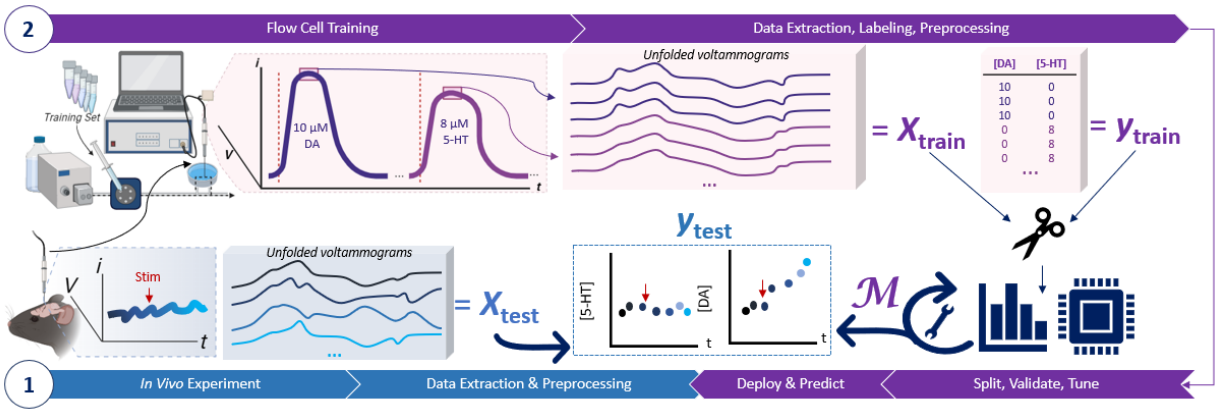

Figure 1.4. Use of flow cell sequential injection analysis for electrode calibration, model training, and inference. An electrode is generally first used *in vivo* (1) followed by post-fouling calibration (2; post-calibration). 'Stim' refers to a stimulation (*e.g.*, pharmacologic, optical, electrical, behavioral). Representative analyte calibration data are obtained (*e.g.,* dopamine (DA), 5-hydroxytryptamine/serotonin (5-HT), *etc.*) using a flow cell. The data are split, the model is trained, tuned, and validated before the final model *M* is used to perform inference on the unknown *in vivo* data (*i.e.*, test data).

1.3.5.1 Training sets

Neurochemical voltammetry seeks to fit a model, empirically, to the relationship between signal response at an electrode (voltammogram for an applied waveform) and the electrode environment (identity and concentration of analyte(s)). Iteratively updating the parameters of the underlying calibration model is called training, and the dataset used for parameter updating is the training or calibration set. In brief, training sets should contain all expected sources of variation, scale with the degrees of freedom of the model, span all concentration ranges and mixtures of analytes/interferents expected to be encountered, and be collected under the same conditions and with the same equipment (*e.g.,* sources of noise) as the test set, defined below.[47]

Training set data can be acquired *in vitro* or *in vivo*. We discuss *in vivo* training sets in detail in ***Section 1.8.3***. *In vitro* training sets are increasingly common and acquired using a flow cell with sequential injection analysis (**Fig. 1.4**). Neurochemicals of interest at known concentrations are prepared in a physiological buffer (*e.g.*, artificial cerebrospinal fluid). Training

sets can be as simple as, for example, five concentrations of dopamine or as complex as several neurochemicals, each across dozens of concentrations, mixtures, and noise conditions. Training set samples are injected at controlled intervals while physiological buffer flows continuously. Training voltammograms are extracted from a stable response area such that the electrode is fully exposed to the sample. To a rough approximation, this process mimics the rapid release and reuptake of neurochemical(s) in a simple and reproducible manner. Efforts are underway to improve flow cell design.[48,49]

Anywhere from one to hundreds of voltammograms may be extracted from a single injection, each corresponding to the sample's known concentration(s). All voltammograms from a single sample are treated as replicates. The final size of the dataset depends on the number of injections, the number of voltammograms extracted per injection, the waveform and sampling frequency, and any pre-processing (described below). Outlier removal procedures (*e.g.,* Cook's distance) can be utilized to remove poor training data.[50] With the dataset in hand, the training, validation, and testing of a suitable machine learning model are performed by dividing the data accordingly.

1.3.5.2 Validation & test sets

We distinguish between two uses of the term "validation". In machine learning, model validation refers to holding out a portion of the training data, known as the validation set, to estimate model performance on unseen data (*i.e.,* cross-validation). This is done such that reasonable hyperparameters can be chosen before deploying the fully trained model with an unknown test set.

In fast neurochemical voltammetry, validation can refer to when a new technique undergoes neurobiological challenges (*e.g., ex vivo* or *in vivo*) with known effects. These challenges can include pharmacologic, stereotaxic, stimulated-based (*i.e.,* optical, electrical, behavioral) experiments in which the expected response of certain neurochemicals of interest are known (*e.g.,* optogenetic stimulation of dopaminergic neurons should produce a dopamine response).[26] If the results agree with domain knowledge, the technique is said to be validated.

To complicate matters, validation, as described in voltammetry, is akin to a test set in machine learning. In the latter, a test set comprises unlabeled input data not seen by the model before model construction. In machine learning, in addition to voltammetry validation data, a test set can contain unlabeled *in vitro* injections (on the same or different electrodes) that have not been used to train the model. Test set data in machine learning are used to gauge model generalizability and to reduce model overfitting. By predicting concentrations sequentially from *in vivo* recordings, a continuous temporal plot over seconds to minutes enables a biological time course to be compared with known experimental events at defined timestamps.

Model training can be carried out using a training set before *in vivo* experiments, in conventional experiments referred to as pre-calibration. Next, *in vivo* experimental data are collected at an implanted electrode. Post-calibration training can also be performed by removing the electrode and using it to obtain *in vitro* training data. Training on electrodes after implantation and biofouling and across multiple (similar) electrodes for large, chemically diverse analyte panels provide data more similar to the test data, as electrodes have been exposed to brain tissue, which can alter electrode surfaces and the resulting calibration responses.[5,51,52] An appropriately trained model should retain only the salient, conserved latent voltammetric features across these environments in order to generalize.

1.4 LINEAR METHODS

Fast voltammetry calibration has relied historically on univariate linear regression to predict concentrations of neurochemicals from voltammograms. The peak current at characteristic voltages (*e.g.,* dopamine oxidation potential) is plotted as a function of known analyte concentration such that the concentration of an unknown (*in vivo*) voltammogram can be predicted.[53] Because peak amplitudes (or integrals[46]) at characteristic potentials are linearly dependent upon the concentration of an analyte (*e.g.*, Randles–Ševčík equation[39]), linear models were a first choice for fast voltammetry. Other uses of linear regression in fast voltammetry include correlation analyses of voltammogram 'templates',[5,43,54] and setting integration boundaries for calculating charge under a faradaic peak.[55]

However, univariate linear regression neglects the majority of the data in voltammograms. It suffers drawbacks associated with voltage-peak overlapping for species common in brain voltammetry measurements (*e.g.,* dopamine and pH changing simultaneously).[56] An attractive alternative is multivariate linear regression, which can reduce noise and interferent effects. However, voltammograms also contain multi-collinear data (*i.e.*, multiple points within a voltammogram are correlated with the same analyte) and datasets with more features than samples ($D>>N$), resulting in regression problems with non-unique or unstable solutions.[47,57] Thus, methods of selecting which variables in the voltammograms to use as predictors are often required.

1.4.1 Dimensionality reduction

One approach to dealing with multicollinearity is dimensionality reduction. Dimensionality reduction creates linear combinations of predictors that explain the variance in a dataset.[47] One of the earliest applications of machine learning for fast voltammetry of neurochemicals was principal components analysis (PCA) followed by linear regression, known as principal components regression (PCR).[34] The PCA technique is considered an unsupervised technique, as the correlation of the input **X** data with the concentration data (**y** matrix) is not considered, only the variance in **X** itself. When the concentrations are regressed on the principal components using linear regression, model fitting and predictions of concentration level for each analyte in the training set can be made. In-depth discussions and tutorials of PCA and PCR for fast voltammetry can be found elsewhere.[34,50,58-60]

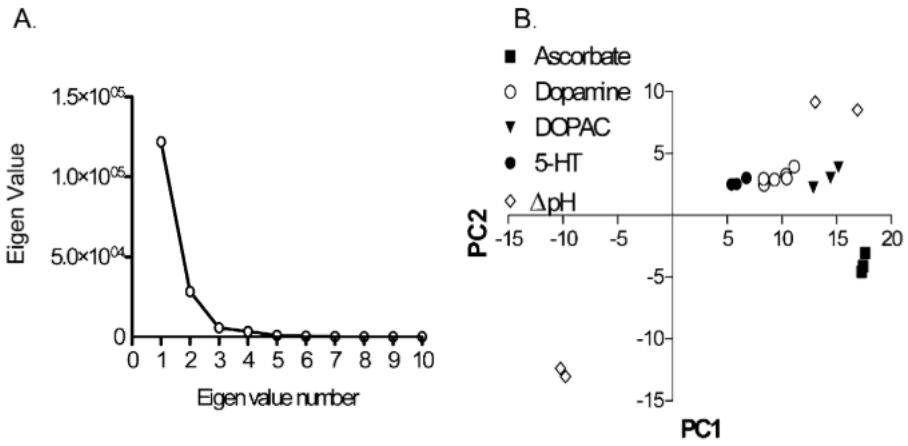

Figure 1.5. Early application of principal components regression (PCR) to fast scan cyclic voltammetry data for neurochemical prediction. DOPAC = 3,4-dihydroxyphenylacetic acid, 5-HT = serotonin. Reprinted with permission from Heien, MLAV; Johnson, MA; Wightman, RM. *Anal Chem* **2004** *76* (19), 5697-5704. Copyright 2004 American Chemical Society.

The first application of PCR to fast-scan cyclic voltammetry (FSCV-PCR) of neurochemicals reduced the dataset from a 1000-dimensional space per voltammogram to 5 dimensions (*i.e.,* a dataset of 30,000 data points became 150 data points). In addition, selectivity was improved by separating the variance contributions in the data (**Fig. 1.5**). Ascorbate, serotonin, 3,4-dihydroxyphenylacetic acid (DOPAC), and pH were resolved from dopamine,

respectively, in two-component mixtures within 10% accuracy for dopamine. The PCR method was validated in rat striatum brain slices, where it differentiated dopamine release (hundreds of nM) *vs*. a pH change of >0.1 units after electrical stimulation. The same study further validated the use of PCR using bovine adrenal medullary cells and revealed vesicular release of norepinephrine and epinephrine . While PCR could discriminate the latter analytes, the temporal resolution of voltammetry was limited as sufficient time is required for epinephrine to adsorb and produce the unique secondary oxidative wave that differentiates it from norepinephrine. A follow-up study validated PCR for quantitating dopamine and pH in the rat nucleus accumbens.[61] Here, an *in vivo* training set was used, as *in vitro* calibration failed, presumably due to electrode fouling. The *in vivo* training set was acquired by varying the electrical stimulation pulse and frequency settings as voltammograms were acquired in the rat brain (***Section 1.8.3***).

Since these two landmark studies in the early 2000s, the PCR technique combined with the triangle FSCV waveform for dopamine detection remains one of the most commonly utilized approaches in the field.[62,63] Extensions and modifications of the FSCV-PCR approach have followed. For example, including background drift in the training set allows the separation of drift from dopamine and pH contributions.[64] Co-detection of glutamate and dopamine using an enzyme-modified electrode and a modified FSCV triangle waveform, respectively, is also possible using PCR.[65] Other analytes detected using FSCV-PCR include adenosine[66], oxygen,[67] serotonin, and dopamine,[68] as well as adenosine triphosphate and hydrogen peroxide using a sawhorse waveform,[69] and a dual-waveform for analyzing norepinephrine and dopamine.[70] The effect of waveform modifications for lowering the detection limit for PCR has also been studied.[71] As an alternative to PCR, multivariate curve resolution with alternating least squares

was also explored for FSCV data, but performed similarly to PCR for dopamine and pH predictions while requiring more involved analyses.[72]

A technique related to PCR is partial least squares regression (PLSR). The origin of the PLSR approach is rooted in chemometrics. Compared to PCR, PLSR is considered a supervised dimensionality reduction approach.[73] While PCR models only the variance in **X** with the assumption that it will relate to **y**, PLSR explicitly considers the co-variance of **X** and **y** when building components, resulting in higher weighting of input variables correlating to response. Thus, PLSR creates dimensions of voltammogram features that relate to concentration and current rather than solely to variations in the current (which could include noise), often resulting in fewer retained components to explain a dataset.

Using a novel rapid pulse waveform, the PLSR approach has been used to co-detect serotonin and dopamine in mouse striatum.[26] A recent report used a modified FSCV waveform with PLSR to detect serotonin and histamine in human hair follicle epithelial cells.[74] The Sombers group has reported several PLSR-based techniques with a double waveform for drift subtraction and pH/H_2O_2 differentiation.[27,75] The PLSR approach outperforms PCR for predicting neurochemical concentrations, as shown for both fast and slow-scan waveforms and rapid pulses.[26,76,77] However, PCR remains the more common approach, perhaps due to the historical use and the abundance of fast voltammetry-specific PCR tutorials.[59] Many extensions to PCR and PLSR exist, including non-linear adaptations; however few have been explored for FSCV. For example, Loewinger explored functional PCR (fPCR) but found it to have inferior performance to PCR.[78]

The introduction of PCR to fast voltammetry set into motion a series of papers on best practices for training and tuning accurate predictive machine learning models *in vitro* or *in vivo*,

for eventual translation and use *in vivo*. These discussions are ongoing to this day. Two examples are discussed below: choosing components and validation by residual analysis. The remaining discussions of multiple electrodes and the construction of valid training sets are discussed in the context of generalizability (***Section 1.8***).

1.4.1.1 Choosing components

Choosing the number of components is the main hyperparameter tuned in PCR and PLSR models. A hyperparameter is a model parameter that is set before training. The components found most valuable for describing the data and performing predictions are usually referred to as primary or retained components, while the discarded components are referred to as secondary or noise components.[47] This tuning helps address the bias-variance tradeoff. If the threshold is set too low and too few components are retained, the data are underfitted and useful information is discarded. In contrast, if too many components are retained, the data are overfitted by modeling noise. While many approaches and discussions on choosing the number of components exist in chemometrics, three main approaches are most utilized for neurochemical fast voltammetry. These are: cumulative variance threshold, Malinowski's F-test, and cross-validation. Setting the number of components based solely on *a priori* knowledge of the sources of variation is strictly not recommended (*e.g.*, a two-component model for a training set of pH and dopamine), as components may or may not be physiochemically relevant to the analytes (alternative methods exist if this is desired).[72,79]

Cumulative variance was used in the seminal work on FSCV-PCR and is still in use today due to its simplicity.[34] Here, all ordered components explaining up to 99.5% of the variance are set as primary components, and the remaining are set as secondary components and discarded.

However, this method assumes noise makes up an arbitrary percentage (*e.g.*, 0.5%) of every data set and is thus unlikely to generalize across laboratories and electrodes.

A formal technique grounded in chemometrics is Malinowski's F-test. This technique sets a dataset-dependent threshold of statistical significance α (*e.g.*, 5-10%) to delineate primary and secondary component assignment. The F-test was compared to cumulative variance selection for PCR data.[58] Here, 119 *in vivo* training sets, each containing five dopamine and five pH voltammograms, were analyzed across different technicians, laboratories and electrodes. Of the 119 training sets, only 25% resulted in the same choice of components by cumulative variance *vs.* F-test, with cumulative variance often retaining more components than the F-test. The F-test removed significantly more noise by selecting an appropriate number of components compared to cumulative threshold for dopamine and pH data. However, authors also showed that predictions remained virtually unchanged in certain cases even when up to four additional secondary components were retained (*i.e.*, predictions made by models with components set by either method were highly correlated). A follow-up report demonstrated that outlier removal techniques such as Cook's distance can be used to guide rank selection.[50]

Cross-validation can also select the number of components. In cross-validation, a portion of the training set is held-out as a validation set. Models are trained with the remaining portion of the training data. The models are then used to make predictions on the validation set as the number of components in the model varies. Cross-validation has been compared to the F-test with mixed results, as determining the optimal number of components by cross-validation can be ambiguous (*e.g.,* determining the 'elbow' point), while the F-test relies on strict statistical assumptions.[80] One recent report found that cross-validation outperformed the F-test, specifically for FSCV PCR data.[81] Regardless, cross-validation remains the *de facto* technique in the wider

machine learning community, although various component selection methods continue to be explored.[80] For fast voltammetry with PLSR, cross-validation remains the most popular component selection method. Notably, the F-test for PLSR component selection has seen little, if any, use in fast voltammetry, perhaps due to PLSR being a supervised technique. A failing of all components-based techniques is that relevant information can be contained within noisy, secondary components.

Many types of cross-validation exist. When *k*-fold cross-validation is used, a certain percentage (defined as a "fold") of the data is held out. For example, 5- and 10-fold cross-validation is common in voltammetry, in which 20% or 10% of the data (*e.g.*, 5 or 10 folds), respectively, are randomly withheld. The folds can also be grouped or stratified by concentration or electrode so that out-of-concentration or out-of-electrode cross-validation is performed.[82] Further, some techniques use a portion of the scans from the same flow cell injection to hold out, while others group solely by separate injections.[36] Choosing components by cross-validation is becoming more commonplace (**Table 1.1**), as is done for most hyperparameter optimization, as the computation involved in large iterations of training during cross-validation has become exceedingly fast. Regardless, the choice of components is a larger topic in the chemometric and machine learning communities that has only recently been studied in fast voltammetry (***Section 1.8.2***).

1.4.1.2 Q_α validation

A model validation technique developed specifically for *in vivo* fast voltammetry with PCR compares the residuals of reconstructed and raw voltammograms, referred to as the Q_α method.[61] If the residuals between the reconstructed (*via* retained PCs) and raw voltammograms of the unknown data set (*i.e., in vivo* data) do not fall within a given threshold α (unrelated to α

of the F-test, but also usually set to 5-10%), the data are rejected as inaccurately quantitated by the model (*i.e.,* a significant source of variance is not accounted for by the training set, but is present in the test set).[58] In theory, this approach rejects voltammograms with unaccounted-for interferents to be estimated by the model. In practice, the approach fails with noisy training data and makes no guarantees on the model's accuracy, only on applicability.[59] Some reports maintain that because Q_α values are distributed in a manner dependent on the dataset, rather than a single value, a universal training set does not exist for *in vivo* training data.[58] While the Q_α approach is useful for identifying potentially erroneous voltammograms simply by way of inputs, it can fail to include appropriate data or exclude inappropriate data when applied across data sets.[60] Further, this method assumes that accurate prediction (output) is correlated with accurate signal reconstruction (input).

1.4.2 Regularization

Regularized linear regression for analyzing fast voltammetry data has been explored as an alternative to PCR and PLSR. Regularization prevents overfitting and addresses multi-collinearity by adding a penalty term to the regression coefficients during training. In voltammetry, rather than define new dimensions as combinations of predictors as in PCR/PLSR, regularization treats each sampled point in the voltammogram as an independent predictor. Each predictor's regression coefficient is penalized to shrink their values towards zero, thus reducing variance.

Regularized approaches include ridge, least absolute shrinkage and selection operator (LASSO), and elastic net regression.[83] Each of these techniques differ in how they penalize the

regression coefficients. For example, ridge regression shrinks the ℓ_2 norm of the regression coefficients while LASSO utilizes the ℓ_1 norm. A benefit of LASSO is sparsity, allowing regression coefficients to be exactly zero. The elastic net combines both the ℓ_1 and ℓ_2 penalties. None of the three approaches will outperform the others universally and must be selected and tuned using cross-validation.

Regularization approaches (referred to here as elastic net electrochemistry) were and continue to be pioneered in fast voltammetry by the Kishida & Montague groups, who also developed working electrode procedures for in-human use.[6,63] Accordingly, elastic net electrochemistry has been used mostly in conscious human subjects undergoing neurosurgical procedures (*i.e.,* deep brain stimulation). The first report was in 2016 using elastic net for dopamine prediction in 17 human subjects.[81] A follow-up study investigated serotonin signaling in 14 humans using LASSO,[84] and later serotonin and dopamine co-detection in 4 humans again using elastic net (**Fig. 1.6**).[85] All studies were performed in the striatum while participants performed decision-making tasks under uncertainty, such as a stock investment game. *In vitro*, the elastic net approach has been extended to oxytocin and vasopressin detection,[86] as well as towards low-amplitude sweep and random-burst pulse waveforms.[87,88] Elastic net electrochemistry is commonly used with large training sets across many electrodes, such that the coefficients of predictors with high variance shrink towards zero, effectively cancelling out points in voltammograms that cause out-of-electrode effects.

Elastic net electrochemistry has been compared to FSCV-PCR.[81] Theoretically, PCR is most closely related to ridge regression, as it does not enforce sparsity. Experimentally, PCR was unreliable at low dopamine concentrations and confounded pH changes with dopamine predictions.[81] Empirically, PCR and PLSR require less training time than elastic net due to the

nature of the hyperparameter search space. Compared to PCR, supervised methods such as PLSR and regularization are less susceptible to reconstructing irrelevant features. Further, an argument can be made that model validation is not a signal reconstruction problem (as in the Q_α approach), but a test set predictive accuracy problem (*i.e.,* the reconstruction accuracy of an input signal is unimportant so long as the model predictions perform well).[85] Because regularization selects individual features rather than linear combinations, model training is less reliant on variations between points and rather relies on variations of points related to the target. While Q_α a maintains that voltammograms containing unaccounted-for variance should not be analyzed at all, cross-validation and test set validation maintains that such variance has been trained to minimally affect model output. Regardless, both techniques can be confounded by interferents contributing similarly to analyte signal.

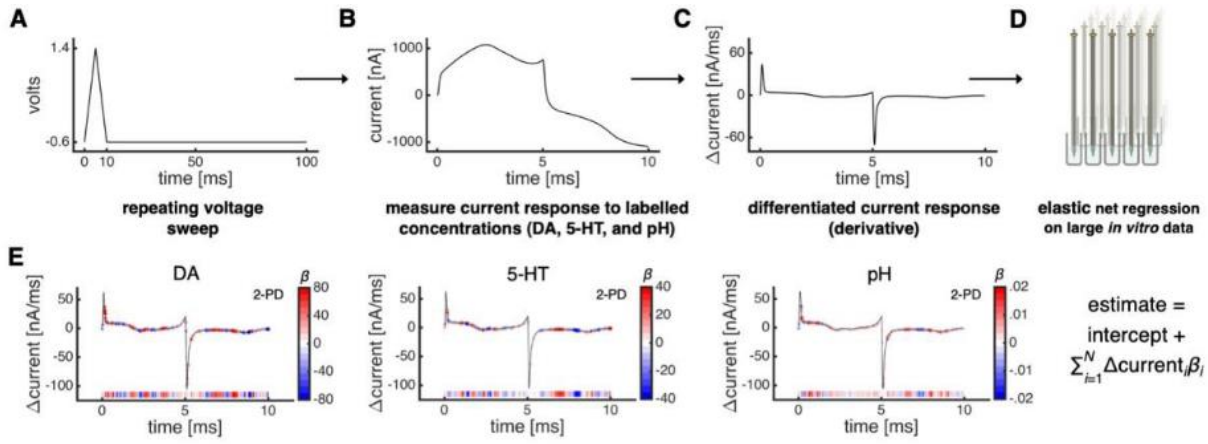

Figure 1.6. Elastic net electrochemistry for dopamine (DA), serotonin (5-HT) and pH prediction. Reproduced with permission under a Creative Commons CC-BY license from Bang, D; Kishida, KT, Lohrenz, T; White, JP; Laxton, AW; Tatter, SB, Fleming, SM, Montague, PR. *Neuron* **2020** *108* (5), 999-1010.

1.4.3 Feature engineering

Fast voltammetry data are pre-processed in several common ways before model training. We refer to these pre-processing procedures as feature engineering because they involve some combination of transforming, excluding, extracting, or otherwise manipulating features prior to prediction.[89] For example, the use of univariate linear regression can be considered manual feature engineering; the analyst decides which point (voltage) from the voltammograms to use for peak amplitude calibration.

Standardization, normalization, and derivative-based approaches are commonly used to adjust the scale of voltammograms before model training. This process improves the speed and accuracy of the training process and can be a required assumption of the underlying model or data distribution (*e.g.,* mean-centered with unit variance). Most techniques utilize standardization (*e.g.,* resulting in features with a mean of zero and standard deviation of one) or normalization (*e.g.*, resulting in features ranging from negative to positive one), while others (such as elastic net electrochemistry) utilize the first-derivative (differentiated voltammogram trace). Pre-processing approaches can alter the weight of certain parts of voltammograms during model training by changing the relative magnitude of the responses. For example, normalization emphasizes peak amplitude. Standardization emphasizes variability, and differentiation emphasizes rates of change (*i.e.,* peak and switching potentials).[26,57,81] Output data (*i.e.,* concentration) can be pre-processed for similar reasons, using *z*-scores for relative changes and a square root function to enforce positivity or non-negativity constraints.[78,84,85]

Various averaging and filtering techniques denoise, deconvolute, or otherwise filter data, usually *via* linear assumptions. For example, deconvolution and Fourier analyses remove non-Faradaic current[90,91] and denoise data.[55,92,93] Other linear transformations and various digital

signal processing protocols continue to be developed for voltammetry-specific uses.[94,95] The Hilbert transform applied to AC-voltammetry data has distinguished serotonin and dopamine.[96] An advantage is that this technique does not rely on assumptions of data stationarity or linearity. Wavelet transformation has been used to preprocess phasic dopamine release images and for compressive FSCV sensing, in which various domain transformations and reconstruction algorithms were compared.[97] Efficient data compression is needed to further develop wireless FSCV systems.[98]

One feature engineering choice that distinguishes voltammetry techniques and models is background subtraction *vs.* background inclusive treatments, discussed in detail elsewhere.[4] Background inclusive voltammetry, paired with machine learning, enabled simultaneous recordings of phasic and tonic dopamine and serotonin, which few, if any, other techniques have been able to do.[26,99,100] The elastic net electrochemistry and rapid pulse voltammetry techniques are some of the few approaches that forgo background subtraction. Indeed, with proper algorithms, tedious pre-processing can be eliminated, and raw data can be used with minimal feature engineering. For example, deep learning techniques, such as convolutional neural networks (CNNs; ***Section 1.6***), excel at automatic feature engineering and perform better when trained with raw data rather than pre-processed data, as shown in fields such as vibrational spectroscopy.[101,102]

More computationally complex feature selection techniques have been explored for similar models in fields other than fast voltammetry (*e.g.,* genetic algorithms).[103-106] Feature selection techniques trade off potential information loss and overfitting for improved model performance at the added expense of computation time. The choice of a feature selection algorithm is usually a guess-and-check approach, as many techniques exist, but none are

guaranteed to generalize. One specific type of feature engineering that has been applied to fast voltammetry (best subset selection) is discussed in the context of transfer learning (***Section 1.8.2***). However, many feature engineering algorithms do not involve 'learnable' parameters, or do not relate directly to concentration quantification, so we do not cover them further here. Meanwhile, some models discussed above "learn" to perform feature selection (regularization) or extraction (dimensionality reduction) during the training process.[104,105]

1.4.4 Extensions of linear models

Generalized linear models (GLMs) are an extension of linear models that enable the underlying distribution of the outcome variables (*e.g.*, analyte concentration) to be assumed to be distributed non-normally. The pioneers of multiple-cyclic square wave voltammetry (MCSWV) used GLMs to predict tonic dopamine concentrations.[107] This study demonstrated the power of probabilistic inference rather than peak-based signal analysis. Further extensions of GLMs should be explored, as these models could account for the temporal correlation between observations (adsorption/desorption between scans) and non-normal distributions while addressing non-linearities in the data.[108]

1.5 NON-LINEAR METHODS

When might non-linear methods be appropriate for voltammetry data? Based on electrochemical theory, the concentrations of analytes undergoing faradaic electron transfer are linearly proportional to the current generated.[39] Thus, using a non-linear model to model a known linear relationship would be inefficient. However, there are cases when non-linearities arise in voltammetry. For example, multi-component mixtures such as dopamine, ascorbic acid, and divalent cations (Mg^{2+}) can exhibit non-linear behavior.[76,109] Temporal electrode drift has also been shown to be non-linear, although, including drift in training sets of linear models works well as a corrective measure.[64] Regardless, the origin of such non-linearities could include biofouling, varying experimental noise sources, surface phenomena affecting electrode responses over time, and other dynamic background changes.[4] Only a handful of non-linear models (excluding deep learning, ***Section 1.6***) have been explored for fast voltammetry data analysis.

1.5.1 Kernel & tree-based approaches

Support vector machines are a popular group of non-linear models capable of classification and regression. Support vector machines transform the original feature space into a higher dimensional space using a kernel, which is then used to create linear decision boundaries. These linear decision boundaries in transformed space can translate to non-linear boundaries in the original space.[83] Matsushita *et al.* used support vector machines to classify phasic dopamine release *vs.* non-release. They achieved up to 96% accuracy on a public dataset of 285 false color plot FSCV images from nine separate recording sessions in rats,[110] but required manual extraction and labeling to generate the training set.

One of the only reported applications of support vector machines to quantify neurotransmitters from fast voltammetry data was for dopamine detection using FSCV.[111] The

authors showed that pre-processed PCA and raw (down-sampled) data could be both classified and regressed using support vector machines. The PCA step was used to reduce training time at the expense of slightly decreased predictive accuracy. Interestingly, classification was first performed on the data to determine if dopamine was present. Only then was regression analysis performed.

Tree-based models segment the predictor variables using splitting rules, creating a tree-like structure. These methods are simple and interpretable. The most simple form is decision tree regression.[112] Few studies have utilized tree-based approaches for neurotransmitter analysis.[113] Fewer, if any, studies used these models for voltammetry data. Instead, bagging, random forests, and boosting approaches can be used to enhance predictive accuracy. These approaches are often called ensemble techniques, as they combine multiple learners. Ensemble methods build a strong prediction model by combining weaker, simpler models, similar to how a random forest averages across a combination of many trees.[83] When using random forests and boosting for phasic dopamine classification, ~72% accuracy was achieved, below the performance of support vector machine and deep learning approaches.[114]

Head-to-head comparisons of fast voltammetry data across various linear and non-linear models are scarce. A report that compared linear, tree-based, k-nearest neighbors, and support vector regression used differential pulse voltammetry to detect dopamine and serotonin in blood serum.[115] Here, linear regression and support vector machines performed the poorest. One reason is that support vector machines move data into higher dimensional space, which is counterintuitive to the reason for applying dimensionality reduction. Perhaps for similar reasons, non-linear dimensionality reduction techniques, including non-linear extensions to PCR and PLSR, are also underreported. The sheer number of features and samples prevalent in

voltammetry data does not pair well with the computational complexity and the poor scaling of nonlinear techniques that require many hyperparameters. Another reason for the dearth of non-linear approaches is poor interpretability (aside from tree-based approaches, which are among some of the most interpretable models; ***Section 1.9***).

However, a separate report compared multiple pre-processing methods and models (linear and non-linear) for detecting ascorbic acid, uric acid, dopamine and nitrate. The study used a glassy carbon electrode and square wave voltammetry for application in human serum.[116] Interestingly, the authors found that a non-linear modification of PLSR utilizing a radial basis function performed best all-around. By contrast, artificial neural networks (***Section 1.6***) were found to be less accurate and required ~100x greater computation time. Fast voltammetry will benefit from large-scale, head-to-head comparisons of various models using neurochemical-specific datasets for brain applications. No single model or class of models has been demonstrated to work well across voltammetry techniques, even for similar classes of analytes.

One of the most comprehensive comparisons of machine learning models for fast voltammetry was completed by Goyal and co-authors using multiple cyclic square wave voltammetry (MCSWV) to detect tonic concentrations of dopamine, norepinephrine and serotonin.[37] Authors compared the performance of PCR, PLSR, support vector regression (SVR), and regularization (ridge, LASSO, elastic net) against a deep learning approach (discussed below). Using a within electrode approach, the SVR drastically outperformed LASSO, EN and PLSR, while PCR and ridge performed the worst (though the deep learning approach performed the best overall). However, PCA was performed prior to regularization to reduce computational time, and PCR/PLSR components were chosen using the variance threshold technique, both of which could bias the performance of these approaches towards worse-than-expected results if

they were tuned in more careful, yet time consuming, manners. Notably, SVR likely performed better for MCSWV data, as this is inherently a higher dimensional technique due to the waveform design. While the deep learning approach outperformed SVR across electrodes, the other shallow learning algorithms that performed worse within electrodes were not tested across electrodes.

1.6 DEEP LEARNING

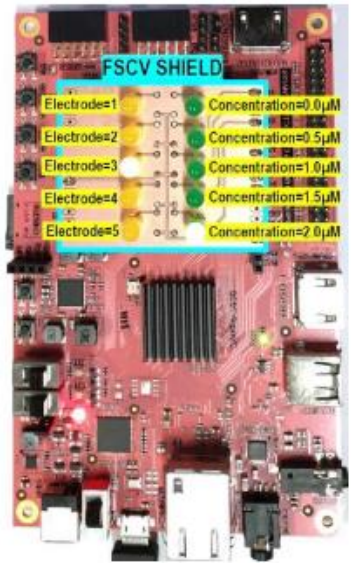

Figure 1.7. An early implementation of deep learning for fast voltammetry. Reproduced with permission from Zhang, Z; Oh, Y; Adams, SD; Bennet, KE; Kouzani, AZ. *IEEE J Biomed Health* **2021** *25* (6), 2248-2259. Copyright © 2021 IEEE.

Deep learning has garnered interest for its ability to model complex non-linear relationships. Due to its recent attention and impact, we cover deep learning in its own section. Excellent introductions to deep learning and artificial neural networks can be found elsewhere.[117,118]

The ability to perform automated feature extraction is a key advantage of deep learning. A disadvantage is the potential for overfitting and high computational cost when a network is fully connected (*i.e.,* all neurons in one layer are connected to all neurons in the next layer). Among other techniques to address these problems, convolutional neural networks (CNNs) have emerged as a leading architecture (*i.e.,* connectivity pattern) for high-dimensional data such as image data. Given that voltammetry data are high-dimensional data with short- and long-range correlations (*i.e*., a single analyte can have redox peaks across many voltages), CNNs are a good candidate architecture to analyze voltammetry data. Other types of layers are used in conjunction with convolutional layers, such as pooling (which can help with the translational invariance associated with small shifts in redox potentials) and dropout (to reduce overfitting).

Early applications of artificial neural networks to FSCV data focused on classifying phasic dopamine release using CNNs.[114,119] As noted earlier, manual analysis of false color plot data for phasic neurotransmitter release is time-consuming and conducive to automation. Matsushita *et al.* reported accuracies exceeding 98% for classifying over 2,000 FSCV images of

20 s recordings with and without electrically evoked ventral tegmental area dopamine release across 35 mice in two different laboratories.[114] The authors explored architectures such as a ten-layer CNN, an Inception v3 network, and YOLOv3. Patarnello *et al.* later achieved 98% accuracy using an ensemble of 60 AlexNet ensembles, each with ~8 layers.[119] Al-Haija *et al.* reported 99% accuracy across 6030 images by using data augmentation and DarkNet, a CNN architecture with ~24 layers.[120]

The first applications of deep learning to predict neurotransmitter concentrations from fast voltammetry data have emerged in the last several years. One of the earliest reports was for dopamine detection.[121] Here, the authors focused on implementing deep learning using less resource-intensive hardware (field programmable gate array) for integration into wearable/wireless hardware (a hardware-software codesign). To reduce computational resource requirements, a CNN was not used. Instead, a fully connected network was trained and then "pruned" to reduce the number of parameters. Interestingly, the model was trained to recognize concentration and the electrode used (as defined by the length of the cut tip of the carbon fiber) from only the voltammograms as input (a 'multi-task' approach). We note that the goal was to classify voltammograms with discrete concentrations of 0, 0.5, 1., 1.5, and 2 μM and identify from which electrode voltammograms were acquired – not true, continuous regression (noted as future work) (**Fig. 1.7**). The authors then reduced the number of parameters by setting thresholds in a custom pruning algorithm approach. They reduced the parameters by a factor of 3 (from 166,102 to 52,193), while achieving slightly higher accuracy (from 96 to 97.2%) after retraining. In addition, the authors compared the pruned artificial neural network concentration identification performance with that of PLSR and PCR. While found the deep learning approach was more accurate for test set accuracy across all five electrodes, PLSR outperformed PCR.[121]

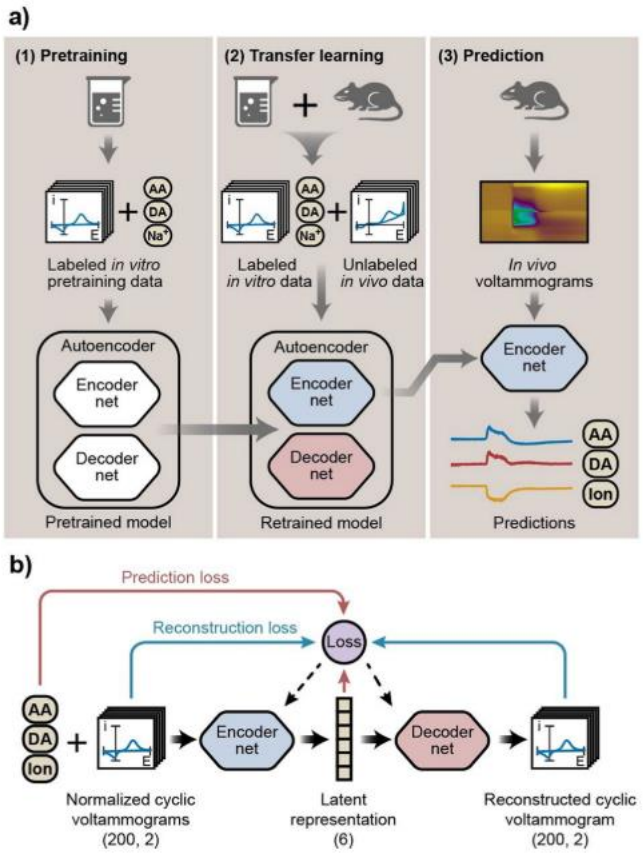

Figure 1.8. Use of autoencoder with semi-supervised learning for FSCV. AA = ascorbic acid, DA = dopamine, Na+/ion = sodium chloride. Reproduced with permission Xue, Y; Ji, W; Jiang, Y; Yu, P; Mao, L. *Angew Chem Int Ed* **2021**, *60*, 23777. Copyright © 2021 Wiley-VCH GmbH.

Xue and coworkers were one of the first to utilize an autoencoder architecture for FSCV (**Fig. 1.8**).[122] Autoencoders consist of encoder and decoder functions, usually modeled by artificial neural networks (here, CNNs). The output of the encoder, and thus the input of the decoder, are a latent feature representation of the original data.[123] The autoencoder was trained to predict ascorbic acid, dopamine and NaCl concentration dynamics. The authors noted that non-faradaic sensing could be accomplished, as shown by NaCl, because autoencoders account for nonlinearities that methods such as PCR cannot.

Notably, this approach used the autoencoder with transfer learning (***Section 1.8.3***). In this process, the authors trained the full model (consisting of an encoder and decoder) using labeled *in vitro* data, as was done in most cases above. The loss function was defined to minimize the error in predicted *vs.* actual concentration, but with an added term for reconstruction loss. In other words, the encoder inputs high-dimensional voltammograms and outputs the encoded, low-dimensional concentrations, while the decoder takes the concentrations and can decode them

back into reconstructed voltammograms. This model is referred to as a "pretrained", as it has not been presented with its specific task or the domain on which to perform inference (*in vivo*).

The pretrained model (encoder and decoder) is then retrained with labeled, *in vitro* training voltammograms and unlabeled *in vivo* voltammograms. Here, the model is trained to minimize reconstruction loss on labeled and unlabeled data, while maintaining accurate concentrations of the labeled data. Thus, the decoder causes the encoder to retain relevant features shared across *in vivo* and *in vitro* data. This is often referred to as semi-supervised or transfer learning, as the data are partly labeled and partly unlabeled (***Section 1.8***). Then, using only the fully trained encoder portion of the model, the concentration predictions are made (**Fig. 1.8**). By minimizing both types of loss, generalizable feature extraction is improved while overfitting is reduced. Here, the authors partly attributed model success to the vapor-grown carbon fiber electrode stability. The final model predicted μM fluxes of ascorbic acid and dopamine and mM fluxes of NaCl, *in vitro* and *in vivo*. For validation, these authors microinfused KCl to induce spreading depression in the rat striatum and 4,4-diisothiocynantostilbene-2-2'-disulfonic acid to measure the inhibition of Cl^- influx. Lastly, the autoencoder approach allowed for reconstructed voltammograms to be studied by means of the decoder net, providing an avenue for statistical validation similar to the use of Q_α for PCR.

Mena and coworkers combined deep learning with fast-scan controlled adsorption voltammetry (FSCAV) for serotonin detection to quantify absolute concentrations.[124] The FSCAV technique is derived from FSCV but utilizes a combination of high-frequency waveform scans and extended holding potentials. Challenges in post-experiment calibration, the non-linear effects that occur post-implantation, variable adsorption properties between electrodes when using FSCAV inspired the use of deep learning for this application.

Two shallow artificial neural networks were built, each with two hidden layers. The first network predicted serotonin concentrations based solely on four voltammogram-specific characteristics, using training data collected on a single electrode or 140 electrodes. While both neural network approaches outperformed linear regression for serotonin prediction, the neural network training approaches performed similarly. This result is interesting because deep learning models are usually thought to improve with increased training data. Another network was built using all training voltammograms (1,100 rather than 4 inputs) from all 140 electrodes. This model performed similarly to the other neural networks but avoided electrode post-calibration, so long as consistent experimental procedures were followed. These authors attributed success to the correlation between background current and electrode sensitivity that can be inferred from including the entirety of the information-rich voltammograms. The model was validated *in vivo* in mouse hippocampus using escitalopram and lipopolysaccharide to increase or decrease serotonin levels, respectively. The calibration-free results were similar to more cumbersome manual approaches.

Rather than predicting phasic or tonic concentrations, a novel data analysis approach was used by Buchanon *et al*. predict the ratio of serotonin to dopamine using a CNN.[125] Here, the authors investigated the co-release of serotonin and dopamine in the mouse striatum. The authors used labeled *in vivo* color plots of pharmacologically verified electrically evoked release of striatal dopamine or hippocampal serotonin. Data augmentation was used to create additional labeled synthetic training data by summing known, randomized ratios of the verified color plots. The authors then generated training sets of 5,000 color plots per animal to predict serotonin-to-dopamine ratios.

Choi and colleagues reported one of the first direct comparisons of FSCV data analysis with PCR *vs.* deep learning (**Fig. 1.9**).[36] For the PCR models, the components were chosen to explain 99.99% of the variance and Q_α was used to determine valid (as defined by reconstruction error) voltammograms. A VGGNet-inspired CNN architecture was used for deep learning with five-fold cross-validation. Dopamine, norepinephrine, epinephrine, serotonin, and pH predictions were compared in single and multi-analyte combinations across five electrodes by training in a flow cell. No significant differences in accuracy were found between PCR and deep learning for single-analyte detection. For multi-analyte mixtures, deep learning was significantly more accurate (by up to 20%) compared to PCR. This *in vitro* result supports the use of CNNs in discerning complex mixtures of neurotransmitters *vs*. a linear model, presumably due to the

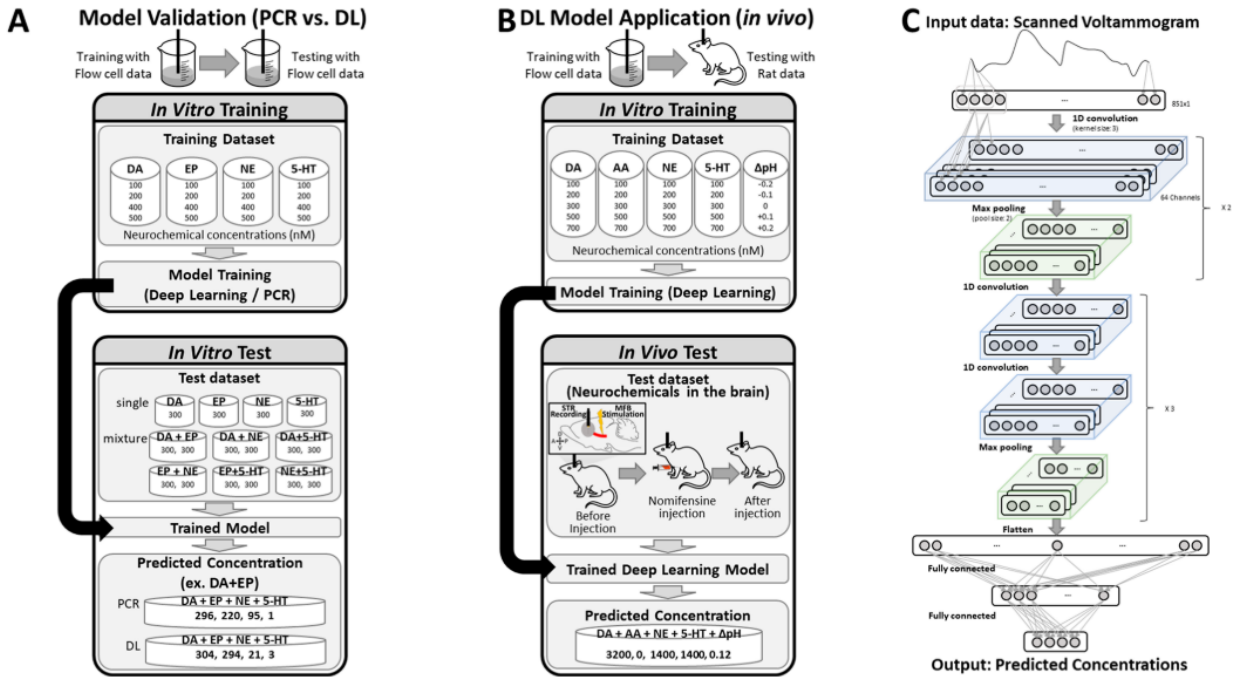

Figure 1.9. Comparison of principal components regression (PCR) and deep learning (DL) for fast scan cyclic voltammetry (FSCV). DA, EP, NE, 5-HT = dopamine, epinephrine, norepinephrine, and serotonin, respectively. Reprinted (adapted) with permission from Choi, H; Shin, H; Cho, HU; Blaha, CD; Heien, ML; Oh, Y; Lee, KH; Jang, DP. *ACS Chemical Neuroscience* **2022** *13* (15), 2288-2297. Copyright 2022 American Chemical Society.

ability of CNNs to model non-linearities that may arise from multi-analyte or multi-electrode effects.

In vivo validation was performed by stimulating the medial forebrain bundle and monitoring phasic dopamine release in the dorsomedial striatum of anesthetized rats, with nomifensine as a pharmacologic challenge.[36] As expected, stimulated dopamine predicted by deep learning increased significantly after nomifensine administration. The pH predictions during electrical stimulation were also significantly increased by approximately +0.1 units compared to pre-drug administration. Serotonin, ascorbic acid, and norepinephrine concentrations did not significantly change. The dopamine results tracked with conventional linear post-calibration. The PCR models trained on more complex mixtures outperformed single-analyte training sets used in earlier applications, supporting the increasingly common use of large, diverse training sets. The authors note the limitations of incomplete training set designs on both PCR and deep learning predictions. Analytes and interferents not present in the training set, but present in the brain, limit *in vivo* generalization. While PCR uses Q_α to identify voltammograms with possible contributions from non-trained analytes, no such approach was employed for deep learning in this report. The approach by Xue *et al*. above allows for signal reconstruction from a deep learning model and could address this concern towards reliability.[122] In sum, deep learning performed the same if not better than conventional linear methods for fast voltammetry, both *in vitro* and *in vivo*.

Twomey *et al*. recently reported a comprehensive comparison of different artificial neural network architectures.[82] They compared out-of-electrode (*i.e.,* performing prediction on voltammograms obtained on a separate electrode from those used to obtain the training voltammograms) performance across a dataset with 76 electrodes for detecting dopamine,

serotonin, and norepinephrine. The architectures included two fully convolutional networks, two multilayer perceptron models of varying size, an InceptionTime network (an ensemble of CNNs based on a specific architecture), and two domain-specific architectures (SSVEPformer and EEG-Transformer) adapted for voltammetry. The InceptionTime model was the best performing model but one of the most susceptible to artificially induced electronic noise. The multi-layer perceptron was the next best performing and was least susceptible to noise. Noise was induced by measurements outside of a Faraday cage with commercial electronic lab equipment nearby. These findings suggest that non-convolutional architectures may be useful for FSCV data. (Fully convolutional networks performed worst in terms of noise and accuracy).

In the same report, larger models (more parameters) did not necessarily improve performance within the architectures studied. Model performance was correlated across analytes, and serotonin prediction was the best indicator of performance. The multilayer perceptron was susceptible to noise because of the derivative as a pre-processing technique. Reducing noise at the source was deemed important in preprocessing since this can have large negative effects on the model. Thus, some manual feature engineering or ensembling may be needed for deep learning. However, eliminating all types of noise is nearly impossible, especially in an *in vivo* environment. Lastly, these authors demonstrated a method of identifying "deviant" probes (*i.e.,* electrodes that fail to generalize/produce inaccurate predictions) by investigating model embeddings. Such an approach, among others, will be useful in aggregating large, multi-electrode training sets and for out-of-electrode predictions.

Following the *in vitro* success of InceptionTime architecture described above, one of the most recent reports by the Montague group was for detection of noradrenaline in human amygdala.[35] Related to the report above, authors used a modified version of the InceptionTime

CNN model, which itself is an ensemble of multiple models. Authors were able to predict serotonin and dopamine in addition to norepinephrine.

Another approach extended a previously developed technique, second-derivative-based background drift removal, to predict tonic dopamine and serotonin using deep learning.[126] The authors used a temporal convolutional network. While results were only demonstrated *in vitro*, the allure of simultaneous analyte detection across timescales remains highly sought after.

One of the most recent reports of solely tonic measurements (~10s temporal resolution) using deep learning[37] was inspired by the autoencoder approach developed by Xue *et al*.[122] Aside from tonic concentration predictions by use of MCSWV and use 2D instead of 1D convolutional blocks, this autoencoder (named DiscrimNet) was trained on datasets across electrodes, rather than within a single electrode. Across-electrode training paradigms are hypothesized to better generalize *in vivo*, in which electrode conditions are significantly altered but the model retains conserved salient features. Further, a key benefit of this across-electrode model is that it does not need to be retrained for additional electrodes and can instead be reused in real-time as voltammetric data are being acquired. The latter possibility has direct applications to closed-loop deep brain stimulation (***Section 1.7***). When *in vivo* data obtained in anesthetized rat nucleus accumbens using naïve electrodes (not included in the training set) were analyzed by DiscrimNet, tonic concentrations of dopamine, serotonin, and norepinephrine followed historical trends and pharmacological challenges to cocaine and oxycodone. Authors attributed success to the higher dimensional data obtained using MCSWV for tonic rather than phasic measurements (especially to aid in differentiating dopamine and norepinephrine), as well as the semi-supervised approach performed across- rather than within-electrodes. Future work on optimizing DiscrimNet to handle awake, behaving subjects, and chronic implantation artifacts is needed.

1.6.1 Are big data required?

A commonly accepted pre-requisite for deep learning is that large datasets are required. Interestingly, while some groups have had success with deep learning across large, multi-electrode data sets, the use of artificial neural networks for calibration-free FSCAV did not find an improvement with a large dataset.[124] Response deviations across electrodes when combining data sets might have contributed. Advanced methods are being developed to improve the subsets of across-electrode datasets that should be combined to create multi-electrode models (***Section 1.8.1***). Other fields are also questioning the 'bigger is better' mentality when it comes to machine learning dataset size.[127]

In general, voltammetry users are trending towards using the latest machine learning advances, and developing techniques that capture or incorporate as much chemical information as possible. The layers of recent deep learning networks range from a couple up to more than a dozen, with the number of parameters exceeding half of a million. However, the number of electrodes, voltammograms, and calibration concentrations/interferents used to train such models varies widely. Some reports utilize dozens of electrodes across tens of thousands of voltammograms, with dozens of varying concentration calibration mixtures. Others still have seen success using far less complicated schemes across only single electrodes, a few calibration samples, and only dozens of trainings voltammograms. Part of the reason for this ambiguity on 'how many training data are required?' is the lack of standardized datasets, evaluation metrics, and inability to assess ground truth *in vivo*.

Table 1.1. Representative sample of novel applications of machine learning to quantify neurochemicals using fast voltammetry. 3MT = 3-methoxytyramine, 5-HIAA = 5-hydroxyindoleacetic acid, 5-HT = serotonin, AA = ascorbic acid, ADO = adenosine, CNN = convolutional neural network, CV = cross validation, DA = dopamine, DOPAC = 3,4-dihydroxyphenylacetic acid, EN = elastic net, EP = epinephrine, GLM = generalized linear model, HVA = homovanillic acid, LASSO = least absolute shrinkage and selection operator, L-DOPA = levodopa, MCSWV = multiple cyclic square wave voltammetry, MLP = multilayer perceptron, n/a = not applicable/not reported/unclear, NE = norepinephrine, PCR = principal components regression, PLSR = partial least squares regression, SVR = support vector regression, UA = uric acid, VT = variance threshold.

Year	Reference	Waveform/Technique	Model(s)	Analyte(s) & Interferents	Model Validation	Training set	Animal Validation/Application	# Electrodes
2004	[34]	Triangle	PCR	DA, 5HT, DOPAC, AA, pH, NE, EP, 3MT, L-DOPA, UA, HVA	VT (99.5%)	*in vitro*	Rat striatum (slice); electrical stimulation and vesicular release	1
2016	[81]	Triangle	PCR, EN	DA, pH	10 fold CV, F-test	*in vitro* (out-of-probe)	Human striatum; sequential investment game	≥2
2018	[84]	Triangle	LASSO	5HT, DA, pH	10 fold CV	*in vitro* (out-of-probe)	Human striatum; sequential investment game	3
2019	[77]	Triangle	PCR, PLSR	DA, AA, DOPAC, 5HT, pH	VT (99.9%), 10 fold CV	*in vitro*	n/a	3
2019	[88]	Random burst	EN, LASSO	5HT, DA, pH, NE, 5HIAA	10 fold CV	*in vitro*	n/a	n/a
2020	[121]	Triangle	PCR, PLSR, MLP	DA	10 fold CV, 5 components	*in vitro*	n/a	5
2020	[85]	Triangle	EN	5HT, DA, pH	10 fold CV	*in vitro* (out-of-probe)	Human striatum; visual motion discrimination task	20
2020	[111]	Triangle	SVR	DA, 5HT, AA, DOPAC, pH	5 fold CV	*in vitro*	Rat nucleus accumbens; electrical stimulation	n/a
2021	[122]	Triangle	Autoencoder	AA, DA, NaCl	n/a	*in vitro* & *in vivo* (semi-supervised)	Rat striatum; pharmacologic validation	1
2021	[26]	Triangle, rapid pulse	PCR, PLSR	DA, 5HT	LOOCV	*in vitro* (post-calibration)	Mouse striatum; stereotaxic, pharmacologic, optogenetic validation	3
2021	[107]	MCSWV	GLM	DA	5 fold CV	*in vitro* (post-calibration)	Rat striatum; pharmacologic validation	6
2021	[87]	Low amplitude burst, low amplitude triangle	EN	5HT, DA, pH, EP	10 fold CV	*in vitro*	n/a	n/a
2022	[36]	Triangle	PCR, CNN	DA, EP, NE, 5HT, pH	VT (99.99%), 5 fold CV	*in vitro* (post-calibration)	Rat striatum; electrical and pharmacologic validation	5
2022	[82]	Triangle	MLP, CNN, Transformers	DA, 5HT, NE, pH	10 fold CV	*in vitro*	n/a	76
2022	[124]	N-shape	MLP	5HT	10 fold CV	*in vitro* (post-calibration)	Mouse hippocampus; electrical and pharmacologic validation	140
2022	[125]	N-shape	CNN	5HT, DA	5 fold CV	*in vivo* (data augmentation)	Mouse hippocampus; electrical and pharmacologic validations	10
2023	[35]	Triangle	CNN	NE, DA, 5HT, pH	10 fold CV	*in vitro* (post-calibration)	Human amygdala, visual affective oddball task	6
2024	[37]	MCSWV	Autoencoder, SVR, LASSO, EN, Ridge, PLSR, PCR	DA, NE, 5HT, UA, pH, DOPAC, AA, ADO, HVA	5-20 fold CV, VT (99%)	*in vitro* & *in vivo* (semi-supervised; out-of-probe)	Rat nucleus accumbens, pharmacologic validation	12

1.7 DATA FUSION, DEVICES & AUXILIARY USES

An exciting area of progress in biosensing, including voltammetry, is data fusion and multi-modal sensors.[20] Data fusion can be homogenous (*i.e.*, combining data from the same sensing mechanism) or multi-modal (combining data from different sensing mechanisms).

Fused homogeneous data can come from a single sensing modality, such as voltammetric electrode arrays,[23,24] in which each electrode can have varying materials, coatings, or waveforms. This concept extends soft sensing and creates a voltammetric "electronic tongue" for the brain.[128] One could envision a scenario where multiple waveforms are applied, each with individual strengths and weaknesses. Ensembled corrections and improvements are made when data or predictions are fused (especially across materials). Some models may be better suited for specific analytes, sensing tonic or phasic release, or could be more tolerant to fouling, drift, or noise. An ensemble of models that can vote on the best concentrations could be useful for future work.

Multi-modal data fusion combines different sensing modalities. For example, field effect transistors measurements were recently combined with voltammetry at carbon-fiber microelectrodes to determine pH.[129] Other instrumentation and techniques combined with voltammetry include electrochemical impedance spectroscopy,[130] iontophoresis and electrophysiology,[131,132] functional magnetic resonance imaging,[133] and optogenetics.[134] As these techniques and devices continue to develop, training combined datasets or combined models could take advantage of the mutual information content.

Voltammetry is conducive to hardware miniaturization and portability, as well as on-device computing.[135-137] This has led to voltammetry being a key component in developing closed-loop deep brain stimulation systems. Such a system would require a device that can

measure neurochemicals *via* voltammetry, analyze the data, make decisions using on-device computing, and respond with optimized electrical stimulation settings to create an Observation-Orientation-Decision-Action loop (**Fig. 1.10**). Machine learning will play a key role in these devices, to quantify neurochemicals using the techniques discussed in this review and for refining stimulation parameters. Several systems are being developed for this purpose.[138-142]

The use of machine learning to develop new voltammetry sensors is unexplored. Other fields have used machine learning to discover new materials and sensors.[143,144] Fast voltammetry may also benefit from the machine-learning-inspired design of electrode materials. The panels of analytes monitored by fast voltammetry are ever-expanding, along with newly developed materials, waveforms, and models. Using data analysis with feedback control to alter waveforms may also see continued development.[145] As done in other fields, connecting these advances in feedback discovery loops could accelerate the development of new voltammetry approaches.[143,146]

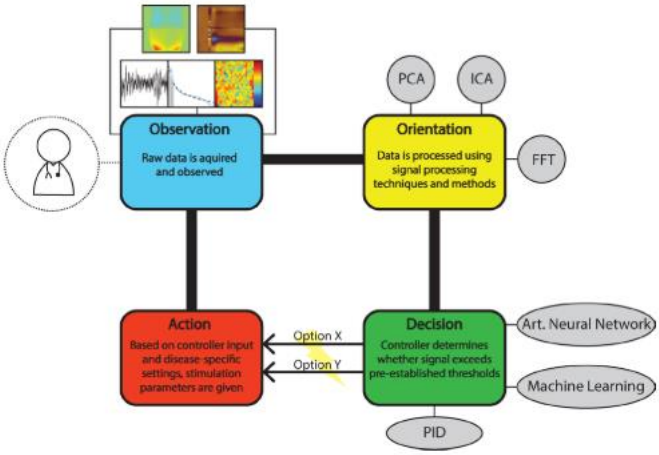

Figure 1.10. Observation-Orientation-Decision-Action loop. Reproduced with permission under a Creative Commons Attribution 4.0 International License from Rojas Cabrera, JM; Blair Price, J; Rusheen, AE; Goyal, A; Jondal, D; Barath, AS; Shin, H; Chang, SY; Bennet, KE; Blaha, CD; Lee, KH. *Reviews in Analytical Chemistry* **2020** *39* (1), 188-199. Copyright © 2020 Juan M. Rojas Cabrera *et al*., published by De Gruyter.

Beyond using machine learning directly for voltammetry data analysis, there are uses of machine learning for auxiliary or complementary experiments to voltammetry. For example, hidden Markov models have been used estimate correlations between pupillometry and noradrenaline,[35] computer vision approaches have been used to relate the facial expressions of

head-fixed mice with brain activity and emotional encodings,[147] and reinforcement learning for studying reward processing.[148]

1.8 TRANSFER LEARNING

Several issues arise from applying *in vitro* calibration to perform predictions on *in vivo* test data. Because the training set and test sets are collected in different environments (*i.e.,* domains) or come from different underlying statistical distributions, generalizing a model trained *in vitro* to perform inference on *in vivo* data presents unique challenges for brain voltammetry. The ground truth of analyte identity and concentration *in vivo* is currently unknowable, subjecting model performance metrics to various biological validations. Obtaining *in vivo* training data is difficult, if not impossible. Yet it is often a statistical requirement that the test data are obtained in the same environment as the training data. While attempts to mimic some *in vivo* conditions can help, such as the use of post-fouled electrodes and/or various buffer and interferent conditions, many electrode surface-chemistry changes occur *in vivo* that simply cannot be replicated *in vitro*. These issues are referred to as a generalizability issue, a beaker-to-brain issue, or an out-of-distribution effect and are the chief concerns when applying machine learning to *in vivo* voltammetry.

There are many possible origins for out-of-distribution shifts. For example, even though a flow cell simulates release and reuptake kinetics, the brain is not “flowing”. Flow cells do not have the same tortuosity and impedance environments as brain tissue. Further, the brain is under intracranial pressure, maintained at body temperature, and contains dissolved gases, among many other differences that are either cumbersome or impossible to mimic *in vitro* or even *ex vivo.* While work is being done to mitigate electrode shifts at the source, such as developing innovative electrode coatings and configurations,[149,150] no technique can truly yet mimic the brain, limiting many techniques to validate in more well-controlled, mimicable, or indirect environments such as blood, urine, or sweat.

This issue of how to combine, train, and perform inference across multiple datasets or domains is not unique to voltammetry. Broadly, this field is referred to as transfer learning. Transferring model calibration across domains, such as different instruments and laboratories, has roots in spectroscopy and chemometrics.[151] There is a rich literature on transfer learning, domain adaptation, and domain generalization, as well as specific guidelines for chemometric applications.[152] Many applications in the biological and medical fields have similar difficulties wherein the training and test data distributions are different. Voltammetry can benefit from adopting complementary approaches. Approaches developed for voltammetry and other techniques are detailed below.

1.8.1 *In vitro* multi-electrode models

Here, the training data are the source domain (beaker) used to make inferences about the target domain (brain) data. Even though the task remains the same between source and target domains (neurotransmitter quantification), the domains differ. The failure of training sets to generalize *in vivo* occurs because our statistical learning algorithms assume that training and test data are from the same domain. This is not to say that using machine learning for *in vivo* voltammetry is unjustified. However, predictions are estimates and must be interpreted carefully, even for simple univariate analysis).[5,153] The less the source and target domains differ, the more likely models will be to generalize.

One solution to model building to generalize across domains that include different electrodes is to obtain larger, aggregated training sets across many electrodes and analytes to produce a generalized representation over time. Large, multi-electrode datasets capture variations

across electrodes, resulting in models that generalize across unseen electrodes. As an extension, we can assume that a model can also generalize to *in vivo* domains because *in vivo* environments impact electrode performance such that each electrode can be considered a 'different' electrode when used in the brain *vs*. the beaker (or flow cell). *In vitro* training sets are getting larger and include more variations through multiple electrodes, analytes, and analyte concentration levels to account for shifts in the marginal or covariate current distributions across a waveform. Along with post-fouled calibrations, we can bridge source and target domains.

Nonetheless, voltammetry microelectrodes are highly heterogeneous. Even within laboratories, they are almost exclusively hand-made with even considerable variations in performance characteristics when made by the same individual. Moreover, different research groups use different fabrication and testing protocols. There are no standardized voltammetry electrode metrics agreed upon by the research community. Models trained from data acquired on one electrode will fail to predict accurately on test data from a different electrode, whether used *in vitro* or *in vivo*. Significant calibration differences also occur between pre-fouled training and post-fouled predictions.[154]

While new electrode materials, fabrication techniques, and standardized testing metrics will help reduce the generalization issue's impact,[12,25,68,155,156] the underlying statistical problem is that training voltammograms for each electrode and the corresponding neurotransmitter concentrations as come from different marginal and conditional distributions, respectively. This is the root source of poor generalizability. Optimal training sets may lie in a subset of the total available aggregate of training data. How should multi-electrode datasets be combined to ensure generalizability (*i.e*., make predictions on electrodes not included in training, in separate domains, or both)?

One approach is to use subsets of multi-electrode data sets. When training across multiple electrodes (and especially when aiming to generalize to electrodes outside the training set, *i.e.,* out-of- electrode samples), voltammograms generated across electrodes can exhibit response variations due to inherent variations in fabrication. Data subsets can be identified where only similar electrode responses to input variables are used to train the underlying model. This idea is supported by previous reports in which subsets of electrodes and measurements were highly correlated for within- and between-subjects/electrode training.[60]

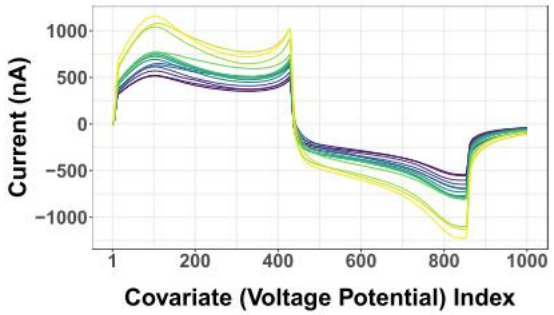

Figure 1.11. Covariate profile similarity weighting. Adapted with permission under a CC-BY-NC-ND 4.0 International license (https://creativecommons.org/licenses/by-nc-nd/4.0/) from Loewinger, G; Patil, P; Kishida, KT; Parmigiani, G. *bioRxiv* **2021** 856385; doi: https://doi.org/10.1101/856385.

Further, if the biology under investigation can be interpreted through relative changes (*e.g.,* z-scores), the over- or under-estimation of transient concentration changes becomes less of an issue. Kishida and co-authors began matching training data across electrodes by comparing shape similarities and found this to improve prediction accuracy and generalizability.[81] To find similar voltammograms, unsupervised learning approaches such as hierarchal clustering can be used to determine data from electrodes with similar responses. Training sets across these electrodes are then combined into single training sets. A later approach by Loewinger *et al.* used covariate profile similarity (CPS) weighting (**Fig. 1.11**).[78] The authors leveraged the fact that covariates (*i.e.*, voltammograms) from the target domain are available prior to modeling, such that unlabeled information can be leveraged similar to semi-supervised transfer learning approach used by Xue *et al*.[122]

A different apporach involves creating multiple models for specific concentration ranges.[81] This is done by selecting training data that are normally distributed around a concentration range of interest. Here, models trained on narrow concentration ranges performed better in multiple use cases. This approach allows for "guess and check", where specialized models for various concentration ranges can be utilized to analyze unknown *in vivo* data, such that appropriate models and concentration ranges can essentially be searched for. The downside is the computational effort to train and apply such models.

An interesting development of novel statistical learning methods, specifically designed to address fast voltammetry dataset ensembles, is detailed by Loewinger and co-workers' called the "study strap ensemble".[78] Here, "studies" refers to *in vitro* training sets of dopamine using FSCV, each acquired at a different electrode. Multi-study learning thus refers to the training of statistical inference models on datasets that combine data from multiple electrodes. Historically, this has been accomplished by either pooling all studies together and fitting a single model to the merged dataset (training on the merged dataset; TOM). Alternatively, separate models are trained on individual datasets and the predictions are averaged (observed-studies ensemble; OSE). The study strap combines both approaches to find the ideal combination of studies using custom-developed algorithms and a tuning parameter that allows fine control over heterogeneous combinations of datasets. The study strap can also be combined with CPS weighting so that only similar studies are combined.

The study strap approach has been evaluated with electrodes not included in the training data (as a proxy for electrodes in the brain, where data distributions shift so much that data are considered as having been collected from a "different" electrode). Performing well across unseen electrodes is a good indicator of *in vivo* generalizability. Here, PCR was used rather than

regularization, as the former offered superior cross-study performance. Per an elastic net electrochemistry protocol, pre-processing included the voltammogram derivative but not background subtraction. The TOM, OSE, and study strap approaches were compared across 15 studies (20,000 samples total) with and without CPS. The improvements of CPS and study strap methods developed in this work matched or outperformed the standard approaches of combining multiple data sets, such as by TOM and OSE, with improvements in root mean squared error of dopamine predictions ranging from 5 – 61%.[78] Study strap algorithms were released as an open-source package. However, these methods are computationally intensive.

1.8.2 Best subset selection

Instead of finding the optimal combination of datasets to create generalizable fast voltammetry models, a separate approach is to find the optimal combination of model features that generalize to unseen data, such as in best subset selection. Best subset selection refers to finding a subset of features from the total set of features to create the model to reduce prediction errors and enhance interpretability.[83] While best subset selection is related to feature engineering and model selection, the applications of best subset selection in fast voltammetry are few and relate directly to domain adaptation applications.

In separate work, the same authors focusing on the study strap extended the best subset selection approach to multi-task learning. Here, analyte predictions at separate electrodes were considered separate tasks,[157] as the marginal distribution of electrode signals, and hence the conditional distribution of the concentration, differed across electrodes. Latent structures were captured across multiple training datasets and models improved performance. Training on

different electrodes uses different regions (features) of voltammograms. How can we create models that leverage such information across electrodes, such that training on all the data is better than training only on data from a single electrode?

One common solution is to enforce sparsity through a penalized error term, as done in regularization.[157] Here, solutions were identified that leveraged data patterns and individual data values. For example, each electrode may have a different pattern of features (*i.e.*, area of analyte activity at the electrode surface) specific to that electrode. Generalizing across electrodes finds conserved patterns across electrodes. The authors deem this approach "support heterogeneity regularization". Compared to conventional approaches for training across multiple electrodes, this new technique outperformed all others in predictions on a held-out electrode. The code to perform multi-task learning was also released as an open-source package.[157]

Best subset selection techniques have also been explored for dimensionality reduction techniques, such as selection of the best subset of principal components. Similar to the above, *"[t]he first few PCs will only be useful for discriminating between groups if within- and between-group variation have the same dominant directions. If this does not happen (and in general there is no particular reason for it to do so) then omitting the low-variance PCs may actually throw away most of the information in x (input) concerning between-group variation".*[158] Thus, selecting PCs by ordered eigenvalue thresholds may not result in optimal subset selection. Other, albeit more computationally demanding selection methods have been used in areas such as spectroscopy and were discussed in the section on feature engineering (*e.g.,* genetic algorithms). These avenues can provide training across multiple electrodes to enhance generalizability. Regardless, best subset selection adds additional computational time on top of dimensionality reduction or regularization approaches.

1.8.3 Uses of *in vivo* data for model training and selection

In the absence of quantitative *in vivo* validation, qualitative *in vivo* validation is still an option. For example, Movassaghi and coworkers showed that the number of components selected by cross-validation did not track with multiple *in vivo* validation challenges when using a multi-electrode training set.[26] Rather, a subset of components provided a worse cross-validation score but improved *in vivo* domain knowledge results. As noted by the authors, *in vitro* validation may not translate *in vivo*, and thus selection of components by cross-validation may be sub-optimal. The inclusion of 'minor' components not in the top-down ordered selection can improve model generalizability. While earlier reports used *in vivo* validation checks (*e.g.,* comparing unexpected food rewards at the beginning and end of a recording session as a proxy for valid *in vivo* dopamine training sets),[5,159,160] model selection can also be done in this manner.

Such techniques contrast with other validation techniques that select components by maximal signal reconstruction. It may be more useful to frame *in vitro* to *in vivo* translation not as an issue of signal reconstruction, but as subset selection. Forcing the selection of a model by its ability to reconstruct signal in one domain makes no guarantees on its generalizability to another domain; this is especially true when multiple electrodes are involved. Thus, selecting variables or components optimally may be a matter of also considering the validity of built-in *in vivo* qualitative checks. For example, if component subsets are selected such that known stereotaxic, pharmacologic, or stimulation-based neurotransmitter release are qualitatively followed, then application to unknown biological dynamic situations are more trustworthy.

Another approach is to select hyperparameters and/or models using domain knowledge from *in vivo* experiments. For example, the predicted concentrations of test data can be compared

across models with different numbers of components or training sets to see which results agree most with known biological ground truths (*i.e.*, non-negative concentrations, stimulation-matched responses, genetically modified animals). To increase confidence, voltammetry experiments are often performed in brain regions with narrow neurochemical diversity to rule out certain interferents or off-target effects. Where possible, validating across separate techniques (*i.e.*, microdialysis) can engender further confidence.[26]

Rather than using *in vivo* data to assess the validity of *in vitro*-trained models, an ostensibly more straightforward solution is to train on *in vivo* data. Nonetheless, training *in vivo* presents unique challenges. Movement artifacts occur when electrodes are implanted in brain tissue. Importantly, there is the issue of ground truth, meaning the inability to know the true concentrations of analytes for *in vivo* training data. In addition to many different neurotransmitters, metabolites, peptides, proteins, ions, and can confound model predictions. Various approaches to *in vivo* training have been studied and advocated. However, technical difficulties remain, especially for chronic electrode implantation.[5] Approaches to monitoring biofouling or otherwise correcting for electrode sensitivity changes across implantation times have been developed.[130,161,162]

In vivo training sets can be compiled by recording voltammograms from brain regions with known responses to stimuli, such as dopamine and pH changes in the nucleus accumbens during electrical stimulation in the substantia nigra/ventral tegmental area (usually performed after the *in vivo* experimental data (*e.g.*, behavioral) has been collected to account for electrode fouling effects).[61] These voltammograms are assigned reference concentrations using traditional *in vitro* flow cell calibration by sequential injection analysis. The labeled *in vivo* training set is then used to predict unknown *in vivo* data. Some groups maintain these training sets can only be

used for one animal, at the same brain location, and using same electrode to prevent erroneous conclusions resulting from variations in calibration factors and voltammogram shapes (*e.g.*, the peak oxidation potential of dopamine can shift hundreds of mV between subjects[50]). So-called unrepresentative training sets can lead to substantial disagreements in concentration estimates depending on the training set used, especially at low signal-to-noise ratios.[50]

Meanwhile, others advocate for the use of 'standard' or 'universal' training sets for use across animals and electrodes. These training sets are "inter-subject", in that a training set on a different animal and different electrode is used to predict data from a different animal on a different electrode. The advent of this approach came about as chronically, as opposed to acutely, implanted electrodes were introduced.[163,164] The advantage of acute recordings is that post-fouled calibration factors obtained *in vitro* are likely to be relevant over the time scale of the *in vivo* experiment due to reduced immune responses and electrode fouling. Chronically implanted electrodes likelier to experience more dynamic environments over implantation periods. Moreover, they are rarely implanted with stimulating electrodes, precluding the use of *in vivo* training sets obtained at the same location or same animal.

Alternatives include unexpected sucrose delivery for *in vivo* training data to produce dopamine transients. However, this approach can underestimate predictions relative to electrical stimulation training sets as the dopamine concentrations spanned[60] for sucrose reward are narrower compared to electrical stimulation. Sucrose delivery is also less time-locked than electrical stimulation. More commonly, the 'standard training set' which uses electrical stimulation from separate subjects, is used. The results of within-subject and standard training sets on unknown *in vivo* data can also agree.[165]

Several reports have compared intra- *vs.* inter-subject training sets for chronic and acute electrodes for dopamine recordings. When *in vivo* training data from different electrodes and different animals were used to make predictions, dopamine transients were underestimated up to 50% as compared to within-subject predictions. This was attributed to the variance in voltammogram response between animals and electrodes. Using a cross-subject/electrode training set also leads to different Qα validation results, meaning the validity of training data defined by residuals depends on whether within or between subject training sets are used.

Similar results exist for multi-electrode studies. As the number of electrodes and training set size increases, more data variance is introduced not directly attributable to dopamine or pH. Thus, principal components bear less resemblance to their analytes and can cause overfitting. Again, PLSR and regularization may avoid this issue by their ability to separate contributions solely from variance in the data that covarying with concentration or by avoiding dimensionality reduction entirely and instead penalizing each individual point in the voltammogram in a supervised manner. This could explain why multi-electrode models have been successful outside of PCR.

Regardless, none of the approaches is perfect; each has its downsides. While the work on within-subjects and electrode *in vivo* training has been developed into a robust procedure, it suffers from problems of scale. The data sets are inherently small. Further, all approaches rely on imperfect *in vitro* calibration to some extent. *In vivo* training sets are not guaranteed to be untainted (for example, H_2O_2 and adenosine can confound pH changes in response to electrical stimulation), are more time-consuming, and cannot readily scale to multi-analyte mixtures.

For these reasons, the use of purely *in vitro* training sets on post-fouled electrodes to analyze *in vivo* data appears to be becoming more popular, alongside alternative models to PCR. This *in vitro* approach allows larger sets of training and test data to be compiled, avoids additional *in vivo* experimentation, and can scale to any level of concentration or mixture of analytes. Novel approaches incorporating *in vivo* data into the training process are being developed in lieu of template *in vivo* training sets. As transfer learning approaches develop, this will surely be an active area of new approaches.

Part of the reason for the growth in the popularity of *in vitro* training may come from the inability of in-human work to undergo *in vivo* training. To avoid calibration and electrical stimulation, in-human work often must forgo pre-calibration due to potential contamination issues. Work in humans, while still a small portion of voltammetry research, has contributed to the rise in popularity of larger, more diverse *in vitro* training sets aimed at better generalization.

In summary, using semi-supervised learning represents a promising avenue to address the generalizability issue by combining unsupervised and supervised approaches. Geoffrey Hinton, one of the founders of modern machine learning, summarizes the potential power of this approach: *"When we're learning to see, nobody's telling us what the right answers are—we just look. Every so often, your mother says 'that's a dog,' but that's very little information. You'd be lucky if you got a few bits of information—even one bit per second—that way. The brain's visual system requires 10^{14} [neural] connections. And you only live for 10^{9} seconds. So it's no use learning one bit per second. You need more like 10^{5} bits per second. And there's only one place you can get that much information—from the input itself."*[166]

1.9 INTERPRETABILITY

The importance of model interpretability in scientific machine learning is gaining increasing attention.[167,168] Interpretability provides context for understanding the machine learning predictions and an avenue to improve model performance.

For component-based models such as PCR, visual inspection of the scores and loadings/regression vectors are important and can be qualitatively assessed for chemical relevance.[50,68,153] Hermans *et al.* visualized how different component selection procedures removed noise from dopamine and pH training sets. Keithley *et al.* interpreted the electrochemical behavior of regression vectors as a model diagnostic tool. They incorporated domain knowledge as to what chemical information additional components were contributing (*e.g.*, the C, QH, and Q peaks of a pH change in voltammograms).[50] Interpreting the residuals can identify how training sets should be augmented because the peak potentials with the sources of error can be identified, and domain experts can infer potential interferents that should be included in training in the future.[50]

Sparse, linear models help interpretability. Some papers have analyzed model coefficients to identify voltammogram subregions of importance. This includes methods such as PLSR (*via* loadings and VIP scores)[26] and elastic net (*via* regression coefficients).[84] Deep learning methods for interpretability have also been used. For example, Choi *et al.* looked at class activation feature maps.[36] Mena and Buchanon *et al.* utilized feature importances.[124,125] Xue *et al.* noted the features retained between single and mixed analyte solutions[122] and Twomey *et al.* examined embeddings.[82]

Background inclusive voltammograms obscure analyte-specific features, which was a key reason for utilizing background subtraction (increased signal-to-noise and analyte peak oxidation and reduction feature identification). Machine learning has repeatedly been shown to utilize what was previously considered uninformative regions of voltammograms, even for applications outside of fast voltammetry, for example, mechanistic electrochemistry.[169] One of the largest effects machine learning has had across voltammetry is to question the importance of non-faradaic currents and motivate the use of new, information-rich waveforms.[4]

1.10 PROGRESS, CHALLENGES & FUTURE DIRECTIONS

The historical problems in voltammetry seem to be converging towards machine learning-inspired solutions. The out-of-electrode and out-of-concentration prediction problems are improved with large training sets and appropriately trained models and subset selection methods, including novel statistical learning adaptations. The multiplexing issue is being overcome as models approach complex training sets with nearly double-digit numbers of analytes (**Table 1.1**). With increased computational power and laboratory automation, more comprehensive training sets and other advances can be expected. However, the utility of larger networks and training sizes remains ambiguous. Still, the trend of head-to-head comparative studies should continue as there is no 'free lunch' when it comes to model selection.[170]

Some issues persist, such as out-of-distribution shifts. The utility of *in vivo* sets has seen decreased use as opposed to *in vitro* training sets with domain knowledge validation. However, the latest advances in using transfer learning and other task-aware approaches may provide a compromise of utilizing both *in vitro* and *in vivo* training data. New developments in fast voltammetry, outside of machine learning, will also inform the appropriate solutions. Improved waveform design and electrode coatings and materials (both for working and reference electrodes), as well as more fundamental understanding of biofouling at these interfaces,[155] may be combined with the data analysis pipelines detailed here to fix the flaws that remain after modeling. Reproducibility of electrode construction and surface chemistries would help generalizability, such as standardized microfabrication.[24] Still, this does not mean voltammetry and machine learning should not be practiced in its current form today. These problems are pervasive throughout many bioanalytical realms, and new biology can and continues to be

learned even when using less-than-ideal techniques. Continued use will only uncover and inspire new solutions to the challenges discussed here.

Successful models must be shared and made available for wide use. Models are unimportant unless others evaluate and use them. While we have reviewed state-of-the-art applications of machine learning to fast voltammetry, the most popular technique among neuroscientists remains the FSCV-PCR method implemented in 2004. As models are developed, they need to be widely disseminated. The rise in the use of open-source machine learning packages is an excellent step in this direction, away from previously commercialized and licensed software. The most popular software is trending towards open-source packages written in R (glmnet) and Python (scikit-learn, TensorFlow, Keras, PyTorch) or commonly academically licensed software such as MATLAB. Developing tutorials or even custom fast voltammetry packages that showcase these new techniques will help push the wider field beyond developers to use these techniques to discover new insights into the brain.

If the community could agree on an open-source baseline dataset to compare consistent metrics across models, this would be a great help.[171] Large-scale publicly available databases often do not contain voltammetry data.[89] In addition, agreed-upon community standards would be beneficial as benchmarking studies, such as in a recently proposed framework for reporting key performance metrics of FSCV carbon electrodes aimed toward varying carbon materials.[156] A similar framework for varying machine learning algorithms could be beneficial. This would allow head-to-head comparisons across models, training sets, and research groups placing new techniques on an even playing field. Universal databases and paradigms would enable large-scale studies. Many similar studies have been carried out for spectroscopy and voltammetric electronic tongues or other slow-scan voltammetry techniques. However, few if any such wide-scale studies

have been conducted for fast voltammetry applications. While advances in architectures and compute times are constantly being made, trade-offs are important to keep in mind if methods are to be used beyond the few leading research groups developing new fast voltammetry machine learning analysis techniques. At what point do miniscule increases in accuracy stop impacting important neurobiological conclusions?

Lastly, we should stand on the shoulders of our peers. This includes related fields like the voltammetric electronic tongue and mechanistic electrochemistry, but also more disparate or broad fields, such as fundamental statistics, chemometrics, and spectroscopy. Many of the issues and problems inherent in voltammetry can be overcome in through inspiration from these fields.

Machine learning will continue to develop alongside fast voltammetry. Practitioners and developers of new methods seem to be increasingly motivated to utilize state-of-the-art machine learning approaches. While the use of these techniques to predict real-time neurochemical dynamics in the brain has not been perfected, advances and contributions to neuroscience will continue to be made.

***Acknowledgements & author contributions*:** CSM conceptualized and drafted the manuscript. AMA supervised the project and edited the manuscript. CSM was supported by the National Science Foundation Graduate Research Fellowship Program (DGE-1650604 and DGE-2034835). Any opinions, findings, and conclusions or recommendations expressed in this material are those of the authors and do not necessarily reflect the views of the National Science Foundation. Biorender.com is acknowledged for figure generation.

1.11 REFERENCES

1. Mistry, A.; Franco, A. A.; Cooper, S. J.; Roberts, S. A.; Viswanathan, V., How machine learning will revolutionize electrochemical sciences. *ACS Energy Lett.* **2021,** *6* (4), 1422-1431. https://doi.org/10.1021/acsenergylett.1c00194
2. Puthongkham, P.; Venton, B. J., Recent advances in fast-scan cyclic voltammetry. *Analyst* **2020,** *145* (4), 1087-1102. https://doi.org/10.1039/c9an01925a
3. Rusheen, A. E.; Gee, T. A.; Jang, D. P.; Blaha, C. D.; Bennet, K. E.; Lee, K. H.; Heien, M. L.; Oh, Y., Evaluation of electrochemical methods for tonic dopamine detection in vivo. *TrAC Trends in Analytical Chemistry* **2020,** *132*, 116049. https://doi.org/10.1016/j.trac.2020.116049
4. Movassaghi, C. S.; Alcañiz Fillol, M.; Kishida, K. T.; McCarty, G.; Sombers, L. A.; Wassum, K. M.; Andrews, A. M., Maximizing electrochemical information: A perspective on background-inclusive fast voltammetry. *Anal. Chem.* **2024**. https://doi.org/10.1021/acs.analchem.3c04938
5. Rodeberg, N. T.; Sandberg, S. G.; Johnson, J. A.; Phillips, P. E. M.; Wightman, R. M., Hitchhiker's guide to voltammetry: Acute and chronic electrodes for in vivo fast-scan cyclic voltammetry. *ACS Chem. Neurosci.* **2017,** *8* (2), 221-234. https://doi.org/10.1021/acschemneuro.6b00393
6. Montague, P. R.; Kishida, K. T., Computational underpinnings of neuromodulation in humans. *Cold Spring Harbor Symp. Quant. Biol.* **2018,** *83*, 71-82. https://doi.org/10.1101/sqb.2018.83.038166
7. Alivisatos, A. P.; Andrews, A. M.; Boyden, E. S.; Chun, M.; Church, G. M.; Deisseroth, K.; Donoghue, J. P.; Fraser, S. E.; Lippincott-Schwartz, J.; Looger, L. L.;

Masmanidis, S.; McEuen, P. L.; Nurmikko, A. V.; Park, H.; Peterka, D. S.; Reid, C.; Roukes, M. L.; Scherer, A.; Schnitzer, M.; Sejnowski, T. J.; Shepard, K. L.; Tsao, D.; Turrigiano, G.; Weiss, P. S.; Xu, C.; Yuste, R.; Zhuang, X., Nanotools for neuroscience and brain activity mapping. *ACS Nano* **2013,** *7* (3), 1850-66. https://doi.org/10.1021/nn4012847

8. Andrews, A. M., The BRAIN Initiative: Toward a chemical connectome. *ACS Chem. Neurosci.* **2013,** *4* (5), 645. https://doi.org/10.1021/cn4001044

9. Su, Y.; Bian, S.; Sawan, M., Real-time in vivo detection techniques for neurotransmitters: A review. *Analyst* **2020,** *145* (19), 6193-6210. https://doi.org/10.1039/D0AN01175D

10. Zhang, Y.; Jiang, N.; Yetisen, A. K., Brain neurochemical monitoring. *Biosens. Bioelectron.* **2021,** *189*, 113351. https://doi.org/10.1016/j.bios.2021.113351

11. Venton, B. J.; Cao, Q., Fundamentals of fast-scan cyclic voltammetry for dopamine detection. *Analyst* **2020,** *145* (4), 1158-1168. https://doi.org/10.1039/C9AN01586H

12. Shao, Z.; Chang, Y.; Venton, B. J., Carbon microelectrodes with customized shapes for neurotransmitter detection: A review. *Anal. Chim. Acta* **2022,** *1223*, 340165. https://doi.org/10.1016/j.aca.2022.340165

13. Ostertag, B. J.; Ross, A. E., The future of carbon-based neurochemical sensing: A critical perspective. *ECS Sens. Plus* **2023,** *2* (4), 043601. https://doi.org/10.1149/2754-2726/ad15a2

14. Liu, R.; Feng, Z.-Y.; Li, D.; Jin, B.; Lan, Y.; Meng, L.-Y., Recent trends in carbon-based microelectrodes as electrochemical sensors for neurotransmitter detection: A review. *TrAC, Trends Anal. Chem.* **2022,** *148*, 116541.

15. Rafi, H.; Zestos, A. G., Recent advances in FSCV detection of neurochemicals via waveform and carbon microelectrode modification. *J. Electrochem. Soc.* **2021,** *168* (5), 057520.

16. Da, Y.; Luo, S.; Tian, Y., Real-time monitoring of neurotransmitters in the brain of living animals. *ACS Appl. Mater. Interfaces* **2023,** *15* (1), 138-157. https://doi.org/10.1021/acsami.2c02740

17. Chen, H.; Kätelhön, E.; Compton, R. G., Machine learning in fundamental electrochemistry: Recent advances and future opportunities. *Curr. Opin. Electrochem.* **2023,** *38*, 101214. https://doi.org/10.1016/j.coelec.2023.101214

18. Sun, J.; Liu, C., What and how can machine learning help to decipher mechanisms in molecular electrochemistry? *Curr. Opin. Electrochem.* **2023,** *39*, 101306. https://doi.org/10.1016/j.coelec.2023.101306

19. Giordano, G. F.; Ferreira, L. F.; Bezerra, Í. R. S.; Barbosa, J. A.; Costa, J. N. Y.; Pimentel, G. J. C.; Lima, R. S., Machine learning toward high-performance electrochemical sensors. *Anal. Bioanal. Chem.* **2023**. https://doi.org/10.1007/s00216-023-04514-z

20. Cui, F.; Yue, Y.; Zhang, Y.; Zhang, Z.; Zhou, H. S., Advancing biosensors with machine learning. *ACS Sens.* **2020,** *5* (11), 3346-3364. https://doi.org/10.1021/acssensors.0c01424

21. Puthongkham, P.; Wirojsaengthong, S.; Suea-Ngam, A., Machine learning and chemometrics for electrochemical sensors: Moving forward to the future of analytical chemistry. *Analyst* **2021,** *146* (21), 6351-6364. https://doi.org/10.1039/D1AN01148K

22. Namuduri, S.; Narayanan, B. N.; Davuluru, V. S. P.; Burton, L.; Bhansali, S., Review—deep learning methods for sensor based predictive maintenance and future perspectives

for electrochemical sensors. *J. Electrochem. Soc.* **2020,** *167* (3), 037552. https://doi.org/10.1149/1945-7111/ab67a8

23. Rafi, H.; Zestos, A. G., Multiplexing neurochemical detection with carbon fiber multielectrode arrays using fast-scan cyclic voltammetry. *Anal. Bioanal. Chem.* **2021,** *413* (27), 6715-6726.

24. Castagnola, E.; Robbins, E. M.; Krahe, D. D.; Wu, B.; Pwint, M. Y.; Cao, Q.; Cui, X. T., Stable in-vivo electrochemical sensing of tonic serotonin levels using PEDOT/CNT-coated glassy carbon flexible microelectrode arrays. *Biosens. Bioelectron.* **2023,** *230*, 115242. https://doi.org/10.1016/j.bios.2023.115242

25. Dunham, K. E.; Venton, B. J., Improving serotonin fast-scan cyclic voltammetry detection: New waveforms to reduce electrode fouling. *Analyst* **2020,** *145* (22), 7437-7446. https://doi.org/10.1039/D0AN01406K

26. Movassaghi, C. S.; Perrotta, K. A.; Yang, H.; Iyer, R.; Cheng, X.; Dagher, M.; Fillol, M. A.; Andrews, A. M., Simultaneous serotonin and dopamine monitoring across timescales by rapid pulse voltammetry with partial least squares regression. *Anal. Bioanal. Chem.* **2021,** *413* (27), 6747-6767. https://doi.org/10.1007/s00216-021-03665-1

27. Meunier, C. J.; Mitchell, E. C.; Roberts, J. G.; Toups, J. V.; McCarty, G. S.; Sombers, L. A., Electrochemical selectivity achieved using a double voltammetric waveform and partial least squares regression: Differentiating endogenous hydrogen peroxide fluctuations from shifts in pH. *Anal. Chem.* **2018,** *90* (3), 1767-1776. https://doi.org/10.1021/acs.analchem.7b03717

28. Andrews, A. M.; Schepartz, A.; Sweedler, J. V.; Weiss, P. S., Chemistry and the BRAIN Initiative. *J. Am. Chem. Soc.* **2014,** *136* (1), 1-2. https://doi.org/10.1021/ja4118347

29. Andrews, A. M.; Bhargava, R.; Kennedy, R.; Li, L.; Sweedler, J. V., The chemistry of thought: The role of the measurement sciences in brain research. *Anal. Chem.* **2017,** *89* (9), 4757. https://doi.org/10.1021/acs.analchem.7b01364

30. Andrews, A. M.; Weiss, P. S., Nano in the brain: Nano-neuroscience. *ACS Nano* **2012,** *6* (10), 8463-4. https://doi.org/10.1021/nn304724q

31. Mitchell, T. M., Machine learning. McGraw-Hill: 1997.

32. Sybrandt, L.; Perone, S. P., Computerized learning machine applied to qualitative analysis of mixtures by stationary electrode polarography. *Anal. Chem.* **1971,** *43* (3), 382-388.

33. Pichler, M. A.; Perone, S. P., Computerized pattern recognition applications to chemical analysis. Development of interactive feature selection methods for the k-nearest neighbor technique. *Anal. Chem.* **1974,** *46* (12), 1790-1798.

34. Heien, M. L. A. V.; Johnson, M. A.; Wightman, R. M., Resolving neurotransmitters detected by fast-scan cyclic voltammetry. *Anal. Chem.* **2004,** *76* (19), 5697-5704. https://doi.org/10.1021/ac0491509

35. Bang, D.; Luo, Y.; Barbosa, L. S.; Batten, S. R.; Hadj-Amar, B.; Twomey, T.; Melville, N.; White, J. P.; Torres, A.; Celaya, X.; Ramaiah, P.; McClure, S. M.; Brewer, G. A.; Bina, R. W.; Lohrenz, T.; Casas, B.; Chiu, P. H.; Vannucci, M.; Kishida, K. T.; Witcher, M. R.; Montague, P. R., Noradrenaline tracks emotional modulation of attention in human amygdala. *Curr. Biol.* **2023,** *33* (22), 5003-5010 e6. https://doi.org/10.1016/j.cub.2023.09.074

36. Choi, H.; Shin, H.; Cho, H. U.; Blaha, C. D.; Heien, M. L.; Oh, Y.; Lee, K. H.; Jang, D. P., Neurochemical concentration prediction using deep learning vs principal

component regression in fast scan cyclic voltammetry: A comparison study. *ACS Chem. Neurosci.* **2022,** *13* (15), 2288-2297. https://doi.org/10.1021/acschemneuro.2c00069

37. Goyal, A.; Yuen, J.; Sinicrope, S.; Winter, B.; Randall, L.; Rusheen, A. E.; Blaha, C. D.; Bennet, K. E.; Lee, K. H.; Shin, H.; Oh, Y., Resolution of tonic concentrations of highly similar neurotransmitters using voltammetry and deep learning. *Mol. Psychiatry* **2024**. https://doi.org/10.1038/s41380-024-02537-1

38. Murphy, K. P., *Probabilistic machine learning: An introduction*. MIT press: 2022.

39. Bard, A. J.; Faulkner, L. R.; White, H. S., *Electrochemical methods: Fundamentals and applications*. John Wiley & Sons: 2022.

40. Bond, A. M., A perceived paucity of quantitative studies in the modern era of voltammetry: Prospects for parameterisation of complex reactions in Bayesian and machine learning frameworks. *J Solid State Electrochem.* **2020,** *24* (9), 2041-2050. https://doi.org/10.1007/s10008-020-04639-6

41. Gundry, L.; Guo, S.-X.; Kennedy, G.; Keith, J.; Robinson, M.; Gavaghan, D.; Bond, A. M.; Zhang, J., Recent advances and future perspectives for automated parameterisation, Bayesian inference and machine learning in voltammetry. *Chem. Comm.* **2021,** *57* (15), 1855-1870. https://doi.org/10.1039/D0CC07549C

42. Chen, H.; Yang, M.; Smetana, B.; Novák, V.; Matějka, V.; Compton, R. G., Discovering electrochemistry with an electrochemistry-informed neural network (ECINN). *Angew. Chem. Int. Ed.* **2024,** *63* (13), e202315937. https://doi.org/10.1002/anie.202315937

43. Robinson, D. L.; Venton, B. J.; Heien, M. L.; Wightman, R. M., Detecting subsecond dopamine release with fast-scan cyclic voltammetry in vivo. *Clin. Chem* **2003,** *49* (10), 1763-73. https://doi.org/10.1373/49.10.1763

44. Puthongkham, P.; Rocha, J.; Borgus, J. R.; Ganesana, M.; Wang, Y.; Chang, Y.; Gahlmann, A.; Venton, B. J., Structural similarity image analysis for detection of adenosine and dopamine in fast-scan cyclic voltammetry color plots. *Anal. Chem.* **2020,** *92* (15), 10485-10494. https://doi.org/10.1021/acs.analchem.0c01214

45. Borman, R. P.; Wang, Y.; Nguyen, M. D.; Ganesana, M.; Lee, S. T.; Venton, B. J., Automated algorithm for detection of transient adenosine release. *ACS Chem. Neurosci.* **2017,** *8* (2), 386-393. https://doi.org/10.1021/acschemneuro.6b00262

46. Espín, L. X.; Asp, A. J.; Trevathan, J. K.; Ludwig, K. A.; Lujan, J. L., Integral methods for automatic quantification of fast-scan-cyclic-voltammetry detected neurotransmitters. *PLOS ONE* **2021,** *16* (7), e0254594. https://doi.org/10.1371/journal.pone.0254594

47. Kramer, R., *Chemometric techniques for quantitative analysis*. CRC Press: Boca Raton, FL, 1998.

48. Hexter, M.; van Batenburg-Sherwood, J.; Hashemi, P., Novel experimental and analysis strategies for fast voltammetry: 2. A troubleshoot-free flow cell for FSCV calibrations. *ACS Meas. Sci. Au* **2023,** *3* (2), 120-126. https://doi.org/10.1021/acsmeasuresciau.2c00059

49. Delong, L. M.; Li, Y.; Lim, G. N.; Wairegi, S. G.; Ross, A. E., A microfluidic electrochemical flow cell capable of rapid on-chip dilution for fast-scan cyclic voltammetry electrode calibration. *Anal. Bioanal. Chem.* **2020,** *412* (24), 6287-6294. https://doi.org/10.1007/s00216-020-02493-z

50. Keithley, R. B.; Wightman, R. M., Assessing principal component regression prediction of neurochemicals detected with fast-scan cyclic voltammetry. *ACS Chem. Neurosci.* **2011,** *2* (9), 514-525. https://doi.org/10.1021/cn200035u

51. Rantataro, S.; Pascual, L. F.; Laurila, T., Electrochemical detection of amine neurotransmitters is drastically different in buffer solutions, in vivo, and cell culture systems. *Electrochem. Commun.* **2024**, 107732. https://doi.org/10.1016/j.elecom.2024.107732

52. Singh, Y. S.; Sawarynski, L. E.; Dabiri, P. D.; Choi, W. R.; Andrews, A. M., Head-to-head comparisons of carbon fiber microelectrode coatings for sensitive and selective neurotransmitter detection by voltammetry. *Anal. Chem.* **2011,** *83* (17), 6658-6666. https://doi.org/10.1021/ac2011729

53. Phillips, P. E. M.; Stuber, G. D.; Heien, M. L. A. V.; Wightman, R. M.; Carelli, R. M., Subsecond dopamine release promotes cocaine seeking. *Nature* **2003,** *422* (6932), 614-618. https://doi.org/10.1038/nature01476

54. Cheer, J. F.; Wassum, K. M.; Heien, M. L. A. V.; Phillips, P. E. M.; Wightman, R. M., Cannabinoids enhance subsecond dopamine release in the nucleus accumbens of awake rats. *J. Neurosci.* **2004,** *24* (18), 4393-4400. https://doi.org/10.1523/jneurosci.0529-04.2004

55. Mena, S.; Dietsch, S.; Berger, S. N.; Witt, C. E.; Hashemi, P., Novel, user-friendly experimental and analysis strategies for fast voltammetry: 1. The analysis kid for FSCV. *ACS Meas. Sci. Au* **2021,** *1* (1), 11-19.

56. Takmakov, P.; Zachek, M. K.; Keithley, R. B.; Bucher, E. S.; McCarty, G. S.; Wightman, R. M., Characterization of local pH changes in brain using fast-scan cyclic

voltammetry with carbon microelectrodes. *Anal. Chem.* **2010,** *82* (23), 9892-9900. https://doi.org/10.1021/ac102399n

57. Díaz-Cruz, J. M.; Esteban, M.; Ariño, C., *Chemometrics in electroanalysis*. 1 ed.; Springer: Cham, Switzerland, 2019; p 202.

58. Keithley, R. B.; Carelli, R. M.; Wightman, R. M., Rank estimation and the multivariate analysis of in vivo fast-scan cyclic voltammetric data. *Anal. Chem.* **2010,** *82* (13), 5541-5551. https://doi.org/10.1021/ac100413t

59. Keithley, R. B.; Mark Wightman, R.; Heien, M. L., Multivariate concentration determination using principal component regression with residual analysis. *TrAC, Trends Anal. Chem.* **2009,** *28* (9), 1127-1136. https://doi.org/10.1016/j.trac.2009.07.002

60. Rodeberg, N. T.; Johnson, J. A.; Cameron, C. M.; Saddoris, M. P.; Carelli, R. M.; Wightman, R. M., Construction of training sets for valid calibration of in vivo cyclic voltammetric data by principal component analysis. *Anal. Chem.* **2015,** *87* (22), 11484-11491. https://doi.org/10.1021/acs.analchem.5b03222

61. Heien, M. L. A. V.; Khan, A. S.; Ariansen, J. L.; Cheer, J. F.; Phillips, P. E. M.; Wassum, K. M.; Wightman, R. M., Real-time measurement of dopamine fluctuations after cocaine in the brain of behaving rats. *Proc. Natl. Acad. Sci. U.S.A.* **2005,** *102* (29), 10023-10028. https://doi.org/10.1073/pnas.0504657102

62. Regan, S. L.; Cryan, M. T.; Williams, M. T.; Vorhees, C. V.; Ross, A. E., Enhanced transient striatal dopamine release and reuptake in Lphn3 knockout rats. *ACS Chem. Neurosci.* **2020,** *11* (8), 1171-1177. https://doi.org/10.1021/acschemneuro.0c00033

63. Kishida, K. T.; Sandberg, S. G.; Lohrenz, T.; Comair, Y. G.; Sáez, I.; Phillips, P. E. M.; Montague, P. R., Sub-second dopamine detection in human striatum. *PLOS ONE* **2011,** *6* (8), e23291. https://doi.org/10.1371/journal.pone.0023291

64. Hermans, A.; Keithley, R. B.; Kita, J. M.; Sombers, L. A.; Wightman, R. M., Dopamine detection with fast-scan cyclic voltammetry used with analog background subtraction. *Anal. Chem.* **2008,** *80* (11), 4040-4048. https://doi.org/10.1021/ac800108j

65. Kimble, L. C.; Twiddy, J. S.; Berger, J. M.; Forderhase, A. G.; McCarty, G. S.; Meitzen, J.; Sombers, L. A., Simultaneous, real-time detection of glutamate and dopamine in rat striatum using fast-scan cyclic voltammetry. *ACS Sens.* **2023,** *8* (11), 4091-4100. https://doi.org/10.1021/acssensors.3c01267

66. Nguyen, M. D.; Lee, S. T.; Ross, A. E.; Ryals, M.; Choudhry, V. I.; Venton, B. J., Characterization of spontaneous, transient adenosine release in the caudate-putamen and prefrontal cortex. *PLOS ONE* **2014,** *9* (1), e87165. https://doi.org/10.1371/journal.pone.0087165

67. Wang, Y.; Venton, B. J., Correlation of transient adenosine release and oxygen changes in the caudate-putamen. *J. Neurochem.* **2017,** *140* (1), 13-23. https://doi.org/10.1111/jnc.13705

68. Jamalzadeh, M.; Cuniberto, E.; Huang, Z.; Feeley, R. M.; Patel, J. C.; Rice, M. E.; Uichanco, J.; Shahrjerdi, D., Toward robust quantification of dopamine and serotonin in mixtures using nano-graphitic carbon sensors. *Analyst* **2024,** *149* (8), 2351-2362. https://doi.org/10.1039/D3AN02086J

69. Ross, A. E.; Venton, B. J., Sawhorse waveform voltammetry for selective detection of adenosine, ATP, and hydrogen peroxide. *Anal. Chem.* **2014,** *86* (15), 7486-7493. https://doi.org/10.1021/ac501229c

70. Jo, T.; Yoshimi, K.; Takahashi, T.; Oyama, G.; Hattori, N., Dual use of rectangular and triangular waveforms in voltammetry using a carbon fiber microelectrode to differentiate norepinephrine from dopamine. *J. Electroanal. Chem.* **2017,** *802*, 1-7. https://doi.org/10.1016/j.jelechem.2017.08.037

71. Rodeberg, N. T.; Johnson, J. A.; Bucher, E. S.; Wightman, R. M., Dopamine dynamics during continuous intracranial self-stimulation: Effect of waveform on fast-scan cyclic voltammetry data. *ACS Chem. Neurosci.* **2016,** *7* (11), 1508-1518. https://doi.org/10.1021/acschemneuro.6b00142

72. Johnson, J. A.; Gray, J. H.; Rodeberg, N. T.; Wightman, R. M., Multivariate curve resolution for signal isolation from fast-scan cyclic voltammetric data. *Anal. Chem.* **2017,** *89* (19), 10547-10555.

73. Wold, S.; Sjöström, M.; Eriksson, L., PLS-regression: A basic tool of chemometrics. *Chemom. Intell. Lab. Syst* **2001,** *58* (2), 109-130. https://doi.org/10.1016/S0169-7439(01)00155-1

74. Agramunt, J.; Parke, B.; Mena, S.; Ubels, V.; Jimenez, F.; Williams, G.; Rhodes, A. D.; Limbu, S.; Hexter, M.; Knight, L.; Hashemi, P.; Kozlov, A. S.; Higgins, C. A., Mechanical stimulation of human hair follicle outer root sheath cultures activates adjacent sensory neurons. *Sci. Adv.* **2023,** *9* (43), eadh3273. https://doi.org/10.1126/sciadv.adh3273

75. Meunier, C. J.; McCarty, G. S.; Sombers, L. A., Drift subtraction for fast-scan cyclic voltammetry using double-waveform partial-least-squares regression. *Anal. Chem.* **2019,** *91* (11), 7319-7327. https://doi.org/10.1021/acs.analchem.9b01083

76. Rouhollahi, A.; Rajabzadeh, R.; Ghasemi, J., Simultaneous determination of dopamine and ascorbic acid by linear sweep voltammetry along with chemometrics using a glassy carbon electrode. *Microchim. Acta* **2007,** *157* (3), 139-147. https://doi.org/10.1007/s00604-006-0668-9

77. Kim, J.; Oh, Y.; Park, C.; Kang, Y. M.; Shin, H.; Kim, I. Y.; Jang, D. P., Comparison study of partial least squares regression analysis and principal component analysis in fast-scan cyclic voltammetry. *Int. J. Electrochem. Sci.* **2019,** *14* (7), 5924-5937. https://doi.org/10.20964/2019.07.03

78. Loewinger, G.; Patil, P.; Kishida, K. T.; Parmigiani, G., Hierarchical resampling for bagging in multistudy prediction with applications to human neurochemical sensing. *Ann. Appl. Stat.* **2022,** *16* (4), 2145-2165, 21. https://doi.org/10.1214/21-aoas1574

79. Reich, G.; Wolf, J.; Long, J. T.; Weber, S. G., Recovery of voltammograms by target factor analysis of current-time data in electrochemical detection. *Anal. Chem.* **1990,** *62* (23), 2643-2646. https://doi.org/10.1021/ac00222a024

80. Saccenti, E.; Camacho, J., Determining the number of components in principal components analysis: A comparison of statistical, crossvalidation and approximated methods. *Chemom. Intell. Lab. Syst* **2015,** *149*, 99-116. https://doi.org/10.1016/j.chemolab.2015.10.006

81. Kishida, K. T.; Saez, I.; Lohrenz, T.; Witcher, M. R.; Laxton, A. W.; Tatter, S. B.; White, J. P.; Ellis, T. L.; Phillips, P. E. M.; Montague, P. R., Subsecond dopamine

fluctuations in human striatum encode superposed error signals about actual and counterfactual reward. *Proc. Natl. Acad. Sci. U.S.A.* **2016,** *113* (1), 200-205. https://doi.org/10.1073/pnas.1513619112

82. Twomey, T.; Barbosa, L.; Lohrenz, T.; Montague, P. R., Deep learning architectures for FSCV, a comparison. *arXiv (Medical Physics)* **2022,** (posted 2022-12-05). https://doi.org/10.48550/arXiv.2212.01960 (accessed 2023-12-12)

83. Hastie, T.; Tibshirani, R.; Friedman, J. H., *The elements of statistical learning: Data mining, inference, and prediction*. 2nd ed.; Springer: New York, NY, 2001.

84. Moran, R. J.; Kishida, K. T.; Lohrenz, T.; Saez, I.; Laxton, A. W.; Witcher, M. R.; Tatter, S. B.; Ellis, T. L.; Phillips, P. E. M.; Dayan, P.; Montague, P. R., The protective action encoding of serotonin transients in the human brain. *Neuropsychopharmacology* **2018,** *43* (6), 1425-1435. https://doi.org/10.1038/npp.2017.304

85. Bang, D.; Kishida, K. T.; Lohrenz, T.; White, J. P.; Laxton, A. W.; Tatter, S. B.; Fleming, S. M.; Montague, P. R., Sub-second dopamine and serotonin signaling in human striatum during perceptual decision-making. *Neuron* **2020,** *108* (5), 999-1010.e6. https://doi.org/10.1016/j.neuron.2020.09.015

86. Spry, K. P. Detection of oxytocin and vasopressin using fast-scan cyclic voltammetry and machine learning methods. M.S. Thesis, Wake Forest University, United States -- North Carolina, 2022.

87. Eltahir, A.; White, J.; Lohrenz, T.; Montague, P. R., Low amplitude burst detection of catecholamines. *bioRxiv (Neuroscience)* **2021,** (posted 2021-08-04). https://doi.org/10.1101/2021.08.02.454747 (accessed 2023-12-12)

88. Montague, P. R.; Lohrenz, T.; White, J.; Moran, R. J.; Kishida, K. T., Random burst sensing of neurotransmitters. *bioRxiv (Neuroscience)* **2019,** (posted 2019-04-13), 607077. https://doi.org/10.1101/607077 (accessed 2023-12-12)

89. Ayres, L. B.; Gomez, F. J. V.; Linton, J. R.; Silva, M. F.; Garcia, C. D., Taking the leap between analytical chemistry and artificial intelligence: A tutorial review. *Anal. Chim. Acta* **2021,** *1161*, 338403. https://doi.org/10.1016/j.aca.2021.338403

90. Johnson, J. A.; Hobbs, C. N.; Wightman, R. M., Removal of differential capacitive interferences in fast-scan cyclic voltammetry. *Anal. Chem.* **2017,** *89* (11), 6166-6174. https://doi.org/10.1021/acs.analchem.7b01005

91. Johnson, J. A.; Rodeberg, N. T.; Wightman, R. M., Measurement of basal neurotransmitter levels using convolution-based nonfaradaic current removal. *Anal. Chem.* **2018,** *90* (12), 7181-7189. https://doi.org/10.1021/acs.analchem.7b04682

92. Atcherley, C. W.; Vreeland, R. F.; Monroe, E. B.; Sanchez-Gomez, E.; Heien, M. L., Rethinking data collection and signal processing. 2. Preserving the temporal fidelity of electrochemical measurements. *Anal. Chem.* **2013,** *85* (16), 7654-7658. https://doi.org/10.1021/ac402037k

93. DeWaele, M.; Oh, Y.; Park, C.; Kang, Y. M.; Shin, H.; Blaha, C. D.; Bennet, K. E.; Kim, I. Y.; Lee, K. H.; Jang, D. P., A baseline drift detrending technique for fast scan cyclic voltammetry. *Analyst* **2017,** *142* (22), 4317-4321. https://doi.org/10.1039/C7AN01465A

94. Kang, S.; Park, J.; Jeong, Y.; Oh, Y.-S.; Choi, J.-W., Second-derivative-based background drift removal for a tonic dopamine measurement in fast-scan cyclic

voltammetry. *Anal. Chem.* **2022,** *94* (33), 11459-11463. https://doi.org/10.1021/acs.analchem.2c01047

95. Laude, N. D.; Atcherley, C. W.; Heien, M. L., Rethinking data collection and signal processing. 1. Real-time oversampling filter for chemical measurements. *Anal. Chem.* **2012,** *84* (19), 8422-8426. https://doi.org/10.1021/ac302169y

96. Anastassiou, C. A.; Patel, B. A.; Arundell, M.; Yeoman, M. S.; Parker, K. H.; O'Hare, D., Subsecond voltammetric separation between dopamine and serotonin in the presence of ascorbate. *Anal. Chem.* **2006,** *78* (19), 6990-6998. https://doi.org/10.1021/ac061002q

97. Zamani, H.; Bahrami, H. R.; Chalwadi, P.; Garris, P. A.; Mohseni, P., C–FSCV: Compressive fast-scan cyclic voltammetry for brain dopamine recording. *IEEE Trans. Neural Syst. Rehabil. Eng.* **2017,** *26* (1), 51-59.

98. Amos, A. N.; Roberts, J. G.; Qi, L.; Sombers, L. A.; McCarty, G. S., Reducing the sampling rate of biochemical measurements using fast-scan cyclic voltammetry for in vivo applications. *IEEE Sens. J.* **2014,** *14* (9), 2975-2980. https://doi.org/10.1109/JSEN.2014.2321479

99. Sadibolova, R.; DiMarco, E. K.; Jiang, A.; Maas, B.; Tatter, S. B.; Laxton, A.; Kishida, K. T.; Terhune, D. B., Sub-second and multi-second dopamine dynamics underlie variability in human time perception. *medRxiv* **2024**, 2024.02. 09.24302276. https://doi.org/10.1101/2024.02.09.24302276

100. Ma, P.; Chen, P.; Tilden, E. I.; Aggarwal, S.; Oldenborg, A.; Chen, Y., Fast and slow: Recording neuromodulator dynamics across both transient and chronic time scales. *Sci. Adv.* **2024,** *10* (8), eadi0643. https://doi.org/10.1126/sciadv.adi0643

101. Yang, J.; Xu, J.; Zhang, X.; Wu, C.; Lin, T.; Ying, Y., Deep learning for vibrational spectral analysis: Recent progress and a practical guide. *Anal. Chim. Acta* **2019,** *1081*, 6-17. https://doi.org/10.1016/j.aca.2019.06.012

102. Zhang, X.; Lin, T.; Xu, J.; Luo, X.; Ying, Y., Deepspectra: An end-to-end deep learning approach for quantitative spectral analysis. *Anal. Chim. Acta* **2019,** *1058*, 48-57. https://doi.org/10.1016/j.aca.2019.01.002

103. Chong, I.-G.; Jun, C.-H., Performance of some variable selection methods when multicollinearity is present. *Chemom. Intell. Lab. Syst* **2005,** *78* (1), 103-112. https://doi.org/10.1016/j.chemolab.2004.12.011

104. Giglio, C.; Brown, S. D., Using elastic net regression to perform spectrally relevant variable selection. *J. Chemom.* **2018,** *32* (8), e3034. https://doi.org/10.1002/cem.3034

105. Fu, G.-H.; Xu, Q.-S.; Li, H.-D.; Cao, D.-S.; Liang, Y.-Z., Elastic net grouping variable selection combined with partial least squares regression (EN-PLSR) for the analysis of strongly multi-collinear spectroscopic data. *Appl. Spectrosc.* **2011,** *65* (4), 402-408. https://doi.org/10.1366/10-06069

106. Prieto, N.; Oliveri, P.; Leardi, R.; Gay, M.; Apetrei, C.; Rodriguez-Méndez, M. L.; de Saja, J. A., Application of a GA–PLS strategy for variable reduction of electronic tongue signals. *Sens. Actuators, B* **2013,** *183*, 52-57. https://doi.org/10.1016/j.snb.2013.03.114

107. Kim, J.; Barath, A. S.; Rusheen, A. E.; Rojas Cabrera, J. M.; Price, J. B.; Shin, H.; Goyal, A.; Yuen, J. W.; Jondal, D. E.; Blaha, C. D.; Lee, K. H.; Jang, D. P.; Oh, Y., Automatic and reliable quantification of tonic dopamine concentrations in vivo using a novel probabilistic inference method. *ACS Omega* **2021,** *6* (10), 6607-6613. https://doi.org/10.1021/acsomega.0c05217

108. Zeger, S. L.; Liang, K.-Y.; Albert, P. S., Models for longitudinal data: A generalized estimating equation approach. *Biometrics* **1988,** *44* (4), 1049-1060. https://doi.org/10.2307/2531734

109. Kallabis, C.; Beyerlein, P.; Lisdat, F., Quantitative determination of dopamine in the presence of interfering substances supported by machine learning tools. *Bioelectrochemistry* **2024,** *157*, 108667. https://doi.org/10.1016/j.bioelechem.2024.108667

110. Matsushita, G. H. G.; Oliveira, L. E. S.; Sugi, A. H.; Cunha, C. d.; Costa, Y. M. G. In *Automatic identification of phasic dopamine release*, 2018 25th International Conference on Systems, Signals and Image Processing (IWSSIP), 20-22 June 2018; 2018; pp 1-5.

111. Siegenthaler, J. Building new tools for measuring and analyzing dopaminergic signaling using fast-scan cyclic voltammetry. Ph.D. Thesis, The University of Arizona, United States -- Arizona, 2020.

112. Kammarchedu, V.; Ebrahimi, A., Advancing electrochemical screening of neurotransmitters using a customizable machine learning-based multimodal system. *IEEE Sens. Lett.* **2023,** *7* (3), 1-4. https://doi.org/10.1109/LSENS.2023.3247002

113. Komoto, Y.; Ohshiro, T.; Yoshida, T.; Tarusawa, E.; Yagi, T.; Washio, T.; Taniguchi, M., Time-resolved neurotransmitter detection in mouse brain tissue using an artificial intelligence-nanogap. *Sci. Rep.* **2020,** *10* (1), 11244. https://doi.org/10.1038/s41598-020-68236-3

114. Matsushita, G. H. G.; Sugi, A. H.; Costa, Y. M. G.; Gomez-A, A.; Da Cunha, C.; Oliveira, L. S., Phasic dopamine release identification using convolutional neural

network. *Comput. Biol. Med.* **2019,** *114*, 103466. https://doi.org/10.1016/j.compbiomed.2019.103466

115. Kumar, S.; Bhagat, A. K.; Bhaiyya, M.; Amreen, K.; Dubey, S. K.; Goel, S., A machine learning approach for simultaneous electrochemical detection of dopamine and serotonin in an optimized carbon thread-based miniaturized device. *IEEE Sens. J.* **2024**. https://doi.org/10.1109/JSEN.2024.3386655

116. Gholivand, M.-B.; Jalalvand, A. R.; Goicoechea, H. C.; Skov, T., Chemometrics-assisted simultaneous voltammetric determination of ascorbic acid, uric acid, dopamine and nitrite: Application of non-bilinear voltammetric data for exploiting first-order advantage. *Talanta* **2014,** *119*, 553-563.

117. Stevens, E.; Antiga, L.; Viehmann, T., *Deep learning with PyTorch*. Manning Publications: 2020.

118. Raschka, S.; Mirjalili, V., *Python machine learning: Machine learning and deep learning with Python, scikit-learn, and TensorFlow 2*. 3rd ed.; Packt Publishing Ltd.: Birmingham, UK, 2019.

119. Patarnello, L.; Celin, M.; Nanni, L., Phasic dopamine release identification using ensemble of AlexNet. *arXiv* **2020**.

120. Al-Haija, Q. A.; Smadi, M.; Al-Bataineh, O. M. In *Identifying phasic dopamine releases using darknet-19 convolutional neural network*, 2021 IEEE International IoT, Electronics and Mechatronics Conference (IEMTRONICS), IEEE: 2021; pp 1-5.

121. Zhang, Z.; Oh, Y.; Adams, S. D.; Bennet, K. E.; Kouzani, A. Z., An FSCV deep neural network: Development, pruning, and acceleration on an FPGA. *IEEE J. Biomed. Health. Inform.* **2020,** *25* (6), 2248-2259.

122. Xue, Y.; Ji, W.; Jiang, Y.; Yu, P.; Mao, L., Deep learning for voltammetric sensing in a living animal brain. *Angew. Chem. Int. Ed.* **2021,** *60* (44), 23777-23783. https://doi.org/10.1002/anie.202109170

123. Michelucci, U., An introduction to autoencoders. *arXiv* **2022**.

124. Mena, S.; Visentin, M.; Witt, C. E.; Honan, L. E.; Robins, N.; Hashemi, P., Novel, user-friendly experimental and analysis strategies for fast voltammetry: Next generation FSCAV with artificial neural networks. *ACS Meas. Sci. Au* **2022,** *2* (3), 241-250. https://doi.org/10.1021/acsmeasuresciau.1c00060

125. Buchanan, A. M.; Mena, S.; Choukari, I.; Vasa, A.; Crawford, J. N.; Fadel, J.; Maxwell, N.; Reagan, L.; Cruikshank, A.; Best, J.; Nijhout, H. F.; Reed, M.; Hashemi, P., Serotonin as a biomarker of toxin-induced Parkinsonism. *Molecular Medicine* **2024,** *30* (1), 33. https://doi.org/10.1186/s10020-023-00773-9

126. Kang, S.; Jeong, Y.; Choi, J. W. In *Simultaneous estimation of tonic dopamine and serotonin with high temporal resolution in vitro using deep learning*, 2023 45th Annual International Conference of the IEEE Engineering in Medicine & Biology Society (EMBC), 24-27 July 2023; 2023; pp 1-4.

127. Li, K.; Persaud, D.; Choudhary, K.; DeCost, B.; Greenwood, M.; Hattrick-Simpers, J., Exploiting redundancy in large materials datasets for efficient machine learning with less data. *Nat. Commun.* **2023,** *14* (1), 7283. https://doi.org/10.1038/s41467-023-42992-y

128. Ciosek, P.; Wróblewski, W., Sensor arrays for liquid sensing–electronic tongue systems. *Analyst* **2007,** *132* (10), 963-978. https://doi.org/10.1039/B705107G

129. Cho, W.; Rafi, H.; Cho, S.; Balijepalli, A.; Zestos, A. G., High resolution voltammetric and field-effect transistor readout of carbon fiber microelectrode biosensors. *Sensors & Diagnostics* **2022,** *1* (3), 460-464.

130. Park, C.; Hwang, S.; Kang, Y.; Sim, J.; Cho, H. U.; Oh, Y.; Shin, H.; Kim, D. H.; Blaha, C. D.; Bennet, K. E., Feasibility of applying Fourier transform electrochemical impedance spectroscopy in fast cyclic square wave voltammetry for the in vivo measurement of neurotransmitters. *Anal. Chem.* **2021,** *93* (48), 15861-15869. https://doi.org/10.1021/acs.analchem.1c02308

131. Kirkpatrick, D. C.; McKinney, C. J.; Manis, P. B.; Wightman, R. M., Expanding neurochemical investigations with multi-modal recording: Simultaneous fast-scan cyclic voltammetry, iontophoresis, and patch clamp measurements. *Analyst* **2016,** *141* (16), 4902-4911. https://doi.org/10.1039/C6AN00933F

132. Takmakov, P.; McKinney, C. J.; Carelli, R. M.; Wightman, R. M., Instrumentation for fast-scan cyclic voltammetry combined with electrophysiology for behavioral experiments in freely moving animals. *Rev. Sci. Instrum.* **2011,** *82* (7), 074302. https://doi.org/10.1063/1.3610651

133. Walton, L. R.; Verber, M.; Lee, S.-H.; Chao, T.-H. H.; Wightman, R. M.; Shih, Y.-Y. I., Simultaneous fMRI and fast-scan cyclic voltammetry bridges evoked oxygen and neurotransmitter dynamics across spatiotemporal scales. *NeuroImage* **2021,** *244*, 118634. https://doi.org/10.1016/j.neuroimage.2021.118634

134. Kim, Y.; Lee, Y.; Yoo, J.; Nam, K. S.; Jeon, W.; Lee, S.; Park, S., Multifunctional and flexible neural probe with thermally drawn fibers for bidirectional synaptic probing in the brain. *ACS Nano* **2024,** *18* (20), 13277-13285. https://doi.org/10.1021/acsnano.4c02578

135. Corva, D. M.; Doeven, E. H.; Parke, B.; Adams, S. D.; Tye, S. J.; Hashemi, P.; Berk, M.; Kouzani, A. Z., SmartFSCV: An artificial intelligence enabled miniaturised FSCV device targeting serotonin. *IEEE Open J. Eng. Med. Biol.* **2024,** *5*, 75-85. https://doi.org/10.1109/OJEMB.2024.3356177

136. Corva, D. M.; Adams, S. D.; Bennet, K. E.; Berk, M.; Kouzani, A. Z., Miniature FSCV devices: A review. *IEEE Sens. J.* **2021,** *21* (12), 13006-13018. 10.1109/JSEN.2021.3069950

137. de Oliveira Filho, J. I.; Faleiros, M. C.; Ferreira, D. C.; Mani, V.; Salama, K. N., Empowering electrochemical biosensors with ai: Overcoming interference for precise dopamine detection in complex samples. *Adv. Intell. Syst.* **2023,** *5* (10), 2300227.

138. Rojas Cabrera, J. M.; Oesterle, T. S.; Rusheen, A. E.; Goyal, A.; Scheitler, K. M.; Mandybur, I.; Blaha, C. D.; Bennet, K. E.; Heien, M. L.; Jang, D. P.; Lee, K. H.; Oh, Y.; Shin, H., Techniques for measurement of serotonin: Implications in neuropsychiatric disorders and advances in absolute value recording methods. *ACS Chem. Neurosci.* **2023**. https://doi.org/10.1021/acschemneuro.3c00618

139. Bozorgzadeh, B.; Schuweiler, D. R.; Bobak, M. J.; Garris, P. A.; Mohseni, P., Neurochemostat: A neural interface SoC with integrated chemometrics for closed-loop regulation of brain dopamine. *IEEE Trans. Biomed. Circuits* **2016,** *10* (3), 654-667. https://doi.org/10.1109/TBCAS.2015.2453791

140. Corva, D. M.; Parke, B.; West, A.; Doeven, E. H.; Adams, S. D.; Tye, S. J.; Hashemi, P.; Berk, M.; Kouzani, A. Z., SmartStim: An artificial intelligence enabled deep brain stimulation device. *IEEE Trans. Med. Robot. Bionics* **2024**, 1-1. https://doi.org/10.1109/TMRB.2024.3381341

141. Lee, K. H.; Lujan, J. L.; Trevathan, J. K.; Ross, E. K.; Bartoletta, J. J.; Park, H. O.; Paek, S. B.; Nicolai, E. N.; Lee, J. H.; Min, H.-K.; Kimble, C. J.; Blaha, C. D.; Bennet, K. E., WINCS harmoni: Closed-loop dynamic neurochemical control of therapeutic interventions. *Sci. Rep.* **2017,** *7* (1), 46675. https://doi.org/10.1038/srep46675

142. Trevathan, J. K.; Yousefi, A.; Park, H. O.; Bartoletta, J. J.; Ludwig, K. A.; Lee, K. H.; Lujan, J. L., Computational modeling of neurotransmitter release evoked by electrical stimulation: Nonlinear approaches to predicting stimulation-evoked dopamine release. *ACS Chem. Neurosci.* **2017,** *8* (2), 394-410. https://doi.org/10.1021/acschemneuro.6b00319

143. Unger, E. K.; Keller, J. P.; Altermatt, M.; Liang, R.; Matsui, A.; Dong, C.; Hon, O. J.; Yao, Z.; Sun, J.; Banala, S.; Flanigan, M. E.; Jaffe, D. A.; Hartanto, S.; Carlen, J.; Mizuno, G. O.; Borden, P. M.; Shivange, A. V.; Cameron, L. P.; Sinning, S.; Underhill, S. M.; Olson, D. E.; Amara, S. G.; Temple Lang, D.; Rudnick, G.; Marvin, J. S.; Lavis, L. D.; Lester, H. A.; Alvarez, V. A.; Fisher, A. J.; Prescher, J. A.; Kash, T. L.; Yarov-Yarovoy, V.; Gradinaru, V.; Looger, L. L.; Tian, L., Directed evolution of a selective and sensitive serotonin sensor via machine learning. *Cell* **2020,** *183* (7), 1986-2002.e26. https://doi.org/10.1016/j.cell.2020.11.040

144. Butler, K. T.; Davies, D. W.; Cartwright, H.; Isayev, O.; Walsh, A., Machine learning for molecular and materials science. *Nature* **2018,** *559* (7715), 547-555. https://doi.org/10.1038/s41586-018-0337-2

145. Kang, Y.; Goyal, A.; Hwang, S.; Park, C.; Cho, H. U.; Shin, H.; Park, J.; Bennet, K. E.; Lee, K. H.; Oh, Y.; Jang, D. P., Enhanced dopamine sensitivity using steered fast-

scan cyclic voltammetry. *ACS Omega* **2021,** *6* (49), 33599-33606. https://doi.org/10.1021/acsomega.1c04475

146. Kelich, P.; Jeong, S.; Navarro, N.; Adams, J.; Sun, X.; Zhao, H.; Landry, M. P.; Vuković, L., Discovery of DNA–carbon nanotube sensors for serotonin with machine learning and near-infrared fluorescence spectroscopy. *ACS Nano* **2022,** *16* (1), 736-745. https://doi.org/10.1021/acsnano.1c08271

147. Dolensek, N.; Gehrlach, D. A.; Klein, A. S.; Gogolla, N., Facial expressions of emotion states and their neuronal correlates in mice. *Science* **2020,** *368* (6486), 89-94. https://doi.org/10.1126/science.aaz9468

148. Liebenow, B.; Jones, R.; DiMarco, E.; Trattner, J. D.; Humphries, J.; Sands, L. P.; Spry, K. P.; Johnson, C. K.; Farkas, E. B.; Jiang, A.; Kishida, K. T., Computational reinforcement learning, reward (and punishment), and dopamine in psychiatric disorders. *Front. Psychiatry* **2022,** *13*. https://doi.org/10.3389/fpsyt.2022.886297

149. Vreeland, R. F.; Atcherley, C. W.; Russell, W. S.; Xie, J. Y.; Lu, D.; Laude, N. D.; Porreca, F.; Heien, M. L., Biocompatible PEDOT:Nafion composite electrode coatings for selective detection of neurotransmitters in vivo. *Anal. Chem.* **2015,** *87* (5), 2600-2607. https://doi.org/10.1021/ac502165f

150. Seaton, B. T.; Hill, D. F.; Cowen, S. L.; Heien, M. L., Mitigating the effects of electrode biofouling-induced impedance for improved long-term electrochemical measurements in vivo. *Anal. Chem.* **2020,** *92* (9), 6334-6340. https://doi.org/10.1021/acs.analchem.9b05194

151. Feudale, R. N.; Woody, N. A.; Tan, H.; Myles, A. J.; Brown, S. D.; Ferré, J., Transfer of multivariate calibration models: A review. *Chemom. Intell. Lab. Syst* **2002,** *64* (2), 181-192.

152. Nikzad-Langerodi, R.; Andries, E., A chemometrician's guide to transfer learning. *J. Chemom.* **2021,** *35* (11), e3373. https://doi.org/10.1002/cem.3373

153. Johnson, J. A.; Rodeberg, N. T.; Wightman, R. M., Failure of standard training sets in the analysis of fast-scan cyclic voltammetry data. *ACS Chem. Neurosci.* **2016,** *7* (3), 349-359. https://doi.org/10.1021/acschemneuro.5b00302

154. Meunier, C. J.; Roberts, J. G.; McCarty, G. S.; Sombers, L. A., Background signal as an in situ predictor of dopamine oxidation potential: Improving interpretation of fast-scan cyclic voltammetry data. *ACS Chem. Neurosci.* **2017,** *8* (2), 411-419. https://doi.org/10.1021/acschemneuro.6b00325

155. Jang, J.; Cho, H.-U.; Hwang, S.; Kwak, Y.; Kwon, H.; Heien, M. L.; Bennet, K. E.; Oh, Y.; Shin, H.; Lee, K. H.; Jang, D. P., Understanding the different effects of fouling mechanisms on working and reference electrodes in fast-scan cyclic voltammetry for neurotransmitter detection. *Analyst* **2024**. https://doi.org/10.1039/D3AN02205F

156. Jamalzadeh, M.; Cuniberto, E.; Shahrjerdi, D., A framework for benchmarking emerging FSCV neurochemical sensors. *Advanced Physics Research* **2023**, 2300079.

157. Loewinger, G.; Behdin, K.; Kishida, K. T.; Parmigiani, G.; Mazumder, R., Multi-task learning for sparsity pattern heterogeneity: A discrete optimization approach. *arXiv* **2022**.

158. Prakash, M.; Narasimha Murty, M., A genetic approach for selection of (near-) optimal subsets of principal components for discrimination. *Pattern Recognit. Lett.* **1995,** *16* (8), 781-787. https://doi.org/10.1016/0167-8655(95)00041-E

159. Clark, J. J.; Collins, A. L.; Sanford, C. A.; Phillips, P. E. M., Dopamine encoding of Pavlovian incentive stimuli diminishes with extended training. *J. Neurosci.* **2013,** *33* (8), 3526-3532. https://doi.org/10.1523/jneurosci.5119-12.2013

160. Phillips, P. E. M.; Wightman, R. M., Critical guidelines for validation of the selectivity of in-vivo chemical microsensors. *TrAC, Trends Anal. Chem.* **2003,** *22* (8), 509-514. https://doi.org/10.1016/S0165-9936(03)00907-5

161. Roberts, J. G.; Toups, J. V.; Eyualem, E.; McCarty, G. S.; Sombers, L. A., In situ electrode calibration strategy for voltammetric measurements in vivo. *Anal. Chem.* **2013,** *85* (23), 11568-11575. https://doi.org/10.1021/ac402884n

162. Meunier, C. J.; Denison, J. D.; McCarty, G. S.; Sombers, L. A., Interpreting dynamic interfacial changes at carbon fiber microelectrodes using electrochemical impedance spectroscopy. *Langmuir* **2020,** *36* (15), 4214-4223. https://doi.org/10.1021/acs.langmuir.9b03941

163. Clark, J. J.; Sandberg, S. G.; Wanat, M. J.; Gan, J. O.; Horne, E. A.; Hart, A. S.; Akers, C. A.; Parker, J. G.; Willuhn, I.; Martinez, V.; Evans, S. B.; Stella, N.; Phillips, P. E. M., Chronic microsensors for longitudinal, subsecond dopamine detection in behaving animals. *Nat. Methods* **2010,** *7* (2), 126-129. https://doi.org/10.1038/nmeth.1412

164. Flagel, S. B.; Clark, J. J.; Robinson, T. E.; Mayo, L.; Czuj, A.; Willuhn, I.; Akers, C. A.; Clinton, S. M.; Phillips, P. E. M.; Akil, H., A selective role for dopamine in stimulus–reward learning. *Nature* **2011,** *469* (7328), 53-57. https://doi.org/10.1038/nature09588

165. Willuhn, I.; Burgeno, L. M.; Everitt, B. J.; Phillips, P. E. M., Hierarchical recruitment of phasic dopamine signaling in the striatum during the progression of cocaine use. *Proc. Natl. Acad. Sci. U.S.A.* **2012,** *109* (50), 20703-20708. https://doi.org/10.1073/pnas.1213460109

166. Gorder, P. F., Neural networks show new promise for machine vision. *Comput. Sci. Eng.* **2006,** *8* (6), 4-8.

167. Dybowski, R., Interpretable machine learning as a tool for scientific discovery in chemistry. *New Journal of Chemistry* **2020,** *44* (48), 20914-20920. https://doi.org/10.1039/D0NJ02592E

168. Oviedo, F.; Ferres, J. L.; Buonassisi, T.; Butler, K. T., Interpretable and explainable machine learning for materials science and chemistry. *Acc. Mater. Res.* **2022,** *3* (6), 597-607. https://doi.org/10.1021/accountsmr.1c00244

169. Hoar, B. B.; Zhang, W.; Xu, S.; Deeba, R.; Costentin, C.; Gu, Q.; Liu, C., Electrochemical mechanistic analysis from cyclic voltammograms based on deep learning. *ACS Meas. Sci. Au* **2022,** *2* (6), 595-604. https://doi.org/10.1021/acsmeasuresciau.2c00045

170. Wolpert, D. H., The lack of a priori distinctions between learning algorithms. *Neural Comput.* **1996,** *8* (7), 1341-1390.

171. Thiyagalingam, J.; Shankar, M.; Fox, G.; Hey, T., Scientific machine learning benchmarks. *Nat. Rev. Phys.* **2022,** *4* (6), 413-420. https://doi.org/10.1038/s42254-022-00441-7

Chapter 2

Call me serotonin

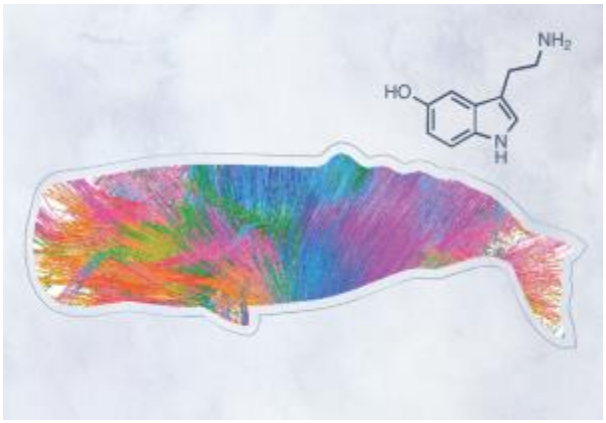

The information in this chapter is adapted with permission from

Movassaghi, C.S.; Andrews, A.M. Call me serotonin. *Nature Chemistry.* **16**, 670 (2024).

Serotonin is known by many names—In science as 5-hydroxytryptamine (5-HT) or enteramine, and in popular culture as the "feel good" chemical or the "happy hormone". Cameron Movassaghi and Anne Andrews discuss the knowns and unknowns of this well-studied yet elusive neurotransmitter.

If necessity is the mother of invention, then serendipity is the mother of serotonin. In 1937, Vittorio Erspamer isolated a mysterious monoamine from the gastric mucosa of rabbits while studying smooth muscle contraction. He coined the initial namesake a portmanteau of *entero*chromaffin cells and unknown *amine* (enteramine).[1] In 1948, Cleveland Clinic researchers investigating hypertension-producing factors isolated a pesky interferent from bovine serum. Due to its presence in blood *serum* as the chemical affecting vascular *tone*, enteramine unknowingly earned a second portmanteau of serotonin.[2] Less common synonyms with etymology rooted in blood clotting research (thrombocytin and thrombotonin) were also reported. Isolated as red crystals, the original vial of serotonin has been preserved to this day. Within five years, a single structure was elucidated and all of the aforementioned names were shown to be the same compound.[3] Soon after, Upjohn Pharmaceutical began synthesizing and selling the research compound under the name serotonin, and the name stuck.

Initial enthusiasm for serotonin dampened as evidence emerged that it was not essential in hypertension (nor for survival as was later learned).[4] Serotonin research thus began in earnest in 1953, when Betty Twarog first identified serotonin in the mammalian brain. Even so, neuroscience was in its infancy and scientists were doubtful of neurotransmitter theory. When biochemist D. W. Woolley found that lysergic acid diethylamide (LSD; a serendipitous synthesis from the prior decade) could block contractions caused by serotonin in the rat uterus, the role of serotonin in psychosis was soon theorized–if LSD could act on serotonin receptors to produce

profound changes in perception, then consciousness might be pharmaceutically accessible. In 1963, Woolley published his seminal work, *The Biochemical Bases of Psychoses or the Serotonin Hypothesis about Mental Illness*,[5] cementing the roles of serotonin and LSD in birthing the field of neurochemistry. The two compounds remain linked to this day and there is renewed interest in the neuroplasticity effects of psychedelics to treat a wide range of mental disorders in which the serotonin system is implicated.[6]

In 1954, iproniazid was developed as a tuberculosis treatment when clinicians noted it produced a euphoric side effect. Iproniazid would become the first antidepressant and the first of an entire class called monoamine oxidase inhibitors. A second class, tricyclic antidepressants, followed shortly thereafter with the report of imipramine in 1958. Research at Eli Lilly yielded fluoxetine (Prozac), the first selective serotonin reuptake inhibitor (SSRI), developed by Fuller, Perry, and Malloy and FDA-approved in 1974.[7] Though this continuing boon of drug development would bring serotonin to the forefront of modern pharmaceutical discourse, serotonin was discovered to be an ancient molecule in evolutionary terms. Various structural and functional specializations of the serotonin system have been preserved in organisms ranging from plants to sea slugs, nematodes, and even bacteria.[8,9] Its role in evolution can be further appreciated by the fact that serotonin acts first not as a neurotransmitter, but as a signaling molecule for neuron growth prior to synapse formation in human development.

It was not until the 1980s that molecular biology research began to uncover the complexity of the serotonin system. One of more than one hundred chemical messengers (neurotransmitters) found in the brain, serotonin is biosynthesized from the essential amino acid tryptophan. Because serotonin cannot cross the blood-brain barrier, tryptophan and 5-hydroxytryptophan act as permeable intermediaries. Serotonin is broken down into 5-

hydroxyindoleacetic acid and excreted in urine or used as the precursor to melatonin. Only ~300,000 of the 85 billion neurons in the human brain use serotonin with ~5% of serotonin found in the brain (>90% is in the gut). Serotonin neurons project from the brain stem to nearly all areas of the central nervous system, including the cortex and spinal cord. The serotonin system has the most known receptor subtypes (at least 14) of any neurotransmitter system. Taken together, serotonin employs an extensive neurochemical wiring system making it an alluring pharmacologic target.

Serotonin has become nearly synonymous with mood and emotion in public discourse. Fluoxetine and other SSRIs remain the most commonly prescribed antidepressants. Their widespread use is in part responsible for the pervasive belief (>80% of the general population) in the serotonin hypothesis of depression (a causal link between serotonin and depression), or the more simplified view that depression is simply a deficiency in serotonin (hit songs and lyrics have been titled as such!). At best, the serotonin hypothesis is an oversimplification. Scientists do not yet know what causes depression or how antidepressants produce their effects when given over weeks to months to years. Moreover, we do not fully understand how serotonin encodes behavioral information.

As such, research on serotonin remains ongoing. For the most complex organ known, delegating a single brain chemical as responsible for something as complex as mood is implausible. In fact, nature has evolved a complex analog system of neurotransmitters that greatly diversifies and empowers brain information encoding–a chemical connectome.[10] The most recent thrusts in systems neuroscience have been towards uncovering emergent brain phenomena through the development of new tools and theories.[11] History repeats itself as studies refuting[12] or confirming[13] empirical evidence for the roles of serotonin in depression continue to

emerge. These debates will assuredly continue until we can truly measure neurochemical dynamics[14] particularly in human brains, which remains a recent, rare, and exceptionally difficult area of research.

The ubiquity of the serotonin system undoubtedly underlies its roles in many behavioral processes, which does not mean that serotonin is solely responsible for these processes (implication is far from causation). Throughout history, humankind has philosophized on the meaning of happiness. It is only fitting that the debate around the proverbial 'happiness' molecule is just as hotly contested. The story of serotonin will be written and re-written, just as its pioneers renamed it many times over. Surrounded by white matter and housed in a whale-shaped brain stem, serotonin is part of the hunt for understanding ourselves – humankind's white whale.[15]

"It is not down on any map; true places never are."

- **Herman Melville, *Moby Dick***

Acknowledgements and Author Contributions: CSM and AMA conceptualized and wrote the manuscript. CSM was supported by the National Science Foundation Graduate Research Fellowship Program (DGE-1650604 and DGE- 2034835). Any opinions, findings, and conclusions or recommendations expressed in this material are those of the authors and do not necessarily reflect the views of the National Science Foundation.

2.1 REFERENCES

1. Whitaker-Azmitia, P. M., The discovery of serotonin and its role in neuroscience. *Neuropsychopharmacology* **1999,** *21* (1), 2-8.
2. Rapport, M. M.; Green, A. A.; Page, I. H., Crystalline serotonin. *Science* **1948,** *108* (2804), 329-330.
3. Tricklebank, M.; Daly, E., *The serotonin system: History, neuropharmacology, and pathology*. Academic Press: 2019.
4. Hendricks, T. J.; Fyodorov, D. V.; Wegman, L. J.; Lelutiu, N. B.; Pehek, E. A.; Yamamoto, B.; Silver, J.; Weeber, E. J.; Sweatt, J. D.; Deneris, E. S., Pet-1 ETS gene plays a critical role in 5-HT neuron development and is required for normal anxiety-like and aggressive behavior. *Neuron* **2003,** *37* (2), 233-247.
5. Woolley, D. W., *The biochemical bases of psychoses or the serotonin hypothesis about mental diseases*. John Wiley and Sons, Inc: 1962.
6. Vargas, M. V.; Dunlap, L. E.; Dong, C.; Carter, S. J.; Tombari, R. J.; Jami, S. A.; Cameron, L. P.; Patel, S. D.; Hennessey, J. J.; Saeger, H. N.; McCorvy, J. D.; Gray, J. A.; Tian, L.; Olson, D. E., Psychedelics promote neuroplasticity through the activation of intracellular 5-HT2A receptors. *Science* **2023,** *379* (6633), 700-706.
7. Fuller, R. W.; Perry, K. W.; Molloy, B. B., Effect of 3-(p-trifluoromethylphenoxy)-N-methyl-3-phenylpropylamine on the depletion of brain serotonin by 4-chloroamphetamine. *J Pharmacol Exp Ther* **1975,** *193* (3), 796-803.
8. Barandouzi, Z. A.; Lee, J.; del Carmen Rosas, M.; Chen, J.; Henderson, W. A.; Starkweather, A. R.; Cong, X. S., Associations of neurotransmitters and the gut

microbiome with emotional distress in mixed type of irritable bowel syndrome. *Sci Rep* **2022,** *12* (1), 1648.

9. Erland, L. A. E.; Murch, S. J.; Reiter, R. J.; Saxena, P. K., A new balancing act: The many roles of melatonin and serotonin in plant growth and development. *Plant Signal Behav* **2015,** *10* (11), e1096469.

10. Andrews, A. M., The BRAIN Initiative: Toward a chemical connectome. *ACS Chem Neurosci* **2013,** *4* (5), 645.

11. Alivisatos, A. P.; Andrews, A. M.; Boyden, E. S.; Chun, M.; Church, G. M.; Deisseroth, K.; Donoghue, J. P.; Fraser, S. E.; Lippincott-Schwartz, J.; Looger, L. L.; Masmanidis, S.; McEuen, P. L.; Nurmikko, A. V.; Park, H.; Peterka, D. S.; Reid, C.; Roukes, M. L.; Scherer, A.; Schnitzer, M.; Sejnowski, T. J.; Shepard, K. L.; Tsao, D.; Turrigiano, G.; Weiss, P. S.; Xu, C.; Yuste, R.; Zhuang, X., Nanotools for neuroscience and brain activity mapping. *ACS Nano* **2013,** *7* (3), 1850-66.

12. Moncrieff, J.; Cooper, R. E.; Stockmann, T.; Amendola, S.; Hengartner, M. P.; Horowitz, M. A., The serotonin theory of depression: A systematic umbrella review of the evidence. *Mol Psychiatry* **2022**, 1-14.

13. Jauhar, S.; Arnone, D.; Baldwin, D. S.; Bloomfield, M.; Browning, M.; Cleare, A. J.; Corlett, P.; Deakin, J. W.; Erritzoe, D.; Fu, C., A leaky umbrella has little value: Evidence clearly indicates the serotonin system is implicated in depression. *Mol Psychiatry* **2023**, 1-4.

14. Nakatsuka, N.; Yang, K.-A.; Abendroth, J. M.; Cheung, K. M.; Xu, X.; Yang, H.; Zhao, C.; Zhu, B.; Rim, Y. S.; Yang, Y.; Weiss, P. S.; Stojanović, M. N.; Andrews, A.

M., Aptamer–field-effect transistors overcome Debye length limitations for small-molecule sensing. *Science* **2018,** *362* (6412), 319.

15. Herman, M., *Moby Dick*. Strelbytskyy Multimedia Publishing: 2020.

Chapter 3

Simultaneous serotonin and dopamine monitoring across timescales by rapid pulse voltammetry with partial least squares regression

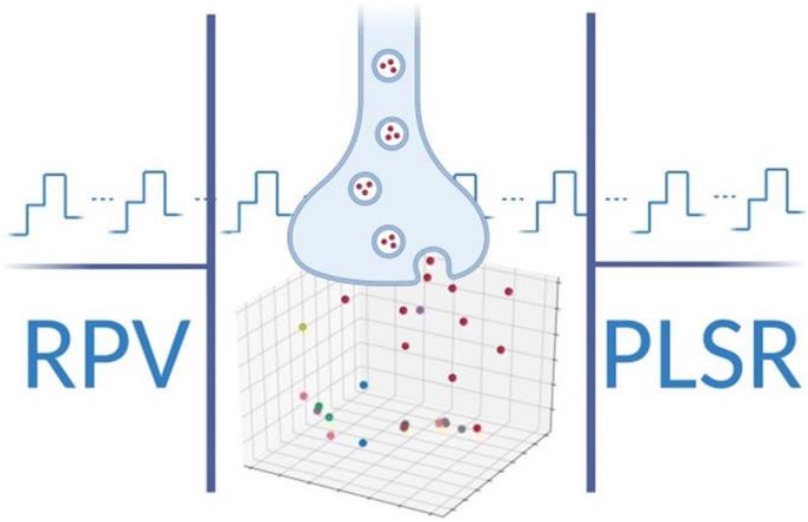

The information in this chapter is adapted with permission from

Movassaghi, C.S.; Perrotta, K.A.; Yang, H.; Iyer, R.; Cheng, X.; Dagher, M.; Alcañiz, M; Andrews, A.M. Simultaneous serotonin and dopamine monitoring across timescales by rapid pulse voltammetry with partial least squares regression. *Analytical and Bioanalytical Chemistry*. **413**, 6747-6767 (2021).

3.1 ABSTRACT

Many voltammetry methods have been developed to monitor brain extracellular dopamine levels. Fewer approaches have been successful in detecting serotonin *in vivo*. No voltammetric techniques are currently available to monitor both neurotransmitters simultaneously across timescales, even though they play integrated roles in modulating behavior. We provide proof-of-concept for rapid pulse voltammetry coupled with partial least squares regression (RPV-PLSR), an approach adapted from multi-electrode systems (*i.e.*, electronic tongues) used to identify multiple components in complex environments. We exploited small differences in analyte redox profiles to select pulse steps for RPV waveforms. Using an intentionally designed pulse strategy combined with custom instrumentation and analysis software, we monitored basal and stimulated levels of dopamine and serotonin. In addition to faradaic currents, capacitive currents were important factors in analyte identification arguing against background subtraction. Compared to fast-scan cyclic voltammetry-principal components regression (FSCV-PCR), RPV-PLSR better differentiated and quantified basal and stimulated dopamine and serotonin associated with striatal recording-electrode position, optical stimulation frequency, and serotonin reuptake inhibition. The RPV-PLSR approach can be generalized to other electrochemically active neurotransmitters and provides a feedback pipeline for future optimization of multi-analyte, fit-for-purpose waveforms and machine learning approaches to data analysis.

3.2. INTRODUCTION

The idea that neurotransmitters function *via* coordinated activities to shape behavior is becoming increasingly supported by *in vivo* studies [1-9]. We recently found that optogenetic stimulation of midbrain dopamine neurons, which drives reward-related behavior [10], produces serotonin release in striatum [11]. Dopamine and serotonin neurons directly and indirectly form circuits with one another [12-14]. Both systems exhibit developmental, functional, and clinical interplay [15,16]. The dopamine and serotonin systems are implicated in diverse behaviors of relevance to neuropsychiatric and neurological disorders, including major depressive and anxiety disorders [17,18], schizophrenia [19,20], substance use disorder [21,22], and Parkinson's disease [23,24]. These and other findings support the overarching hypothesis that multiple neurochemical systems, and particularly, the dopamine and serotonin systems, function (or dysfunction) concertedly [25-27].

Neurochemical signaling encodes biologically relevant information across multiple timescales [28]. Tonic (basal) neurotransmitter levels arise from clocklike neural firing over minutes to hours to days. Phasic (transient) changes in neurotransmitter levels are rapid (tens of milliseconds to seconds) and are hypothesized to result from synchronized bursts of neural firing in response to evoked or naturally occurring stimuli [29-33]. The ability to monitor transitory neurochemical events, in conjunction with changes in tonic signaling, will enable a more comprehensive understanding of how chemical neurotransmission encodes behaviorally relevant information [34,35].

A variety of techniques are available for *in vivo* neurochemical monitoring with various advantages and disadvantages [36-39]. Here, we focus on voltammetry methods, including fast-scan cyclic voltammetry (FSCV), to detect electroactive neurotransmitters. The use of small carbon-

fiber microelectrodes (5-30 μm diameter) [40,41] and high sampling rates (10-100 Hz) [42,43] in FSCV can be used to differentiate release *vs*. reuptake processes [44]. While widely employed, FSCV suffers from poor analyte specificity. Overlapping oxidation (and reduction) profiles of structurally similar neurochemicals, many of which occur at low concentrations, make *in vivo* measurements of transmitters other than dopamine difficult with FSCV [45]. Moreover, FSCV is limited by the need for background subtraction of large capacitive currents generated during voltage sweeps at fast scan rates. Background subtraction precludes tonic (basal) neurotransmitter determinations and measurements over longer time frames, (*e.g.*, minutes-hours), due to current drift [46,47].

Several novel waveforms have been developed that improve and expand various aspects of sweep-wave voltammetry [42,48]. Fast-scan controlled absorption voltammetry (FSCAV) enables determination of basal dopamine or serotonin levels [34,49,50]. Other adsorption waveforms and accumulation electrodes have been reported [51,52]. Sombers and coworkers devised a waveform that allowed prediction and subtraction of electrochemical drift for measurements of dopamine, adenosine, and H_2O_2 [53], as well as sweep waveforms to detect the opioid peptide met-enkephalin, H_2O_2, and pH [54,55].

Complex waveforms that combine sweeps or staircases with square-wave pulses have been reported. Multiple cyclic square-wave voltammetry was used to quantify tonic dopamine *in vivo* with 10-s resolution [56]. Improvements in selectivity and sensitivity were made using fast-cyclic square-wave voltammetry (FCSWV) [57] and N-FCSWV [58] for monitoring dopamine and serotonin *in vivo*, respectively. Multiplexing has not yet been achieved with square-wave voltammetry—two different waveforms were needed to measure dopamine [57] *vs.* serotonin [58]. Additionally, capacitive current simulation, which relies on assumptions about exponential current decay, was needed for background subtraction. Venton and coworkers used single-walled carbon nanotube electrodes

with FSCV to measure simultaneous changes in dopamine and serotonin *in vivo* [59]. The carbon nanotube coating reduced the formation of oxidative byproducts of serotonin and increased the cathodic currents of dopamine and serotonin, improving analyte discrimination *via* more distinct reduction profiles [60].

Principal components analysis (PCA) [61] and principal components regression (PCR) [62,63] have been used for multiplexing *via* dimensionality reduction in FSCV, with PCR capable of quantitative predictions. Another dimensionality reduction method widely used in chemometrics is partial least squares regression (PLSR) [64]. The PLSR approach is a supervised machine learning technique (*i.e.*, it models input and output); PCA and PCR are considered unsupervised (*i.e.*, only input data is modeled). The use of PLSR was shown to improve predictive accuracy over PCR when analyzing FSCV data for mixtures of neurochemicals [65]. Other uses included prediction and correction of FSCV background drift and pH changes [53,55]. Kishida and colleagues pioneered combining FSCV with regularized linear regression (*i.e.,* elastic net electrochemistry) for sub-second monitoring of evoked dopamine [66,67] and serotonin [68,69] in human striatum during decision making tasks.

While newer waveforms and data processing methods have advanced neurochemical measurements, no single voltammetry technique yet enables tonic and phasic levels of multiple neurotransmitters to be determined simultaneously. To address this, we demonstrate a two-pronged approach to improve waveform design and data analysis. We gained inspiration from the voltammetric electronic tongue (VET) [70], used to measure analytes in food [71,72], beverages [73,74], and wastewater [75]. Rather than using conventional pulse waveforms, 'smart' pulse waveforms are designed for VET sensing. These pulse trains are initially constructed based on the electrochemical characteristics of the analytes of interest [76]. Pulse widths and amplitudes, as well as pulse train

frequencies, among other factors, are optimized to extract distinguishing electrochemical characteristics for data processing [77,78]. Smart pulse design has been shown to outperform conventional [76] and random [71] pulse waveforms using the VET method.

Data generated by the VET method have been analyzed using a multivariate technique, commonly PLSR [72,74]. As PLSR models covariance, the model prioritizes variations in input (current response) that correspond to qualitative and quantitative changes in output (analyte classification and concentration) [64]. As such, differences in the Helmholtz double layer, mass transport, analyte concentrations and adsorption, and other dynamic electrode surface properties occurring during an applied pulse are considered as potential sources of analyte specific information. This information is encoded in the transient responses of faradaic and non-faradaic currents. By including faradaic and non-faradaic current responses as input to the model (*i.e.,* not background subtracting), the PLSR model selects aspects of the current response that covary with analyte identity and concentration. This is opposed to background subtracted methods, where some information is discarded prior to model input to increase signal-to-noise. Potentially relevant information in the background is then lost.

An appropriately trained model can handle voltammetry data without the need for background subtraction, noise filtering/removal, or drift subtraction. In addition to VET studies, regularized regression applied to FSCV has been used to demonstrate that appropriately trained models benefit from information beyond analyte redox potentials when background subtraction is avoided [67,69]. The use of regularized regression accounted for drift and noise, similar to PLSR.

Here, we report on the initial development of rapid pulse voltammetry coupled with PLSR (RPV-PLSR) using a smart pulse approach. By avoiding background subtraction, RPV-PLSR

utilizes faradaic and nonfaradaic current to improve analyte identification and quantification power. Inclusion of the background current also enables tonic and phasic concentration predictions in a single experiment at fast timescales (*i.e.*, limited only by waveform frequency).

3.3. MATERIALS & METHODS

3.3.1. Chemicals

Dopamine hydrochloride (#H8502) and serotonin hydrochloride (#H9523) were purchased from Sigma Aldrich (St. Louis, MO). Artificial cerebrospinal fluid (aCSF) for *in vitro* experiments consisted of 147 mM NaCl (#73575), 3.5 mM KCl (#05257), 1.0 mM NaH_2PO_4 (#17844), 2.5 mM $NaHCO_3$ (#88208) purchased from Honeywell Fluka (Charlotte, NC), and 1.0 mM $CaCl_2$ (#499609) and 1.2 mM $MgCl_2$ (#449172) purchased from Sigma Aldrich. The aCSF solution was adjusted to pH 7.3 ± 0.03 using HCl (Fluka, #84415). The phosphate-buffered mobile phase for high performance liquid chromatography (HPLC) consisted of 96 mM NaH_2PO_4, 3.8 mM Na_2HPO_4 (Fluka #71633), pH 5.4, 2-2.8% MeOH (EMD #MX0475), 50 mg/L EDTA·Na_2 (Sigma #03682), and 500 mg/L sodium decanesulfonate (TCI #I0348) in water. All aqueous solutions were made using ultrapure water (Milli-Q, Millipore, Billerica, MA).

3.3.2. *In vitro* experiments

For *in vitro* training data used for preliminary method validation, carbon fiber microelectrodes were fabricated as described previously [41] with minor modifications. Single 7-µm-diameter carbon fibers (Specialty Materials, Lowell, MA) were vacuum-aspirated into borosilicate glass capillaries (Sutter Instrument Company, Novato, CA). Each capillary was pulled to produce two electrodes by tapering and sealing using a micropipette puller (P-1000, Sutter Instrument Company, Novato, CA). Electrode tips were cleaned with 100% isopropanol (Fisher A416P, for electronic use) for 10 min and dried at 90-100 ℃ for 10-20 min. Electrode tips were then sealed by dipping in non-conductive epoxy (Epoxy Technology Inc., Billerica, MA) for 7-10 min twice at a 1 h interval at

room temperature. Epoxied electrodes were dried at 90-100 ℃ overnight. Prior to testing, electrode tips were blunt-cut using a surgical scalpel under a microscope to create 7-μm-diameter disk shaped conducting surfaces. Bare silver wire (0.010-inch diameter, A-M Systems, Sequim, WA) was cleaned using a polishing cloth and inserted into working electrode capillaries to serve as the electrical connection (**Fig. S3.1**). The electrodes were backfilled with 2 M aqueous NaCl for electrical connection. Reference electrodes (RE-5B Ag/AgCl, BASi, West Lafayette, IN) used for all *in vitro* experiments were maintained in oversaturated aqueous KCl. Fresh aCSF was delivered to a flow cell at a constant flow rate of 2.5-2.7 mL/min by a peristaltic pump. (**Fig. S3.1**). Standards (180 μL) of dopamine, serotonin, and their mixtures were injected *via* an autoinjector (VICI E60 Actuator, Valco Instruments Co. Inc., Houston, TX) in pseudo-random order at >5 min intervals.

3.3.3. *In vivo* experiments

3.3.3.1. Animals: Subjects were virgin female mice generated at the University of California, Los Angeles (UCLA) from a $DAT^{IREScre}$ lineage (Jackson Laboratory, stock no. 006660) on a C57Bl/6J background *via* heterozygote mating. All surgeries were carried out under aseptic conditions with isoflurane anesthesia (5% isoflurane for induction, 1.5-2% for maintenance) on a KOPF Model 1900 Stereotaxic Alignment System (KOPF, Tujunga, CA). After each surgery, mice were administered the analgesic carprofen (5 mg/kg, 1 mg/mL, sc) for the first three days, and an antibiotic (amoxicillin, 0.25 mg/mL) and analgesic (ibuprofen, 0.25 mg/mL) in drinking water for 14 days post-surgery.

3.3.3.2. RPV-PLSR: Three mice first underwent a surgical procedure for head-bar implantation. A pair of rectangular head-bars (9 mm × 7 mm × 0.76 mm, 0.6 g each, laser cut from stainless steel

at Fab2Order) were attached to the sides of the skull by C&B-METABOND (**Fig. S3.1**; Parkell, Edgewood, NY). The Cre-dependent adeno-associated viral vector (AAV) was obtained from the University of North Carolina Vector Core (Chapel Hill, NC). A nanoinjector was used to deliver 600 nL of 7.8×10^{12}/mL AAV5/Syn-Flex-ChrimsonR-tdT unilaterally into the ventral tegmental area (VTA)/substantia nigra (SN) area (AP -3.08 mm, ML ±1.20 mm, DV -4.00 mm from Bregma). Then, a 200 μm diameter ferrule-coupled optical fiber (0.22 NA, Thorlabs, Newton, NJ) was implanted (AP -3.08 mm, ML ±1.20 mm, DV -3.80 mm from Bregma *via* the same path of viral vector injection) to deliver optical stimulation during experiments.

After surgery, mice were pair-housed with cagemates to recover for at least 2-3 weeks and to allow for expression of genes of interest before an additional craniotomy surgery. During this time, subjects were trained to acclimate to the head-fixed testing condition for 15-30 min/session × 6-10 sessions. Two craniotomies were carried out 24 h ahead of testing days. A piece of skull (2.0 mm width × 2.0 mm length, centered at AP +1.0 mm, ML ±1.0 mm from Bregma) above the striatum (STR) of the same hemisphere as the AAV injection site was removed for working electrode insertion. For the Ag/AgCl reference electrode, a 0.4 mm diameter hole (centered AP +2.8 mm, ML ±2.0 mm from Bregma) was made in the skull on the side contralateral to the AAV injection site. The dura remained intact for both surgical areas. All surgery areas were first sealed with a thin layer of Kwik-Cast & Kwik-Sil (World Precision Instruments, Sarasota, FL) and then covered with a thin layer of C&B-METABOND. Animals were allowed to recover for 24 h.

On the testing day, each mouse was transferred and mounted to the head-fixed stage *via* its head-bars (**Fig. S3.1**). After a 10 min habituation period, the C&B-METABOND cover, Kwik-Cast & Kwik-Sil seal, and dura above the recording and reference electrode sites were carefully

removed. A Ag/AgCl reference electrode made from bleached silver wire was lowered into the brain. An optical fiber was calibrated to 10 mW/mm^2 daily prior to fiber coupling. Optical stimulation was generated *via* a 532 nm MGL-III-532 laser (Changchun New Industries Optoelectronics Tech. Col, Ltd, Changchun, P. R. China). Square pulses of 50% duty at 30 or 40 Hz for 20 s were used to deliver optical stimulation at >5 min intervals. One subject received a dose of escitalopram (20 mg/kg, sc). Basal and optically stimulated responses were collected before and beginning 1 h after drug administration.

The working electrode (PEDOT:Nafion carbon fiber microelectrode) was sterilized using 70% ethanol, rinsed with saline, and lowered into the striatum for voltammetry measurements *via* a 1 μm-precision motorized digital micromanipulator (MP-225, Sutter Instrument, Novato, CA). The PEDOT:Nafion coated electrodes were fabricated as per published protocols [79]. Each electrode had a cylindrical conducting surface that was 5-μm in diameter and ~75 μm in length. When lowered to a new recording depth, the electrode baseline was restabilized for at least 10 min before continuing stimulations.

During testing, sweetened milk diluted with water was delivered to the subject every 2 hr. Subject behavior was monitored for signs of distress. After the experiment, each subject was prepared for histological verification of Chrimson expression, recording electrode position, and the position of the optical fiber. At the end of each *in vivo* experiment, electrodes were removed and post-calibrated using standards of dopamine, serotonin, and their mixtures in physiological saline to generate the training set data.

3.3.3.3. Microdialysis: Mice (*N*=3) at 3-6 months of age were Chrimson-transfected, had an optical fiber implanted, and were trained to be head-fixed, as described above. Two-three weeks after

Chrimson-transfection, a second surgery was carried out first to implant a CMA/7 guide cannula for a microdialysis probe aimed at the dSTR (AP+1.00 mm, ML±1.75 mm, DV-3.10 mm from Bregma) into the same hemisphere as the viral delivery and fiber implant site (see above). The guide cannula was secured to the skull with C&B-METABOND. Animals recovered from the surgery for at least three days before microdialysis. Subjects underwent online microdialysis testing for one day. Following testing, the microdialysis probe was removed and the brain of each mouse was prepared for histology to verify the microdialysis probe and optical fiber placements, and Chrimson expression. Microdialysis probe and optical fiber tracks were visualized using light microscopy.

On the night before microdialysis (ZT10-12), each mouse was briefly anesthetized with isoflurane (1-3 min) for insertion of a CMA/7 microdialysis probe (1 mm length, 6 kDa cutoff, CMA8010771; Harvard Apparatus, Holliston, MA) into the guide cannula. Subjects were returned to their home cages after insertion and aCSF was continuously perfused through the probe at 2-3 μL/min for 30-60 min followed by a 0.3 μL/min flow rate for an additional 12-14 h to allow stabilization of the brain tissue surrounding the probe.

On the testing day, subjects were relocated to the head-stage recording set-up and allowed to habituate for at least 30 min before basal data collection. Optical stimulation was performed as described above, except the pulses were delivered at 10 Hz for 5 min. The first stimulation was delivered at ~ZT-2 after 6-18 basal dialysate samples were collected and analyzed. Prior to reverse dialysis of escitalopram (10 μM), three optical stimulations were delivered at 1-h intervals. After 90-120 min of intrastriatal drug perfusion, an additional three optical stimulations were delivered at 1-h intervals while drug perfusion was continued.

High performance liquid chromatography was performed using an Amuza HTEC-500 integrated system (Amuza Corporation [formally known as Eicom], San Diego, CA). An Eicom Insight autosampler was used to inject standards and Eicom EAS-20s online autoinjectors were used to collect and inject microdialysis dialysates [80]. Chromatographic separation was achieved using an Eicom PP-ODS II column (4.6 mm ID x 30 mm length, 2 μm particle diameter). The column temperature was maintained at 21 °C. The volumetric flow rate was 450-500 μL/min. Electrochemical detection was performed using an Eicom WE-3G graphite working electrode with an applied potential of +450 mV *vs.* a Ag/AgCl reference electrode.

Standard curves encompassed physiological concentration ranges of serotonin and dopamine in dialysates (0-10 nM). The limit of detection was ≤302 amol (6.05 pM) for each analyte; the practical limit of quantification was ≤916 amol (18.3 pM). Dialysate samples were collected online at 5-min intervals using a dialysate flow rate of 1.8 μL/min and injected immediately onto the HPLC system for analysis.

3.3.4. Voltammetry data acquisition and analysis

3.3.4.1. Measurement hardware: Voltammetry measurements were carried out using a two-electrode configuration *via* a Ag/AgCl reference electrode and a carbon fiber microelectrode working electrode. Waveforms were generated using a PC with a PCI-6221 data acquisition card (National Instruments (NI), Austin, TX) to control an EI-400 potentiostat (Cypress Systems, USA) and a custom 'headstage' analog pre-amplifier. Potentials were applied to the reference electrode while the working electrode was tied to the zero-potential terminal (virtual ground) of the pre-amplifier circuit. The pre-amplifier was designed to output an analog voltage proportional to

electrode current. Detailed information on the custom headstage design is in the Supplemental Information (**Fig. S3.2**). The output voltage was amplified by the EI-400, then sampled and quantified by an analog-to-digital converter on the NI PCI-6221 data acquisition card.

3.3.4.2. Measurement software: An in-house software program was developed for this study. The software was programmed in MATLAB (R2016a; The MathWorks, Inc., Natick, MA) and consisted of three modules. (1) The signal generation module enabled the design of multi-step waveforms at user-specified potentials, scan rates, sampling and fundamental frequencies, and numbers of sampled points per waveform period. (2) The MATLAB Data Acquisition Toolbox enabled event-driven communication during the measurement process. Waveforms were loaded from the signal generation module while the user specified the measurement start and stop points, along with optional parameters for stimulation or injection events. The data acquisition card generated the analog potential signal and the stimulation signal and digitized the resulting current. Voltammograms for each measurement cycle and the temporal evolution of current at potentials of interest were plotted in real-time. At the end of each measurement, digitized current measurement data were stored in MATLAB files. (3) The data processing module displayed the acquired data in a variety of user-specified formats, allowed for user-defined background subtraction, digital filtering and signal averaging, and generated MATLAB or Excel files to be extracted for machine learning models.

3.3.4.3. Waveforms: Three different waveforms were used herein. (1) A four-step rapid pulse waveform consisting of -0.4 V to +0.2 V to +0.8 V to -0.1 V to -0.4 V at 2 ms per step applied at 10 Hz for *in vitro* RPV to investigate differentiating serotonin from dopamine (**Fig. 3.1a**). (2) A triangle waveform [41] for FSCV from -0.4 V to +1.2 V to -0.4 V at a scan rate of 400 ms/V delivered at 10 Hz for *in vitro* comparisons with the RPV waveform (**Fig. 3.1b**). (3) A combination of the

four-step rapid pulse and triangle waveforms described above. Each waveform was delivered in an alternating manner at 5 Hz *in vivo* and during post calibration (**Fig. 3.1c**).

3.3.4.4. Machine learning: Data were extracted from raw MATLAB files into Excel and imported into Python using Pandas 0.25.1 and Jupyter 6.0.1 notebooks. All models were built using the Python 3.7.4 programming language in Jupyter notebooks using NumPy 1.16.5, SciPy 1.3.1, and scikit-learn 0.22.1 [81]. Data visualization was *via* matplotlib 3.1.1. Per each model built, data were normalized unless otherwise noted using either the ℓ_1, ℓ_2 or maximum norm, as chosen by grid search [81].

3.3.5 Statistics

Statistical analyses for *in vivo* data (two-tailed *t*-tests; Table S3.1) were carried out using Prism, v.9.1.0 (GraphPad Inc., La Jolla, CA). Basal data over six timepoints just prior to the first optical stimulation were averaged for N=3 microdialysis mice and N=1 RPV mouse. The areas under the curve for microdialysis stimulation peaks were calculated using four dialysate samples after the onset of stimulation. Due to faster sampling, the areas under the curve for RPV stimulation peaks were calculated using fifty-two points post stimulation onset. Data are expressed as means ± standard errors of the mean (SEMs). Throughout, P<0.05 was considered statistically significant.

3.4. RESULTS & DISCUSSION

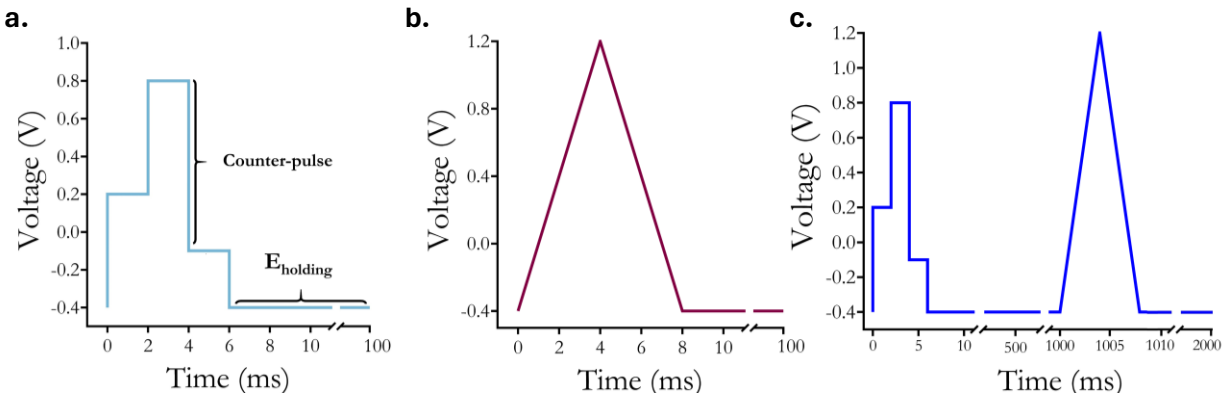

Figure 3.1. Voltammetry waveforms used in this study. (**a**) Four-step rapid pulse voltammetry (RPV) pulsed waveform. (**b**) Fast-scan cyclic voltammetry (FSCV) triangle waveform. (**c**) Combined RPV-FSCV waveform.

We designed and evaluated an initial rapid pulse waveform *in vitro* for dopamine and serotonin co-detection (**Fig. 3.1a**) and to compare with a triangle waveform [41](**Fig. 3.1b**). For *in vivo* experimentation, we alternated the rapid pulse and triangle waveforms (RPV-FSCV; **Fig. 3.1c**). Experimental paradigms utilizing these waveforms are shown in **Fig. 3.2.** The RPV-FSCV waveform was used to facilitate within-subjects' comparisons (**Fig. 3.2a**). For experiments in mice, electrodes were post-calibrated *in vitro* to produce training set data (**Fig. 3.2b**). Training set data for each waveform were used to build machine learning regression models to classify and to quantify dopamine and serotonin (**Fig. 3.2c**). Multiple waveform-model combinations were compared in the context of cross-validation accuracy and predicted *in vivo* responses.

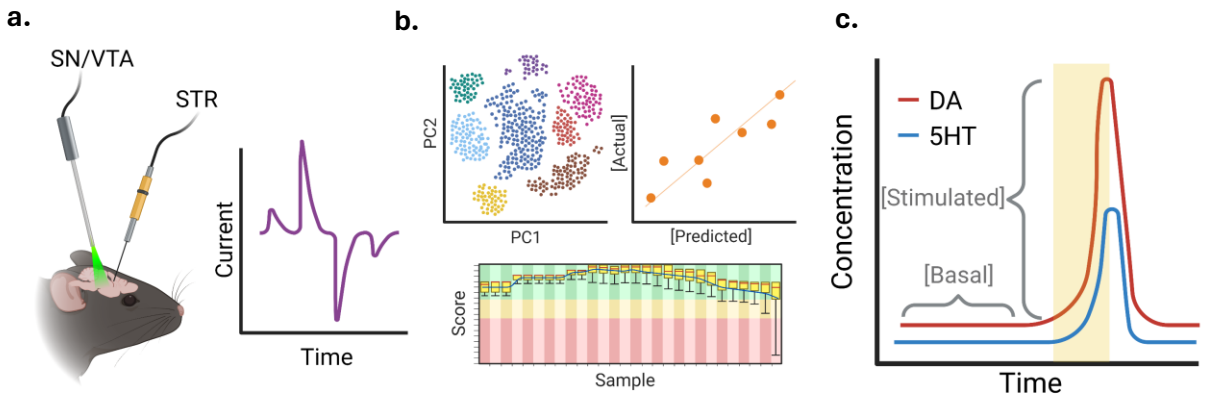

Figure 3.2. General scheme for rapid pulse voltammetry-principle least squares regression (RPV-PLSR). (**a**) Dopamine neurons in the substantia nigra and ventral tegmental area (SN/VTA) of DAT^{IREScre} mice were transfected with the excitatory opsin Chrimson. Basal and optically stimulated dopamine and serotonin levels were recorded from the striatum (STR) using the alternating RPV-fast-scan cyclic voltammetry waveform (Fig. 3.1c). (**b**) Electrodes used for *in vivo* measurements were then post-calibrated to provide data to build a PLSR model for analyte identification and quantification. (**c**) The *in vivo* data were analyzed using the model.

3.4.1. Rapid pulse waveform design: We designed an initial rapid pulse waveform (**Fig. 3.1a**) based on potentials characteristic of commonly used dopamine or serotonin FSCV waveforms (**Fig. 3.1b**). The rapid pulse waveform employed a starting potential of -0.4 V, similar to a commonly used dopamine FSCV waveform [82] (**Fig. 3.1b**), but with steps to +0.2 V and -0.1 V, similar to the voltages scanned during the N-FSCV waveform used for preventing serotonin adsorption on electrode surfaces and to promote reduction of serotonin, respectively [83]. A step to +0.8 V was included to ensure the oxidation of serotonin and dopamine, while preventing capacitive currents from reaching the maximum current limits of our hardware, which occurs with large potential steps. Employing intermediate pulses (*e.g.,* +0.2 V and -0.1 V) has been shown to increase analyte discrimination and precision for VETs [77]. Both faradaic and non-faradaic currents at intermediate steps contribute analyte-specific information more so than a single, large amplitude pulse step directly to the redox potential of interest (*i.e.*, from -0.4 V directly to +0.8 V), which

would be dominated by capacitive current. In the future, intermediate steps can be added to reach +1.3 V, the upper potential commonly used for dopamine detection and recently optimized for serotonin detection [48]. This high upper potential was not used for this proof-of-concept experiment for simplification and to keep the pulse duration short. Employing a counter pulse completes the redox cycle and generates additional information on analyte identity, as demonstrated in electronic tongue pulse design [76].

3.4.2. *In Vitro* Model Construction: Data preprocessing is critical to the training and use of machine learning models, such as PLSR. Here, we use the terms 'feature' or 'variable' interchangeably to refer to the current response at a given time point in a voltammogram. We refer to a voltammogram as a 'sample' determined using a particular combination of analyte concentrations (*in vitro*) or at a particular time relative to a stimulation event (*in vivo*).

Preprocessing typically involves mean-centering (setting means across all samples at each feature equal to zero) and either standardization (scaling the data to have unit variance at each feature across all samples) or normalization (scaling the input features to unit length). Mean-centering is done to simplify the computation process and should not affect model output [64]. Standardization is commonly used to remove magnitude-related effects, while normalization is used to preserve them. All are commonly accepted practices in the machine learning field, as well as for PLSR in chemometrics [64].

Previous implementations of FSCV with PCR[39] or PLSR[42] did not employ mean-centering or data standardization. By forgoing these procedures, the magnitudes of the original current responses were preserved. This caused the PCR or PLSR models to weigh regions of larger current

amplitude (*i.e.,* redox peaks) more heavily compared to low amplitude regions (*i.e.,* noise). For techniques like FSCV, which rely mainly on variations in peak current responses for classification and quantification of analytes, non-standardized data make sense. The model should focus mostly on the variances at the highest peak magnitudes to correlate current magnitudes with concentration. However, pulse techniques, such as the VET and RPV, are explicitly designed *not* to rely solely on peak currents for quantification. Instead, the entire voltammogram is treated as a holistic source of predictive data. Thus, data are standardized, as the model should not treat larger current responses with greater importance.

To investigate the effects of standardization on RPV data, we used a variable selection technique. The *in vitro* raw RPV voltammograms are shown in **Figure 3.3a.** The samples obtained (1000 data points or 'features') were then represented in 1000 dimensions or principal components (PCs), each of which described some amount of variance in the data. The PCs were formed *via* a linear combination of the original variables and weighted projection coefficients, known as loadings [84]. Loading vectors of greatest magnitude and similar direction in the factor space represented greater correlation.

Variable selection is the process of determining the features to present to the model as input. The relevance of different features can be examined through various methods based on the algorithm used. For PLSR, a variable importance in the projection (VIP) score can be mathematically calculated for each feature [85]. Generally, VIP scores >1 indicate variables that are important for the model to learn from the training data; features with scores <1 are considered less important. Thus, VIP scores can be used to evaluate waveform responses and serve three purposes. First, the VIP scores allow us to evaluate if RPV-PLSR is truly using current responses (features) not just from faradaic currents, but also from noise or capacitive currents. Second, the VIP scores

allow us to evaluate how preprocessing affects feature importance (*e.g.*, standardized *vs.*

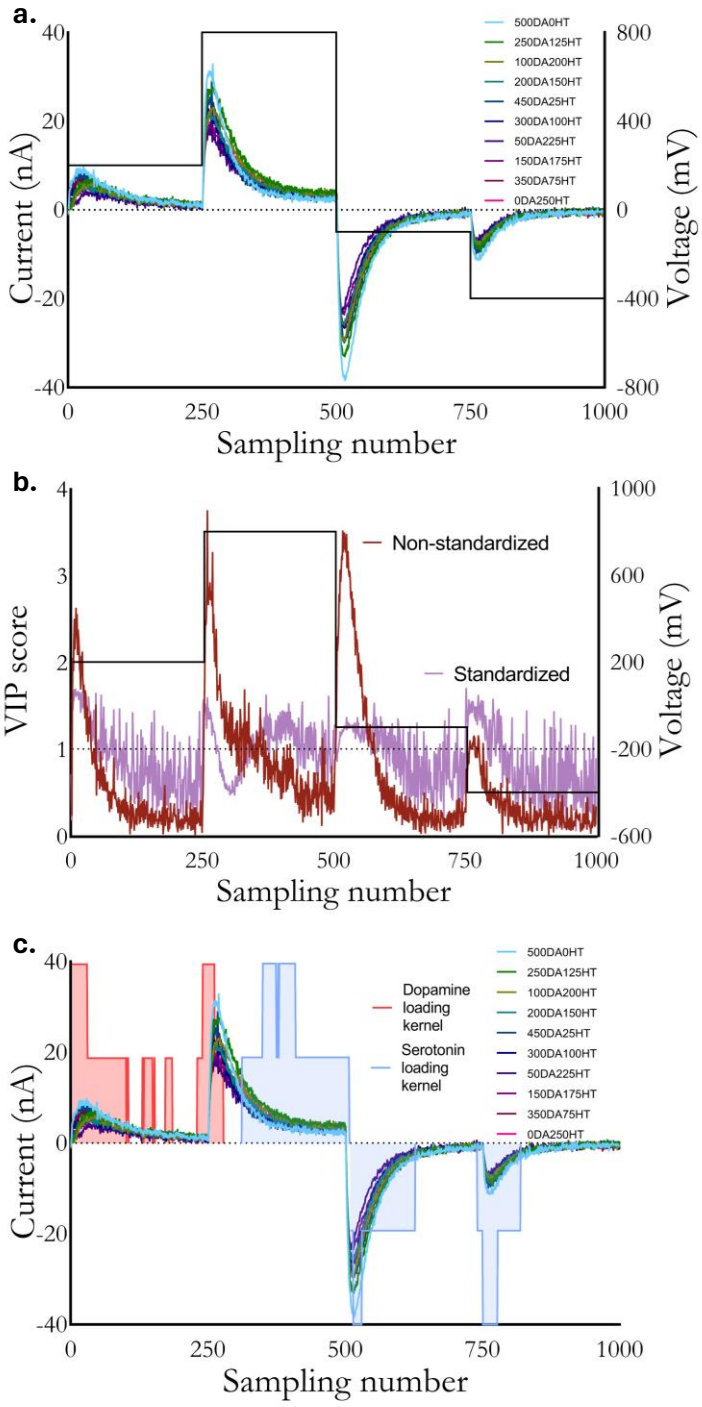

Figure 3.3 (a) Rapid pulse voltammograms of varying dopamine (DA) and serotonin (5HT) combinations (nM). The pulse waveform is overlaid. **(b)** Variable importance in the projection (VIP) scores for non-standardized *vs.* standardized data obtained from Fig. 3.3a. **(c)** Loadings analysis overlaid with Fig. 3.3a.

non-standardized data). And third, areas of the pulse response that are consistently more important for the model can be considered for more frequent sampling in future pulse designs, whereas areas of the current response that consistently have low VIP scores can be excluded by either reducing their sampling or removing that part of the pulse train. The VIP scores can be used as another metric to systematically optimize waveforms for a given analyte panel.

Preliminary analyses demonstrated that RPV-PLSR with standardized data are not dominated by magnitude-related effects and use areas of current response that historically have been discarded (**Fig. 3.3b**). For standardized data, the number of features with VIP scores >1 was 518 out of a possible 1000 features. For non-standardized data, the VIP scores clearly mimicked the magnitude of the current response. Moreover, the number of VIP scores >1 was only 231/1000. Standardizing the data allowed for a more than doubling of 'important' features and these features spanned areas of the voltammogram dominated by non-faradaic current.

The use of non-faradaic current by the model is further supported by an analysis of the PLSR loadings (**Fig. 3.3c**). The magnitude of the projection of the **X** loading vectors onto the **Y** loading vectors was calculated as a mathematical representation of the strength of the correlation that each data point had with different combinations of dopamine and serotonin. To visualize regions of the voltammograms most informative for the model, a moving average kernel was applied to map each variable to low, medium, or high correlation (no shading, 50% shading, or 100% shading, respectively). Areas of the voltammograms with the highest shaded heights were most useful for that analyte (regardless of sign; positive or negative values are arbitrary). For example, the current response of the second pulse step (points 250-500) had high red-shaded areas during capacitive charging illustrating non-faradaic contributions to modeling dopamine.

Meanwhile, the majority of the decay of the second pulse step, which would include faradic and non-faradaic contributions, was heavily used for modeling serotonin.

Similar to the VIP scores (**Fig. 3.3b**), **Figure 3.3c** demonstrates that RPV pulses can be optimized using PLSR analyses (*e.g.*, the last two pulses could be shortened to improve temporal resolution as the tail-ends of each decay are not shaded). These findings support the theory behind intelligent (and iterative) pulse design in RPV and the key idea that background subtracted methods, like FSCV, are likely to be inferior in terms of generating information needed to specify analytes and their concentrations, particularly in complex mixtures, because key information in capacitive current decay is removed. Instead, the VET-based approach used for RPV is a 'soft' technique, agnostically collecting information across the entire pulse train [86]. The capacitive current increases transiently and then decays exponentially due to the presence of charged and polar compounds. Concurrently, faradaic current approaches a limiting value based on the diffusion and adsorption rates of electroactive species. Using multivariate analysis, and specifically, dimensionality reduction, the model is trained on trends across the pulse train, not the response of individual currents, such as in univariate calibration [87].

Our findings are further supported by similar results for elastic net electrochemistry [88], in which the authors used non-background subtracted voltammograms obtained using a FSCV triangular waveform to train an elastic net model, a regularized linear regression technique with some similarities to supervised dimensionality reduction techniques like PLSR [89]. The large magnitude (*i.e.,* important) regularization coefficients, similar to the large magnitude loadings and VIP scores discussed above, were found to span areas of the voltammogram outside of the expected peak faradaic responses of dopamine and serotonin [66,69].

A key difference between RPV and FSCV is that RPV is a pulse method having current decay across each pulse step. Since faradaic and capacitive currents evolve at different rates, each point in the decay provides unique information that is potentially useful for distinguishing analytes. That is, a stepped pulse approach is more information rich when coupled with a regression model compared to a sweep method, even if background subtraction is bypassed in the latter. Further, because RPV uses a bespoke pulse design, which can increase sensitivity when combined with electrode surface modifications [90], temporal resolution can be maximized by changing the pulse parameters. The waveform parameters in **Figure 3.1a** are simply a starting point.

Table 3.1. Training set concentrations for *in vivo* post-calibration.

Mouse	Injection	Dopamine (μM)	Serotonin (μM)
1	1	0.0	0.0
		5.0	0.0
	2	0.0	0.0
		0.0	4.0
	3	0.0	0.0
		2.0	2.0
2	1	0.0	0.0
		4.0	0.0
	2	0.0	0.0
		0.0	3.0
	3	0.0	0.0
		1.5	1.5
3	1	0.0	0.0
		5.0	0.0
	2	0.0	0.0
		0.0	5.0
	3	0.0	0.0
		2.0	2.0

3.4.3. *In Vivo* Model Construction & Deployment: Based on our preliminary *in vitro* RPV findings and the availability of suitable animal subjects from an ongoing study [11], we conducted a pilot *in vivo* study with RPV-PLSR. This small study was designed to compare the feasibility of an RPV waveform (that was admittedly unoptimized) with a commonly used FSCV waveform, early in our development of RPV and before continuing with the validation and creation of larger and more complex *in vitro* RPV training sets. We have found that advancing to *in vivo* experiments sooner in methods development helps to guide our *in vitro* efforts (sometimes in unexpected and fruitful ways) [91,92].

We designed a combined rapid pulse-triangle waveform (RPV-FSCV) for use in conjunction with an optogenetic stimulation paradigm. The red-shifted opsin Chrimson was virally transfected into midbrain dopamine neurons in DAT$^{IRES\textit{cre}}$ mice. Four weeks later, carbon-fiber microelectrodes coated with PEDOT:Nafion [79] were used to measure dopamine and serotonin in the striatum (STR). Optical stimulation (532 nm, 30 or 40 Hz, 20 s) was delivered to dopamine cell bodies in the substantia nigra/ventral tegmental area (SN/VTA) while the combined waveform (**Fig. 3.1c**) was applied to the carbon fiber microelectrode with each alternating waveform at 5 Hz. After several stimulations, the selective serotonin reuptake inhibitor (SSRI) escitalopram was administered, and stimulation continued one-hour post administration. Similar paradigms have been used to examine dopamine in STR [93]. Electrodes were then removed and used to obtain post-calibration training data for PLSR analysis (**Table 3.1**).

Training set samples (one normalized, non-background subtracted voltammogram per standard) were used to train and to cross-validate the PLSR model. While our hypothesis that standardization allows the model to place emphasis on response areas unrelated to magnitude was supported by our *in vitro* data (**Fig. 3.3b**), initial analyses of *in vivo* data using standardization

resulted in negative predicted basal concentrations for dopamine, serotonin, or both. Nonetheless, dopamine and serotonin showed the expected qualitative and quantitative (nanomolar) responses to stimulation.

By removing magnitude related effects *via* standardization, identification of analytes was possible, but quantitation became less reliable. We attributed this to the limited size and concentration range of the training set; standardization emphasizes variability. For accurate quantitation, standardization requires large data sets to train the model adequately on small-magnitude variations. Conversely, the VIP scores for the normalized data mimicked the non-standardized data in **Figure 3.3b**, meaning that lower magnitude responses were still considered by the model due to inclusion of the background, but not as heavily as in standardization. Thus, normalization was used as the preprocessing method for the *in vivo* data to retain current amplitudes associated with a small training set size and for comparison to previous studies [63,65].

After training the PLSR model, the number of components was optimized. The variance explained by the model is a function of the number of components included. For PLSR, the first component always explains the maximal covariance in the data, with successive decreases in covariance explained by additional components (*i.e.,* the first component explains more covariance than the second, which explains more than the third, and so on). The total number of components equals the number of samples, at which the data set is fully reconstructed (the cumulative variance explained reaches 100%). The model is then deployed with an *a priori* number of components such that only the most relevant features that lead to accurate analyte identification and quantification are used to make predictions, while the less relevant features (unrelated noise) are not utilized. Notably, 'noise' as defined by background subtraction may differ from 'noise' as defined by a PLSR model, meaning the background must be included to allow the PLSR model to

discern in the number of components. The number of components can be estimated based on training set conditions and domain knowledge (*i.e.,* if the degrees of freedom of the system under study are known), or determined empirically, commonly by hyperparameter tuning during cross-validation.

To determine the variance in the *Y* variable (concentration) explained by the model, R^2Y scores were calculated (**Table 3.2**). To estimate the generalizability of the model, Q^2Y scores were calculated (*i.e.,* cross-validated R^2Y scores that serve as a proxy for predictive accuracy) using leave-one-out cross-validation because of the small training set size [94]. Given the known two-component calibration and variability of cross-validation errors for small training sets [95-97], we opted to deploy the two-component PLSR model *in vivo* at the expense of a lower *in vitro* cross-validation score ($Q^2Y = 0.1$ for two components *vs.* $Q^2Y = 0.6$ for three components). Although ostensibly detrimental to the model, selecting a model with higher cross validation error can prevent overfitting, especially in the case of noisy training data [98]. The two-component model was used to predict *in vivo* concentrations of dopamine and serotonin simultaneously across time in a single subject.

Table 3.2. Training (R^2Y) and cross-validation (Q^2Y) accuracy metrics for each background subtracted (no (N)/yes (Y))/waveform/model combination.

Model	Waveform	Background Subtraction	Components	R^2Y			Q^2Y		
				2	*3*	*5*	*2*	*3*	*5*
PLSR	Pulse	N		0.408	0.823	0.857	0.072	0.574	0.662
		Y		0.754	0.821	0.874	0.550	0.548	0.555
	Triangle	N		0.720	0.760	0.880	0.420	0.439	0.582
		Y		0.653	0.770	0.844	0.386	0.478	0.034
PCR	Pulse	N		0.356	0.421	0.876	0.033	-0.053	0.651
		Y		0.545	0.563	0.571	0.369	0.396	0.364
	Triangle	N		0.415	0.667	0.784	0.112	0.405	0.430
		Y		0.413	0.490	0.566	0.170	0.273	0.265

As input to the RPV-PLSR model, for each stimulation, 300 scans (120 s total) were extracted that included 150 scans prior to stimulation (60 s) and 150 scans after the onset of stimulation (60 s). As output, the model predicted dopamine and serotonin concentrations for each scan based on the post-calibration training set. A moving average filter was applied to smooth and to align concentration *vs.* time plots. Basal concentrations were calculated as pre-stimulation baseline averages of the first 100 scans. Stimulated concentrations were defined as the areas under the curve for the stimulation peaks. Representative concentration-time plots are shown in **Figure 3.4**.

During the experiment, the carbon fiber microelectrode was lowered from the dorsal striatum to the ventral striatum (dSTR and vSTR, respectively). Multiple stimulations were delivered at each position relative to the surface of the brain The average predicted basal concentration increased for dopamine and decreased for serotonin moving from dSTR to vSTR (**Fig. 3.4a,b,** respectively). These trends are in general agreement with previously reported dorsoventral dopamine and serotonin gradients in striatum [99], which is known to be

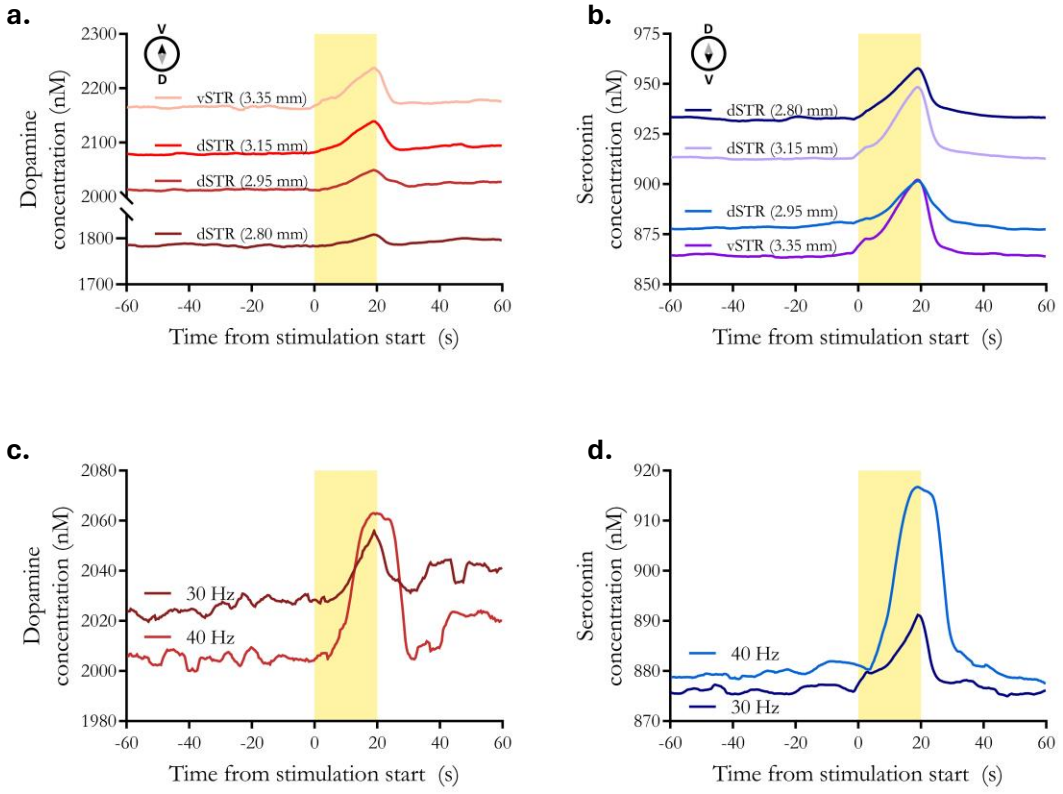

Figure 3.4. ***In vivo*** **dopamine and serotonin monitoring using rapid-pulse voltammetry with partial least squares regression (RPV-PLSR) analysis (a,b)** Time courses of dopamine or serotonin at various dorsoventral striatal positions measured with RPV-PLSR (*n*=3 at 2.80 mm, *n*=5 at 2.95 mm, *n*=7 at 3.15 mm, and *n*=3 at 3.35 mm for a total of 18 recordings in a single representative mouse). **(c.d)** Time courses of dopamine or serotonin measured in dorsal striatum (dSTR) in response to representative sequential 40 Hz and 30 Hz optical stimulations of midbrain dopamine neurons (*n*=1).

neurochemically diverse [100]. To investigate the effects of stimulation strength, we applied a 40 Hz stimulation in the dorsal striatum and after ~5 min, applied a 30 Hz stimulation at the same electrode position. Higher frequency stimulation produced greater stimulated dopamine [101,102] and serotonin release (**Fig. 3.4c,d**).

The predicted basal concentrations are most likely overestimates of actual concentrations given that we biased our *in vivo* training set towards higher dopamine and serotonin concentrations in this proof-of-concept study. Given this limitation, the relative differences of the simultaneous dopamine and serotonin levels under varying stimulation paradigms and model-waveform combinations are more important than absolute concentrations. Optical stimulation of dopamine neurons expressing the excitatory opsin Chrimson produced dopamine release detected by RPV-PLSR (**Fig. 3.4a,c**). The RPV-PLSR model, which was trained to differentiate dopamine and serotonin, also predicted serotonin release (**Fig. 3.4b,d**). Our recent microdialysis findings support the idea that optical stimulation of midbrain dopamine neurons produces serotonin release [11]. Linked dopamine and serotonin in the striatum has been reported elsewhere [60].

To increase our confidence in RPV-PLSR predictions, we compared the effects of serotonin transporter inhibition on basal and stimulated serotonin and dopamine using RPV-PLSR *vs.* microdialysis. The latter is a 'gold standard' neurochemical monitoring method that relies on chromatographic separations for analyte identification and quantification [92,103]. Similar to RPV, DAT^{irescre} mice were transfected with Chrimson for optical excitation of midbrain dopamine neurons during microdialysis [11]. Dialysis samples were collected at 5 min intervals and analyzed immediately online by HPLC with electrochemical detection. The optical stimulation was 5 min to match the dialysate sampling time. For RPV, we optically stimulated dopamine neurons for 20 s and sampled at 5 Hz.

Following administration of the selective serotonin reuptake inhibitor (SSRI) escitalopram, we observed potentiation of optically evoked serotonin (*i.e.*, greater area under the curve) determined by RPV-PLSR and microdialysis (**Fig. 3.5a,b**). Administration of an SSRI increases stimulated serotonin overflow due to reduced reuptake of serotonin by high affinity serotonin transporters [58,104,105]. Serotonin reuptake inhibition also led to a 60% increase in basal serotonin levels [91] observed *via* microdialysis (**Fig. 3.5b**). By contrast, RPV-PLR predicted a small relative decrease in basal extracellular serotonin (2%) (**Fig. 3.5a**).

One factor contributing to the RPV-PLSR prediction of lower basal serotonin following escitalopram involves the high concentration and limited number of standards used in the PLSR training set, which may result in insensitivity to modest changes. The RPV training set employed low micromolar concentration standards, whereas the predicted reduction in serotonin basal levels after escitalopram was only ~20 nM. Another factor potentially contributing to the discrepant effects of escitalopram on basal serotonin levels is the difference in the routes of drug administration. Mice in the microdialysis study received intrastriatal infusion of escitalopram, whereas mice in the RPV study were administered a subcutaneous drug injection. Systemic injection of an SSRI activates inhibitory 5HT1A autoreceptors on serotonin cell bodies [106,107]. This negative feedback reduces serotonin neuron firing, which acutely results in reduced serotonin release in terminals regions like the striatum. Local infusion of escitalopram circumvents activation of somatodendritic 5HT1A receptors and produces an increase in terminal region serotonin levels [91].

Like serotonin, we observed escitalopram-induced potentiation of optically evoked dopamine by RPV-PLSR and microdialysis (**Fig 3.5c,d**). Local perfusion of escitalopram did not affect basal dopamine levels determined by microdialysis (**Fig 3.5d**), while subcutaneous injection

of escitalopram was associated with a small (5%) increase in predicted basal dopamine levels by RPV-PLSR (**Fig 3.5c**). As discussed, limitations of the training set used for RPV-PLSR, as well as the different routes of escitalopram administration may underlie variations in the basal dopamine outcomes.

Despite the high selectivity of escitalopram for serotonin transporters and low affinity for dopamine transporters [108], the serotonin and dopamine systems are linked. Serotonin neurons innervate the SN and VTA, and both systems project to subcortical and cortical regions (*e.g.,* striatum, frontal cortex., dorsomedial thalamus, cerebral cortex) [109,110]. Serotonin receptors expressed on dopamine neurons in the striatum mediate dopamine release [111,112]. Moreover, human imaging studies suggest that citalopram and/or escitalopram increase striatal dopamine levels [113] and dopamine transporter binding (as a compensatory response) [114,115], presumably *via* increases in extracellular serotonin. Regardless of differences in absolute concentrations, microdialysis acts as external validation to confirm that optogenetic stimulation of dopamine neurons releases striatal serotonin and escitalopram potentiates optically stimulated dopamine. Overall, these findings indicate that RPV can be used to detect pharmacologically induced changes in the stimulated release of two neurotransmitters simultaneously *in vivo*.

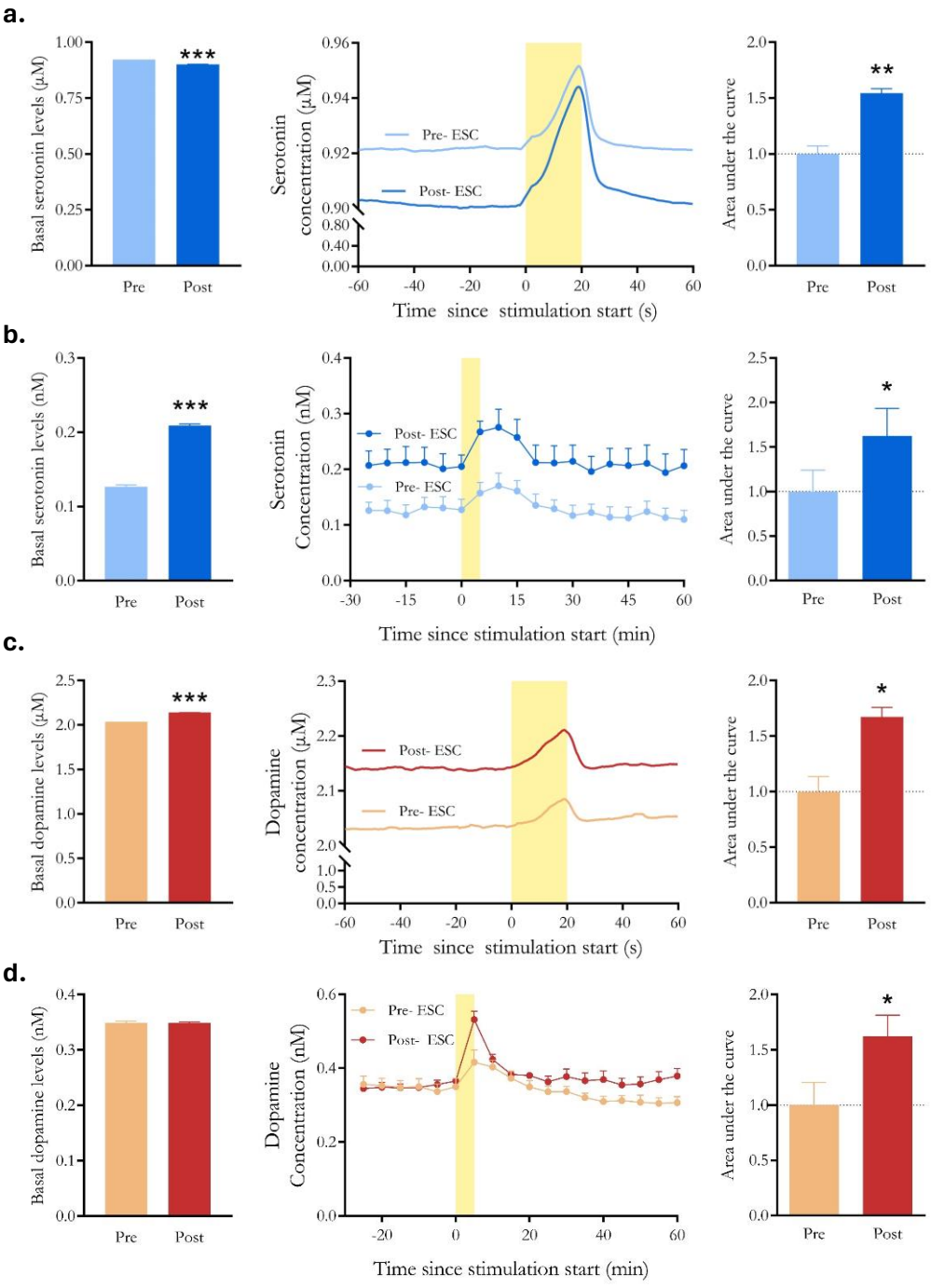
a.
Basal serotonin levels (µM)
Pre
Post
***
Serotonin concentration (µM)
Pre- ESC
Post- ESC
Time since stimulation start (s)
Area under the curve
**
b.
Basal serotonin levels (nM)
***
Serotonin Concentration (nM)
Post- ESC
Pre- ESC
Time since stimulation start (min)
*
c.
Basal dopamine levels (µM)
***
Dopamine concentration (µM)
Post- ESC
Pre- ESC
Time since stimulation start (s)
*
d.
Basal dopamine levels (nM)
Dopamine Concentration (nM)
Pre- ESC
Post- ESC
Time since stimulation start (min)
*

Figure 3.5. Responses to the selective serotonin reuptake inhibitor escitalopram by rapid pulse voltammetry with partial least squares regression analysis (RPV-PLSR) *vs.* microdialysis. Time courses are shown in the center panels for serotonin determined by **(a)** RPV-PLSR or **(b)** microdialysis and dopamine by **(c)** RPV-PLSR or **(d)** microdialysis. Escitalopram (20 mg/kg) was administered subcutaneously at t=-60 min for RPV-PLSR or perfused continuously into the dorsal striatum (10 μM) for microdialysis beginning at t=-90 min. Optical stimulation of Chrimson-transfected dopamine neurons occurred during the time periods marked by yellow bars. Basal serotonin or dopamine concentrations before and after/during escitalopram administration are shown in the left bar graphs. Stimulation-induced increases in serotonin or dopamine before *vs.* after/during escitalopram are shown in the right bar graphs and are calculated as areas under the curve. **P*<0.05, ***P*<0.01, and ****P*<0.001 (See Table S3.1 and Methods for statistical details).

3.3.4. Waveform-Model Combination Comparisons: To compare waveforms and analyses, R^2Y and Q^2Y scores were generated for different model/waveform/background subtracted combinations using the *in vivo* post-calibration training set data (**Table 3.1)**. In addition to two-component models, R^2Y and Q^2Y values were computed for three- and five-component models (**Table 3.2**) due to literature precedent [65]. Greater numbers of components were expected and found to produce erroneous results (negative concentrations, noisy oscillations), likely due to model overfitting. This supported our choice of the two-component model to analyze the *in vivo* results, rather than models with higher cross validation scores [98]. However, due to the large increase in both R^2Y and Q^2Y moving from two to three components (an 'elbow' point; see **Fig. S3.3**), three-component models were chosen to compare cross-validation scores across models. In all cases, training data were pre-processed with mean-centering and normalization.

We sought to answer three questions regarding RPV-PLSR in the context of the current training set data and to guide future studies. 1) How does RPV-PLSR compare, in terms of prediction, with previously developed FSCV-PCR (*i.e.,* background-subtracted voltammograms obtained *via* a triangle waveform (**Fig. 3.1b**) and analyzed by PCR)? 2) Does including

background current data in RPV-PLSR result in a benefit over background subtracted RPV-PLSR, as suggested by **Fig. 3.3c**? 3) Does RPV-PLSR provide more information about analyte identification/quantification than FSCV-PCR or other possible combinations (*e.g.*, why not use FSCV-PLSR?). We discuss various combinations below and find that each step of RPV-PLSR is needed to result in the optimal combination. For each combination, only the voltammograms for the relevant waveform were extracted to build the model (*i.e.,* voltammograms from the triangle waveform were extracted when referring to FSCV; voltammograms from the pulse waveform were extracted when referred to RPV).

3.3.4.1. Comparing RPV-PLSR to FSCV-PCR: Having demonstrated the non-background subtracted RPV-PLSR waveform-model combination, the effects of striatal recording electrode position, optical stimulation frequency, and SSRI administration were examined using background subtracted FSCV data and PCR analysis (**Fig. 3.6**). The FSCV-PCR model has been used for dopamine or serotonin monitoring [62]. Because background currents, which contain information about tonic neurotransmitters levels, are removed, the 'basal' levels predicted by the FSCV-PCR model are not meaningful and thus, were not considered.

Optically stimulated release of dopamine (**Fig. 3.6a,c**) and serotonin (**Fig. 3.6b,d,e**) were predicted by a two component FSCV-PCR model. However, the stimulated concentrations were predicted to be much larger (~1 μM) than by RPV-PLSR and on the high end of literature reported values [34,116,117]. No increases in optically evoked release were detected in association with higher frequency stimulation for either dopamine or serotonin for FSCV-PCR analyses (**Fig. 3.6c,d**) or for serotonin following SSRI administration (**Fig. 3.6e**).

To ensure the model had enough components included to pick up on these differences, we tried increasing the number of components in the FSCV-PCR model from three to five. These additional components did not cause the serotonin traces to be distinguished by stimulation paradigm (data not shown; *i.e.,* the concentration traces looked the same for both 30 and 40 Hz stimulation frequency regardless of the number of components beyond two). This suggests that the model did have enough degrees of freedom, but was undertrained and consistently predicting a response that was not related to serotonin. Meanwhile, dopamine traces began to lose noticeable stimulation responses and showed increased noise as the number of components was increased from three to five, indicating that for this data set, two or three components appear to be better.

The results thus far support the notion that PLSR can deal more efficiently with noise and interferents when trained *in vitro* and used *in vivo* because PLSR models covariation of input and output, rather than just input, as in PCR. We did notice similarities in predicted responses for FSCV-PCR and FSCV-PLSR suggesting that overall, more training data and training across common interferents was needed. Further, RPV-PCR produced similar traces in the same concentration range for dopamine compared to RPV-PLSR (1.8 to 2.3 μM). Serotonin traces showed more variation (larger SEMs) and slightly larger predicted concentrations (1.05 to

1.10 µM) but remained responsive to the stimulation paradigms. In both cases, stimulated responses were on the same order of magnitude as RPV-PLSR (10-100 nM). This is despite the

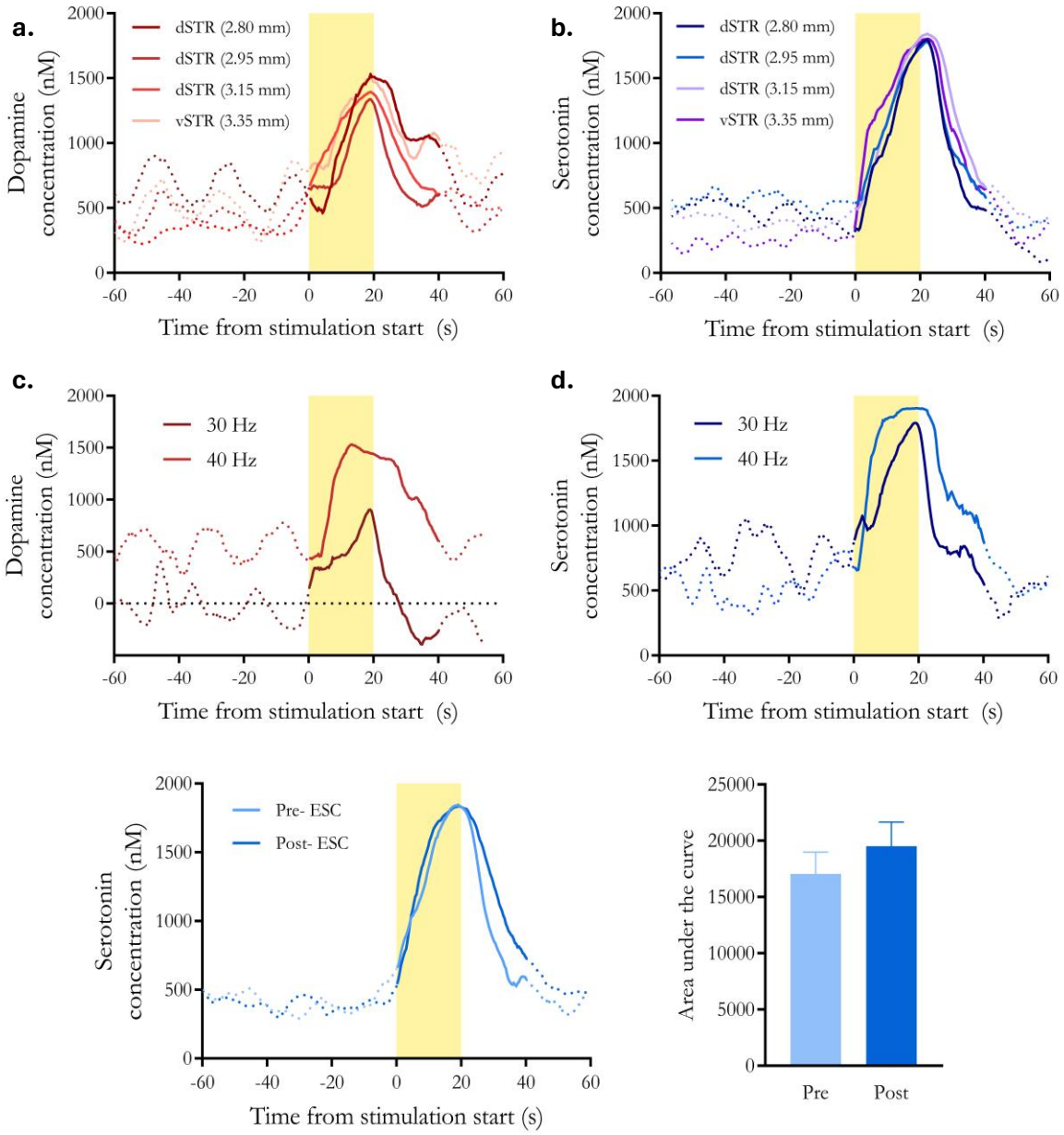

Figure 3.6. Predictions using a two component fast-scan cyclic voltammetry-principle components (FSCV-PCR) model for dopamine and serotonin *in vivo* (a,b) Time courses of dopamine and serotonin, respectively, at various dorsoventral striatal recording electrode positions determined by FSCV-PCR. **(c,d)** Time courses of dopamine and serotonin, respectively in response to 40 Hz *vs.* 30 Hz stimulations predicted by FSCV-PCR. **(e)** Time course (left) and area under the curve (right) of serotonin for pre- and post- escitalopram administration using FSCV-PCR.

low cross-validation score, again supporting the need to cautiously interpret these scores when small training sets are used. For these reasons, we could not state definitively the necessity for PLSR over PCR, other than to state that previous methods support the use of supervised learning over PCR for FSCV [66]. Because PLSR has been compared to PCR elsewhere [65,84,89], we do not compare results further here.

3.3.4.2. The need for including background current. We hypothesized that avoiding background subtraction would result in information gain for the RPV-PLSR model. We indeed observed greater cross validation scores for nonbackground-subtracted compared to background-subtracted RPV-PLSR models (**Table 3.2**). However, this trend was not consistent across waveform-model combinations. The FSCV-PLSR and RPV-PCR analyses showed worse cross-validation accuracy without background subtraction (0.48 compared to 0.44 and 0.40 compared to -0.05, respectively), while the FSCV-PCR cross-validation score improved without background subtraction (0.27 compared to 0.41). Because no clear trend in cross-validation was present when background current was subtracted *vs.* not, we suspect that information gain may be waveform and model dependent. Regardless, nonbackground-subtracted voltammograms obtained by our smart pulse waveform and analyzed by PLSR (*i.e.*, RPV-PLSR) resulted in the highest three-component R^2Y (0.82) and Q^2Y (0.57) scores of all background/waveform/model combinations examined (**Table 3.2**). These variation and accuracy metrics suggest that RPV-PLSR may be better at modelling and predicting dopamine and serotonin concentrations, at least based on the limited training data.

3.3.4.3. Comparisons of further waveform/model combinations. Other waveform/model/background subtraction combinations were explored (**Table 3.2**). Two, three, and five component models were trained and used to analyze the *in vivo* post-calibration training

set data. While RPV-PCR and FSCV-PLSR behaved somewhat similarly to RPV-PLSR and FSCV-PCR (**Fig. S3.4, S3.5**), in all other cases, except those discussed above, we did not find consistent, biologically relevant responses to stimulation paradigms (optical or pharmacological). Although it is possible these models would begin to produce meaningful results with more training data, we note that only the RPV-PLSR method worked reasonably well for this small data set. The RPV-PLSR method, compared to other waveform/model combinations, predicted the most reasonable relative differences when monitoring dopamine and serotonin across stimulation and pharmacologic paradigms. The absolute concentrations, however, should always be regarded as estimates, especially when using dimensionality reduction models [118]. Nonetheless, we attribute the success of RPV-PLSR to the wealth of information in the pulse and the parsimony of the PLSR model. When combined, our findings support the idea that RPV-PLSR can be used to extract maximally relevant information, even with small training set sizes.

3.3.5. Study Limitations and Future Directions: We note the following limitations of this proof-of-concept study. The first is training set size. While increased training set size should improve model generalizability [88,119], training sets with similar sizes to ours (**Table 3.1**; N=18) have been used in previous studies [66,67]. The second limitation is the robustness of our training set. Notably, we did not train for responses to interferents (*e.g.,* 5-hydroxyindoleacetic acid, 3,4-dihydroxyphenylacetic acid, ascorbic acid), changes in pH or ionic salt concentrations (*e.g.,* Na^+, K^+, Ca^{2+}, Mg^{2+}), any of which could conflate capacitive current responses in the PLSR model. This is a potential reason for the likely overestimated basal concentrations [120]. While our findings *in vivo* correspond with previously reported biological phenomena and relative trends, our basal

concentrations are outside of what is expected for dopamine and serotonin based on previous voltammetry and microdialysis studies (~10–1000 nM and ~1–100 nM, respectively) [34,56,103,121].

In the future, we plan to design more robust training sets that include interferents, pH changes, and ionic strength changes to investigate their influence on RPV-PLSR. However, most metabolites of dopamine and serotonin are not expected to change extracellularly (at least over short time frames) during stimulation because they are metabolized intracellularly [122-124]. Further, because the RPV-PLSR model was trained using data across a four-step (*i.e.,* intermediate) pulse voltammogram, it is less likely for the dimensionality reduction to confound interferents across multiple potential steps and time points. While varying pH was not considered in this training set, similar approaches have demonstrated pH insensitivity for dopamine and serotonin when using supervised learning, as opposed to unsupervised techniques (*i.e.,* PCR) [66,69].

Artifacts from ionic and pH changes during stimulated neurotransmitter release occur regardless of background subtraction [120,125]. Some literature suggests that physiological changes in pH and divalent cationic salt concentrations may pose less of an interference problem for biogenic amines when using pulsed voltammetry [126], as opposed to FSCV, especially with Nafion-coated electrodes [127], potentially due to different surface binding mechanisms. The PEDOT:Nafion electrodes used here provide some selectivity against the anionic interferents mentioned above and reduce acute (6 h) biofouling [79], bolstering confidence in our predictions of cationic neurotransmitters.

Long term (chronic) recordings can lead to variability in electrode responses due to biofouling. We will continue to calibrate multiple electrodes post-fouling (that is, after *in vivo* recording), which should account for some variability introduced over the course of brain

implantation. We plan to increase the training size in future training sets, such that the model is trained on artifacts of fouling and other confounding factors mentioned above. We hypothesize that with increased training data, nonspecific signals can be parsed out by PLSR, or another supervised model. In theory, we could add short, highly anodic pulses (*i.e.*, 1.3 V *vs.* Ag/AgCl) to try to renew electrode surfaces (electrochemical cleaning as employed in VETs [86] and FSCV [118]). Larger, historical training sets may also require ensemble weighting schemes to account for electrode variation [119].

At present, we do not directly compare RPV-PLSR to elastic net electrochemistry [88], another supervised learning technique. Theoretical comparisons of their underlying statistical approaches can be found elsewhere [89]. Instead, we note that dimensionality reduction techniques usually require less computation time than regularized techniques, suggesting the RPV-PLSR should scale well for larger training sets, which is a long-term goal of both techniques. However, both dimensionality reduction (PLSR) and regularization (elastic net) seek to prevent overfitting in some manner, whether by introducing sparsity in the latter case or by projecting data to a lower-dimension feature space in the former. Thus, both methods improve robustness of predictions. The two methods can be combined as a form of variable selection due to their supervised nature (*i.e.,* EN-PLS) [128,129]. In fact, the RPV approach can theoretically be combined with any appropriate supervised regression technique that enables feature selection, representing a paradigm shift in design and analysis of waveform-model combinations.

Based on the initial findings arising from the non-background-subtracted, supervised machine learning regression model (RPV-PLSR), we plan to optimize the pulse waveforms presented here, guided by feature selection as discussed earlier. Supervised learning techniques can enable iterative construction and optimization of fit-for-purpose waveforms to expand

measurements to diverse sets of electroactive neurotransmitters (*e.g.*, dopamine, serotonin, norepinephrine, *etc.*). We will also explore other pre-processing and feature selection techniques, as well as more advanced supervised regression models. Larger training sets across many electrodes with more diverse analyte/interferent panels will be needed [118]. Further validation and alternatives to *in vitro* training (*i.e.,* relying on domain knowledge and stimulation paradigms, in addition to cross-validation metrics) should be explored to bolster confidence for *in vivo* predictions when using dimensionality reduction and regularization models that are trained and validated *in vitro*, but applied *in vivo*. Indeed, other areas of the physical sciences are currently working to address model generalizability through embeddings, representations, and domain knowledge [130]. Based on the current findings, future *in vivo* experiments can be designed more robustly to continue to investigate whether data processing models can distinguish and identify analytes in the complex brain matrix (*e.g.,* validation using DAT inhibitors, dopamine and serotonin synthesis inhibitors, and *in vivo* standard addition). Overall, we foresee a new paradigm in which fit-for-purpose pulses are iteratively constructed with feature selection feedback (**Scheme 3.1**).

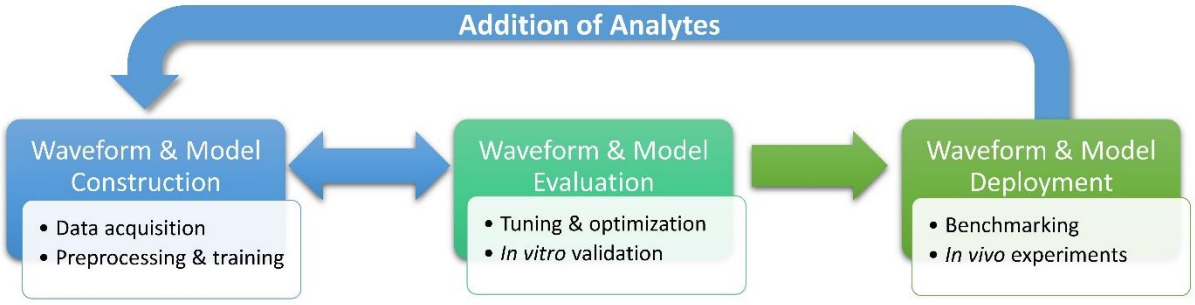

Scheme 3.1. Rapid pulse voltammetry-machine learning optimization scheme.

The coupling of voltammetry with more sophisticated pattern recognition and statistical tools is part of a global shift in scientific data analysis. Applications of machine learning in the physical sciences have skyrocketed over the last decade [131]. Other chemistry disciplines, such as materials, physical, and organic chemistry, were early adopters, but modern machine learning techniques have been underutilized in electrochemistry, specifically voltammetry [132,133]. While advanced techniques, such as deep learning, have been used for classification of voltammograms [134,135], its counterpart (regression) is less often reported [88,119]. The development of this novel voltammetric technique (RPV) coupled with fit-for-purpose machine learning (ML) pipelines (broadly defined as RPV-ML) represents a new paradigm for electroanalytical classification and quantitation of multiplexed neurochemical responses across timescales. This single, customizable technique allows for multiplexed neurotransmitter measurements in real-time in behaving animals, representing a step towards decoding neurotransmission at the molecular scale.

3.5 CONCLUSIONS

All three aspects of RPV appear essential for its success: intelligent pulse design, avoiding background subtraction, and supervised regression (*i.e.*, PLSR). We have demonstrated that the RPV-PLSR combined paradigm can identify and quantify two neurotransmitters *in vitro*. When dopamine neurons were optically stimulated, the RPV-PLSR model detected serotonin release *in vivo*, which corroborates a novel finding by microdialysis using the same experimental paradigm (*i.e.*, opsin, transfection and stimulation location, and recording location) [11]. Compared to FSCV-PCR and other waveform/model combinations, RPV-PLSR was better equipped to detect changes induced by different stimulation frequencies. When an SSRI was administered, RPV-PLSR detected increases in stimulated serotonin levels. Overall, our experimental pipeline demonstrates proof-of-concept for a reliable new technique that can detect biologically relevant (*i.e.,* nM) changes in basal and stimulated levels of multiple neurotransmitters simultaneously across biologically relevant timescales (*i.e.,* stimulated and basal levels over ms to h).

Acknowledgements and Author Contributions: The authors gratefully acknowledge Prof. M. L. Heien for PEDOT:Nafion-coated electrodes, Ayaka Hachisuka for technical assistance with animal surgeries, histology, and the optical setup, Prof. Sotiris Masmanidis for mice and resources for in vivo voltammetry experiments, and Sara Erwin for assistance during in vivo experiments. Biorender.com is acknowledged for figure generation. AMA, MAF, and HY conceived of the work. MAF and RI programmed the voltammetry data acquisition software. MAF and HY customized the voltammetry headstage from a commercial pre-amplifier. HY, XC, and MAF conducted the *in vitro* experiments. HY, KAP, XC, and MD conducted the *in vivo*

experiments. CSM trained the PLSR models and analyzed the voltammetry data. HY, KAP, and MD analyzed the microdialysis data. AMA, CSM, and KAP interpreted the results. CSM, AMA, KAP, and HY wrote the manuscript with assistance from all authors. Funding from the National Institute on Drug Abuse (DA045550) and National Institute of Mental Health (MH106806) was received. CSM was supported by the National Science Foundation Graduate Research Fellowship Program (DGE-1650604 and DGE- 2034835). Any opinions, findings, and conclusions or recommendations expressed in this material are those of the authors and do not necessarily reflect the views of the National Science Foundation.

3.6 SUPPLEMENTARY INFORMATION

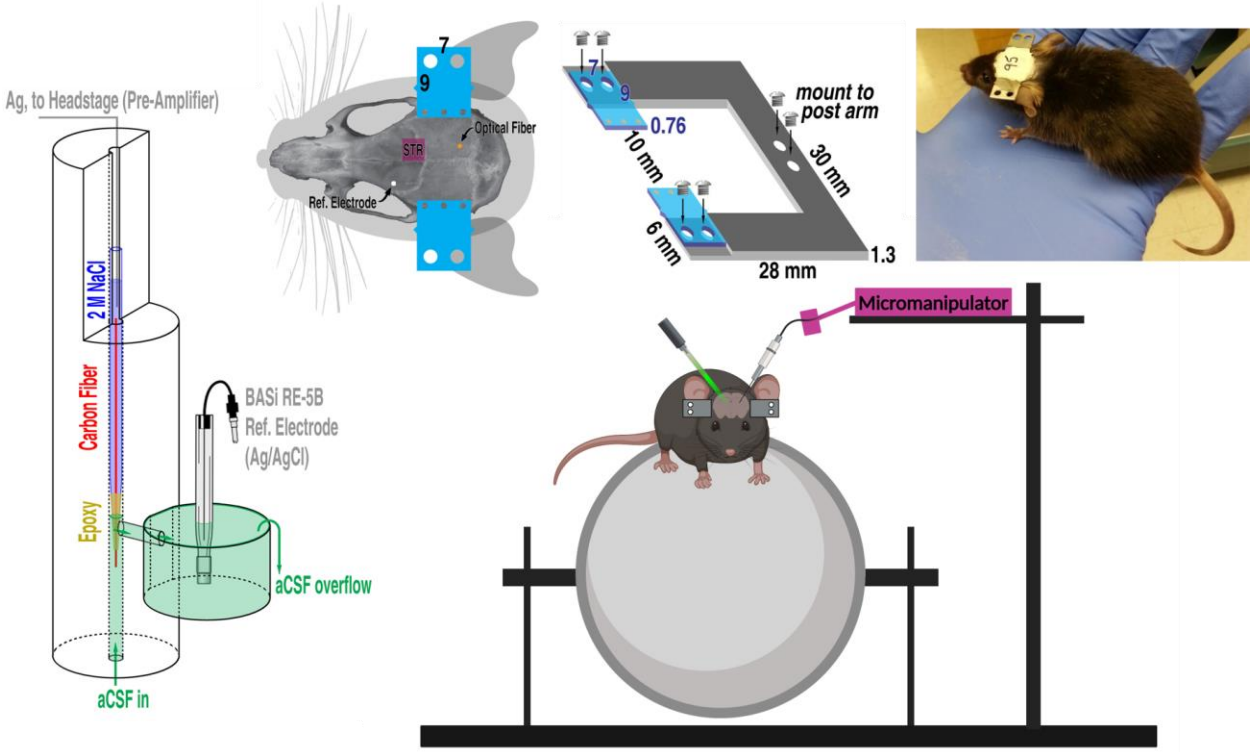

Figure S3.1. Experimental set-up for *in vitro* carbon-fiber microelectrode calibration (flow cell, left) and *in vivo* experiments (right). Photograph courtesy of Wesley Smith.

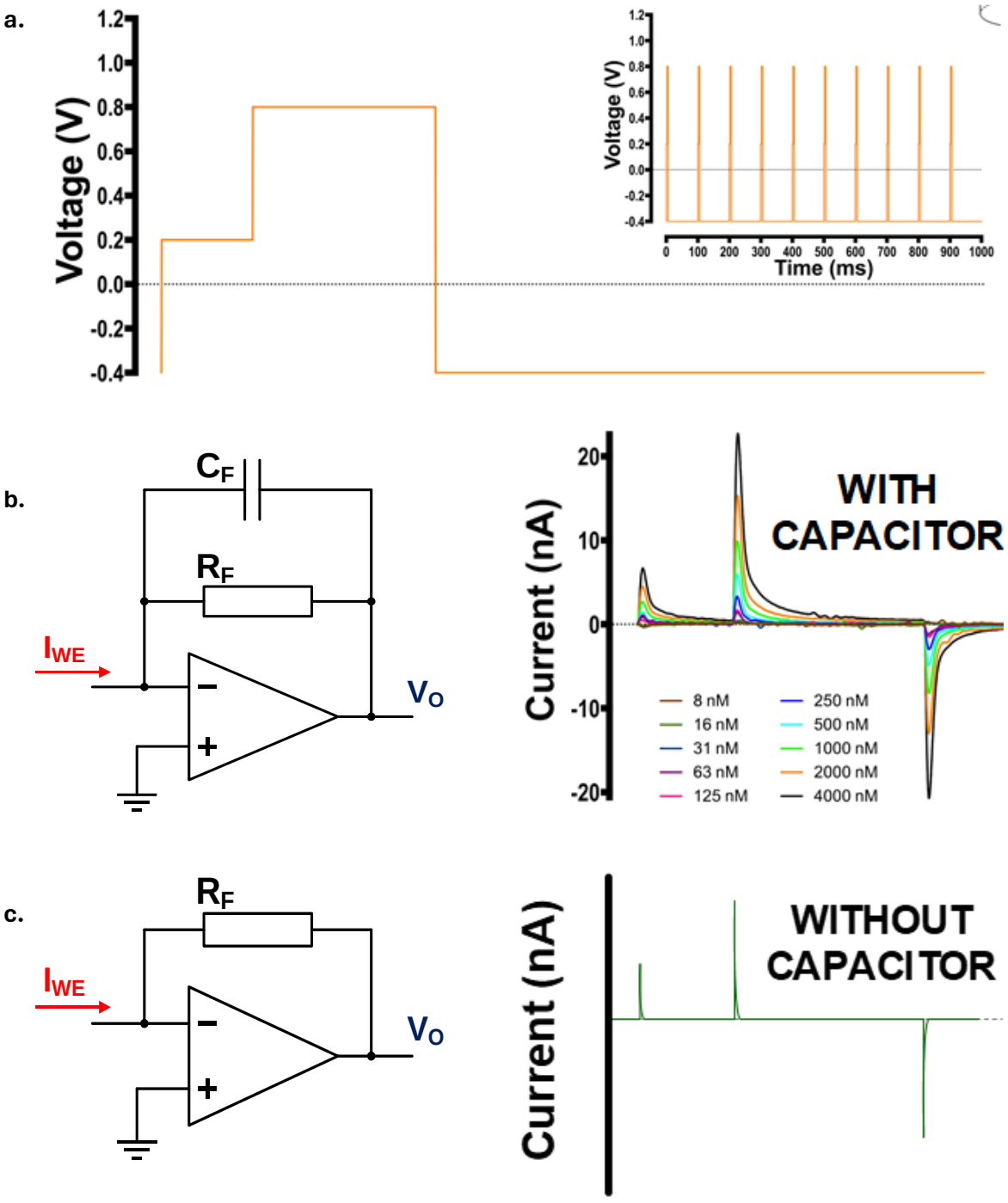

Figure S3.2. Effect of the transimpedance amplifier used in the custom headstage
(a) Representative pulse applied to the electrochemical system. **(b)** Circuit diagram for the transimpedance amplifier (amplifier with feedback resistor R_F in parallel with feedback capacitor C_F) to convert current from the working electrode (I_{WE}) into output voltage (V_O) (left). Representative voltammograms with the capacitor in parallel (right). **(c)** Circuit diagram for amplifier without feedback capacitor (left). Representative voltammogram (right).

The rapid pulse voltammetry (RPV) waveform is shown in **Figure S3.2a**. For this circuit (**Fig. S3.2b**), the relationship between the output voltage and the working electrode current is given by the differential equation:

$$\frac{V_O}{R_F} + C_F \cdot \frac{dV_O}{dt} = -I_{WE} \quad \textbf{(3.1)}$$

If the feedback capacitor is not present (**Fig. S3.2c**), the relationship is given by:

$$V_O = -R_F \cdot I_{WE} \quad \textbf{(3.2)}$$

Transimpedance amplifiers often include a feedback capacitor connected in parallel to the feedback resistor for signal stabilization and filtering purposes. The drawback of their use is that the feedback capacitor disrupts the direct proportionality between measured current and output voltage (**Equation 3.1**). Instead, the output signal will deform (*i.e.,* the exponential current decay will be delayed) according to the differential present in Equation 3.1 (**Fig. S3.2b**). In most cases, the latter is not desired.

For RPV, we purposefully included a feedback capacitor (**Fig. S3.2b**) to allow a smoother, longer duration of the pulse response. Important electrochemical information is present within the nonfaradaic and faradaic currents immediately after a pulse, on the order of tens of microseconds. Without a feedback capacitor, these currents decay too quickly to be sampled with high enough time resolution by the data acquisition system (8 μs sampling rate; 125 kHz). With a feedback capacitor of appropriate capacitance, the output voltage response is spread out over a longer temporal duration. This additional decay time affords the PLSR model more data points to

be sampled from key electrochemical events that would otherwise be missed or under-sampled. While we recognize these electronic components preclude the analysis of an electrochemical system by equivalent circuit analysis, due to the deformation of the original working electrode signal, we note our purpose here is to obtain relevant information for the PLSR model, not to gain mechanistic insights at the electrode surface. Further, the capacitor also helps to stabilize and to reduce the noise of the output signal.

For these reasons, we implemented the feedback capacitor as shown in **Figure S3.2b**. The value of the capacitor was determined empirically to produce the desired smoothing and decay time of the signal, depending on the pulse sequence applied. For our set up, this value was found to be approximately 100 pF.

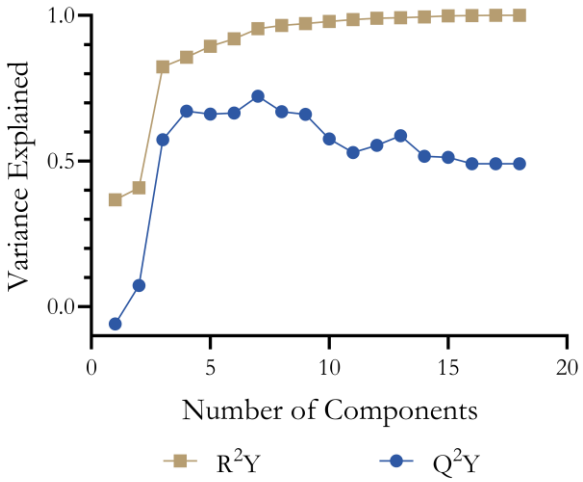

Figure S3.3. Cumulative training (R^2Y) and prediction (Q^2Y) score metrics for the RPV-PLSR model with respect to the number of components.

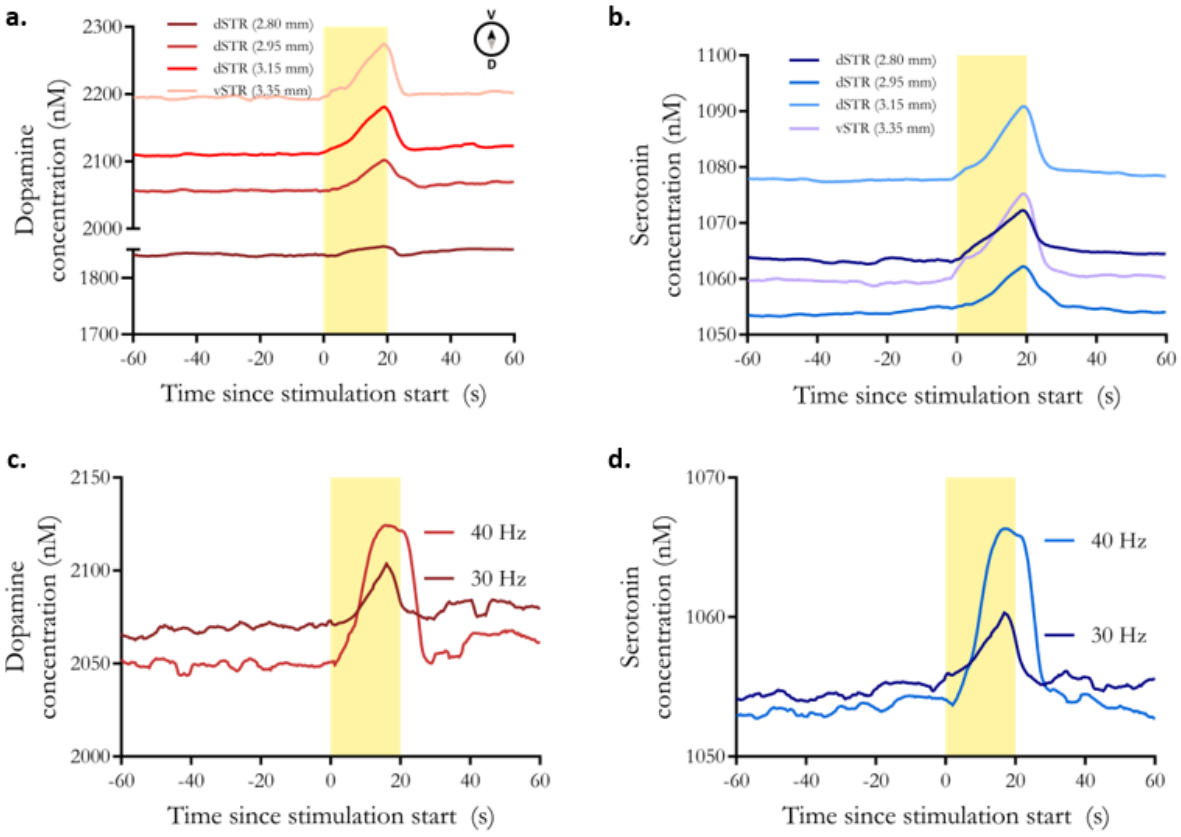

Figure S3.4. *In vivo* dopamine and serotonin monitoring using rapid-pulse voltammetry with principal components regression (RPV-PCR) analysis (a,b) Time courses of dopamine or serotonin at various dorsoventral striatal positions measured with RPV-PCR. **(c.d)** Time courses of dopamine or serotonin measured in dorsal striatum (dSTR) in response to a representative 40 Hz or 30 Hz sequential optical stimulations of midbrain dopamine neurons.

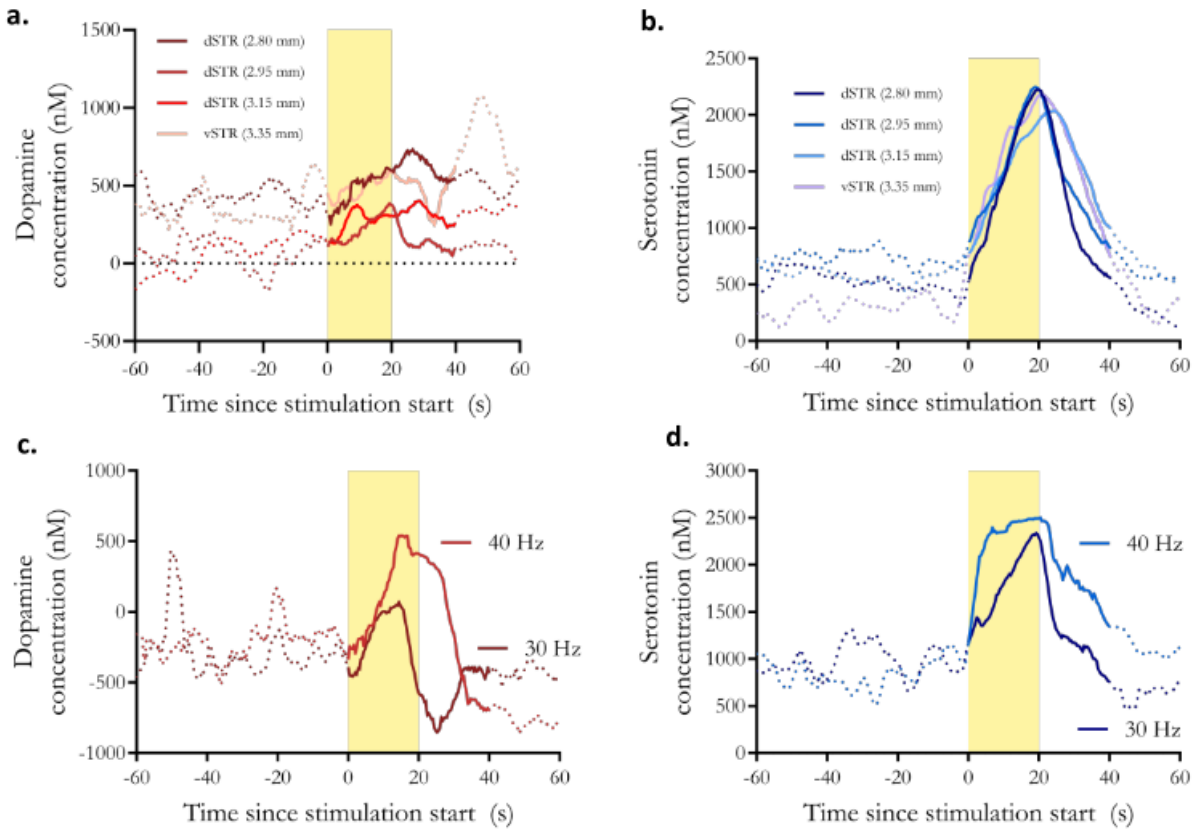

Figure S3.5. Predictions using a FSCV-PLSR model for dopamine and serotonin *in vivo*
(a,b) Time courses of dopamine and serotonin, respectively, at various dorsoventral striatal recording electrode positions determined by FSCV-PLSR. **(c,d)** Time courses of dopamine and serotonin, respectively in response to 30 Hz *vs.* 40 Hz stimulations predicted by FSCV-PLSR.

Table S3.1. Statistical summary.

Figure	Comparison	Test	Statistics	Significant?
3.5A, left	Basal 5HT RPV: pre- SSRI *vs.* post- SSRI	Paired *t*-test	t(5)=238	*P*<0.001
3.5A, right	AUC 5HT RPV: pre- SSRI *vs.* post- SSRI	Unpaired *t*-test	t(5)=5.92	*P*<0.01
3.5B, left	Basal 5HT microdialysis: pre- SSRI *vs.* post- SSRI	Paired *t*-test	t(4)=21.7	*P*<0.001
3.5B, right	AUC 5HT microdialysis: pre- SSRI *vs.* post- SSRI	Paired *t*-test	t(8)=2.67	*P*<0.05
3.5C, left	Basal DA RPV: pre- SSRI *vs.* post- SSRI	Paired *t*-test	t(5)=544	*P*<0.001
3.5C, right	AUC DA RPV: pre- SSRI *vs.* post- SSRI	Unpaired *t*-test	t(5)=3.823	*P*<0.05
3.5D, left	Basal DA microdialysis: pre- SSRI *vs.* post- SSRI	Paired *t*-test	t(4)=0.030	ns
3.5D, right	AUC DA microdialysis: pre- SSRI *vs.* post- SSRI	Paired *t*-test	t(8)=2.843	*P*<0.05

The *t*-tests were two-tailed and paired or unpaired depending on whether matching numbers of pre- *vs.* post SSRI samples were available.

3.7 REFERENCES

1. Marcinkiewcz, C. A.; Mazzone, C. M.; D'Agostino, G.; Halladay, L. R.; Hardaway, J. A.; DiBerto, J. F.; Navarro, M.; Burnham, N.; Cristiano, C.; Dorrier, C. E.; Tipton, G. J.; Ramakrishnan, C.; Kozicz, T.; Deisseroth, K.; Thiele, T. E.; McElligott, Z. A.; Holmes, A.; Heisler, L. K.; Kash, T. L., Serotonin engages an anxiety and fear-promoting circuit in the extended amygdala. *Nature* **2016,** *537* (7618), 97-101. https://doi.org/10.1038/nature19318
2. Hashemi, P.; Dankoski, E. C.; Lama, R.; Wood, K. M.; Takmakov, P.; Wightman, R. M., Brain dopamine and serotonin differ in regulation and its consequences. *Proc. Natl. Acad. Sci. U.S.A.* **2012,** *109* (29), 11510-11515. https://doi.org/10.1073/pnas.1201547109
3. Cheer, J. F.; Heien, M. L. A. V.; Garris, P. A.; Carelli, R. M.; Wightman, R. M., Simultaneous dopamine and single-unit recordings reveal accumbens GABAergic responses: Implications for intracranial self-stimulation. *Proc. Natl. Acad. Sci. U.S.A.* **2005,** *102* (52), 19150-19155. https://doi.org/10.1073/pnas.0509607102
4. Ngernsutivorakul, T.; Steyer, D. J.; Valenta, A. C.; Kennedy, R. T., In vivo chemical monitoring at high spatiotemporal resolution using microfabricated sampling probes and droplet-based microfluidics coupled to mass spectrometry. *Anal. Chem.* **2018,** *90* (18), 10943-10950. https://doi.org/10.1021/acs.analchem.8b02468
5. Tecuapetla, F.; Patel, J. C.; Xenias, H.; English, D.; Tadros, I.; Shah, F.; Berlin, J.; Deisseroth, K.; Rice, M. E.; Tepper, J. M.; Koos, T., Glutamatergic signaling by mesolimbic dopamine neurons in the nucleus accumbens. *J. Neurosci.* **2010,** *30* (20), 7105-7110. https://doi.org/10.1523/jneurosci.0265-10.2010

6. Amilhon, B.; Lepicard, È.; Renoir, T.; Mongeau, R.; Popa, D.; Poirel, O.; Miot, S.; Gras, C.; Gardier, A. M.; Gallego, J.; Hamon, M.; Lanfumey, L.; Gasnier, B.; Giros, B.; El Mestikawy, S., VGLUT3 (vesicular glutamate transporter type 3) contribution to the regulation of serotonergic transmission and anxiety. *J. Neurosci.* **2010,** *30* (6), 2198-2210. https://doi.org/10.1523/jneurosci.5196-09.2010

7. Mingote, S.; Chuhma, N.; Kalmbach, A.; Thomsen, G. M.; Wang, Y.; Mihali, A.; Sferrazza, C.; Zucker-Scharff, I.; Siena, A.-C.; Welch, M. G.; Lizardi-Ortiz, J.; Sulzer, D.; Moore, H.; Gaisler-Salomon, I.; Rayport, S., Dopamine neuron dependent behaviors mediated by glutamate cotransmission. *eLife* **2017,** *6*, e27566. https://doi.org/10.7554/eLife.27566

8. Root, D. H.; Barker, D. J.; Estrin, D. J.; Miranda-Barrientos, J. A.; Liu, B.; Zhang, S.; Wang, H.-L.; Vautier, F.; Ramakrishnan, C.; Kim, Y. S.; Fenno, L.; Deisseroth, K.; Morales, M., Distinct signaling by ventral tegmental area glutamate, GABA, and combinatorial glutamate-GABA neurons in motivated behavior. *Cell Rep.* **2020,** *32* (9), 108094. https://doi.org/10.1016/j.celrep.2020.108094

9. Wang, H.-L.; Zhang, S.; Qi, J.; Wang, H.; Cachope, R.; Mejias-Aponte, C. A.; Gomez, J. A.; Mateo-Semidey, G. E.; Beaudoin, G. M. J.; Paladini, C. A.; Cheer, J. F.; Morales, M., Dorsal raphe dual serotonin-glutamate neurons drive reward by establishing excitatory synapses on VTA mesoaccumbens dopamine neurons. *Cell Rep.* **2019,** *26* (5), 1128-1142.e7. https://doi.org/10.1016/j.celrep.2019.01.014

10. Lee, K.; Claar, L. D.; Hachisuka, A.; Bakhurin, K. I.; Nguyen, J.; Trott, J. M.; Gill, J. L.; Masmanidis, S. C., Temporally restricted dopaminergic control of reward-conditioned

movements. *Nat. Neurosci.* **2020,** *23* (2), 209-216. https://doi.org/10.1038/s41593-019-0567-0

11. Dagher, M.; Perrotta, K. A.; Erwin, S. A.; Hachisuka, A.; Ayer, R.; Masmanidis, S.; Yang, H.; Andrews, A. M., Optogenetic stimulation of midbrain dopamine neurons produces striatal serotonin release. *ACS Chem. Neurosci.* **2022,** *13* (7), 946-958.
12. Di Giovanni, G.; Esposito, E.; Di Matteo, V., Role of serotonin in central dopamine dysfunction. *CNS Neurosci. Ther.* **2010,** *16* (3), 179-194. https://doi.org/10.1111/j.1755-5949.2010.00135.x
13. Aman, T. K.; Shen, R.-Y.; Haj-Dahmane, S., D2-like dopamine receptors depolarize dorsal raphe serotonin neurons through the activation of nonselective cationic conductance. *J. Pharmacol. Exp. Ther.* **2007,** *320* (1), 376-385. https://doi.org/10.1124/jpet.106.111690
14. Lee, E. H. Y.; Geyer, M. A., Dopamine autoreceptor mediation of the effects of apomorphine on serotonin neurons. *Pharmacol. Biochem. Behav.* **1984,** *21* (2), 301-311. https://doi.org/10.1016/0091-3057(84)90230-2
15. Niederkofler, V.; Asher, T. E.; Dymecki, S. M., Functional interplay between dopaminergic and serotonergic neuronal systems during development and adulthood. *ACS Chem. Neurosci.* **2015,** *6* (7), 1055-1070. https://doi.org/10.1021/acschemneuro.5b00021
16. Tan, S. K. H.; Hartung, H.; Schievink, S.; Sharp, T.; Temel, Y., High-frequency stimulation of the substantia nigra induces serotonin-dependent depression-like behavior in animal models. *Biol. Psychiatry* **2013,** *73* (2), e1-e3. https://doi.org/10.1016/j.biopsych.2012.07.032

17. Altieri, S.; Singh, Y.; Sibille, E.; Andrews, A. M., Serotonergic pathways in depression. In *Neurobiology of Depression*, CRC Press: 2011; Vol. 20115633, pp 143-170.

18. Nestler, E. J., Role of the brain's reward circuitry in depression: Transcriptional mechanisms. *Int. Rev. Neurobiol.* **2015,** *124*, 151-70. https://doi.org/10.1016/bs.irn.2015.07.003

19. Simpson, E. H.; Kellendonk, C.; Ward, R. D.; Richards, V.; Lipatova, O.; Fairhurst, S.; Kandel, E. R.; Balsam, P. D., Pharmacologic rescue of motivational deficit in an animal model of the negative symptoms of schizophrenia. *Biol. Psychiatry* **2011,** *69* (10), 928-935. https://doi.org/10.1016/j.biopsych.2011.01.012

20. Sumiyoshi, T.; Kunugi, H.; Nakagome, K., Serotonin and dopamine receptors in motivational and cognitive disturbances of schizophrenia. *Front. Neurosci.* **2014,** *8*, 395. https://doi.org/10.3389/fnins.2014.00395

21. Rothman, R. B.; Blough, B. E.; Baumann, M. H., Dual dopamine/serotonin releasers as potential medications for stimulante and alcohol addictions. *The AAPS Journal* **2007,** *9* (1), E1-E10. https://doi.org/10.1208/aapsj0901001

22. Skowronek, M. H.; Laucht, M.; Hohm, E.; Becker, K.; Schmidt, M. H., Interaction between the dopamine D4 receptor and the serotonin transporter promoter polymorphisms in alcohol and tobacco use among 15-year-olds. *Neurogenetics* **2006,** *7* (4), 239-246. https://doi.org/10.1007/s10048-006-0050-4

23. Eskow Jaunarajs, K. L.; George, J. A.; Bishop, C., L-DOPA-induced dysregulation of extrastriatal dopamine and serotonin and affective symptoms in a bilateral rat model of Parkinson's disease. *Neuroscience* **2012,** *218*, 243-256. https://doi.org/10.1016/j.neuroscience.2012.05.052

24. Stahl, S. M., Parkinson's disease psychosis as a serotonin-dopamine imbalance syndrome. *CNS Spectr.* **2016,** *21* (5), 355-359. https://doi.org/10.1017/S1092852916000602

25. Avery, M. C.; Krichmar, J. L., Neuromodulatory systems and their interactions: A review of models, theories, and experiments. *Front. Neural Circuits* **2017,** *11*, 108. https://doi.org/10.3389/fncir.2017.00108

26. Zangen, A.; Nakash, R.; Overstreet, D.; Yadid, G., Association between depressive behavior and absence of serotonin-dopamine interaction in the nucleus accumbens. *Psychopharmacology (Berl)* **2001,** *155* (4), 434-439. https://doi.org/10.1007/s002130100746

27. Andrews, A. M., The BRAIN Initiative: Toward a chemical connectome. *ACS Chem. Neurosci.* **2013,** *4* (5), 645. https://doi.org/10.1021/cn4001044

28. Sarter, M.; Kim, Y., Interpreting chemical neurotransmission in vivo: Techniques, time scales, and theories. *ACS Chem. Neurosci.* **2015,** *6* (1), 8-10. https://doi.org/10.1021/cn500319m

29. Dreyer, J. K.; Herrik, K. F.; Berg, R. W.; Hounsgaard, J. D., Influence of phasic and tonic dopamine release on receptor activation. *J. Neurosci.* **2010,** *30* (42), 14273-83. https://doi.org/10.1523/jneurosci.1894-10.2010

30. Hajós, M.; Allers, K. A.; Jennings, K.; Sharp, T.; Charette, G.; Sík, A.; Kocsis, B., Neurochemical identification of stereotypic burst-firing neurons in the rat dorsal raphe nucleus using juxtacellular labelling methods. *Eur. J. Neurosci.* **2007,** *25* (1), 119-126. https://doi.org/10.1111/j.1460-9568.2006.05276.x

31. Hajós, M.; Gartside, S. E.; Villa, A. E. P.; Sharp, T., Evidence for a repetitive (burst) firing pattern in a sub-population of 5-hydroxytryptamine neurons in the dorsal and median raphe nuclei of the rat. *Neuroscience* **1995,** *69* (1), 189-197. https://doi.org/10.1016/0306-4522(95)00227-A

32. Hajós, M.; Sharp, T., Burst-firing activity of presumed 5-HT neurones of the rat dorsal raphe nucleus: Electrophysiological analysis by antidromic stimulation. *Brain Res.* **1996,** *740* (1), 162-168. https://doi.org/10.1016/S0006-8993(96)00869-4

33. Sulzer, D.; Cragg, S. J.; Rice, M. E., Striatal dopamine neurotransmission: Regulation of release and uptake. *Basal Ganglia* **2016,** *6* (3), 123-148. https://doi.org/10.1016/j.baga.2016.02.001

34. Abdalla, A.; Atcherley, C. W.; Pathirathna, P.; Samaranayake, S.; Qiang, B.; Peña, E.; Morgan, S. L.; Heien, M. L.; Hashemi, P., In vivo ambient serotonin measurements at carbon-fiber microelectrodes. *Anal. Chem.* **2017,** *89* (18), 9703-9711. https://doi.org/10.1021/acs.analchem.7b01257

35. Atcherley, C. W.; Wood, K. M.; Parent, K. L.; Hashemi, P.; Heien, M. L., The coaction of tonic and phasic dopamine dynamics. *Chem. Comm.* **2015,** *51* (12), 2235-2238. https://doi.org/10.1039/C4CC06165A

36. Alivisatos, A. P.; Andrews, A. M.; Boyden, E. S.; Chun, M.; Church, G. M.; Deisseroth, K.; Donoghue, J. P.; Fraser, S. E.; Lippincott-Schwartz, J.; Looger, L. L.; Masmanidis, S.; McEuen, P. L.; Nurmikko, A. V.; Park, H.; Peterka, D. S.; Reid, C.; Roukes, M. L.; Scherer, A.; Schnitzer, M.; Sejnowski, T. J.; Shepard, K. L.; Tsao, D.; Turrigiano, G.; Weiss, P. S.; Xu, C.; Yuste, R.; Zhuang, X., Nanotools for neuroscience

and brain activity mapping. *ACS Nano* **2013,** *7* (3), 1850-66. https://doi.org/10.1021/nn4012847

37. Watson, C. J.; Venton, B. J.; Kennedy, R. T., In vivo measurements of neurotransmitters by microdialysis sampling. *Anal. Chem.* **2006,** *78* (5), 1391-1399. https://doi.org/10.1021/ac0693722

38. Bucher, E. S.; Wightman, R. M., Electrochemical analysis of neurotransmitters. *Annu. Rev. Anal. Chem.* **2015,** *8* (1), 239-261. https://doi.org/10.1146/annurev-anchem-071114-040426

39. Su, Y.; Bian, S.; Sawan, M., Real-time in vivo detection techniques for neurotransmitters: A review. *Analyst* **2020,** *145* (19), 6193-6210. https://doi.org/10.1039/D0AN01175D

40. Logman, M. J.; Budygin, E. A.; Gainetdinov, R. R.; Wightman, R. M., Quantitation of in vivo measurements with carbon fiber microelectrodes. *J. Neurosci. Methods* **2000,** *95* (2), 95-102. https://doi.org/10.1016/s0165-0270(99)00155-7

41. Singh, Y. S.; Sawarynski, L. E.; Dabiri, P. D.; Choi, W. R.; Andrews, A. M., Head-to-head comparisons of carbon fiber microelectrode coatings for sensitive and selective neurotransmitter detection by voltammetry. *Anal. Chem.* **2011,** *83* (17), 6658-6666. https://doi.org/10.1021/ac2011729

42. Puthongkham, P.; Venton, B. J., Recent advances in fast-scan cyclic voltammetry. *Analyst* **2020,** *145* (4), 1087-1102. https://doi.org/10.1039/c9an01925a

43. Bunin, M. A.; Prioleau, C.; Mailman, R. B.; Wightman, R. M., Release and uptake rates of 5-hydroxytryptamine in the dorsal raphe and substantia nigra reticulata of the rat brain.

J. Neurochem. **1998,** *70* (3), 1077-1087. https://doi.org/10.1046/j.1471-4159.1998.70031077.x

44. Walters, S. H.; Shu, Z.; Michael, A. C.; Levitan, E. S., Regional variation in striatal dopamine spillover and release plasticity. *ACS Chem. Neurosci.* **2020,** *11* (6), 888-899. https://doi.org/10.1021/acschemneuro.9b00577

45. Nakatsuka, N.; Andrews, A. M., Differentiating siblings: The case of dopamine and norepinephrine. *ACS Chem. Neurosci.* **2017,** *8* (2), 218-220. https://doi.org/10.1021/acschemneuro.7b00056

46. Heien, M. L. A. V.; Khan, A. S.; Ariansen, J. L.; Cheer, J. F.; Phillips, P. E. M.; Wassum, K. M.; Wightman, R. M., Real-time measurement of dopamine fluctuations after cocaine in the brain of behaving rats. *Proc. Natl. Acad. Sci. U.S.A.* **2005,** *102* (29), 10023-10028. https://doi.org/10.1073/pnas.0504657102

47. Venton, B. J.; Cao, Q., Fundamentals of fast-scan cyclic voltammetry for dopamine detection. *Analyst* **2020,** *145* (4), 1158-1168. https://doi.org/10.1039/C9AN01586H

48. Dunham, K. E.; Venton, B. J., Improving serotonin fast-scan cyclic voltammetry detection: New waveforms to reduce electrode fouling. *Analyst* **2020,** *145* (22), 7437-7446. https://doi.org/10.1039/D0AN01406K

49. Atcherley, C. W.; Laude, N. D.; Parent, K. L.; Heien, M. L., Fast-scan controlled-adsorption voltammetry for the quantification of absolute concentrations and adsorption dynamics. *Langmuir* **2013,** *29* (48), 14885-92. https://doi.org/10.1021/la402686s

50. West, A.; Best, J.; Abdalla, A.; Nijhout, H. F.; Reed, M.; Hashemi, P., Voltammetric evidence for discrete serotonin circuits, linked to specific reuptake domains, in the mouse

medial prefrontal cortex. *Neurochem. Int.* **2019,** *123*, 50-58. https://doi.org/10.1016/j.neuint.2018.07.004

51. Dengler, A. K.; McCarty, G. S., Microfabricated microelectrode sensor for measuring background and slowly changing dopamine concentrations. *J. Electroanal. Chem.* **2013,** *693*, 28-33. https://doi.org/10.1016/j.jelechem.2013.01.022

52. Kim, S. Y.; Oh, Y. B.; Shin, H. J.; Kim, D. H.; Kim, I. Y.; Bennet, K.; Lee, K. H.; Jang, D. P., 5-hydroxytryptamine measurement using paired pulse voltammetry. *Biomed. Eng. Lett* **2013,** *3* (2), 102-108. https://doi.org/10.1007/s13534-013-0093-z

53. Meunier, C. J.; McCarty, G. S.; Sombers, L. A., Drift subtraction for fast-scan cyclic voltammetry using double-waveform partial-least-squares regression. *Anal. Chem.* **2019,** *91* (11), 7319-7327. https://doi.org/10.1021/acs.analchem.9b01083

54. Calhoun, S. E.; Meunier, C. J.; Lee, C. A.; McCarty, G. S.; Sombers, L. A., Characterization of a multiple-scan-rate voltammetric waveform for real-time detection of met-enkephalin. *ACS Chem. Neurosci.* **2019,** *10* (4), 2022-2032. https://doi.org/10.1021/acschemneuro.8b00351

55. Meunier, C. J.; Mitchell, E. C.; Roberts, J. G.; Toups, J. V.; McCarty, G. S.; Sombers, L. A., Electrochemical selectivity achieved using a double voltammetric waveform and partial least squares regression: Differentiating endogenous hydrogen peroxide fluctuations from shifts in pH. *Anal. Chem.* **2018,** *90* (3), 1767-1776. https://doi.org/10.1021/acs.analchem.7b03717

56. Oh, Y.; Heien, M. L.; Park, C.; Kang, Y. M.; Kim, J.; Boschen, S. L.; Shin, H.; Cho, H. U.; Blaha, C. D.; Bennet, K. E.; Lee, H. K.; Jung, S. J.; Kim, I. Y.; Lee, K. H.; Jang, D. P., Tracking tonic dopamine levels in vivo using multiple cyclic square wave

voltammetry. *Biosens. Bioelectron.* **2018,** *121*, 174-182. https://doi.org/10.1016/j.bios.2018.08.034

57. Park, C.; Oh, Y.; Shin, H.; Kim, J.; Kang, Y.; Sim, J.; Cho, H. U.; Lee, H. K.; Jung, S. J.; Blaha, C. D.; Bennet, K. E.; Heien, M. L.; Lee, K. H.; Kim, I. Y.; Jang, D. P., Fast cyclic square-wave voltammetry to enhance neurotransmitter selectivity and sensitivity. *Anal. Chem.* **2018,** *90* (22), 13348-13355. https://doi.org/10.1021/acs.analchem.8b02920

58. Shin, H.; Oh, Y.; Park, C.; Kang, Y.; Cho, H. U.; Blaha, C. D.; Bennet, K. E.; Heien, M. L.; Kim, I. Y.; Lee, K. H.; Jang, D. P., Sensitive and selective measurement of serotonin in vivo using fast cyclic square-wave voltammetry. *Anal. Chem.* **2020,** *92* (1), 774-781. https://doi.org/10.1021/acs.analchem.9b03164

59. Swamy, B. E. K.; Venton, B. J., Carbon nanotube-modified microelectrodes for simultaneous detection of dopamine and serotoninin vivo. *Analyst* **2007,** *132* (9), 876-884. https://doi.org/10.1039/B705552H

60. Zhou, F.-M.; Liang, Y.; Salas, R.; Zhang, L.; De Biasi, M.; Dani, J. A., Corelease of dopamine and serotonin from striatal dopamine terminals. *Neuron* **2005,** *46* (1), 65-74. https://doi.org/10.1016/j.neuron.2005.02.010

61. Hermans, A.; Keithley, R. B.; Kita, J. M.; Sombers, L. A.; Wightman, R. M., Dopamine detection with fast-scan cyclic voltammetry used with analog background subtraction. *Anal. Chem.* **2008,** *80* (11), 4040-4048. https://doi.org/10.1021/ac800108j

62. Heien, M. L. A. V.; Johnson, M. A.; Wightman, R. M., Resolving neurotransmitters detected by fast-scan cyclic voltammetry. *Anal. Chem.* **2004,** *76* (19), 5697-5704. https://doi.org/10.1021/ac0491509

63. Keithley, R. B.; Mark Wightman, R.; Heien, M. L., Multivariate concentration determination using principal component regression with residual analysis. *TrAC, Trends Anal. Chem.* **2009,** *28* (9), 1127-1136. https://doi.org/10.1016/j.trac.2009.07.002

64. Wold, S.; Sjöström, M.; Eriksson, L., PLS-regression: A basic tool of chemometrics. *Chemom. Intell. Lab. Syst* **2001,** *58* (2), 109-130. https://doi.org/10.1016/S0169-7439(01)00155-1

65. Kim, J.; Oh, Y.; Park, C.; Kang, Y. M.; Shin, H.; Kim, I. Y.; Jang, D. P., Comparison study of partial least squares regression analysis and principal component analysis in fast-scan cyclic voltammetry. *Int. J. Electrochem. Sci.* **2019,** *14* (7), 5924-5937. https://doi.org/10.20964/2019.07.03

66. Kishida, K. T.; Saez, I.; Lohrenz, T.; Witcher, M. R.; Laxton, A. W.; Tatter, S. B.; White, J. P.; Ellis, T. L.; Phillips, P. E. M.; Montague, P. R., Subsecond dopamine fluctuations in human striatum encode superposed error signals about actual and counterfactual reward. *Proc. Natl. Acad. Sci. U.S.A.* **2016,** *113* (1), 200-205. https://doi.org/10.1073/pnas.1513619112

67. Kishida, K. T.; Sandberg, S. G.; Lohrenz, T.; Comair, Y. G.; Sáez, I.; Phillips, P. E. M.; Montague, P. R., Sub-second dopamine detection in human striatum. *PLOS ONE* **2011,** *6* (8), e23291. https://doi.org/10.1371/journal.pone.0023291

68. Bang, D.; Kishida, K. T.; Lohrenz, T.; White, J. P.; Laxton, A. W.; Tatter, S. B.; Fleming, S. M.; Montague, P. R., Sub-second dopamine and serotonin signaling in human striatum during perceptual decision-making. *Neuron* **2020,** *108* (5), 999-1010.e6. https://doi.org/10.1016/j.neuron.2020.09.015

69. Moran, R. J.; Kishida, K. T.; Lohrenz, T.; Saez, I.; Laxton, A. W.; Witcher, M. R.; Tatter, S. B.; Ellis, T. L.; Phillips, P. E. M.; Dayan, P.; Montague, P. R., The protective action encoding of serotonin transients in the human brain. *Neuropsychopharmacology* **2018,** *43* (6), 1425-1435. https://doi.org/10.1038/npp.2017.304

70. Winquist, F.; Wide, P.; Lundström, I., An electronic tongue based on voltammetry. *Anal. Chim. Acta* **1997,** *357* (1), 21-31. https://doi.org/10.1016/S0003-2670(97)00498-4

71. Campos, I.; Masot, R.; Alcañiz, M.; Gil, L.; Soto, J.; Vivancos, J. L.; García-Breijo, E.; Labrador, R. H.; Barat, J. M.; Martínez-Mañez, R., Accurate concentration determination of anions nitrate, nitrite and chloride in minced meat using a voltammetric electronic tongue. *Sens. Actuators, B* **2010,** *149* (1), 71-78. https://doi.org/10.1016/j.snb.2010.06.028

72. Labrador, R. H.; Masot, R.; Alcañiz, M.; Baigts, D.; Soto, J.; Martínez-Mañez, R.; García-Breijo, E.; Gil, L.; Barat, J. M., Prediction of NaCl, nitrate and nitrite contents in minced meat by using a voltammetric electronic tongue and an impedimetric sensor. *Food Chem.* **2010,** *122* (3), 864-870. https://doi.org/10.1016/j.foodchem.2010.02.049

73. Ivarsson, P.; Holmin, S.; Höjer, N.-E.; Krantz-Rülcker, C.; Winquist, F., Discrimination of tea by means of a voltammetric electronic tongue and different applied waveforms. *Sens. Actuators, B* **2001,** *76* (1), 449-454. https://doi.org/10.1016/S0925-4005(01)00583-4

74. Winquist, F.; Krantz-Rülcker, C.; Wide, P.; Lundström, I., Monitoring of freshness of milk by an electronic tongue on the basis of voltammetry. *Meas Sci Technol* **1998,** *9* (12), 1937-1946. https://doi.org/10.1088/0957-0233/9/12/002

75. Ciosek, P.; Wróblewski, W., Sensor arrays for liquid sensing–electronic tongue systems. *Analyst* **2007,** *132* (10), 963-978. https://doi.org/10.1039/B705107G

76. Campos, I.; Alcañiz, M.; Masot, R.; Soto, J.; Martínez-Máñez, R.; Vivancos, J.-L.; Gil, L., A method of pulse array design for voltammetric electronic tongues. *Sens. Actuators, B* **2012,** *161* (1), 556-563. https://doi.org/10.1016/j.snb.2011.10.075

77. Fuentes, E.; Alcañiz, M.; Contat, L.; Baldeón, E. O.; Barat, J. M.; Grau, R., Influence of potential pulses amplitude sequence in a voltammetric electronic tongue (VET) applied to assess antioxidant capacity in aliso. *Food Chem.* **2017,** *224*, 233-241. https://doi.org/10.1016/j.foodchem.2016.12.076

78. Tian, S.-Y.; Deng, S.-P.; Chen, Z.-X., Multifrequency large amplitude pulse voltammetry: A novel electrochemical method for electronic tongue. *Sens. Actuators, B* **2007,** *123* (2), 1049-1056. https://doi.org/10.1016/j.snb.2006.11.011

79. Vreeland, R. F.; Atcherley, C. W.; Russell, W. S.; Xie, J. Y.; Lu, D.; Laude, N. D.; Porreca, F.; Heien, M. L., Biocompatible PEDOT:Nafion composite electrode coatings for selective detection of neurotransmitters in vivo. *Anal. Chem.* **2015,** *87* (5), 2600-2607. https://doi.org/10.1021/ac502165f

80. Sampson, M. M.; Yang, H.; Andrews, A. M., Advanced microdialysis approaches resolve differences in serotonin homeostasis and signaling. In *Compendium of in vivo monitoring in real-time molecular neuroscience*, WORLD SCIENTIFIC: 2017; pp 119-140.

81. Pedregosa, F.; Varoquaux, G.; Gramfort, A.; Michel, V.; Thirion, B.; Grisel, O.; Blondel, M.; Prettenhofer, P.; Weiss, R.; Dubourg, V., Scikit-learn: Machine learning in Python. *J. Mach. Learn. Res.* **2011,** *12*, 2825-2830.

82. Heien, M. L. A. V.; Phillips, P. E. M.; Stuber, G. D.; Seipel, A. T.; Wightman, R. M., Overoxidation of carbon-fiber microelectrodes enhances dopamine adsorption and increases sensitivity. *Analyst* **2003,** *128* (12), 1413-1419. https://doi.org/10.1039/B307024G

83. Jackson, B. P.; Dietz, S. M.; Wightman, R. M., Fast-scan cyclic voltammetry of 5-hydroxytryptamine. *Anal. Chem.* **1995,** *67* (6), 1115-20. https://doi.org/10.1021/ac00102a015

84. Kramer, R., *Chemometric techniques for quantitative analysis*. CRC Press: Boca Raton, FL, 1998.

85. Chong, I.-G.; Jun, C.-H., Performance of some variable selection methods when multicollinearity is present. *Chemom. Intell. Lab. Syst* **2005,** *78* (1), 103-112. https://doi.org/10.1016/j.chemolab.2004.12.011

86. Ivarsson, P.; Johansson, M.; Höjer, N.-E.; Krantz-Rülcker, C.; Winquist, F.; Lundström, I., Supervision of rinses in a washing machine by a voltammetric electronic tongue. *Sens. Actuators, B* **2005,** *108* (1), 851-857. https://doi.org/10.1016/j.snb.2004.12.088

87. Winquist, F., Voltammetric electronic tongues – basic principles and applications. *Microchim. Acta* **2008,** *163* (1), 3-10. https://doi.org/10.1007/s00604-007-0929-2

88. Montague, P. R.; Kishida, K. T., Computational underpinnings of neuromodulation in humans. *Cold Spring Harbor Symp. Quant. Biol.* **2018,** *83*, 71-82. https://doi.org/10.1101/sqb.2018.83.038166

89. Hastie, T.; Tibshirani, R.; Friedman, J. H., *The elements of statistical learning: Data mining, inference, and prediction*. 2nd ed.; Springer: New York, NY, 2001.

90. Kawagoe, K. T.; Zimmerman, J. B.; Wightman, R. M., Principles of voltammetry and microelectrode surface states. *J. Neurosci. Methods* **1993,** *48* (3), 225-240. https://doi.org/10.1016/0165-0270(93)90094-8

91. Yang, H.; Sampson, M. M.; Senturk, D.; Andrews, A. M., Sex- and SERT-mediated differences in stimulated serotonin revealed by fast microdialysis. *ACS Chem. Neurosci.* **2015,** *6* (8), 1487-1501. https://doi.org/10.1021/acschemneuro.5b00132

92. Yang, H.; Thompson, A. B.; McIntosh, B. J.; Altieri, S. C.; Andrews, A. M., Physiologically relevant changes in serotonin resolved by fast microdialysis. *ACS Chem. Neurosci.* **2013,** *4* (5), 790-8. https://doi.org/10.1021/cn400072f

93. O'Neill, B.; Patel, J. C.; Rice, M. E., Characterization of optically and electrically evoked dopamine release in striatal slices from digenic knock-in mice with DAT-driven expression of channelrhodopsin. *ACS Chem. Neurosci.* **2017,** *8* (2), 310-319. https://doi.org/10.1021/acschemneuro.6b00300

94. Martens, H. A.; Dardenne, P., Validation and verification of regression in small data sets. *Chemom. Intell. Lab. Syst* **1998,** *44* (1), 99-121. https://doi.org/10.1016/S0169-7439(98)00167-1

95. Braga-Neto, U. M.; Dougherty, E. R., Is cross-validation valid for small-sample microarray classification? *Bioinformatics* **2004,** *20* (3), 374-380. https://doi.org/10.1093/bioinformatics/btg419

96. Isaksson, A.; Wallman, M.; Göransson, H.; Gustafsson, M. G., Cross-validation and bootstrapping are unreliable in small sample classification. *Pattern Recognit. Lett.* **2008,** *29* (14), 1960-1965. https://doi.org/10.1016/j.patrec.2008.06.018

97. Varoquaux, G., Cross-validation failure: Small sample sizes lead to large error bars. *NeuroImage* **2018,** *180*, 68-77. https://doi.org/10.1016/j.neuroimage.2017.06.061

98. Ng, A. Y. In *Preventing "overfitting" of cross-validation data*, International Conference on Machine Learning (ICML), Citeseer: 1997; pp 245-253.

99. Zhang, L.; Doyon, W. M.; Clark, J. J.; Phillips, P. E.; Dani, J. A., Controls of tonic and phasic dopamine transmission in the dorsal and ventral striatum. *Mol. Pharmacol.* **2009,** *76* (2), 396-404. https://doi.org/10.1124/mol.109.056317

100. Brimblecombe, K. R.; Cragg, S. J., The striosome and matrix compartments of the striatum: A path through the labyrinth from neurochemistry toward function. *ACS Chem. Neurosci.* **2017,** *8* (2), 235-242. https://doi.org/10.1021/acschemneuro.6b00333

101. Hill, D. F.; Parent, K. L.; Atcherley, C. W.; Cowen, S. L.; Heien, M. L., Differential release of dopamine in the nucleus accumbens evoked by low-versus high-frequency medial prefrontal cortex stimulation. *Brain Stimul.* **2018,** *11* (2), 426-434. https://doi.org/10.1016/j.brs.2017.11.010

102. Wightman, R. M.; Amatorh, C.; Engstrom, R. C.; Hale, P. D.; Kristensen, E. W.; Kuhr, W. G.; May, L. J., Real-time characterization of dopamine overflow and uptake in the rat striatum. *Neuroscience* **1988,** *25* (2), 513-523. https://doi.org/10.1016/0306-4522(88)90255-2

103. Mathews, T. A.; Fedele, D. E.; Coppelli, F. M.; Avila, A. M.; Murphy, D. L.; Andrews, A. M., Gene dose-dependent alterations in extraneuronal serotonin but not dopamine in mice with reduced serotonin transporter expression. *J. Neurosci. Methods* **2004,** *140* (1-2), 169-81. https://doi.org/10.1016/j.jneumeth.2004.05.017

104. Daws, L. C.; Toney, G. M.; Davis, D. J.; Gerhardt, G. A.; Frazer, A., In vivo chronoamperometric measurements of the clearance of exogenously applied serotonin in the rat dentate gyrus. *J. Neurosci. Methods* **1997,** *78* (1), 139-150. https://doi.org/10.1016/S0165-0270(97)00144-1

105. Wood, K. M.; Hashemi, P., Fast-scan cyclic voltammetry analysis of dynamic serotonin reponses to acute escitalopram. *ACS Chem. Neurosci.* **2013,** *4* (5), 715-720. https://doi.org/10.1021/cn4000378

106. Dawson, L. A.; Watson, J. M., Vilazodone: A 5-HT1A receptor agonist/serotonin transporter inhibitor for the treatment of affective disorders. *CNS Neurosci. Ther.* **2009,** *15* (2), 107-117. https://doi.org/10.1111/j.1755-5949.2008.00067.x

107. Gartside, S. E.; Umbers, V.; Hajós, M.; Sharp, T., Interaction between a selective 5-HT1A receptor antagonist and an SSRI in vivo: Effects on 5-HT cell firing and extracellular 5-HT. *Br. J. Pharmacol.* **1995,** *115* (6), 1064-1070. https://doi.org/10.1111/j.1476-5381.1995.tb15919.x

108. Owens, M. J.; Knight, D. L.; Nemeroff, C. B., Second-generation SSRIs: Human monoamine transporter binding profile of escitalopram and R-fluoxetine. *Biol. Psychiatry* **2001,** *50* (5), 345-50. https://doi.org/10.1016/s0006-3223(01)01145-3

109. Conio, B.; Martino, M.; Magioncalda, P.; Escelsior, A.; Inglese, M.; Amore, M.; Northoff, G., Opposite effects of dopamine and serotonin on resting-state networks: Review and implications for psychiatric disorders. *Mol. Psychiatry* **2020,** *25* (1), 82-93. https://doi.org/10.1038/s41380-019-0406-4

110. Watabe-Uchida, M.; Zhu, L.; Ogawa, Sachie K.; Vamanrao, A.; Uchida, N., Whole-brain mapping of direct inputs to midbrain dopamine neurons. *Neuron* **2012,** *74* (5), 858-873. https://doi.org/10.1016/j.neuron.2012.03.017

111. Alex, K. D.; Pehek, E. A., Pharmacologic mechanisms of serotonergic regulation of dopamine neurotransmission. *Pharmacology & Therapeutics* **2007,** *113* (2), 296-320. https://doi.org/10.1016/j.pharmthera.2006.08.004

112. Navailles, S.; De Deurwaerdère, P., Presynaptic control of serotonin on striatal dopamine function. *Psychopharmacology (Berl)* **2011,** *213* (2), 213-242. https://doi.org/10.1007/s00213-010-2029-y

113. Smith, G. S.; Ma, Y.; Dhawan, V.; Chaly, T.; Eidelberg, D., Selective serotonin reuptake inhibitor (SSRI) modulation of striatal dopamine measured with [11C]-raclopride and positron emission tomography. *Synapse* **2009,** *63* (1), 1-6. https://doi.org/10.1002/syn.20574

114. Warwick, J. M.; Carey, P. D.; Cassimjee, N.; Lochner, C.; Hemmings, S.; Moolman-Smook, H.; Beetge, E.; Dupont, P.; Stein, D. J., Dopamine transporter binding in social anxiety disorder: The effect of treatment with escitalopram. *Metab. Brain Dis.* **2012,** *27* (2), 151-158. https://doi.org/10.1007/s11011-012-9280-3

115. de Win, M. M. L.; Habraken, J. B. A.; Reneman, L.; van den Brink, W.; den Heeten, G. J.; Booij, J., Validation of [123I]β-CIT SPECT to assess serotonin transporters in vivo in humans: A double-blind, placebo-controlled, crossover study with the selective serotonin reuptake inhibitor citalopram. *Neuropsychopharmacology* **2005,** *30* (5), 996-1005. https://doi.org/10.1038/sj.npp.1300683

116. Altieri, S. C.; Yang, H.; O'Brien, H. J.; Redwine, H. M.; Senturk, D.; Hensler, J. G.; Andrews, A. M., Perinatal vs genetic programming of serotonin states associated with anxiety. *Neuropsychopharmacology* **2015,** *40* (6), 1456-70. https://doi.org/10.1038/npp.2014.331

117. Hashemi, P.; Dankoski, E. C.; Petrovic, J.; Keithley, R. B.; Wightman, R. M., Voltammetric detection of 5-hydroxytryptamine release in the rat brain. *Anal. Chem.* **2009,** *81* (22), 9462-71. https://doi.org/10.1021/ac9018846

118. Rodeberg, N. T.; Sandberg, S. G.; Johnson, J. A.; Phillips, P. E. M.; Wightman, R. M., Hitchhiker's guide to voltammetry: Acute and chronic electrodes for in vivo fast-scan cyclic voltammetry. *ACS Chem. Neurosci.* **2017,** *8* (2), 221-234. https://doi.org/10.1021/acschemneuro.6b00393

119. Loewinger, G.; Patil, P.; Kishida, K. T.; Parmigiani, G., Multi-study learning for real-time neurochemical sensing in humans using the "study strap ensemble". *bioRxiv* **2021**, 856385. https://doi.org/10.1101/856385

120. Johnson, J. A.; Hobbs, C. N.; Wightman, R. M., Removal of differential capacitive interferences in fast-scan cyclic voltammetry. *Anal. Chem.* **2017,** *89* (11), 6166-6174. https://doi.org/10.1021/acs.analchem.7b01005

121. Gardier, A. M.; David, D. J.; Jego, G.; Przybylski, C.; Jacquot, C.; Durier, S.; Gruwez, B.; Douvier, E.; Beauverie, P.; Poisson, N.; Hen, R.; Bourin, M., Effects of chronic paroxetine treatment on dialysate serotonin in 5-HT1B receptor knockout mice. *J. Neurochem.* **2003,** *86* (1), 13-24. https://doi.org/10.1046/j.1471-4159.2003.01827.x

122. Meiser, J.; Weindl, D.; Hiller, K., Complexity of dopamine metabolism. *Cell Commun. Signal* **2013,** *11* (1), 34. https://doi.org/10.1186/1478-811X-11-34

123. Mohammad-Zadeh, L. F.; Moses, L.; Gwaltney-Brant, S. M., Serotonin: A review. *J. Vet. Pharmacol. Ther.* **2008,** *31* (3), 187-199. https://doi.org/10.1111/j.1365-2885.2008.00944.x

124. Qi, Z.; Miller, G. W.; Voit, E. O., Mathematical models of dopamine metabolism in parkinson's disease. In *Systems biology of Parkinson's disease*, Wellstead, P.; Cloutier, M., Eds. Springer New York: New York, NY, 2012; pp 151-171.

125. Takmakov, P.; Zachek, M. K.; Keithley, R. B.; Bucher, E. S.; McCarty, G. S.; Wightman, R. M., Characterization of local pH changes in brain using fast-scan cyclic voltammetry with carbon microelectrodes. *Anal. Chem.* **2010,** *82* (23), 9892-9900. https://doi.org/10.1021/ac102399n

126. Yoshimi, K.; Weitemier, A., Temporal differentiation of pH-dependent capacitive current from dopamine. *Anal. Chem.* **2014,** *86* (17), 8576-8584. https://doi.org/10.1021/ac500706m

127. Gerhardt, G. A.; Hoffman, A. F., Effects of recording media composition on the responses of Nafion-coated carbon fiber microelectrodes measured using high-speed chronoamperometry. *J. Neurosci. Methods* **2001,** *109* (1), 13-21. https://doi.org/10.1016/S0165-0270(01)00396-X

128. Fu, G.-H.; Xu, Q.-S.; Li, H.-D.; Cao, D.-S.; Liang, Y.-Z., Elastic net grouping variable selection combined with partial least squares regression (EN-PLSR) for the analysis of strongly multi-collinear spectroscopic data. *Appl. Spectrosc.* **2011,** *65* (4), 402-408. https://doi.org/10.1366/10-06069

129. Giglio, C.; Brown, S. D., Using elastic net regression to perform spectrally relevant variable selection. *J. Chemom.* **2018,** *32* (8), e3034. https://doi.org/10.1002/cem.3034

130. Vasudevan, R. K.; Ziatdinov, M.; Vlcek, L.; Kalinin, S. V., Off-the-shelf deep learning is not enough, and requires parsimony, Bayesianity, and causality. *Npj Comput. Mater.* **2021,** *7* (1), 16. https://doi.org/10.1038/s41524-020-00487-0

131. Carleo, G.; Cirac, I.; Cranmer, K.; Daudet, L.; Schuld, M.; Tishby, N.; Vogt-Maranto, L.; Zdeborová, L., Machine learning and the physical sciences. *Rev. Mod. Phys.* **2019,** *91* (4), 045002. https://doi.org/10.1103/RevModPhys.91.045002

132. Gundry, L.; Guo, S.-X.; Kennedy, G.; Keith, J.; Robinson, M.; Gavaghan, D.; Bond, A. M.; Zhang, J., Recent advances and future perspectives for automated parameterisation, Bayesian inference and machine learning in voltammetry. *Chem. Comm.* **2021,** *57* (15), 1855-1870. https://doi.org/10.1039/D0CC07549C

133. Bond, A. M., A perceived paucity of quantitative studies in the modern era of voltammetry: Prospects for parameterisation of complex reactions in Bayesian and machine learning frameworks. *J Solid State Electrochem.* **2020,** *24* (9), 2041-2050. https://doi.org/10.1007/s10008-020-04639-6

134. Matsushita, G. H. G.; Sugi, A. H.; Costa, Y. M. G.; Gomez-A, A.; Da Cunha, C.; Oliveira, L. S., Phasic dopamine release identification using convolutional neural network. *Comput. Biol. Med.* **2019,** *114*, 103466. https://doi.org/10.1016/j.compbiomed.2019.103466

135. Ye, J.-J.; Lin, C.-H.; Huang, X.-J., Analyzing the anodic stripping square wave voltammetry of heavy metal ions via machine learning: Information beyond a single voltammetric peak. *J. Electroanal. Chem.* **2020,** *872*, 113934. https://doi.org/10.1016/j.jelechem.2020.113934

Chapter 4

Maximizing electrochemical information: A perspective on background-inclusive fast voltammetry

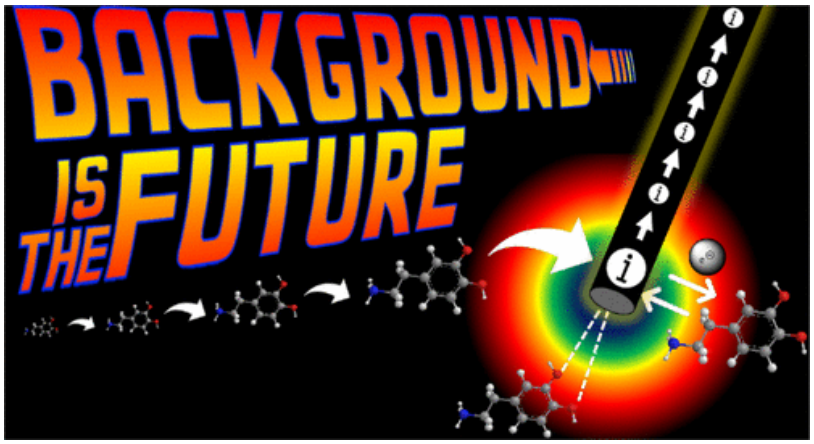

The information in this chapter is adapted with permission from

Movassaghi, C.S.; Alcañiz, M.; Kishida, K.T.; McCarty, G.; Sombers, L.A.; Wassum, K.M.; Andrews, A.M. Maximizing electrochemical information: A perspective on background-inclusive fast voltammetry. *Analytical Chemistry.* **96**, 6097-6105 (2024).

4.1 ABSTRACT

This Perspective encompasses a focused review of the literature leading to a tipping point in electroanalytical chemistry. We tie together the threads of a “revolution” quietly in the making for years through the work of many authors. Long-held misconceptions about the use of background subtraction in fast voltammetry are addressed. We lay out future advantages that accompany background-inclusive voltammetry, particularly when paired with modern machine-learning algorithms for data analysis.

4.2 INTRODUCTION.

Background subtraction for bioanalytical voltammetry was first reported in the 1980s.[1,2] Its purpose, as originally described, was to increase signal-to-noise or otherwise aid in visualizing small faradaic currents (tens of nanoamperes (nA) or less) produced by neurotransmitter release associated with biological stimulus events. Small, analyte-related currents occur amid large capacitive currents (hundreds of nA) produced by the high scan rates used in fast-scan cyclic voltammetry (FSCV). For almost four decades, background subtraction has been de rigueur in fast voltammetry (*e.g.,* FSCV,[3,4] FSCAV,[5] FCSWV[6]). Today, even the smallest stimulus peaks associated with endogenous transients can be readily identified by fast voltammetry and related techniques with modern data acquisition and analysis capabilities.[7-10]

While often discarded, background currents can be sources of electrochemical information for analyte identification.[11-15] Moreover, retaining background currents overcomes a pitfall associated with fast voltammetry–the inability to use the same waveform to measure basal neurotransmitter levels and stimulus-related events contemporaneously.

"The study of basal levels of neurotransmitters and their dynamics requires a means of isolating the portion of the background current arising from neurotransmitter redox reactions."

–Johnson *et al*. **2018**[16]

In this perspective, we delve into the practice of background subtraction, developed during a period when electronic sampling and computational capabilities were less advanced. We outline

the advantages of forgoing background subtraction, at least under some circumstances. While we frame this perspective in the context of neurochemical detection, the ideas developed are relevant to voltammetry for other types of analytes.

Background currents are comprised of faradaic and non-faradaic contributions and noise (*e.g.,* electrical, environmental). In neurochemical studies, the background current is represented by a voltammogram relative to a paired experimental stimulus event and is commonly determined within a 30-90 s recording window immediately before event recording. Background voltammograms are often averages of consecutive pre-stimulus scans (*e.g.,* 5-10 voltammograms), which improves the signal-to-noise ratio for background-subtracted traces. The process of background subtraction produces differential measurements (*i.e.*, determinations of current after *vs.* before a defined time point). The applicability of the defined background current relative to the length of the recording window depends on signal stability and other factors discussed below.

***Pitfalls associated with background subtraction*.** Seminal papers on background subtraction explicitly stated that its purpose was to facilitate peak visualization and calibration when manual peak selection and integration were often required.[1] Based on its original purpose, we suggest background subtraction may no longer be needed. Moreover, in some cases, information inherent in background currents can be used to improve analyte identification and quantitation, particularly for multi-analyte detection.

We suspect that background subtraction remains prevalent partly because the term is somewhat of a misnomer. That is, background subtraction is not background correction. Background subtraction can not remove dynamic nonspecific current contributions. Thus, it may

not result in selective analyte current. Nonetheless, background subtraction is often employed with the underlying implication that analyte-specific faradaic current changes remain after stimulus events.[17] During the recording period after a stimulus, however, the concentrations of non-target analytes (*i.e.*, interferents) and ions at the electrode surface change in response to the stimulus. Some of these species are redox-active (*e.g.*, neurotransmitter metabolites). As such, they contribute to nonspecific changes in faradaic current. Other species, while not electrochemically active, affect electrical double-layer behavior and thus, contribute to changes in non-faradaic current. While non-charged, non-electroactive species (*e.g*., glucose) do not directly affect current responses in physiological media,[18] such species can impact electrode surface accessibility.

In neurochemistry, any type of stimulus contributes to nonspecific current changes, including stimuli delivered *in vivo (e.g.,* behavioral stimuli), *ex vivo* (*e.g.*, tissue slice electrical or optical stimulation), or *in vitro (e.g*., single-cell analyses involving spritzing with secretagogues). Changes in the concentrations of charged molecules and ions, whether electroactive or not, affect capacitive currents due to uncompensated resistance. Fluctuations occur in the concentrations of ions inherent in the processes underlying neurotransmitter release and reuptake (*e.g.,* pH shifts and ion changes tied to action potentials, Na^+/K^+ ATPase activity, and active transport). Background subtraction cannot correct for the effects of these dynamic processes.[19] A few clever yet cumbersome approaches to correct partially for nonspecific current dynamics exist, as studied by Johnson and colleagues.[20]

"FSCV data analysis typically employs digital subtraction of the background using the current measured before the neurobiological phenomena of interest. This method is effective for signal

isolation given background stability. However, if neurotransmitter release is accompanied by factors that affect the background, the subtracted data contain artifacts."

–Johnson *et al*. **2017**[20]

In best-case scenarios, background subtraction preserves much of the post-stimulus neurotransmitter-related data. However, background subtraction can remove relevant, or even introduce irrelevant, features. Wosiak and co-workers have investigated these effects.[17]

"Due to the existence of induced charging currents, the capacitive contribution to the total current is different from the capacitive current measured in the absence of electroactive species…Consequently, the conventional background subtraction method may be inaccurate in these situations."

–Wosiak *et al*. **2020**[17]

Additionally, background subtraction cannot correct for drift, which is dynamic during FSCV recording periods.[21] Several papers address the drift that remains after background subtraction.[22,23] While background subtraction can improve temporal current responses for short recording periods (*e.g*., <90 s), this approach assumes that drift is due solely to capacitive current instability that does not change measurably after the background is determined and over the recording period.[24] Newer, more effective approaches to deal with drift are aimed at extending the time frame of FSCV recordings.[22,23,25,26] However, as also noted by Johnson, the chemistry at the electrode surface is complicated and dependent on the surrounding microenvironment.[20]

"Interactions with the carbon surface, through either adsorption or involvement in surface reactions, may alter these responses and contribute to the background-subtracted

voltammograms. Indeed, nonfaradaic and faradaic currents have been seen in background-subtracted voltammograms taken during pH changes."

–Johnson *et al*. **2017**[20]

Background currents in voltammetry are inherently dynamic, which is at the root of these misconceptions. Changes occur in the background signal, defined as the current generated by everything except the analyte of interest, even on the timescale that background subtraction is employed. Background signals are impacted by changes in electrode surface chemistries (*e.g.*, analyte or interferant adsorption, electrode surface group oxidation, biofouling) and by changes in ion concentrations associated with action potentials, transporter-mediated reuptake ($[Na^+]$, $[K^+]$), and exocytosis ($[H^+]$, $[Ca^{2+}]$). Subtracting the background preceding stimulus events, although previously useful for improving peak identification, ignores these dynamic processes by incorrectly assuming a static microenvironment during the user-defined recording periods typical in FSCV (*e.g.,* 30-90 s). As we propose, background subtraction can also reduce predictive accuracy in certain cases. Indeed, previous studies have shown that background changes can lead to misinterpretations of biological findings.[27,28]

This is not to say that all voltammetry studies using background-subtracted approaches are invalid, nor that background-inclusive data is superior in all cases. Voltammetry would not have advanced without background subtraction. There is likely a "Goldilocks zone" where background-subtracted and non-background-subtracted interpretations largely agree.

We simply advocate reconsidering the significant information included in the background current. Data analyses using background subtraction *vs.* background inclusion are not mutually

exclusive; one can analyze and compare both approaches using the same data. However, as background-inclusive fast voltammetry has emerged relatively recently in neuroscience compared to its predecessor, few studies have compared these approaches directly.[11,29] Regardless of the approach employed, data must always be interpreted with caution. For in the words of statistician Goerge Box, all models are wrong, but some are useful.[30]

Regardless of whether background subtraction is used or not, there are pervasive issues for *in vivo* voltammetry. Perhaps the most significant is the difficulty in generalizing *in vitro* calibration data, including calibration parameters estimated by machine learning models, to *in vivo* data.

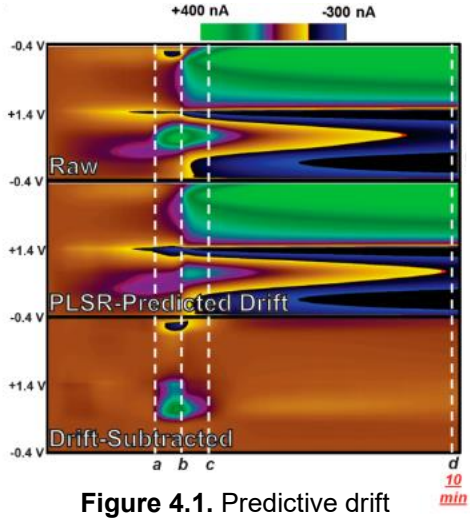

Figure 4.1. Predictive drift modeling generalizes *in vivo*. Reproduced from Meunier, C. J.; McCarty, G. S.; Sombers, L. A. *Anal. Chem.* **2019**, *91*, 7319-7327 (ref 23). Copyright 2019 American Chemical Society.

Here, we refer to machine learning models as those performing multivariate calibration – a supervised regression model (*e.g.,* principal components regression (PCR), partial least-squares regression (PLSR), elastic net, artificial neural network) is trained on voltammograms of known concentration to predict voltammograms of unknown concentration.[31] The inability to deploy background-subtracted models trained *in vitro* (*i.e.*, FSCV-PCR) to give consistent and reliable *in vivo* results has been demonstrated.[32-34] This failure is, in part, thought to be due to the adsorption of interferents, especially metal cations and electro-inactive species such as proteins, which are rarely accounted for.[19] No training paradigm can yet mimic the complex environment in the brain. However, even for a single analyte such as dopamine, a voltammetry technique paired with a suitable machine learning model that better bridges this *in vitro-in vivo* "generalization

gap" would be extremely powerful; the state-of-the-art in the field is moving towards this approach.[13,35-40] Background-inclusive models appear to be a critical step in reducing the generalization gap due to the underutilized information content in background currents, as discussed by Movassaghi and co-workers.[11]

"As such, differences in the Helmholtz double layer, mass transport, analyte concentrations and adsorption, and other dynamic electrode surface properties occurring during an applied pulse are considered potential sources of analyte-specific information. This information is encoded in the transient responses of faradaic and non-faradaic currents. By including faradaic and non-faradaic current responses as input to the model *(i.e.*, not background subtracting), the [model] selects aspects of the current response that covary with analyte identity and concentration. This is opposed to background-subtracted methods, where some information is discarded prior to model input to increase signal-to-noise. Potentially relevant information in the background is then lost."

–Movassaghi *et al.* **2021**[11]

Statistical approaches to domain generalization, adaptation, and transfer learning offer promising improvements over classical chemometric validation techniques such as residual analysis.[31,37,38,41,42] Nonetheless, some consider a barrier to the use of machine learning models in voltammetry the fact that the predictions can only be considered estimates until methods of ground-truth validation are possible. For neurochemical studies, *in vivo* experimental checks can inform predictive model selection and increase confidence and generalizability.[11] These include confirming how analyte concentrations correlate with stereotaxic electrode positioning, stimulation frequency, pharmacology, behavior, and comparisons with other *in vivo* neurochemical methods, *e.g.*, microdialysis.

Dealing with dynamics–let the machines learn: Given the shortcomings of background subtraction described above, how should chemists and neuroscientists deal with background signal dynamics that impede generalization? A logical solution is background correction.

However, background correction methods assume a temporally based parametric relationship within the signal that has the same issues of masking chemically interesting dynamics and can suffer similar pitfalls as background subtraction. A different approach to dealing with dynamic backgrounds is simply to train analysis models with the background current included (*i.e.,* do not background subtract). Meunier *et al.* have shown several demonstrations.[15,23]

"The model, validated both in adrenal slice and live brain tissue, enables information encoded in the shape of the background voltammogram to determine electrochemical parameters that are critical for accurate quantification."

–Meunier *et al*. **2017**[15]

Can machine learning models be effectively and accurately trained with dynamic backgrounds included? Or do dynamic backgrounds preclude the ability to obtain specific (*i.e*., trainable) electrochemical information? In machine learning terms, we aim to find a low-dimensional yet generalizable representation of the analytes, interferents, background current, irrelevant capacitive interference, *etc*. in the model. Sombers and coworkers have shown this is indeed possible, reporting a drift-prediction model that generalized across multiple electrodes (**Fig. 4.1**).[23]

"Thus, it is clearly possible to develop effective models for subtraction of drift from fast voltammetric data that are not specific to any given electrode, to reveal both rapid and gradual changes in analyte concentration over time."

–Meunier *et al*. **2019**[23]

Due to the prevalence of background subtraction for over three decades, suggesting its abstinence may seem controversial. Yet, in the last few years, avoiding background subtraction

has been shown to be more reliable and robust for dopamine predictions than background-subtracted FSCV in the hands of experienced users.[11,29] This is due to the application of modern machine learning methods that negate the need to use background subtraction to increase signal-to-noise. These pattern recognition algorithms are advanced enough to be trained on and to predict raw data extraordinarily accurately.

To lend additional credence to the idea of forgoing background subtraction, we point to studies in the mechanistic electrochemistry field. As opposed to using background-subtracted voltammograms to train machine learning models to predict analyte identity and concentration, fundamental electrochemistry studies use background-inclusive voltammograms to fit simulated and experimental data, including non-faradaic current.[43-45] These reports further demonstrate the utility of non-faradaic information in models of electrochemical processes beyond concentration quantification. For example, areas of voltammograms not typically used in the manual assignment of electrochemical reaction mechanisms are now being used by deep learning classifiers for automated mechanistic assignment.[46] Similar reports have emerged for fast voltammetry in terms of analyte quantification; *vide infra*.

The combined use of suitable supervised regression models and non-background subtracted voltammograms as training data has been demonstrated repeatedly in recent literature to be more powerful than using background-subtracted data. For example, Kishida *et al.* showed that conventional background-subtracted FSCV-principal components regression (PCR) predictions were both unreliable for dopamine at low concentrations and confused changes in pH for dopamine, when compared to an elastic net model trained with the same non-background subtracted data (**Fig. 4.2**).[29] Here, a pH change of 0.2 units resulted in a 250 nM dopamine prediction error (0 nM dopamine was present but 250 nM was predicted). Meanwhile, the non-

background subtracted data, when modeled, not only increased dopamine sensitivity (S/N ratio) but also did not confound pH for dopamine (roughly 0 nM dopamine was predicted for the same 0.2-unit pH change).

Importantly, a 'good' signal-to-noise ratio as defined by the human eye, for example following background subtraction, is not directly comparable to a 'good' signal-to-noise ratio for a machine learning model where signal-to-noise is not based on the single-point, amplitude-based metric used for classical calibration curves. For machine learning models, entire voltammograms, each described by thousands of data points, are now being analyzed. The impact is demonstrated by non-background-subtracted data yielding higher sensitivity than background-subtracted data. Movassaghi *et al*. recently reported findings on the improved performance of background-inclusive models when compared directly to background-subtracted models.[11] Further, Kishida *et al.* and Movassaghi *et al.* demonstrated that their models were using areas of the voltammograms normally discarded during background subtraction (*i.e.*, non-faradaic areas; **Fig. 4.3**).[11,29]

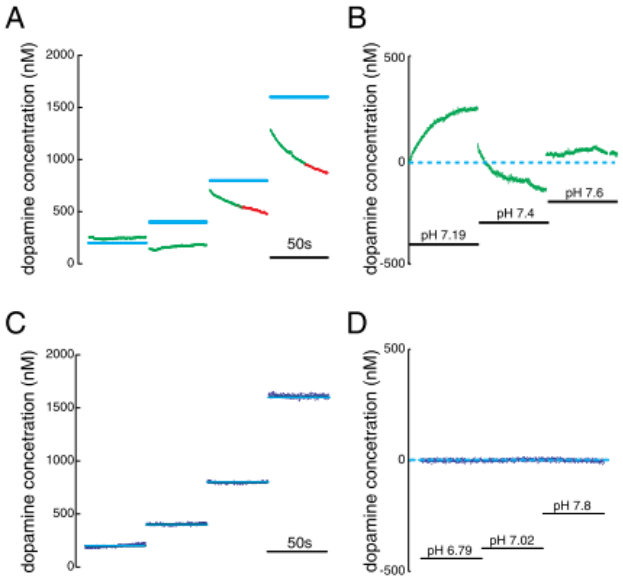

Figure 4.2. (A) Test set performance using an FSCV-PCR model trained on background subtracted voltammograms for varying dopamine concentrations at pH 7.4 and **(B)** versus varying pH at constant dopamine (0 nM). **(C,D)** The same test set performance using an FSCV-elastic net model trained on non-background subtracted data. Reproduced from Kishida, K. T.; Saez, I.; Lohrenz, T.; Witcher, M. R.; Laxton, A. W.; Tatter, S. B.; White, J. P.; Ellis, T. L.; Phillips, P. E. M.; Montague, P. R. *Proc. Natl. Acad. Sci. U.S.A.* **2016**, *113*, 200-205 (ref 29). https://creativecommons.org/licenses/by/4.0/

Background subtraction can be thought of as a form of manual feature engineering useful for identifying oxidation and reduction peak currents for univariate linear regression, while multivariate models essentially perform automatic feature engineering. Thus, machine learning has overcome and surpassed the need for background subtraction as originally proposed. Rather than focusing on a small subset of the information in voltammograms, we can now utilize all voltammogram information.

One question is why non-background-subtracted techniques were not focused on sooner? For one, the resolution of previous generations of data acquisition cards was an impediment to approaches aimed at deconvoluting varying contributions of faradaic and non-faradaic current.[2] Data sampling speeds available today are an order of magnitude faster (*i.e.,* <100 kHz *vs.* >1 MHz). The increases in data density mean processes previously seen at 10-µs intervals are now captured at 1-µs intervals–the timescale of resolvable adsorptive/capacitive charging processes at carbon fiber microelectrodes (*i.e.*, RC equivalent circuit-time constants of ~4-40 µs have been demonstrated both empirically and theoretically).[20]

Moreover, large-scale and chemically diverse training sets were not, and generally, are still not utilized. Early reports of supervised regression models for background-subtracted fast voltammetry were trained solely on dopamine over a handful of concentrations and occasionally, a couple of metabolites at single concentrations, across dozens of voltammograms.[47] The most advanced models today consist of far more robust experimental designs with training sets containing multiple concentrations of analytes, metabolites, H^+ and other ions, multiple electrodes, and so on, across thousands of voltammograms.[38,48] As state-of-the-art (*i.e.,* deep learning) models are developed,[35,37,39,46] electrochemists will also likely find greater success in maximizing the information content of data acquisition. Examples include the fusing of multiple

data sources,[45] the ability to perform inference on out-of-distribution data,[38] and the use of physics-informed[43] and probabilistic[49] models. These areas are likely to yield complementary advances for machine learning and voltammetry that extend beyond neurochemical detection toward electroanalytical chemistry *writ large*.

While previous work has shown there is important information in the capacitive/non-faradaic/background current, few methods have capitalized on background-inclusive models to improve analyte predictions. We surmise the future of fast voltammetry will rely increasingly on background-inclusive machine learning models because of the marked increases in performance associated with utilizing capacitive (non-faradaic) current information. The latter is especially useful as an additional source of information for discriminating highly overlapping electrochemical signals, as shown for serotonin and dopamine (**Fig. 4.3**).[11,48] Adsorption, interfacial surface chemistry, drift, and other contributions, all affect capacitive, in addition to faradaic currents. Subtracting the background removes relevant information that mathematical algorithms can use for more robust training and thus, more accurate predictions. In addition to improvements in

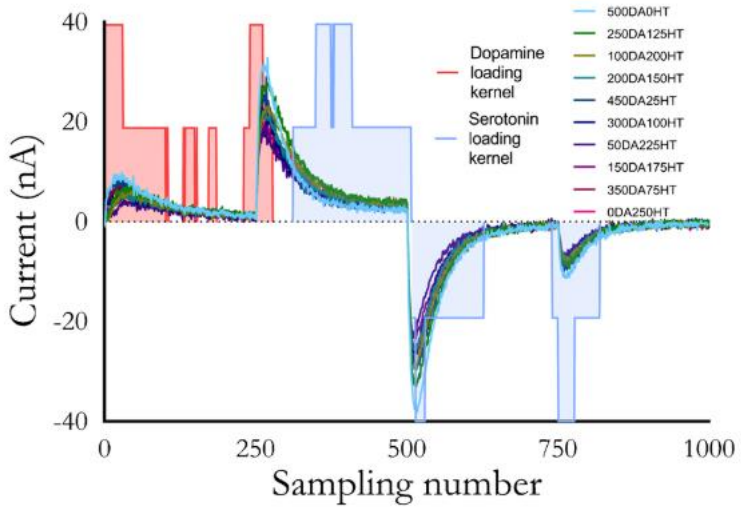

Figure 4.3. Model loadings analysis by analyte for rapid pulse voltammetry. Large loadings for dopamine and serotonin in the early portions of specific steps indicates the model is gaining analyte-specific information from portions of the current traces dominated by capacitive current. Reproduced from Movassaghi, C. S.; Perrotta, K. A.; Yang, H.; Iyer, R.; Cheng, X.; Dagher, M.; Fillol, M. A.; Andrews, A. M. *Anal. Bioanal. Chem.* **2021**, *413*, 6747-6767 (ref 11). http://creativecommons.org/licenses/by/4.0/

sampling, better digital electronics and data acquisition cards can now be used to drive more rapid potential changes with high slew rates.

Waveform woes: powerful pulses or skillful sweeps? The pulse *versus* sweep waveform debate has permeated the history of voltammetry (much like an earlier debate between the "sparks" and the "soups" regarding the nature of communication at synapses[50]). Osteryoung advocated as early as 1993 for a 'pulse revolution', suggesting that progress in electronics and computing would advance pulse voltammetry in a postmodernist era.[51] Ironically, prior to FSCV adoption, electroanalytical chemists avoided fast cyclic voltammetry because of the large background currents generated by fast sweeps. Once background subtraction appeared to alleviate issues associated with large and temporally evolving background currents in FSCV, the use of pulse techniques fell by the wayside because of their slow temporal resolution (associated with differential sampling between non-faradaic and faradaic currents and slow electronics).[2] However, if the background current is indeed no longer an issue and is an information-rich source of information, then electroanalytical chemists are free to explore the use of pulse waveforms thirty years after Osteryoung's prediction.

> "Although the principles of capacitive and faradic current had already been widely known, the straight nature of [pulse voltammetry], where it is easy to separate capacitive and faradic current, has been overlooked, and not utilized for voltammetric recordings in the brain."
>
> –Yoshimi *et al*. **2014**[52]

Both sweep and pulse waveforms enable users to customize start and stop potentials for different waveform segments. Sweep techniques offer customizable scan rates, whereas pulse

techniques allow customizable step potentials and hold times. In fact, a digitally generated sweep signal is a series of small pulses. One argument against sweep voltammetry is that variable scan rates do not provide a different type of fundamental chemical information. That is linear scans (sweeps) inextricably link time with potential and faradaic with capacitive current. In any case, variable scan rates,[53] multiple scan rates,[54] and multi-sweep voltammetry methods[55-58] have been developed.

In theory, pulsed voltammetry provides fundamentally distinguishable faradaic and non-faradaic information, whereas fast-sweep voltammetry does not. In the latter, the capacitive current is rapidly evolving throughout the waveform, making it difficult to separate faradaic from non-faradaic current contributions. Nonetheless, these different sources of current need not be separated to be practically accurate or useful for quantifying an analyte (although, formally modeling these separate contributions can be useful for other tasks, such as equivalent circuit models[59]). In step potentials, even for fast steps, the full capacitive decay profiles (change in current over the step time) provide information to parse capacitive and faradaic current contributions. Yoshimi *et al.* were one of the first to demonstrate that a single rectangular pulse could differentiate dopamine and pH, even in the presence of serotonin and ascorbate, solely by changes in the capacitive current response, without explicit training sets.[52] Meanwhile, dopamine and pH predictions were confounded in FSCV.

Following this work, Wightman and coworkers, who originally promulgated background subtraction in FSCV, reported a convolution-removal technique for the oft-ignored contributions from monovalent ions (K^+, Na^+),[20] and extended this thinking to divalent cations (Mg^{2+}, Ca^{2+}).[16] For example, background-subtracted FSCV-PCR confused a 120 mM change in [K^+] as a 1.5 µM change in dopamine, when no actual change in dopamine occurred.[20] Only when the PCR model was trained across [K^+] or when the deconvolution technique was used did the model not confuse K^+ for dopamine (**Fig. 4.4**). However, training a model across [K^+] requires repeating the original training set while varying [K^+], increasing in training times and samples. The deconvolution technique required another computation step and augmentation of the waveform and has only been tested for the case of a single analyte. Interestingly, this deconvolution method relies on a small amplitude *pulse* integrated with the FSCV *sweep* to separate the expected capacitive ionic current.

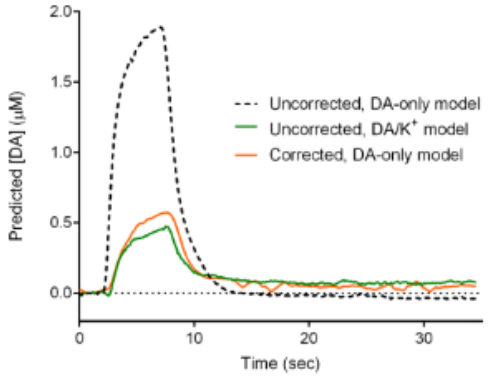

Figure 4.4. Dopamine (DA) predictions from FSCV data containing 120 mM K^+ for an actual value of 500 nM dopamine. Reproduced from Johnson, J. A.; Hobbs, C. N.; Wightman, R. M. *Anal. Chem*. **2017**, *89*, 6166-6174 (ref 20). Copyright 2017 American Chemical Society.

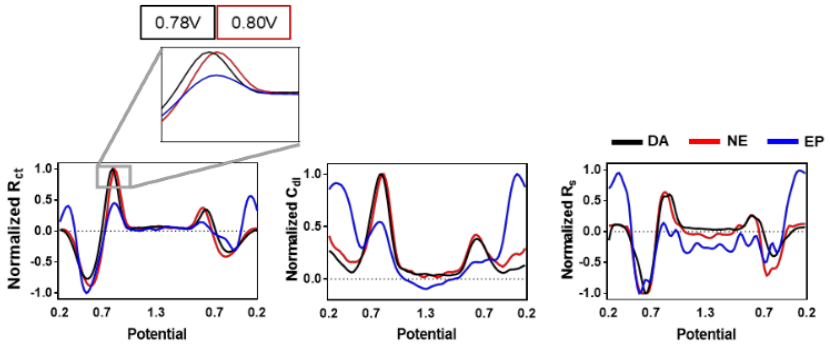

Figure 4.5. Analyte-specific equivalent circuit voltammograms for dopamine (DA), norepinephrine (NE), and epinephrine (EP). Reproduced from Park, C.; Hwang, S.; Kang, Y.; Sim, J.; Cho, H. U.; Oh, Y.; Shin, H.; Kim, D. H.; Blaha, C. D.; Bennet, K. E. *Anal. Chem*. **2021**, *93*, 15861-15869 (ref 14). Copyright 2021 American Chemical Society.

Sweep waveforms remain widely used. Sweeps contain important information in their backgrounds, as shown for non-background subtracted elastic net FSCV.[13] Non-background subtracted FSCV paired with elastic net analysis has been used to decode dopamine and serotonin signaling in human striatum involved in decision making.[9,29,48] Moreover, deep learning algorithms have been used with non-background-subtracted FSCV to determine sub-second norepinephrine signals in human amygdala associated with the emotional regulation of attention.[40] Sombers and coworkers have not only reported on the ability of FSCV with machine learning to predict voltammetric drift[23] and the usefulness of background voltammograms as accurate experimental parameter predictors,[60] they explored the impedance (*i.e.,* capacitive) characteristics of electrodes and analyte-containing solutions through electrochemical impedance spectroscopy (EIS).[61,62] Similarly, later work by the Jang group advocated for modeling analyte-specific equivalent circuit parameters (**Fig. 4.5**) and utilizing double-layer capacitance as a feature to improve biofouling robustness.[14] This work used a novel pulse voltammetry technique.

Using only square wave voltammetry (SWV), Cobb and Macpherson showed that circuit parameters can be extracted directly from the non-faradaic regions in SWV, circumventing the need for EIS.[63] Circuit parameters can then be used to differentiate responses unique to

electrolyte *vs.* analyte concentration dynamics or serotonin biofouling. *In vivo* voltammetry experiments are plagued by the confounding factors of unknown electrolyte composition dynamics and surface biofouling. The non-faradaic information contained within pulses has direct utility in addressing this aspect of the generalization gap (*vide supra*).

"The SWV capacitance data can be used to provide real time monitoring on whether a changing faradaic signal is due to concentration changes of the electrochemically active analyte or fouling of the electrode."

–Cobb *et al*. **2019**[63]

The studies discussed above advocate for the utility of pulse voltammetry, beyond its being complementary to FSCV. Moreover, two methods to date on background-inclusive, customized, rapid or 'burst' pulses have both achieved detection of notoriously difficult analyte mixtures, *i.e.*, co-detection of dopamine and serotonin,[11] and dopamine and norepinephrine (**Fig. 4.6**).[64,65] Rapid pulse voltammetry was also used to demonstrate the first evidence of combined measurements of basal neurotransmitter levels and stimulated release *via* a single technique.[11] Outside of bioanalytical voltammetry, the usefulness of pulse-induced capacitive current has been demonstrated repeatedly and is becoming more commonplace as advanced data acquisition and analysis speeds enable its exploration. The voltammetric electronic tongue community has recognized the importance of modeling information contained in non-faradaic current, in addition to faradaic current, for decades, especially in complex environments.[66-69] The high information content of pulses and their accessible capacitive currents is also gaining attention for electrochemical measurements in other fields.[70,71]

For neurochemical analyses, the debate on pulse *versus* sweep waveforms is expected to continue. While neurochemical fast voltammetry has been tailored towards sweeps, pulses offer relatively unexplored information and use cases. Some have advocated for the complementary use of separate pulse and sweep waveforms (*i.e.,* data fusion),[52] while the Heien, Jang, and Lee groups have pioneered techniques that combine sweeps and pulses into single waveforms.[6,72-74] Others have concatenated pulse and sweep waveforms for a variety of electrochemical detection purposes.[75,76] Approaches outside of the DC-realm (*i.e.,* AC-voltammetry)[77] are also garnering a resurgence of interest when combined with machine learning.[44,78] Regardless of waveform type, we propose that non-background subtracted approaches are well suited to facilitate the union of voltammetry and machine learning due to the importance of the capacitive current included in the training sets.

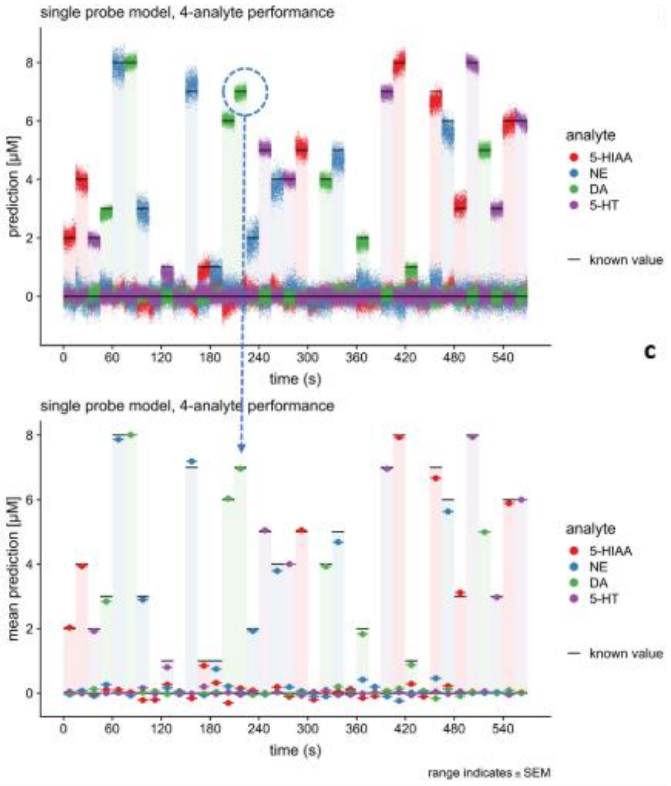

Figure 4.6. Analyte (dopamine (DA), norepinephrine (NE), serotonin (5-HT), and 5-hydroxyindoleacetic acid (5-HIAA)) predictions from randomized pulse voltammetry. Reproduced with permission from Montague, P. R.; Lohrenz, T.; White, J.; Moran, R. J.; Kishida, K. T. *bioRxiv (Neuroscience)* **2019**, (ref 64). Copyright 2019 The Authors.

To extract maximal neurochemical information from the brain, we recommend that voltammetry practitioners extract maximal information from their data to provide information on absolute vs. relative changes in stimulated neurotransmitter levels, basal neurotransmitter levels,

and simultaneous analyte monitoring. Based on the publications reviewed here on the importance of non-faradaic information and the versatility of waveforms (sweeps and pulses) in voltammetry, the next major advances for *in vivo* voltammetry appear likely to come from background-inclusive approaches paired with machine learning. There are many recent examples of movement in this direction inside and outside of the chemical neuroscience community.[11,14,16,20,44-46,64,65,71,72,74,79].

If there is a solution to the pervasive problems that have plagued voltammetry for decades preventing the full electrochemical exploration of the chemical communication systems of the brain and beyond, recent evidence points to a need to reconsider the use of background subtraction. Broadly speaking, all practitioners of voltammetry should consider maximizing the information inherent in their experimental data and complementing domain knowledge with their analysis toolkit of choice.

"There is scientific value to capturing more current data generated during square wave voltammetry…it contains valuable information about the double layer charging and interfacial processes occurring at short timescales. More specifically…analyzing the current-time data from the non-Faradaic region of the potential pulse can provide crucial information."

–Abeykoon *et al*. **2022**[71]

Acknowledgments and Contributions:

CSM was supported by the National Science Foundation Graduate Research Fellowship Program (DGE-1650604 and DGE-2034835). Any opinions, findings, conclusions, or recommendations expressed in this material are those of the authors and do not necessarily reflect the views of the National Science Foundation. CSM and AMA conceived of the work and wrote the initial draft. All authors provided significant edits, revisions, and feedback.

4.3 REFERENCES

1. Millar, J.; Stamford, J. A.; Kruk, Z. L.; Wightman, R. M., Electrochemical, pharmacological and electrophysiological evidence of rapid dopamine release and removal in the rat caudate nucleus following electrical stimulation of the median forebrain bundle. *Eur. J. Pharmacol.* **1985,** *109* (3), 341-348. https://doi.org/10.1016/0014-2999(85)90394-2
2. Baur, J. E.; Kristensen, E. W.; May, L. J.; Wiedemann, D. J.; Wightman, R. M., Fast-scan voltammetry of biogenic amines. *Anal. Chem.* **1988,** *60* (13), 1268-1272. https://doi.org/10.1021/ac00164a006
3. Venton, B. J.; Cao, Q., Fundamentals of fast-scan cyclic voltammetry for dopamine detection. *Analyst* **2020,** *145* (4), 1158-1168. https://doi.org/10.1039/C9AN01586H
4. Kawagoe, K. T.; Zimmerman, J. B.; Wightman, R. M., Principles of voltammetry and microelectrode surface states. *J. Neurosci. Methods* **1993,** *48* (3), 225-240. https://doi.org/10.1016/0165-0270(93)90094-8
5. Atcherley, C. W.; Laude, N. D.; Parent, K. L.; Heien, M. L., Fast-scan controlled-adsorption voltammetry for the quantification of absolute concentrations and adsorption dynamics. *Langmuir* **2013,** *29* (48), 14885-92. https://doi.org/10.1021/la402686s
6. Park, C.; Oh, Y.; Shin, H.; Kim, J.; Kang, Y.; Sim, J.; Cho, H. U.; Lee, H. K.; Jung, S. J.; Blaha, C. D.; Bennet, K. E.; Heien, M. L.; Lee, K. H.; Kim, I. Y.; Jang, D. P., Fast cyclic square-wave voltammetry to enhance neurotransmitter selectivity and sensitivity. *Anal. Chem.* **2018,** *90* (22), 13348-13355. https://doi.org/10.1021/acs.analchem.8b02920

7. Wassum, K. M.; Tolosa, V. M.; Tseng, T. C.; Balleine, B. W.; Monbouquette, H. G.; Maidment, N. T., Transient extracellular glutamate events in the basolateral amygdala track reward-seeking actions. *J. Neurosci.* **2012,** *32* (8), 2734-2746. https://doi.org/10.1523/jneurosci.5780-11.2012

8. Borgus, J. R.; Wang, Y.; DiScenza, D. J.; Venton, B. J., Spontaneous adenosine and dopamine cotransmission in the caudate-putamen is regulated by adenosine receptors. *ACS Chem. Neurosci.* **2021,** *12* (23), 4371-4379. https://doi.org/10.1021/acschemneuro.1c00175

9. Moran, R. J.; Kishida, K. T.; Lohrenz, T.; Saez, I.; Laxton, A. W.; Witcher, M. R.; Tatter, S. B.; Ellis, T. L.; Phillips, P. E. M.; Dayan, P.; Montague, P. R., The protective action encoding of serotonin transients in the human brain. *Neuropsychopharmacology* **2018,** *43* (6), 1425-1435. https://doi.org/10.1038/npp.2017.304

10. Howe, M. W.; Tierney, P. L.; Sandberg, S. G.; Phillips, P. E. M.; Graybiel, A. M., Prolonged dopamine signalling in striatum signals proximity and value of distant rewards. *Nature* **2013,** *500* (7464), 575-579. https://doi.org/10.1038/nature12475

11. Movassaghi, C. S.; Perrotta, K. A.; Yang, H.; Iyer, R.; Cheng, X.; Dagher, M.; Fillol, M. A.; Andrews, A. M., Simultaneous serotonin and dopamine monitoring across timescales by rapid pulse voltammetry with partial least squares regression. *Anal. Bioanal. Chem.* **2021,** *413* (27), 6747-6767. https://doi.org/10.1007/s00216-021-03665-1

12. Fuentes, E.; Alcañiz, M.; Contat, L.; Baldeón, E. O.; Barat, J. M.; Grau, R., Influence of potential pulses amplitude sequence in a voltammetric electronic tongue (VET) applied to assess antioxidant capacity in aliso. *Food Chem.* **2017,** *224*, 233-241. https://doi.org/10.1016/j.foodchem.2016.12.076

13. Montague, P. R.; Kishida, K. T., Computational underpinnings of neuromodulation in humans. *Cold Spring Harbor Symp. Quant. Biol.* **2018,** *83*, 71-82. https://doi.org/10.1101/sqb.2018.83.038166

14. Park, C.; Hwang, S.; Kang, Y.; Sim, J.; Cho, H. U.; Oh, Y.; Shin, H.; Kim, D. H.; Blaha, C. D.; Bennet, K. E., Feasibility of applying Fourier transform electrochemical impedance spectroscopy in fast cyclic square wave voltammetry for the in vivo measurement of neurotransmitters. *Anal. Chem.* **2021,** *93* (48), 15861-15869. https://doi.org/10.1021/acs.analchem.1c02308

15. Meunier, C. J.; Roberts, J. G.; McCarty, G. S.; Sombers, L. A., Background signal as an in situ predictor of dopamine oxidation potential: Improving interpretation of fast-scan cyclic voltammetry data. *ACS Chem. Neurosci.* **2017,** *8* (2), 411-419. https://doi.org/10.1021/acschemneuro.6b00325

16. Johnson, J. A.; Rodeberg, N. T.; Wightman, R. M., Measurement of basal neurotransmitter levels using convolution-based nonfaradaic current removal. *Anal. Chem.* **2018,** *90* (12), 7181-7189. https://doi.org/10.1021/acs.analchem.7b04682

17. Wosiak, G.; Coelho, D.; Carneiro-Neto, E. B.; Pereira, E. C.; Lopes, M. C., Numerical resolving of net faradaic current in fast-scan cyclic voltammetry considering induced charging currents. *Anal. Chem.* **2020,** *92* (23), 15412-15419. https://doi.org/10.1021/acs.analchem.0c03026

18. Pasta, M.; La Mantia, F.; Cui, Y., Mechanism of glucose electrochemical oxidation on gold surface. *Electrochim. Acta* **2010,** *55* (20), 5561-5568. https://doi.org/10.1016/j.electacta.2010.04.069

19. Takmakov, P.; Zachek, M. K.; Keithley, R. B.; Bucher, E. S.; McCarty, G. S.; Wightman, R. M., Characterization of local pH changes in brain using fast-scan cyclic voltammetry with carbon microelectrodes. *Anal. Chem.* **2010,** *82* (23), 9892-9900. https://doi.org/10.1021/ac102399n

20. Johnson, J. A.; Hobbs, C. N.; Wightman, R. M., Removal of differential capacitive interferences in fast-scan cyclic voltammetry. *Anal. Chem.* **2017,** *89* (11), 6166-6174. https://doi.org/10.1021/acs.analchem.7b01005

21. Heien, M. L. A. V.; Khan, A. S.; Ariansen, J. L.; Cheer, J. F.; Phillips, P. E. M.; Wassum, K. M.; Wightman, R. M., Real-time measurement of dopamine fluctuations after cocaine in the brain of behaving rats. *Proc. Natl. Acad. Sci. U.S.A.* **2005,** *102* (29), 10023-10028. https://doi.org/10.1073/pnas.0504657102

22. DeWaele, M.; Oh, Y.; Park, C.; Kang, Y. M.; Shin, H.; Blaha, C. D.; Bennet, K. E.; Kim, I. Y.; Lee, K. H.; Jang, D. P., A baseline drift detrending technique for fast scan cyclic voltammetry. *Analyst* **2017,** *142* (22), 4317-4321. https://doi.org/10.1039/C7AN01465A

23. Meunier, C. J.; McCarty, G. S.; Sombers, L. A., Drift subtraction for fast-scan cyclic voltammetry using double-waveform partial-least-squares regression. *Anal. Chem.* **2019,** *91* (11), 7319-7327. https://doi.org/10.1021/acs.analchem.9b01083

24. Robinson, D. L.; Venton, B. J.; Heien, M. L.; Wightman, R. M., Detecting subsecond dopamine release with fast-scan cyclic voltammetry in vivo. *Clin. Chem* **2003,** *49* (10), 1763-73. https://doi.org/10.1373/49.10.1763

25. Seaton, B. T.; Hill, D. F.; Cowen, S. L.; Heien, M. L., Mitigating the effects of electrode biofouling-induced impedance for improved long-term electrochemical measurements in

vivo. *Anal. Chem.* **2020,** *92* (9), 6334-6340. https://doi.org/10.1021/acs.analchem.9b05194

26. Kang, Y.; Goyal, A.; Hwang, S.; Park, C.; Cho, H. U.; Shin, H.; Park, J.; Bennet, K. E.; Lee, K. H.; Oh, Y.; Jang, D. P., Enhanced dopamine sensitivity using steered fast-scan cyclic voltammetry. *ACS Omega* **2021,** *6* (49), 33599-33606. https://doi.org/10.1021/acsomega.1c04475

27. Collins, A. L.; Greenfield, V. Y.; Bye, J. K.; Linker, K. E.; Wang, A. S.; Wassum, K. M., Dynamic mesolimbic dopamine signaling during action sequence learning and expectation violation. *Sci. Rep.* **2016,** *6* (1), 20231. https://doi.org/10.1038/srep20231

28. Hamid, A. A.; Pettibone, J. R.; Mabrouk, O. S.; Hetrick, V. L.; Schmidt, R.; Vander Weele, C. M.; Kennedy, R. T.; Aragona, B. J.; Berke, J. D., Mesolimbic dopamine signals the value of work. *Nat. Neurosci.* **2016,** *19* (1), 117-126. https://doi.org/10.1038/nn.4173

29. Kishida, K. T.; Saez, I.; Lohrenz, T.; Witcher, M. R.; Laxton, A. W.; Tatter, S. B.; White, J. P.; Ellis, T. L.; Phillips, P. E. M.; Montague, P. R., Subsecond dopamine fluctuations in human striatum encode superposed error signals about actual and counterfactual reward. *Proc. Natl. Acad. Sci. U.S.A.* **2016,** *113* (1), 200-205. https://doi.org/10.1073/pnas.1513619112

30. Box, G. E. P., Science and statistics. *J. Am. Stat. Assoc.* **1976,** *71* (356), 791-799. https://doi.org/10.1080/01621459.1976.10480949

31. Keithley, R. B.; Mark Wightman, R.; Heien, M. L., Multivariate concentration determination using principal component regression with residual analysis. *TrAC, Trends Anal. Chem.* **2009,** *28* (9), 1127-1136. https://doi.org/10.1016/j.trac.2009.07.002

32. Rodeberg, N. T.; Johnson, J. A.; Cameron, C. M.; Saddoris, M. P.; Carelli, R. M.; Wightman, R. M., Construction of training sets for valid calibration of in vivo cyclic voltammetric data by principal component analysis. *Anal. Chem.* **2015,** *87* (22), 11484-11491. https://doi.org/10.1021/acs.analchem.5b03222

33. Johnson, J. A.; Rodeberg, N. T.; Wightman, R. M., Failure of standard training sets in the analysis of fast-scan cyclic voltammetry data. *ACS Chem. Neurosci.* **2016,** *7* (3), 349-359. https://doi.org/10.1021/acschemneuro.5b00302

34. Rodeberg, N. T.; Sandberg, S. G.; Johnson, J. A.; Phillips, P. E. M.; Wightman, R. M., Hitchhiker's guide to voltammetry: Acute and chronic electrodes for in vivo fast-scan cyclic voltammetry. *ACS Chem. Neurosci.* **2017,** *8* (2), 221-234. https://doi.org/10.1021/acschemneuro.6b00393

35. Choi, H.; Shin, H.; Cho, H. U.; Blaha, C. D.; Heien, M. L.; Oh, Y.; Lee, K. H.; Jang, D. P., Neurochemical concentration prediction using deep learning vs principal component regression in fast scan cyclic voltammetry: A comparison study. *ACS Chem. Neurosci.* **2022,** *13* (15), 2288-2297. https://doi.org/10.1021/acschemneuro.2c00069

36. Mena, S.; Visentin, M.; Witt, C. E.; Honan, L. E.; Robins, N.; Hashemi, P., Novel, user-friendly experimental and analysis strategies for fast voltammetry: Next generation FSCAV with artificial neural networks. *ACS Meas. Sci. Au* **2022,** *2* (3), 241-250. https://doi.org/10.1021/acsmeasuresciau.1c00060

37. Xue, Y.; Ji, W.; Jiang, Y.; Yu, P.; Mao, L., Deep learning for voltammetric sensing in a living animal brain. *Angew. Chem. Int. Ed.* **2021,** *60* (44), 23777-23783. https://doi.org/10.1002/anie.202109170

38. Loewinger, G.; Patil, P.; Kishida, K. T.; Parmigiani, G., Hierarchical resampling for bagging in multistudy prediction with applications to human neurochemical sensing. *Ann. Appl. Stat.* **2022,** *16* (4), 2145-2165, 21. https://doi.org/10.1214/21-aoas1574

39. Twomey, T.; Barbosa, L.; Lohrenz, T.; Montague, P. R., Deep learning architectures for FSCV, a comparison. *arXiv (Medical Physics)* **2022,** (posted 2022-12-05). https://doi.org/10.48550/arXiv.2212.01960 (accessed 2023-12-12)

40. Bang, D.; Luo, Y.; Barbosa, L. S.; Batten, S. R.; Hadj-Amar, B.; Twomey, T.; Melville, N.; White, J. P.; Torres, A.; Celaya, X.; Ramaiah, P.; McClure, S. M.; Brewer, G. A.; Bina, R. W.; Lohrenz, T.; Casas, B.; Chiu, P. H.; Vannucci, M.; Kishida, K. T.; Witcher, M. R.; Montague, P. R., Noradrenaline tracks emotional modulation of attention in human amygdala. *Curr. Biol.* **2023,** *33* (22), 5003-5010 e6. https://doi.org/10.1016/j.cub.2023.09.074

41. Zhuang, F.; Qi, Z.; Duan, K.; Xi, D.; Zhu, Y.; Zhu, H.; Xiong, H.; He, Q., A comprehensive survey on transfer learning. *Proc. IEEE* **2020,** *109* (1), 43-76. https://doi.org/10.1109/JPROC.2020.3004555

42. Nikzad-Langerodi, R.; Andries, E., A chemometrician's guide to transfer learning. *J. Chemom.* **2021,** *35* (11), e3373. https://doi.org/10.1002/cem.3373

43. Chen, H.; Kätelhön, E.; Compton, R. G., Machine learning in fundamental electrochemistry: Recent advances and future opportunities. *Curr. Opin. Electrochem.* **2023,** *38*, 101214. https://doi.org/10.1016/j.coelec.2023.101214

44. Gundry, L.; Guo, S.-X.; Kennedy, G.; Keith, J.; Robinson, M.; Gavaghan, D.; Bond, A. M.; Zhang, J., Recent advances and future perspectives for automated

parameterisation, Bayesian inference and machine learning in voltammetry. *Chem. Comm.* **2021,** *57* (15), 1855-1870. https://doi.org/10.1039/D0CC07549C

45. Sun, J.; Liu, C., What and how can machine learning help to decipher mechanisms in molecular electrochemistry? *Curr. Opin. Electrochem.* **2023,** *39*, 101306. https://doi.org/10.1016/j.coelec.2023.101306

46. Hoar, B. B.; Zhang, W.; Xu, S.; Deeba, R.; Costentin, C.; Gu, Q.; Liu, C., Electrochemical mechanistic analysis from cyclic voltammograms based on deep learning. *ACS Meas. Sci. Au* **2022,** *2* (6), 595-604. https://doi.org/10.1021/acsmeasuresciau.2c00045

47. Heien, M. L. A. V.; Johnson, M. A.; Wightman, R. M., Resolving neurotransmitters detected by fast-scan cyclic voltammetry. *Anal. Chem.* **2004,** *76* (19), 5697-5704. https://doi.org/10.1021/ac0491509

48. Bang, D.; Kishida, K. T.; Lohrenz, T.; White, J. P.; Laxton, A. W.; Tatter, S. B.; Fleming, S. M.; Montague, P. R., Sub-second dopamine and serotonin signaling in human striatum during perceptual decision-making. *Neuron* **2020,** *108* (5), 999-1010.e6. https://doi.org/10.1016/j.neuron.2020.09.015

49. Bond, A. M., A perceived paucity of quantitative studies in the modern era of voltammetry: Prospects for parameterisation of complex reactions in Bayesian and machine learning frameworks. *J Solid State Electrochem.* **2020,** *24* (9), 2041-2050. https://doi.org/10.1007/s10008-020-04639-6

50. Valenstein, E. S., *The war of the soups and the sparks: The discovery of neurotransmitters and the dispute over how nerves communicate*. Columbia University Press: 2005.

51. Osteryoung, J., Voltammetry for the future. *Acc. Chem. Res.* **1993,** *26* (3), 77-83. https://doi.org/10.1021/ar00027a001

52. Yoshimi, K.; Weitemier, A., Temporal differentiation of pH-dependent capacitive current from dopamine. *Anal. Chem.* **2014,** *86* (17), 8576-8584. https://doi.org/10.1021/ac500706m

53. Hashemi, P.; Dankoski, E. C.; Petrovic, J.; Keithley, R. B.; Wightman, R. M., Voltammetric detection of 5-hydroxytryptamine release in the rat brain. *Anal. Chem.* **2009,** *81* (22), 9462-71. https://doi.org/10.1021/ac9018846

54. Calhoun, S. E.; Meunier, C. J.; Lee, C. A.; McCarty, G. S.; Sombers, L. A., Characterization of a multiple-scan-rate voltammetric waveform for real-time detection of met-enkephalin. *ACS Chem. Neurosci.* **2019,** *10* (4), 2022-2032. https://doi.org/10.1021/acschemneuro.8b00351

55. Meunier, C. J.; Mitchell, E. C.; Roberts, J. G.; Toups, J. V.; McCarty, G. S.; Sombers, L. A., Electrochemical selectivity achieved using a double voltammetric waveform and partial least squares regression: Differentiating endogenous hydrogen peroxide fluctuations from shifts in pH. *Anal. Chem.* **2018,** *90* (3), 1767-1776. https://doi.org/10.1021/acs.analchem.7b03717

56. Kim, S. Y.; Oh, Y. B.; Shin, H. J.; Kim, D. H.; Kim, I. Y.; Bennet, K.; Lee, K. H.; Jang, D. P., 5-hydroxytryptamine measurement using paired pulse voltammetry. *Biomed. Eng. Lett* **2013,** *3* (2), 102-108. https://doi.org/10.1007/s13534-013-0093-z

57. Oh, Y.; Park, C.; Kim, D. H.; Shin, H.; Kang, Y. M.; DeWaele, M.; Lee, J.; Min, H.-K.; Blaha, C. D.; Bennet, K. E.; Kim, I. Y.; Lee, K. H.; Jang, D. P., Monitoring in vivo changes in tonic extracellular dopamine level by charge-balancing multiple waveform

fast-scan cyclic voltammetry. *Anal. Chem.* **2016,** *88* (22), 10962-10970. https://doi.org/10.1021/acs.analchem.6b02605

58. Jang, D. P.; Kim, I.; Chang, S.-Y.; Min, H.-K.; Arora, K.; Marsh, M. P.; Hwang, S.-C.; Kimble, C. J.; Bennet, K. E.; Lee, K. H., Paired pulse voltammetry for differentiating complex analytes. *Analyst* **2012,** *137* (6), 1428-1435. https://doi.org/10.1039/C2AN15912K

59. Ramón, J. E.; Martínez-Ibernón, A.; Gandía-Romero, J. M.; Fraile, R.; Bataller, R.; Alcañiz, M.; García-Breijo, E.; Soto, J., Characterization of electrochemical systems using potential step voltammetry. Part I: Modeling by means of equivalent circuits. *Electrochim. Acta* **2019,** *323*, 134702. https://doi.org/10.1016/j.electacta.2019.134702

60. Roberts, J. G.; Toups, J. V.; Eyualem, E.; McCarty, G. S.; Sombers, L. A., In situ electrode calibration strategy for voltammetric measurements in vivo. *Anal. Chem.* **2013,** *85* (23), 11568-11575. https://doi.org/10.1021/ac402884n

61. Mitchell, E. C.; Dunaway, L. E.; McCarty, G. S.; Sombers, L. A., Spectroelectrochemical characterization of the dynamic carbon-fiber surface in response to electrochemical conditioning. *Langmuir* **2017,** *33* (32), 7838-7846. https://doi.org/10.1021/acs.langmuir.7b01443

62. Meunier, C. J.; Denison, J. D.; McCarty, G. S.; Sombers, L. A., Interpreting dynamic interfacial changes at carbon fiber microelectrodes using electrochemical impedance spectroscopy. *Langmuir* **2020,** *36* (15), 4214-4223. https://doi.org/10.1021/acs.langmuir.9b03941

63. Cobb, S. J.; Macpherson, J. V., Enhancing square wave voltammetry measurements via electrochemical analysis of the non-faradaic potential window. *Anal. Chem.* **2019,** *91* (12), 7935-7942. https://doi.org/10.1021/acs.analchem.9b01857

64. Montague, P. R.; Lohrenz, T.; White, J.; Moran, R. J.; Kishida, K. T., Random burst sensing of neurotransmitters. *bioRxiv (Neuroscience)* **2019,** (posted 2019-04-13), 607077. https://doi.org/10.1101/607077 (accessed 2023-12-12)

65. Eltahir, A.; White, J.; Lohrenz, T.; Montague, P. R., Low amplitude burst detection of catecholamines. *bioRxiv (Neuroscience)* **2021,** (posted 2021-08-04). https://doi.org/10.1101/2021.08.02.454747 (accessed 2023-12-12)

66. Winquist, F.; Wide, P.; Lundström, I., An electronic tongue based on voltammetry. *Anal. Chim. Acta* **1997,** *357* (1), 21-31. https://doi.org/10.1016/S0003-2670(97)00498-4

67. Winquist, F., Voltammetric electronic tongues – basic principles and applications. *Microchim. Acta* **2008,** *163* (1), 3-10. https://doi.org/10.1007/s00604-007-0929-2

68. Alcañiz, M.; Vivancos, J.-L.; Masot, R.; Ibañez, J.; Raga, M.; Soto, J.; Martínez-Máñez, R., Design of an electronic system and its application to electronic tongues using variable amplitude pulse voltammetry and impedance spectroscopy. *J. Food Eng.* **2012,** *111* (1), 122-128. https://doi.org/10.1016/j.jfoodeng.2012.01.014

69. Campos, I.; Alcañiz, M.; Masot, R.; Soto, J.; Martínez-Máñez, R.; Vivancos, J.-L.; Gil, L., A method of pulse array design for voltammetric electronic tongues. *Sens. Actuators, B* **2012,** *161* (1), 556-563. https://doi.org/10.1016/j.snb.2011.10.075

70. Kraikaew, P.; Jeanneret, S.; Soda, Y.; Cherubini, T.; Bakker, E., Ultrasensitive seawater pH measurement by capacitive readout of potentiometric sensors. *ACS Sens.* **2020,** *5* (3), 650-654. https://doi.org/10.1021/acssensors.0c00031

71. Abeykoon, S. W.; White, R. J., Continuous square wave voltammetry for high information content interrogation of conformation switching sensors. *ACS Meas. Sci. Au* **2023,** *3* (1), 1-9. https://doi.org/10.1021/acsmeasuresciau.2c00044

72. Shin, H.; Oh, Y.; Park, C.; Kang, Y.; Cho, H. U.; Blaha, C. D.; Bennet, K. E.; Heien, M. L.; Kim, I. Y.; Lee, K. H.; Jang, D. P., Sensitive and selective measurement of serotonin in vivo using fast cyclic square-wave voltammetry. *Anal. Chem.* **2020,** *92* (1), 774-781. https://doi.org/10.1021/acs.analchem.9b03164

73. Shin, H.; Goyal, A.; Barnett, J. H.; Rusheen, A. E.; Yuen, J.; Jha, R.; Hwang, S. M.; Kang, Y.; Park, C.; Cho, H.-U.; Blaha, C. D.; Bennet, K. E.; Oh, Y.; Heien, M. L.; Jang, D. P.; Lee, K. H., Tonic serotonin measurements in vivo using N-shaped multiple cyclic square wave voltammetry. *Anal. Chem.* **2021,** *93* (51), 16987-16994. https://doi.org/10.1021/acs.analchem.1c02131

74. Oh, Y.; Heien, M. L.; Park, C.; Kang, Y. M.; Kim, J.; Boschen, S. L.; Shin, H.; Cho, H. U.; Blaha, C. D.; Bennet, K. E.; Lee, H. K.; Jung, S. J.; Kim, I. Y.; Lee, K. H.; Jang, D. P., Tracking tonic dopamine levels in vivo using multiple cyclic square wave voltammetry. *Biosens. Bioelectron.* **2018,** *121*, 174-182. https://doi.org/10.1016/j.bios.2018.08.034

75. Fedorowski, J.; LaCourse, W. R., A review of pulsed electrochemical detection following liquid chromatography and capillary electrophoresis. *Anal. Chim. Acta* **2015,** *861*, 1-11. https://doi.org/10.1016/j.aca.2014.08.035

76. Jo, T.; Yoshimi, K.; Takahashi, T.; Oyama, G.; Hattori, N., Dual use of rectangular and triangular waveforms in voltammetry using a carbon fiber microelectrode to differentiate

norepinephrine from dopamine. *J. Electroanal. Chem.* **2017,** *802*, 1-7. https://doi.org/10.1016/j.jelechem.2017.08.037

77. Anastassiou, C. A.; Patel, B. A.; Arundell, M.; Yeoman, M. S.; Parker, K. H.; O'Hare, D., Subsecond voltammetric separation between dopamine and serotonin in the presence of ascorbate. *Anal. Chem.* **2006,** *78* (19), 6990-6998. https://doi.org/10.1021/ac061002q

78. Jaworski, A.; Wikiel, H.; Wikiel, K., Benefiting from information-rich multi-frequency AC voltammetry coupled with chemometrics on the example of on-line monitoring of leveler component of electroplating bath. *Electroanalysis 35* (1), e202200478. https://doi.org/10.1002/elan.202200478

79. Ye, J.-J.; Lin, C.-H.; Huang, X.-J., Analyzing the anodic stripping square wave voltammetry of heavy metal ions via machine learning: Information beyond a single voltammetric peak. *J. Electroanal. Chem.* **2020,** *872*, 113934. https://doi.org/10.1016/j.jelechem.2020.113934

Chapter 5

Machine-learning-guided design of pulse voltammetry waveforms

Part of the information in this chapter is in preparation for submission and has been adapted here.

Movassaghi, C.S.; Perrotta, K.A.; Curry, M.E.; Nashner, A.N.; Nguyen, K.K.; Wesely, M.E.; Alcañiz, M.; Liu, C.; Meyer, A.S.; Andrews, A.M.

5.1 ABSTRACT

Voltammetry is widely used to detect and quantify oxidizable or reducible species in complex environments. The neurotransmitter serotonin epitomizes an analyte that is challenging to detect *in situ* due to low concentrations and co-existing similarly structured analytes and interferents. We developed rapid-pulse voltammetry for brain neurotransmitter monitoring due to the high information content in non-background-subtracted faradaic and non-faradic current responses at each pulse step. Here, we illustrate how Bayesian optimization can be used to hone searches for optimized rapid pulse waveforms in prohibitively large combinatorial spaces. Our machine-learning-guided workflow outperformed random and human-guided waveform designs and is tunable *a priori* to enable selective analyte detection. We interpreted the black box optimizer to gain insights into the logic of machine-learning-guided waveform design. Our approach is straightforward and generalizable for a variety of single and multi-analyte problems requiring optimized electrochemical waveform solutions.

5.2 INTRODUCTION

Voltammetry is widely employed across many fields, including energy storage,[1,2] catalysis,[3] organic synthesis,[4] and electroanalysis (*i.e.,* neuroscience,[5-7] diagnostics,[8] environmental applications,[9] and food and beverage analysis[10]). Despite the variety of analytes suitable for voltammetry, few design principles exist to enable voltammetry waveforms to be identified and optimized systematically. This lack of objectively guided waveform design and optimization imposes significant limitations on voltammetry for single- or multi-analyte detection and monitoring applications.

In chemical neuroscience, voltammetry is broadly used to characterize and quantify electroactive neurotransmitter release and reuptake.[11-13] Recent progress has focused on developing novel electrode materials, coatings, or data analysis procedures to improve selectivity and sensitivity in the brain.[11,14-21] Meanwhile, voltammetry waveform development (*i.e.,* selecting optimal waveform parameters for detecting a particular analyte) has remained largely unchanged for decades. It relies principally upon historic performers (*e.g.,* pre-patterned waveforms), heuristics, and grid search.[22,23]

For neurochemistry applications, historic performers include fast-scan cyclic voltammetry (FSCV) using triangle or N-shape waveforms for detecting evoked dopamine[24] or serotonin,[25] respectively, *in vivo*. Modifying these waveforms can alter the technique's desired sensitivity, selectivity, and temporal resolution.[22,26-28] For example, the development of fast-cyclic square-wave voltammetry has improved the sensitivity and selectivity of dopamine[29] and serotonin[30] detection by superimposing triangle and N-shape waveforms, respectively, on pre-patterned staircase waveforms. Further waveform modifications have led to fast-scan controlled absorption

voltammetry and multiple cyclic square-wave voltammetry to determine basal dopamine[31] or serotonin levels.[32,33] These approaches require separate waveforms to measure separate analytes and timescales, and were derived from the triangle and N-shape waveforms in a guess-and-check manner (**Fig. 5.1**, top).

To enable multi-analyte monitoring (*e.g.*, simultaneous serotonin and dopamine detection) across timescales (*i.e.*, quantification of basal and stimulated neurotransmitter levels using the same waveform in the same recording session), we developed rapid pulse voltammetry (RPV).[34] The latter utilizes background-inclusive (*i.e.,* non-background subtracted) data, requiring waveform design to produce informative background currents.[35] The design of our original generation (OG) RPV waveform is described in the pilot study.[34] While also based on characteristic oxidation and reduction potentials in the triangle and N-shape waveforms, rapid pulses, rather than a fast sweep, reduced fouling and evoked informative faradaic and non-faradaic currents. The resulting current-time fingerprints from our original generation (OG) RPV waveform yielded analyte-specific information that can be used by partial least squares regression (PLSR) or other supervised regression models (*e.g.*, artificial neural networks, elastic net) to distinguish analytes and predict their concentrations. Because the OG waveform was inspired by heuristics from the voltammetric electronic tongue (VET) field for 'soft' sensing (*e.g.,* intermediate and counter pulses),[36-38] we refer to this as VET-inspired design (**Fig. 5.1**, middle).

Having shown that our VET-inspired OG design outperformed conventional waveforms,[34] we sought an expandable and generalizable approach to designing rapid pulse waveforms. Because tuning specific waveform parameters can improve analyte-specific currents,[11,22,39] we hypothesized that optimal RPV waveforms for serotonin and dopamine co-detection (and many more analytes) exist but remain undiscovered due to a lack of design principles.

To address the waveform space problem (*infra vide*), we focused first on the difficult analyte, serotonin. Serotonin is involved in modulating mood, anxiety, and reward-related behavior *via* brain circuits.[40-44] It is also a key gut hormone and plays a role in spinal pain transmission and immune function.[45-48] Serotonin is a challenging target to detect using voltammetry due to its relatively low physiological concentrations (high pM to low nM),[41] colocalization with other neurotransmitters having similar redox profiles (*e.g.*, dopamine), and irreversible oxidation byproducts[49] that can foul electrodes. A waveform development paradigm to discover optimized serotonin waveforms would likely generalize to other neurochemicals and types of analytes.

When developing RPV or other complex waveforms, a prohibitively large number of step or segment combinations impedes exhaustive empirical investigation, even for small numbers of steps or segments. Step/segment voltages, lengths, order, and hold times are all variables for investigation when exploring and optimizing waveforms that can have complex effects on electrochemical signals.[26] While a 'guess and check' approach has yielded a handful of useful conventional and VET-inspired waveforms mentioned above, one-parameter-at-a-time or randomized[50,51] optimization approaches do not take advantage of the rich information diversity encoded in complex waveforms, leaving the overall waveform search space relatively unexplored.

Recently, Bayesian optimization[52-55] has navigated intractable physiochemical search spaces effectively when combined with experimental training data.[56-58] This adaptive experimentation approach presents an opportunity to pair machine learning with electroanalysis to create a new waveform development paradigm (**Fig. 5.1**, bottom). Here, we present a Bayesian optimization workflow that generates fit-for-purpose voltammetry waveforms for selective serotonin detection. To our knowledge, a systematic machine-learning-based approach to designing, testing, and optimizing analyte-specific waveforms has not yet been reported. We show that voltammogram information depends on specific potentials occurring in specific order and timing, confirming the need for a parsimonious search approach across parameter dimensions. An active learning approach outperformed randomly designed and domain expert-designed waveforms after only a handful of iterations. Importantly, our methods can be straightforwardly extended to designing any voltammetry waveform for any electroactive analyte to discover new and perhaps non-intuitive waveforms, optimized specifically for application-specific metrics.

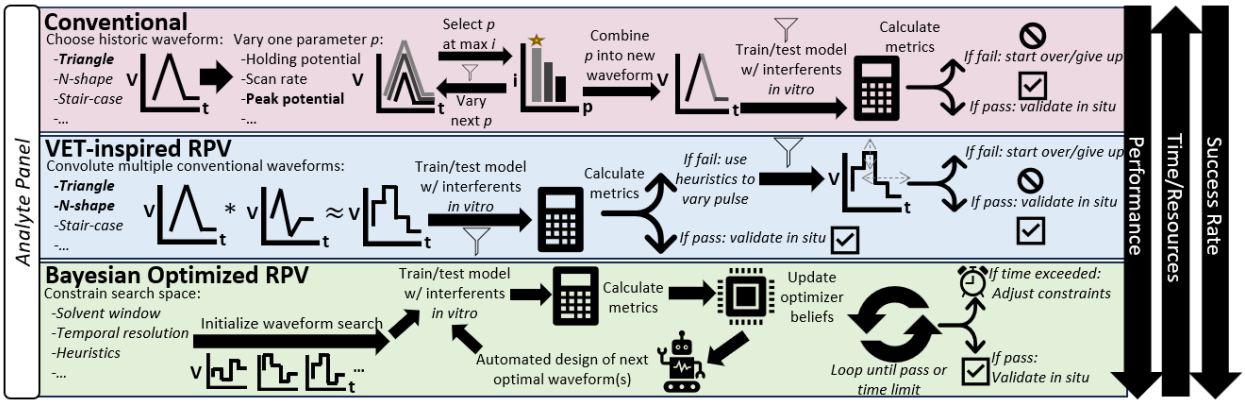

Figure 5.1. Approaches to voltammetry waveform design. Funnels denote likely bottlenecks. RPV = rapid pulse voltammetry.

5.3 RESULTS

The SeroOpt workflow casts waveform development as black box optimization.

We designed the following Bayesian optimization workflow for robust, iterative, and adaptive voltammetric waveform development (**Fig. 5.2**). We sought to identify an input (a rapid pulse waveform) related to an optimal output objective (sensor performance metric; *e.g.*, serotonin detection accuracy) by an unknown, ground-truth objective function (the black box). This function can only be accessed by obtaining experimental training data on various waveform-metric combinations, approximating the black-box function using a surrogate model, and then querying the model to generate an input (waveform) corresponding to a predicted objective optimum. The generated waveform is tested experimentally, and the true objective value for that waveform is

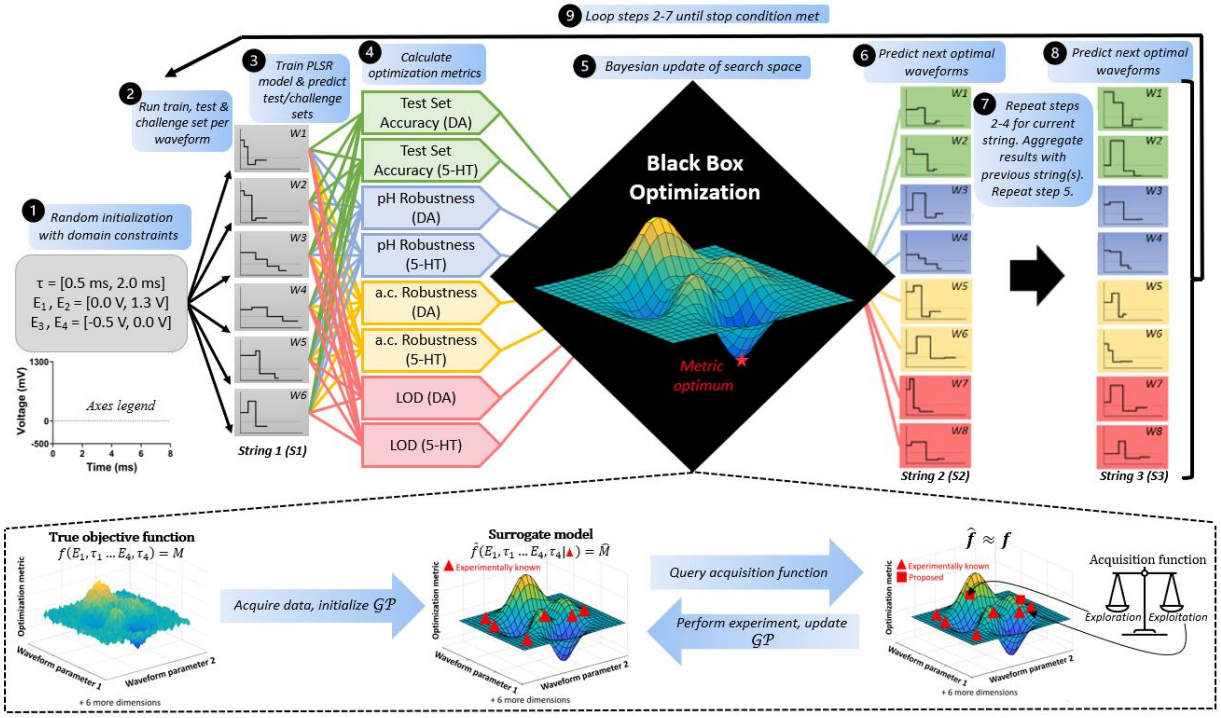

Figure 5.2. Bayesian optimization workflow for machine learning-guided RPV waveform design for serotonin (5-HT) and dopamine (DA). An example visualization of optimization landscapes is shown (bottom). GP = Gaussian process, M = metric, W = Waveform, S = String, a.c. = altered cation; ˆ represents estimation of true value

provided as new training data for the next round of optimization. This sequential feedback loop is

known as Bayesian optimization because the surrogate model is provided updated data on each iteration. Each of the workflow steps is described in detail below.

Search space constraints & initialization by embedding domain knowledge.

Each training waveform **W** was embedded as a vector in 8-dimensional space such that **W** $\coloneqq$ [E_1, τ_1, E_2, τ_2, E_3, τ_3, E_4, τ_4] (**Fig. 5.2,** step 1). Here, E_i is each potential step (V) and τ_i is each step hold time (ms). In this initial design, for eventual comparison with our original generation (OG) human-designed four-step waveform[34] (**Fig. 5.3a**), we constrained the search space to four steps per waveform, with E_1 and E_2 constrained to 0-1.3 V and E_3 and E_4 constrained to -0.5-0 V. These constraints ensured that waveforms remained inside the solvent window[26] and encoded a 'pulse/counter-pulse' (*i.e.,* anodic steps followed by cathodic steps) concept from VET theory.[59] We constrained τ to 0.5-2.0 ms based on our preliminary results showing that capacitive current decays fully after ~2 ms, yet important features are contained in as little as ~0.5 ms.[34] Pulses as short as 0.5 ms contain valuable information and do not result in voltage cross-talk (*i.e.*, residual capacitive current from successive voltage steps).[30,31] To limit the number of parameters, the hold time was defined as $(100 - \sum_{i=1}^{4} \tau_i)$ ms, so each pulse was applied at 10 Hz; the holding potential was defined as E_4.

To initialize a model of the relationship between waveform and objective (*i.e.*, the optimization metric), six waveforms were randomly generated using the constraints above (**Fig. 5.2**, step 1). The choice of six waveforms was arbitrary and was within the number of waveforms that could be experimentally evaluated in a single day. We refer to this collection of random initialization waveforms as string 1 (S1).

Model calibration & optimization metrics allow for relevant objective functions.

We obtained experimental calibration curves (**Table 5.1**) for each waveform (gray boxes, **Fig. 5.2**) to train a partial-least squares regression (PLSR) model as demonstrated previously.[34] The PLSR model predicted the test and challenge set sample concentrations of serotonin and dopamine (**Fig. 5.2**, steps 2-3; see *Methods* for definitions of train, test, and challenge samples). These predictions were used to calculate the eight optimization metrics listed (**Fig. 5.2**, step 4; defined in **Table S5.1**). All metrics were calculated on all waveforms in each string, unless otherwise noted (**Fig. 5.2**, steps 2-4). We focus on the results for the second waveform (W2) of each string, which is optimized across strings for the serotonin test set prediction accuracy metric. The latter is the mean absolute error in the PLSR model predictions of test samples T1-4 (including a blank; **Table S5.1**), thus creating a minimization task (maximum accuracy implies minimal error). We chose mean absolute error rather than relative error due to the presence of the blank (null true concentration).

The choice of test set accuracy as an optimization metric was motivated by several factors. First, we pursued single-objective optimization for simplicity and a lack of user-friendly open-source software to perform multi-objective human-in-the-loop optimization. Having to choose only a single metric to focus on, test set accuracy is an attractive choice as it is a direct measure of waveform performance instead of alternatives, such as PLSR model-specific metrics (*e.g.,* scores clustering). The use of model-specific metrics is less-physically meaningful and would limit the extendibility of our method. Using physically meaningful parameters such as test set accuracy, our workflow remains model-agnostic (*i.e.,* any model that performs supervised regression prediction can be used). For similar reasons of retaining metrics in raw form, we chose not to combine multiple metrics into a single objective task (*e.g.,* scalarization[60]).

Second, we encoded selectivity in our test and challenge set design. Our calibration curve varies the concentrations of all analytes and interferents across the training, test, and challenge sets used to build and evaluate the PLSR models (**Table 5.1**). If the PLSR model for a given waveform confuses any interferent for serotonin, this will be represented in the test or challenge set accuracy metric for serotonin as it will contribute to the mean absolute error. Thus, serotonin test and challenge set accuracy is a proxy for selectivity in varying dopamine, 5-HIAA, ascorbate, DOPAC, pH, and K^+/Na^+ concentrations (see *Methods*).

Lastly, other analytical figures of merit that could be used as optimization metrics (sensitivity, limit of detection (LOD), linear range, *etc*.) are irrelevant if model accuracy and selectivity are not first established. For example, we included LOD as an alternative optimization metric (**Fig. 5.2**). While optimizing for LOD improved signal-to-noise ratio, as expected (**Fig. S5.2**), the selectivity performance of LOD-optimized waveforms (inferred *via* test and challenge set accuracy) was poor. Thus, we did not continue to optimize for LOD in subsequent campaigns but were still able to utilize these waveforms as training data by calculating their other metrics. For these reasons, we focused on test set accuracy. Specifically, we focused on serotonin (5-HT) because it is historically a more difficult analyte to detect by voltammetry. Its concentrations are approximately 10-fold lower than dopamine in striatum and serotonin has complex redox mechanisms and fouling processes.[25]

Regardless, we included other optimization metrics in our workflow rather than solely serotonin test set accuracy to explore which metrics have an objective landscape that is 'optimizable'. As this was a first attempt, we had no guarantee that the serotonin test set accuracy was a viable choice of metric. We also wanted to investigate other analytes and metrics for future use with multi-objective optimization. For example, we included dopamine-specific metrics in the

scheme for comparison with our original RPV work because serotonin/dopamine co-detection is a long-term goal for multi-objective optimization.[34,61]

Pursuing a single metric would entail only a single waveform tested per string, which is inefficient in preparing the complex calibration curves used here. By calculating and incorporating the additional metrics for all waveforms, instead of optimizing on only a single metric per waveform, our approach allows seven additional experimental points to be explored per string. Thus, performing single objective optimization across multiple metrics in parallel is a way of exploring 'optimizable' metrics and obtaining additional training data per string in a simple yet sample-efficient manner. For example, if test set accuracy failed as an optimizable metric for serotonin, we could pivot to an alternative metric.

Parallel single objective optimization of multiple metrics.

The waveform embeddings and corresponding experimentally determined metrics were used to train the surrogate models (*i.e.*, Gaussian processes)[54] of the unknown objective functions (**Fig. 5.2**, step 5). As mentioned, only single-objective optimization was performed on each metric. Separate Gaussian processes were trained (one for each metric; eight total) in parallel on the aggregated data after evaluating each string. An acquisition function (*i.e.*, expected improvement)[54] finds the optima of each surrogate function and outputs the next most likely waveform that will improve each respective metric (**Fig. 5.2**, step 6). The process then repeats (**Fig. 5.2**, steps 7-9). The overall workflow is illustrated in **Figures 5.2** and **S5.8**.

The eight waveforms (each corresponding to optimization for one of the eight metrics) output from the first optimization loop of this workflow are shown as string 2 (S2). These eight

new waveforms were generated for S2 with each new waveform optimized on a single metric (*i.e.,* using the training data generated from S1 (**Fig. 5.2**, steps 4-6)). Because S1 was randomly generated to initialize the surrogate model, S2 represented the first iteration of optimized waveforms generated by the workflow.

We repeated the optimization loop by obtaining experimental calibration curve data using each new S2 waveform. We then calculated the individual optimization metrics, aggregated the data with the previous string(s) (*e.g.*, all S3 waveforms were predicted using all S1 *and* S2 data, one metric at a time), and predicted the next set of optimal S3 waveforms for each metric (**Fig. 5.2,** steps 7-8). This process was repeated again to generate four waveform strings in total (**Fig. 5.2**, step 9). We refer to the group of strings as S1-4. Each string had eight waveforms (W1-8) corresponding to eight separate metrics, except the initial string (S1), which had only six randomly generated waveforms (arbitrary). Collectively, all four strings and their associated waveforms were referred to as run 1 (R1).

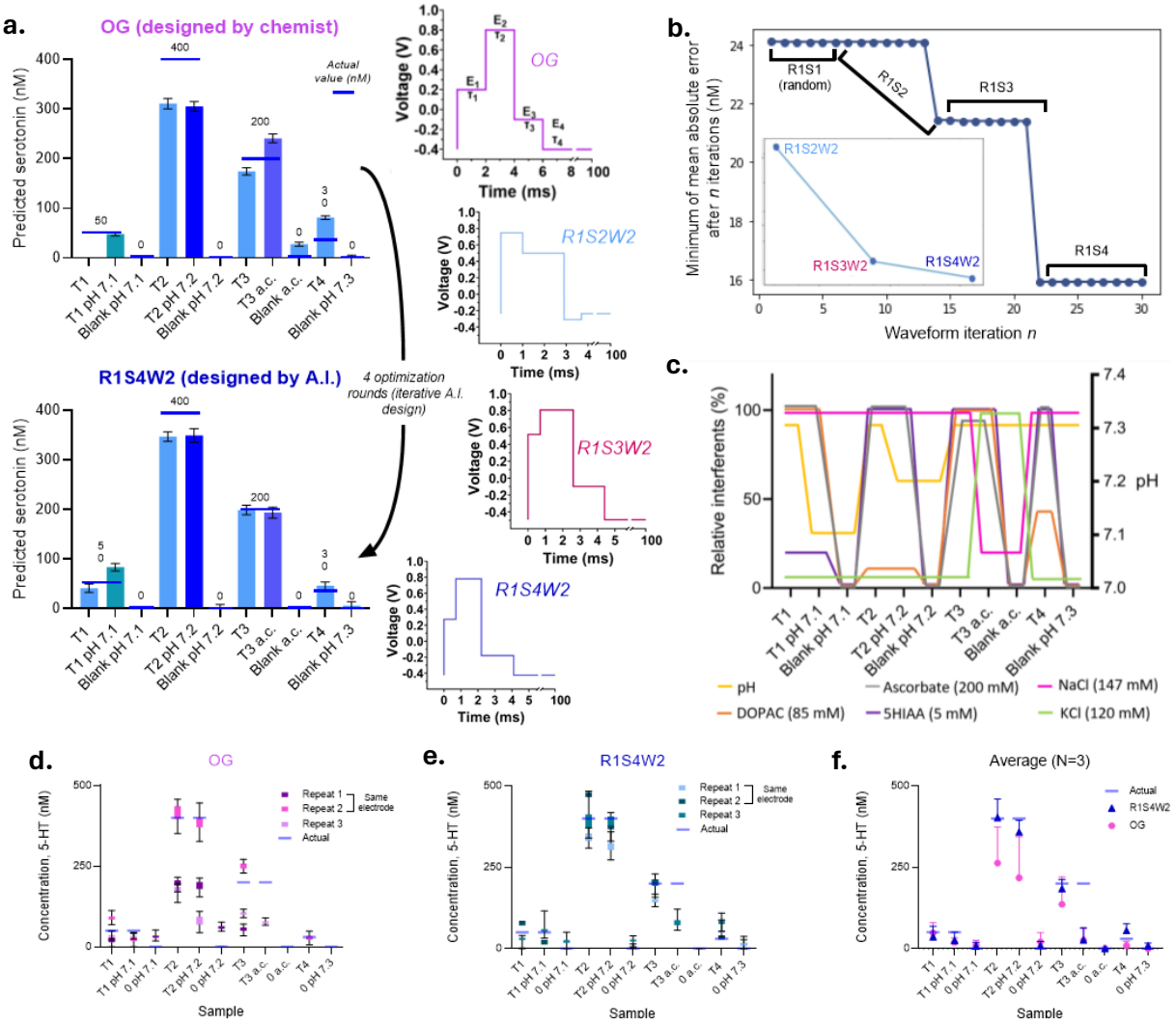

Figure 5.3. a) Bayesian optimization waveform (R1S4W2; bottom) outperforms the original generation (OG) human-designed RPV waveform (top) after four iterations. Error bars represent standard deviation. **b)** Convergence plot of the minima of 5-HT test set accuracy per string. The waveforms optimized specifically for 5-HT test set accuracy (W2) are shown on the inset. **c)** Varied interferents encountered in the test and challenge set samples (a.c. = altered cationic salt concentrations). **d)** Test and challenge set results for the OG waveform in triplicate across two electrodes. Error bars represent minimum and maximum values predicted. **e)** Test and challenge set results for the optimized serotonin waveform (R1S4W2) in triplicate across two electrodes. Error bars represent minimum and maximum values predicted. **f)** Average of d,e. Error bars represent standard deviation.

Machine learning outperforms human-guided waveform design.

Across R1, three new waveforms were generated by optimizing for serotonin test set accuracy (S1W2 was random; the three successive (S2W2, S3W2, S4W2) were each more 'optimal' than the last). The evolution of the serotonin accuracy waveform across three successive strings was compared to our initial RPV OG waveform (**Fig. 5.3a**). We noticed similarities between the OG waveform and the final optimized waveform, R1S4W2 (**Fig. 5.3a**, top right and bottom right, respectively). In the first run, the final waveform generated by our Bayesian optimization scheme near perfectly mimicked our chemically intuitive choices for the potentials of the waveform design; they differed only by ~100 mV or less. The remarkable differences were in the individually optimized step lengths (τ) for R1S4W2. Values of τ are rarely optimized individually and instead are set to a global value decided by one-factor-at-a-time optimization under single experimental conditions (*e.g.,* 2 ms for all steps in the OG design).[29-32,34]

Even though R1S4W2 was only 5.5 ms long, it outperformed the OG which was 8 ms. Given the similarity in pulse potentials, the increase in data fidelity was attributed partially to changes in the hold times of each step; that is, Bayesian optimization was able to generate better-performing choices of τ.

While a 2.5 ms difference in overall pulse length was ostensibly negligible, at data rates of 1 MHz, this equates to a reduction of 2500 data points per scan. This reduction can easily save gigabytes of unneeded data that otherwise would have to be stored, and save computation time wasted during multi-hour experiments. Decreasing the overall length of the rapid pulse sequence also opens opportunities to increase the temporal resolution to >10 Hz or design more complex pulses with additional steps while retaining 10 Hz sampling.

We did not simply 'get lucky' or stumble across a similar waveform randomly, as the convergence plot (**Fig. 5.3b**) shows that for each optimization string (S2-S4), the waveform optimized for serotonin test set accuracy (W2) found a new minimum for serotonin prediction error during each iteration. This improvement across strings suggests that the surrogate model is learning a reasonable representation of the optimization landscape for serotonin accuracy.

Explicit and implicit discovery of interferent-agnostic waveforms.

We next compared the results for the test and challenge set samples from the OG waveform to R1S4W2 (which should be the best-yet waveform for test set serotonin performance). Indeed, R1S4W2 outperformed the OG waveform for serotonin detection in the test set samples and the challenge set samples (see *Methods*). The train and test sets contain samples with varying levels of three physiologically relevant metabolites (DOPAC, 5-HIAA, ascorbate). Meanwhile, the challenge set samples have physiologically relevant pH, Na^+, and K^+ levels that were held constant in the training set (**Fig. 5.3a,c**, samples denoted pH 7.1, pH 7.2, and altered cations or "a.c."). The optimized serotonin waveform R1S4W2 outperformed the OG waveform for interferents it was explicitly (DOPAC, 5-HIAA, ascorbate) and not explicitly (pH, Na^+/K^+) trained on. For example, while the OG waveform confounded changes in pH and Na^+/K^+ contained in the challenge set, the R1S4W2 waveform did not suffer similar problems (see samples T2 pH 7.2, T3 a.c., blank a.c. for each waveform in **Fig. 5.3a**). This result was not due to the waveform not sensing a change in current for varying cation concentrations or being 'electrochemically silent'.[62] Increases in current (hundreds of nA) were evident when aCSF a.c. blanks were injected compared to normal aCSF blanks (**Fig. S5.5b**). Similar responses were noted for pH blanks.

To investigate whether the initial results for R1S4W2 outperforming the OG waveform were precise and robust, the waveforms and training/test/challenge sets were run in triplicate across two different electrodes (**Fig. 5.3d-f**). We determined that the R1S4W2 waveform increased prediction accuracy for test samples 1-4 by ~20% compared to the OG waveform. We found that the agnostic behavior towards pH was reproducible for R1S4W2 and not the OG. However, we did notice that the T3 a.c. challenge sample accuracy was not reproducible across electrodes for either waveform. We attribute this to differences in the fabrication of the electrodes. Standardizing the fabrication of fast voltammetry electrodes, along with multi-objective optimization with reproducibility as a metric, will help alleviate this issue. Regardless, the performance of R1S4W2 as an early optimization candidate showing enhanced test and challenge set accuracy demonstrates the success and future promise of SeroOpt.

The SeroOpt workflow is reproducible and outperforms random search.

To investigate whether Bayesian optimization was simply "getting lucky" and not gleaning chemically relevant information, this process was repeated starting with a new set of six random waveforms and carried out for four strings as described above (**Fig. 5.4**). We refer to this as run 2 (R2). Note that data are aggregated across strings in each run, data between runs are not aggregated. The runs are kept separate to compare, from a new randomized initialization, whether four rounds of Bayesian optimization can repeatedly produce improved waveforms. We do not expect the convergence of R2 on the same waveform as R1. The search space is vast and given only a small subset of waveforms, converging on the same optima is unlikely. Rather, if R1 and R2 both find improved waveforms faster than the randomized waveforms, we can then examine the black box models to see what makes the optimizer decide on 'good' waveforms (*vide infra*).

In all cases, except for the first run of pH and a.c. challenge samples, the average serotonin test/challenge set error was lower when using the optimized serotonin waveforms (W2,4,6,8 for S2,3,4 of R1 and R2), when compared to the average for the randomly generated S1 waveforms of R1 and R2 (**Fig. 5.4**). The error minima were lower in all cases for the optimized waveforms; random search never produced a better waveform than Bayesian optimization. For example, while each W2 in R1 improved across strings, R2S2W2 immediately found a 5-fold lower minima than the starting initialization. Thus, new random initialization can cause the discovery of new waveforms in local minima. Continuing this optimization indefinitely may lead to the discovery of global optima.

These results suggests the following. On average, Bayesian optimization produces better waveforms than randomly generated or chemist-enabled waveforms. Bayesian optimization finds waveforms corresponding to error minima better than random chance. The Bayesian optimization surrogate model (*i.e.,* Gaussian process) effectively models the relationship between voltammetry waveforms and performance, as the minima only occurred for waveforms optimized specifically for serotonin detection. (In addition to outperforming random waveforms, waveforms optimized for solely dopamine did not outperform those optimized for serotonin when assessing serotonin output metric accuracy). For example, using the randomly generated waveforms, the average serotonin accuracy was ~45 nM. By optimizing for any serotonin parameter, the average serotonin accuracy was improved to 34 nM (24% improvement). While an ostensibly small return on investment, this is only the first iteration of this protocol, and the results consistently outperform the few standard alternatives to waveform design.

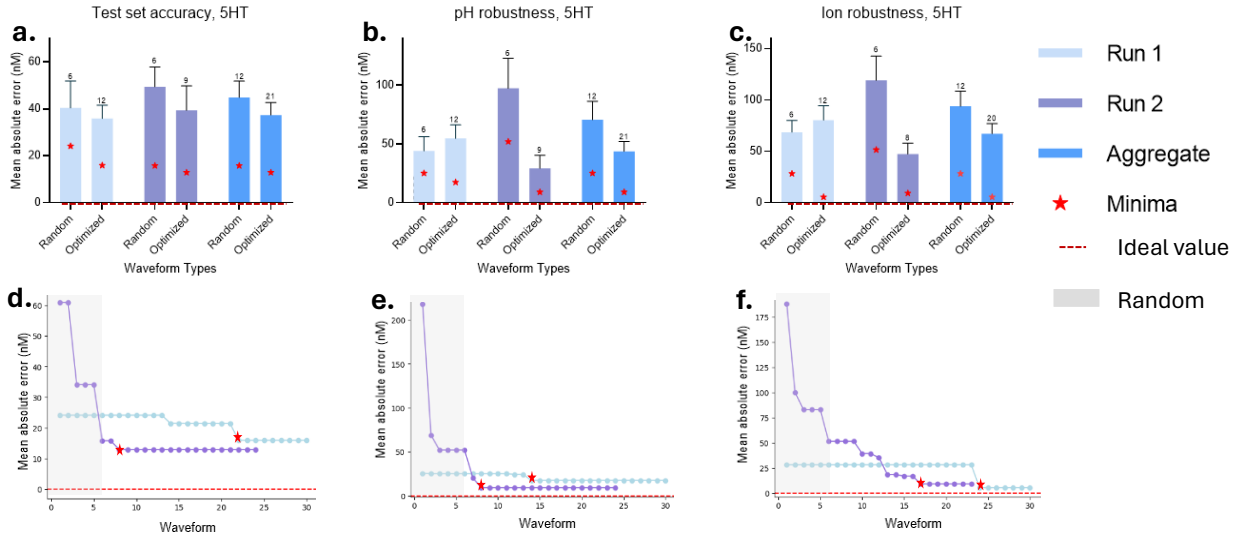

Figure 5.4. Bayesian optimization outperforms random search. Average mean absolute error for run 1, run 2 and the aggregate of both runs are shown for serotonin test set accuracy **(a)**, pH robustness **(b),** and ion robustness **(c)**. Error bars represent standard deviation. Sample size is shown atop the bars. The minima of error is for each group of waveforms is denoted by a red star. Random refers to string 1 waveforms only. Optimized refers to waveforms optimized for 5-HT performance (*i.e.,* W2,4,6,8). **(d-f)** Convergence plots corresponding to a-c, respectively, showing current minimum mean absolute error at each waveform iteration. Gray boxes represent random initialization waveform regions.

Fine-grained waveform parameter tuning improves predictive performance.

In total, 55 waveforms were tested experimentally (the OG waveform, 12 randomly generated waveforms from R1S1 and R2S2, and 42 Bayesian optimized waveforms from R1 and R2 S2-4) with their corresponding metrics given as optimization training data. The generated waveforms covered a wide search space across all the waveform parameters (**Fig. 5.5**). Clusters of points are interpreted as exploitation, while isolated points are interpreted as exploration. A key advantage of Bayesian optimization is that the acquisition function parsimoniously explores a search space with the exploration-exploitation trade-off in mind.[54] Bayesian optimization judiciously explored the search space over 55 waveforms. At the time of writing and to our

knowledge, this is the largest optimization scheme covered in neurochemical voltammetry waveform development.

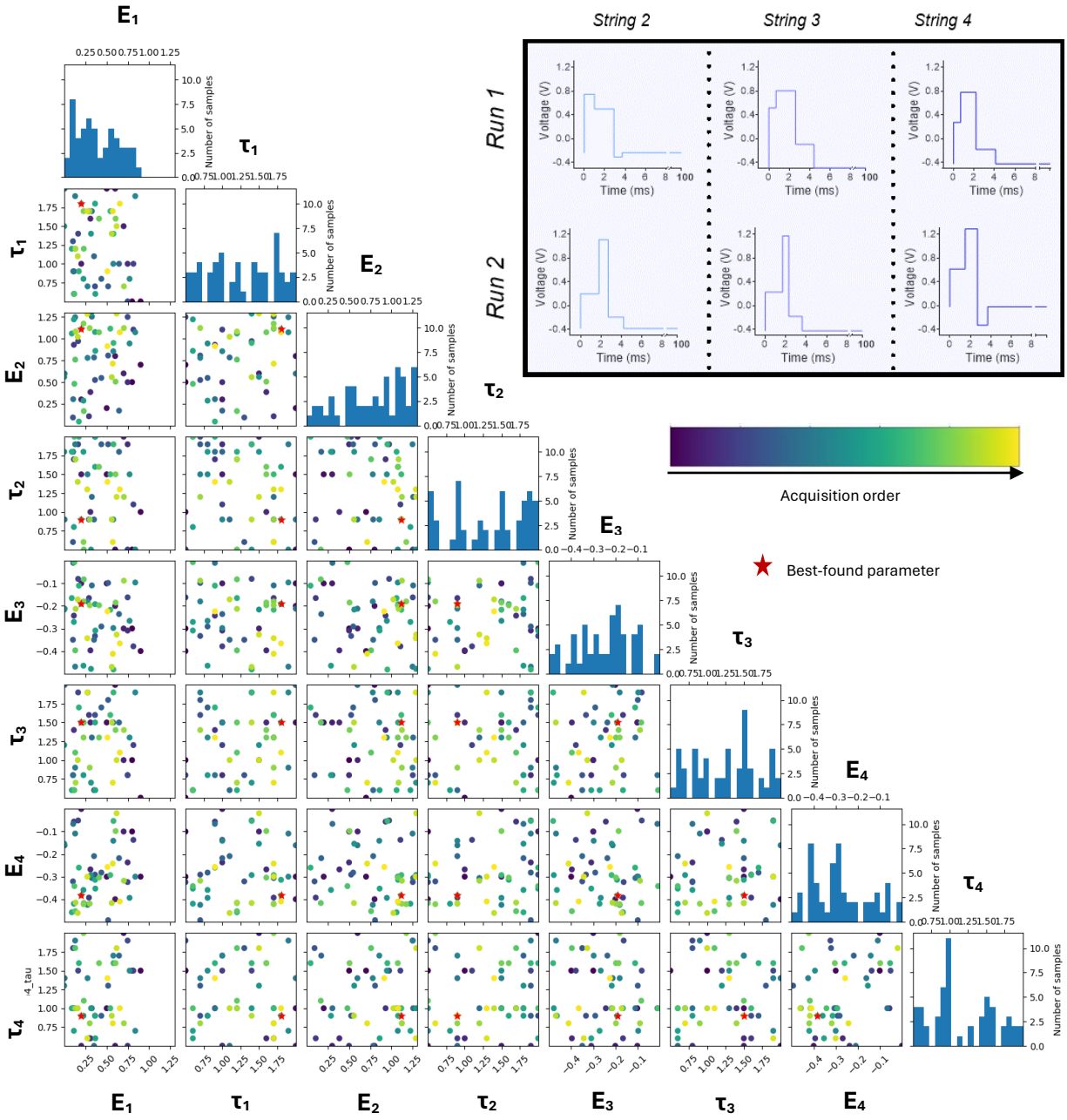

Figure 5.5 Search space of all waveforms tested experimentally from runs 1 and 2. Red star represents optimum parameters. Histograms represent the frequency of that parameter value in the waveforms tested. **(inset)** Evolution of the predicted Bayesian optimization waveforms across two separate Bayesian optimization runs, 1 and 2**,** for serotonin accuracy metric in blue (W2). String 1 not shown as they were randomly generated.

Data for all waveforms and metrics are provided (**Tables S5.2, S5.3**). We noticed that for serotonin accuracy (W2), the predicted waveforms between R1 and R2 looked similar, especially for S3 and S4 (**Fig. 5.5**, inset). The serotonin accuracy waveforms share characteristics with the OG waveform across R1 and R2. They exhibit low to high potential steps for the oxidative potential steps and high to low potential steps for the reductive potential steps. By S4, all waveforms prefer the 'intermediate' anodic pulse step concept described in VET literature, in which a relatively low amplitude E_1 step before a higher amplitude E_2 step prevents signal saturation and enhances concentration discrimination.[37] Further, most waveforms exhibited a large amplitude counter-pulse (*e.g.,* a large difference between E_2 and E_3 to complete the redox cycle).[59] The fact that the model is learning these domain knowledge heuristics in these four iterations suggests it can also learn more complex, higher order interactions.

Waveform optimizations occurred with relatively small changes in E and τ, even for waveforms as simple as four steps as shown here. Tuning these waveforms can result in drastic waveform differences, and this effect is relatively unexplored in a systematic, multi-variate manner as done here. For example, R1S4W6 and R1S3W8 differed by $\leq$0.04 V and $\leq$0.9 ms in E and τ (**Table S5.2**). Yet, R1S3W8 outperformed R1S4W6 for serotonin test set, pH and ion accuracy, with up to nearly 50% reduction in error (**Table S5.3**).

To test whether this effect was due to differences in electrodes across strings (separate electrodes were used across strings to encourage generalizability across electrodes), we compared two similar waveforms tested on the same electrode: R2S1W2 and R2S1W3. These waveforms differed only by $\leq$0.15 V and $\leq$ 1.2 ms, yet R2S1W2 outperformed R2S1W3 in all serotonin metrics (**Table S5.2, S5.3**). Thus, small and otherwise "insignificant" changes in step potential and

holding time can produce major accuracy differences. These findings support the importance of a technique like Bayesian optimization to tune parameters with fine-grained adjustments.

The order of the steps in the rapid pulse also matters. For example, R1S1W1 and R1S4W3 are nearly identical, except for the order of their pulses. Yet, R1S1W1 outperformed R1S4W3 in all categories by up to five-fold (**Tables S5.2, S5.3**).

Interpretable machine learning reveals waveform parameter interactions and learnable heuristics

Aside from the qualitative explanations above, interpretable machine learning methods[63] can be applied to 'open the black box' and assess how Bayesian optimization decides upon improved waveforms. We used a global, model-agnostic technique known as partial dependence plots (PDPs) to visualize how varying waveform parameters affects the surrogate model predictions.[63] The PDPs are useful for non-parametric models, such as Gaussian processes, that are not directly interpretable.[63] Essentially, PDPs average the predictions from the model over samples where all parameters, except the ones of interest, are held constant. The effect of changing just the parameter(s) of interest can then be inferred (*i.e.,* the partial dependence of a feature).

The PDPs for aggregated runs (R1 and R2 combined) and individual runs are shown for the serotonin test set accuracy metric (**Figs. 5.6a, S5.3, S5.4**, respectively). We focus on the aggregated models because these have more total samples and thus, are more likely to uncover meaningful relationships. The 2D plots on the diagonal represent the average effect of a metric while varying that parameter. Generally, the more a PDP plot for a particular feature varies, the more important that feature. Conversely, flat lines indicate either unimportant or interacting

features. The aggregated data PDP (**Fig. 5.6a**) confirm a complex and interacting optimization landscape. For example, E_3 oscillates, E_4 is parabolic, and E_1 and τ_1 are monotonically decreasing or increasing, respectively. The 3D contour plots below the diagonal represent average effects on each metric while varying two waveform parameters. Because we minimize error, the purple shading represents the optimal (minima) regions, while the yellow regions represent maxima.

The PDPs have some weaknesses. First, PDPs represent averages, meaning heterogenous interactions can be obfuscated (*e.g.,* an effect on one-half of the data may be averaged out by an opposite effect on the other half). Thus, non-varying parameters in PDPs could be misinterpreted. To confirm this, we examine individual conditional expectation (ICE) plots. The ICE plots show the individual contributions that make up the averages in the PDP plots.[63] Thus, the 2D PDPs (blue lines, **Fig. 5.6a**) have matching structure with the average ICE plots (blue lines, **Fig. 5.6b**). The individual instances (gray lines, **Fig. 5.6b**) show that there are heterogeneous effects hidden by the PDP averages for some parameters. For example, τ_1, E_3 and E_4 have traces that do not all follow the same general trends. Thus, varying these parameters is dependent on heterogeneous interactions between the other waveform parameters. Meanwhile, the remaining parameters E_1, E_2, τ_2, τ_3 and τ_4 all appear to follow the same general trends (flat lines suggesting non-interacting waveform parameters).

As an alternative to PDP and ICE plots, we used Shapley additive explanations (SHAP) plots.[63] The SHAP values enable interpretations of how features contribute to individual model predictions. The SHAP plots confirmed that E_3, E_4, τ_1, and E_1 were the most important features. **Figure 5.6c** shows the spread of the SHAP value per feature. Further, the heterogeneous effects, particularly in E_3 and E_4, are confirmed by the different colors of the feature values that do not cluster on a single side.

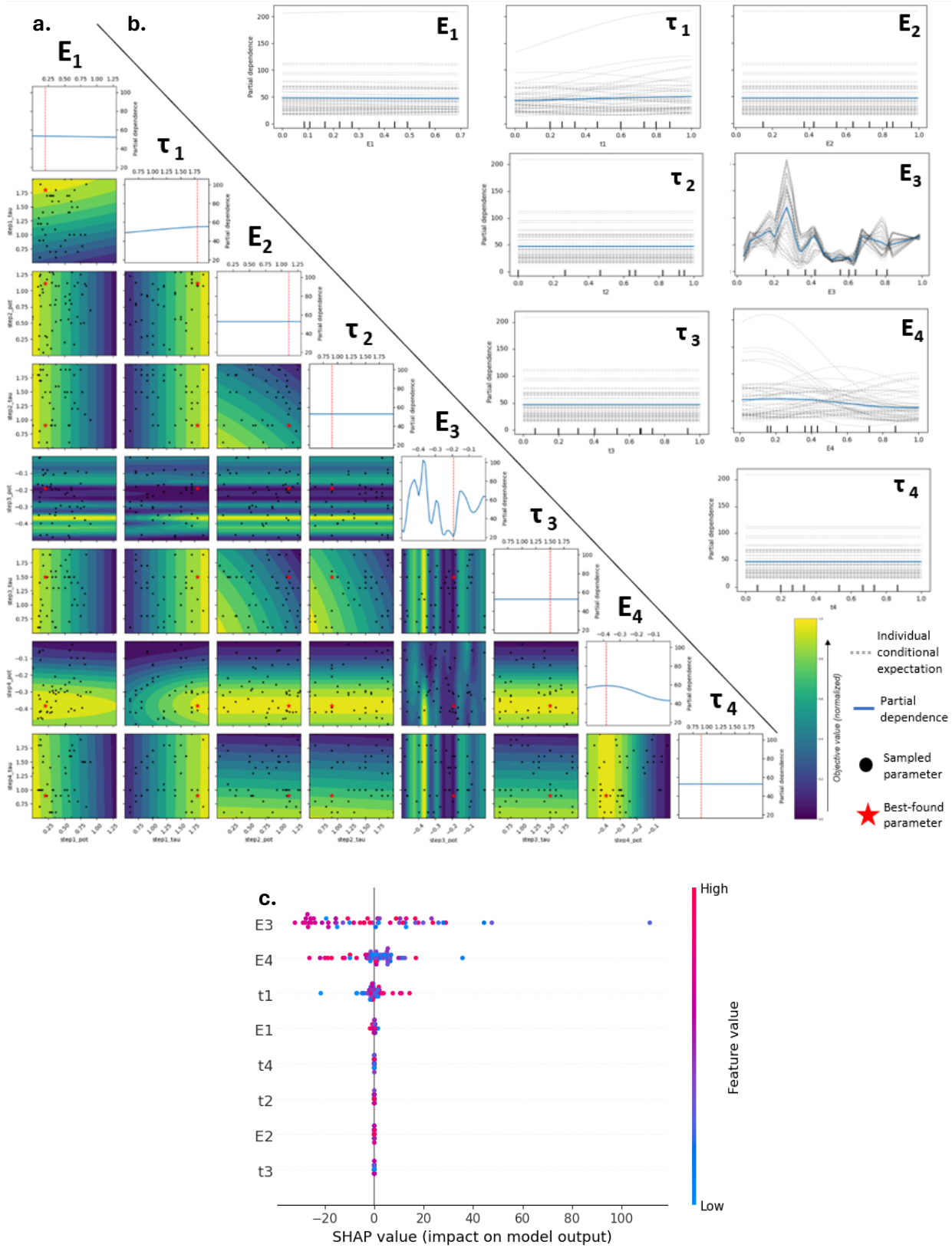

Figure 5.6. a) Partial dependence plot. **b)** Individual conditional expectation plots. Ticks represent deciles of the feature values. **c)** Shapley additive explanations summary plot.

5.4 DISCUSSION

Bayesian optimization enables data-driven experimental design to identify global optima in high-dimensional search spaces across complex interaction parameters.[55] It has been widely applied across diverse fields, including automated machine learning,[64] robotics,[65] sensor design,[66] materials discovery,[56,67] and chemical reaction optimization.[57,68] Despite its advantages and versatility, applications of Bayesian optimization to analytical chemistry and specifically, electrochemistry are still uncommon.[69-72] We are not aware of previous applications of Bayesian optimization to voltammetry waveform design.

Other approaches can be used to design waveforms (*e.g.*, first-principles, chemometric screening, design of experiments). However, these approaches suffer from limitations associated with limited computational complexity, an exponential number of experiments required per parameter, resource intensity (labor, time, materials, *etc*.), and/or the inability to account for confounding waveform parameter interactions.[64] Our attempts to use feature selection to identify key waveform step potentials and lengths were confounded by the magnitude of the current response and the pulse pattern (**Fig. S5.1**).

We introduced an experimental design framework to embed voltammetry waveforms and their corresponding electroanalytical performance into a Bayesian optimization workflow. Rather than optimizing for an electrochemical response, the accuracy of supervised regression models was optimized directly by including model accuracy metrics as the objectives. We explored which model metrics were optimizable by simultaneously performing parallel single-objective optimization loops across eight metrics (**Fig. 5.2**). We found that serotonin test set accuracy

optimization was sample-efficient, reproducible, and outperformed domain-guided and randomly designed waveforms across multiple metrics (**Fig. 5.3**).

We showed that in two separately initialized optimization campaigns consisting of four strings or 'rounds', we generated waveforms selective for serotonin in the presence of interferents (**Fig. 5.4**). Previous applications of Bayesian optimization in other fields achieved improvement in as few as three or four string-like iterations (*i.e.,* low data regimes). The behavior we observed was not unexpected.[56,57,65,66] Notably, our selectivity challenges were more arduous and efficient than many standard waveform validation schemes that test only a single interferent or interferent concentration after the waveform is developed for the analyte of interest.

Selectivity is a major barrier to effective waveform design, especially for background-inclusive and multi-analyte waveforms. Most voltammetry approaches achieve selectivity by either training a machine-learning model, modifying the waveform, or changing the electrode material. Rather than independently adopting one of the latter approaches, our data-driven waveform design uses the predictive performance of a machine learning model as feedback to modify waveform parameters – the black box model decides what waveform would generate accurate PLSR predictions.

In addition to 5-HIAA, DOPAC, and ascorbate, monovalent cation concentrations (*i.e.*, Na^+, K^+, H^+) fluctuate in the extracellular space upon neural stimulation due to the biophysics of membrane polarization and repolarization, transporter dynamics, and elevated O_2 consumption (and CO_2/carbonic acid/H^+ production) associated with synchronized action potentials.[67] Thus, these species represent key interferents to test in the presence of analytes, as electrodes will likely encounter changes in interferent concentrations under real-world (*in vivo*) conditions.

The literature suggests that certain voltage pulses can deconvolute monoamine neurotransmitter responses from cation changes.[68-70] Thus, we hypothesized our search space would contain inherently interferent agnostic waveforms. That is, we expected to find waveforms whose voltammograms, when modeled in low-dimensional spaces by PLSR, are selective for features specific only to the analytes of interest (dopamine and serotonin) and not features that are affected by interferents. If a waveform-model combination can ignore cation interferent effects (*i.e.,* is cation agnostic), training across such interferents is unnecessary. Thus, we built the search for agnostic waveforms into our Bayesian workflow in an implicit manner by introducing the concept of a challenge set.

Challenge set samples illustrated that SeroOpt can identify implicitly (*i.e.,* requiring no explicit training samples) interferent agnostic waveforms (**Fig. 5.3a**). While the literature has demonstrated cationic interferent agnostic waveforms,[62,68-70] our approach required no manual or additional data processing, and instead automatically designed the agnostic waveforms. Combining the information content of an optimized waveform with a powerful machine learning model (PLSR) enabled this agnostic behavior.

Because step potential,[37,59] step order,[36] and hold time[71] or potential[69] can impact waveform performance, other pulse techniques that simply layer steps at constant potential steps and times could maximize their performance by tuning these parameters similarly to the manner presented here.[38] Adding more pulses could deteriorate model performance, as useless steps add noise to the data.[38] Thus, careful selection of the number of steps is paramount. We confirmed this by noting performance differences across waveforms with only slight parameter differences. We attribute this to the unique faradaic and non-faradaic processes that occurred at sub-ms timescales.[62,68,70,72]

Optimization of individual pulse step lengths results in different transient redox responses from preceding pulses to become the starting state for succeeding pulses, as opposed to letting the current decay to steady state. A non-steady-state approach has been shown to discriminate compounds better using VETs,[71] yet a lack of methods for optimizing individual step lengths has prevented wide adoption of this optimization practice. Differentiation of dopamine from norepinephrine has been accomplished using pulses with differences as small as 0.1 V though without systematic design patterns.[73]

Potential mechanisms for the success of interferent agnostic waveforms include diffusion layer depletion of the interfering species by the onset pulse (E_1/τ_1),[74] and other differentiating information provided by unique pulse sequences and transient responses of the rapid pulses to the model.[68,70,71] More optimization campaigns, interpretability techniques, and the use of numerical simulation of species at electrode surfaces could uncover the phenomena at play.

Regardless, the finding that interferent agnostic waveforms can be identified and optimized, especially when forgoing background subtraction, shows the utility of including historically categorized "non-specific" capacitive currents. These findings support the idea that analyte-specific information from appropriately designed waveforms occurs in the background current. This information is captured by our model without explicit training, even in the presence of interferents that affect the double layer. Previous reports have shown that pH and Na^+/K^+ fluxes can cause hundreds to thousands of nM in prediction error *in vitro*.[68,75] For the same fluxes, our waveform-model combinations show only tens of nM error or less, and do not require explicit training, specialized waveform augmentation, or data analysis.

We noticed that across runs and interpretability methods, E_1 or τ_1 (onset pulse/time), E_2 and E_3 (pulse/counter pulse[59]), and E_4 (holding) were continually ranked as the most important features for the surrogate models of serotonin test set accuracy. These parameters represent four known heuristics: counter pulse potential (E_3, useful for analyte confirmation),[59] holding potential (E_4, for analyte accumulation, sensitivity, and reduced serotonin fouling),[26] and τ_1 and E_1 (onset time/intermediate potential; useful for selectivity and diffusion layer depletion).[74] Further meta-analyses of these behaviors will provide important insights into unexpected electrochemical optimization design patterns.

Small amplitude onset pulses have been shown to improve the deconvolution and differentiation of ions such as pH,[70] Na^+ and K^+,[68] along with small amplitude onset sweeps for drift and pH.[62,76] Again, carefully designed waveform tuning can result in explicit and implicit interferent agnostic waveforms. Other waveform parameters deemed unimportant in this study might be associated with the imposed constraints affecting the full exploration of parameter space or our relatively small sample size. Further, the interpretability methods are also estimates of the surrogate model, which itself is an estimate. Thus, our interpretations must be taken lightly as correlations, not causation.

The SeroOpt paradigm is immediately extendable to more than 4 steps (8 parameters) to create more complex waveforms. Future research into other optimization metrics, supervised regression and surrogate models/kernels, and additional analytes is underway. For example, pulses have been shown to differentiate norepinephrine from dopamine.[73]

We note the extendibility of our waveform embedding approach. This embedding can be used for any waveform type, such as sweeps, where the parameter values represent the slopes (scan

rate) of each segment, along with parameters for start and stop potentials. Pulse and sweep designs can also be combined.[74] Similar approaches could also extend to embedding AC voltammetry parameters (*e.g.*, amplitude, phase).[77] Thus, rather than starting from a historic performer and exploring new waveforms one factor a time, entirely new waveforms can be discovered *de novo*. Our approach will help to accelerate waveform development for new single- and multi-analyte panels in environments hindered by selectivity or other difficult-to-optimize metrics.

Further exploration of waveforms with this agnostic behavior and using multi-objective optimization are underway. While this study focused on serotonin, we serendipitously identified promising co-detection waveforms for dopamine, serotonin, and ion robustness (**Fig. S5.5**). The next steps include reproducibility tests, multi-objective optimization, and *in vivo* application to explore optimal co-detection waveforms.

5.5 METHODS

Chemicals

Serotonin (5-HT) standards, dopamine (DA) standards, and artificial cerebrospinal fluid (aCSF) solutions were purchased from and prepared as described in previous literature.[34] The standards for 5-hydroxyindoleacetic acid (5-HIAA) (#H8876), 3,4-dihydroxyphenylacetic acid (DOPAC) (#850217), and ascorbic acid (#A92902) were purchased from Sigma-Aldrich (St. Louis, MO). The aCSF solution was adjusted on the day of the experiments to pH 7.1, 7.2 or 7.3 ± 0.03 using HCl (Fluka, #84415). Altered cation (a.c.) aCSF buffer contained the following ion composition: 31 mM NaCl (#73575), 120 mM KCl (#05257), 1.0 mM NaH_2PO_4 (#17844), 2.5 mM $NaHCO_3$ (#88208) purchased from Honeywell Fluka (Charlotte, NC), and 1.0 mM $CaCl_2$ (#499609) and 1.2 mM $MgCl_2$ (#449172) purchased from Sigma-Aldrich. All aqueous solutions were made using Milli-Q grade or higher water (Sigma-Aldrich).

Electrode fabrication and polymerization

Carbon fiber microelectrodes were fabricated as follows: 7-μm diameter carbon fibers (T650/35, Cytec Carbon Fiber) were vacuum-aspirated into O.D. 1.2 mm, I.D. 0.69 mm, 10 cm length borosilicate glass capillaries (Sutter Instrument Company, Novato, CA, B120-69-10). A micropipette puller (P-1000, Sutter Instrument Company, Novato, CA) was used to pull each capillary into two electrodes by tapering and sealing the glass around the carbon fiber. Four-part epoxy (Sigma Aldrich, Spurr Low Viscosity Embedding Kit- EM0300) was backfilled into the tip of each electrode. Epoxied electrodes were dried at 70 °C for 8-12 h. Electrode tips were cut to ~100 μm using micro-scissors under an inverted microscope. For electrical conduction, the

electrodes were backfilled with a non-toxic metal alloy of gallium-indium-tin, Galinstan (Alfa Aesar, 14634-18). Bare copper wire (0.0253-in. diameter, Archor B22) was polished using a 600-grit polishing disc and inserted into working electrode capillaries to serve as the electrical connection to the potentiostat. Epoxy (Loctite EA 1C) was then placed around the top of each electrode to secure the Cu wire in place. The epoxy was cured for 24 h at room temperature.

Electrode tips were cleaned with HPLC-grade isopropanol (Sigma Aldrich #34863) for 10 min. Electrodes were then overoxidized by applying a static 1.4 V potential for 20 min.[78] Low-density EDOT:Nafion solution was made by first creating a 40 mM EDOT stock; 100 µL of this stock was added to 200 µL of Nafion and diluted with 20 mL of acetonitrile.[14] A triangle waveform (1.5 V to -0.8 V to 1.5 V) was applied using a CHI Instruments Electrochemical Analyzer 15x at 100 mV/s to generate a PEDOT:Nafion coating on each electrode.

In vitro experiments

Reference electrodes were made by placing 0.025-inch silver wire (A-M Systems, 783500) into bleach for 10 minutes. Each reference electrode was rinsed with distilled water before being used in experiments. A flow cell (NEC-FLOW-1, Pine Research Instrumentation Inc.) was combined with a VICI air actuated injector (220-0302H; VICI Valco Instruments, Houston, TX) to make measurements. An HPLC pump by Dionex (Sunnyvale, California) moved aCSF through the flow cell at a constant flow rate of 1.0 mL/min (**Fig. 5.7**).

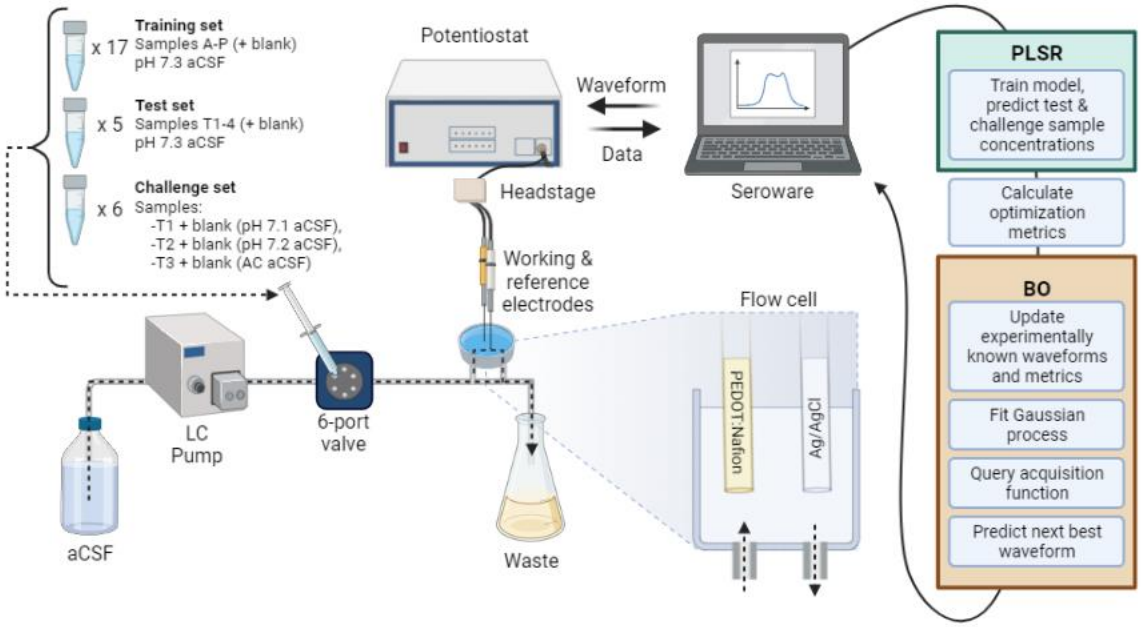

Figure 5.7. Workflow for parallel Bayesian optimization of voltammetric waveforms with intrinsic interferent selectivity.

Standard concentrations were selected using a fractional factorial box design (**Table 5.1**). This is a chemometric approach that designs a multi-dimensional 'box' spanning analytes, their concentrations, and experimental conditions of interest.[64,79] We selected a fractional approach to bias towards low analyte concentrations and small relative changes. High accuracy and precision in the nM range are important for monitoring basal and stimulated neurotransmitter levels using a single technique. The fractional approach avoids a full factorial design,

Table 5.1. Training, test and challenge set concentrations, in order of injection. All solutions prepared in artificial cerebrospinal fluid; a.c. = altered cations.

Set	Sample	DA (nM)	5-HT (nM)	5-HIAA (µM)	DOPAC (µM)	Ascorbate (µM)	pH (units)	KCl (mM)	NaCl (mM)
Training	Blank	0	0	0	0	0	7.3	3.5	147
	A	300	0	6	80	200	7.3	3.5	147
	B	1000	20	10	70	110	7.3	3.5	147
	C	0	120	6	90	190	7.3	3.5	147
	D	450	350	4	0	130	7.3	3.5	147
	E	600	500	1	10	170	7.3	3.5	147
	Blank	0	0	0	0	0	7.3	3.5	147
	F	160	250	2	20	180	7.3	3.5	147
	G	700	300	0	0	100	7.3	3.5	147
	H	80	160	10	60	100	7.3	3.5	147
	I	20	60	0	50	160	7.3	3.5	147
	J	40	40	2	100	120	7.3	3.5	147
	Blank	0	0	0	0	0	7.3	3.5	147
	K	800	10	8	30	150	7.3	3.5	147
	L	500	0	0	0	100	7.3	3.5	147
	M	0	250	0	0	100	7.3	3.5	147
	N	0	0	10	0	100	7.3	3.5	147
	O	0	0	0	50	100	7.3	3.5	147
	P	0	0	0	0	100	7.3	3.5	147
	Blank	0	0	0	0	0	7.3	3.5	147
Test	T1	750	50	1	85	200	7.3	3.5	147
	T2	100	400	5	9	200	7.3	3.5	147
	T3	400	200	5	85	190	7.3	3.5	147
	T4	70	30	5	35	200	7.3	3.5	147
	Blank	0	0	0	0	0	7.3	3.5	147
Challenge (pH)	T1 pH	750	50	1	85	200	7.1	3.5	147

	Blank pH	0	0	0	0	0	7.1	3.5	147
	T2 pH	100	400	5	9	200	7.2	3.5	147
	Blank pH	0	0	0	0	0	7.2	3.5	147
Challenge (a.c.)	T3 a.c.	400	200	5	85	190	7.3	120	31
	Blank a.c.	0	0	0	0	0	7.3	120	31

which would require orders of magnitude (and prohibitively) more calibration samples. In contrast, traditional calibration sets are less information-rich and can lead to spurious correlations when training a multiplexed method with overlapping signals from analytes and interferents.[64] The training and test sets effectively span the concentrations and combinations of interest without correlation (**Fig. S5.6**). Ascorbate was included in all samples (except blanks) for antioxidant properties. The concentrations of dopamine, serotonin, 5-HIAA, DOPAC, and ascorbate were altered by physiologically relevant changes in concentration throughout, so the model could be trained and tested across all analytes.

Solutions of aCSF were bubbled with nitrogen for at least ten minutes before sample preparation. All training and test samples were made fresh from stocks stored at -80 ˚C. All solutions were adjusted to the corresponding pH each day prior to aliquoting. All solutions were kept covered from light and stored on ice during the experiments.

We define a training set (*i.e.*, calibration set) as known concentration analyte mixtures, *i.e.,* "standards", used to train a PLSR model. A test set is defined as known concentration analyte mixtures not used during training, but instead held out and used to measure model performance. Test set samples only include samples with conditions incurred in the training set (*i.e.*, the same

buffer conditions). We define "challenge" samples as additional test set samples prepared at conditions not included or varied in the training set, such as varying pH and cationic buffer salt concentrations (**Table 5.1**; see *Data Analysis*). We define an injection blank or zero (0) as an injected solution containing only aCSF.

Training, test, and challenge sets were injected (~1 mL into a 500 µL loop) into a flow cell using a six-port valve (**Fig. 5.7**). The valve was switched to the inject position for ~20 s per injection. The time between injections was ≥ 200 s, depending on the waveform and time for the current to return to baseline. Samples were injected in a pseudo-randomized but consistent order. Within each string, the waveform calibration curves were completed across consecutive days. All waveforms within a string were acquired with the same electrode. A different electrode was used for each string to ensure the robustness of the waveform optimization. All waveforms were conditioned for ≥ 10 min in aCSF before acquiring data.

Voltammetry hardware and software

A two-electrode configuration *via* an Ag/AgCl reference electrode and a carbon fiber microelectrode working electrode was used. A PC with a PCIe-6363 data acquisition card (National Instruments (NI), Austin, TX) was used to control a WaveNeuro One FSCV Potentiostat System (NEC-WN-BASIC, Pine Research Instrumentation Inc.) with a 1,000 nA/V headstage amplifier (AC01HS2, Pine Research Instrumentation Inc.). The copper wire of the working electrode and the silver wire reference electrode were inserted into a microelectrode-headstage coupler (AC01HC0315-5, Pine Research Instrumentation Inc.) that connected the electrodes to the potentiostat.

In-house software was developed for RPV and described in our previous paper.[34] The software has since been updated and named SeroWare. Details regarding SeroWare and open-source access to the program will be described in an upcoming manuscript.

Bayesian optimization

Bayesian optimization was carried out using the open-source Python package Scikit-Optimize.[80] This software uses an 'ask and tell' interface. First, the search space was constrained as described in *Results*. The surrogate model (Gaussian process regressor with a Matérn and white noise kernel, and uniform prior) was initialized through the 'tell' interface using vectorized and normalized String 1 waveform parameters and optimization metrics. A Matérn kernel was chosen due to its flexibility, and the assumption that the true objective function of the waveform parameters is not infinitely differentiable (*i.e.*, the potentials and time applied by the potentiostat/data acquisition card are discretized to some degree).

The acquisition function (expected improvement) was then minimized using the 'ask' interface to generate a vectorized waveform to be experimentally queried. Kernel hyperparameters (*i.e.,* length scale, smoothness) and the acquisition function were optimized automatically by the limited-memory Broyden–Fletcher–Goldfarb–Shanno (L-BFGS) algorithm in the software package. The acquisition function returned a vectorized waveform that was then created in SeroWare format for data acquisition. After experimental results were obtained with the predicted waveform, the metrics of all previous waveforms were aggregated with the newest metrics and the Bayesian optimizer was updated using the 'tell' interface to set new query points using the 'ask' interface. In this work, increments of voltage were rounded to the nearest 0.001 V and increments

of time were rounded to the nearest 0.1 ms. To interpret the model, built-in partial dependence functions to Scikit-Learn and Scikit-Optimize were used, along with the SHAP Python package.

Data analysis

Data were extracted using in-house custom acquisition software written in MATLAB 2016a. Models were built as described in previous literature using open-source Python packages (Scikit-Learn).[34,81] Briefly, roughly 40-100 voltammograms were extracted per sample injection. All voltammograms were normalized, and the number of components was chosen using 5-fold cross-validation. Optimization metrics were then calculated using the final model (**Table S5.1**).

Drift training: The PLSR model was trained to account for drift using voltammograms collected throughout the experiment while aCSF containing interferents was flowed and injections were not occurring (~2 h). We define these voltammograms as "background blanks". They are portions of the data when no samples are being injected. The injection blanks correct for injection artifacts while the background blanks correct for drift (**Fig. S5.7**)**.** Data, in which drift was evident, were extracted from these background epochs and labeled as 'zero' analyte concentrations to teach the model what drift, as opposed to analyte-containing, voltammograms, look like. Background blanks were in addition to data from injections of aCSF alone (*i.e.*, injection blanks), which account for flow cell injection artifacts.

We found this process to increase the accuracy and precision of the PLSR predictions. It was generalizable to test set samples. We attribute this to a low-dimensional representation of drift learned by the model (**Fig. S5.7**). All concentration predictions were constrained to be ≥ 0 (*i.e.*,

domain knowledge dictates concentrations cannot be negative. Negative concentration predictions were replaced with 0).

Optimization metrics: The eight different optimization metrics were dopamine accuracy (mean absolute error of the test set predictions), serotonin accuracy (mean absolute error of the test set predictions), variance of the test set blanks (proxy for LOD) for zero dopamine or serotonin, mean absolute error for dopamine or serotonin in altered cation (a.c.) aCSF (ion robustness challenge samples), and varying pH aCSF (pH robustness challenge samples) (**Table S5.1**). Due to experimental time constraints, the LOD metric was excluded from the optimization panel for the second run of Bayesian optimization (R2). This resulted in 30 unique waveforms for the first run (six random in String 1, plus three strings of 8), and a total of 24 waveforms for the second run (six random in String 1, plus three rounds of 6). In R1 and R2 combined, 55 unique waveforms were tested (with the additional OG RPV waveform that was also tested; **Table S5.2**).

Challenge samples: Test samples (T1-T4), prepared at pH 7.3, were used to assess dopamine and serotonin accuracy and LOD. Some test samples (T1-T3) were also prepared in aCSF at pH 7.1 or pH 7.2, and in aCSF with altered cation concentrations (Na^+ and K^+) to assess the accuracy of dopamine and serotonin predictions in the presence of changing H^+, Na^+, and K^+ concentrations expected *in vivo*. We refer to these specially prepared test samples as 'challenge' samples (**Table 5.1**, **Fig. S5.1**). These samples enabled sparse training set size. Thus, we were able to optimize for interferent agnostic waveforms without explicitly training on these interferents. For example, training across variations in pH or other cations would require partial or up to full-fold increases

in the samples injected. As an efficient alternative, we optimized for accuracy on the challenge set samples without any increase in training set size. Thus, the optimization goal of challenge samples was to find a waveform inherently agnostic to changes in pH or cations, rather than a waveform that was 'trainable' across these interferents. In this case, the interferents implicitly optimized are pH and monovalent cations, but this is extendable to any *a priori* domain knowledge of interferents expected. This is especially useful in situations such as voltammetry in which the matrix of the training data differs from the application of the model (*i.e., in vitro* to *in vivo* generalizability).

Acknowledgments & Author Contributions

AMA, ASM, CL, CSM and KAP conceived of the work and designed the experiments. ANN, CSM, KKN, KAP, MEC and MEW performed all experiments. CSM and KAP analyzed the data. CSM wrote the code for the regression and Bayesian optimization models. KAP performed statistical analyses. AMA, ASM, MA and CL guided the project. All authors contributed to and approved the final version of the manuscript. The authors acknowledge Biorender.com for figure generation. CSM was supported by the National Science Foundation Graduate Research Fellowship Program (DGE-1650604 and DGE- 2034835). Any opinions, findings, and conclusions or recommendations expressed in this material are those of the authors and do not necessarily reflect the views of the National Science Foundation.

5.6 SUPPLEMENTARY INFORMATION

Table S5.1. Optimization metric calculations for Bayesian optimization runs 1 and 2.

Waveform #	Optimization metric	Calculation
1	DA test set accuracy	Mean absolute error of PLSR DA predictions for all test set samples (T1, T2, T3, T4, 0) at pH 7.3
2	5-HT test set accuracy	Mean absolute error of PLSR 5-HT predictions for all test set samples (T1, T2, T3, T4, 0) at pH 7.3
3	DA pH robustness	Mean absolute error of PLSR DA predictions for challenge samples T1 (pH 7.1), 0 (pH 7.1), T2 (pH 7.2), 0 (pH 7.2)
4	5-HT pH robustness	Mean absolute error of PLSR 5-HT predictions for challenge samples T1 (pH 7.1), 0 (pH 7.1), T2 (pH 7.2), 0 (pH 7.2)
5	DA ion robustness	Mean absolute error of PLSR DA predictions for challenge samples T3 (a.c.), 0 (a.c.)
6	5-HT ion robustness	Mean absolute error of PLSR 5-HT predictions for challenge samples T3 (a.c.), 0 (a.c.)
7	DA limit of detection (LOD) *(Run 1 only)*	Standard deviation of the PLSR DA predictions of blanks, i.e., 0 (pH 7.3)
8	5-HT limit of detection (LOD) *(Run 1 only)*	Standard deviation of the PLSR 5-HT predictions of blanks, i.e., 0 (pH 7.3)

Table S5.2. Waveform parameters for all strings and runs of Bayesian optimization.

Run	*String*	*Waveform*	E_1 (V)	τ_1 (ms)	E_2 (V)	τ_2 (ms)	E_3 (V)	τ_3 (ms)	E_4 (V)	τ_4 (ms)	*Hold time (ms)*
1	1	1	0.800	0.5	0.500	0.5	-0.300	1.0	-0.100	1.5	96.5
		2	0.900	0.5	0.700	1.0	-0.400	0.5	-0.300	1.5	96.5
		3	0.500	2.0	0.200	1.5	-0.100	1.5	-0.300	1.0	94.0
		4	0.600	2.0	0.800	0.5	-0.200	2.0	-0.400	0.5	95.0
		5	0.200	1.0	0.300	1.5	-0.100	1.5	0.000	0.5	95.5
		6	0.700	1.5	0.600	2.0	-0.300	1.0	-0.100	2.0	93.5
	2	1	0.308	1.6	0.385	1.0	-0.397	1.5	-0.268	0.6	95.3
		2	0.747	1.0	0.499	1.9	-0.309	0.8	-0.237	0.5	95.8
		3	0.113	0.9	0.930	1.7	-0.243	1.4	-0.056	1.0	95.0
		4	0.291	1.7	0.106	0.9	-0.165	1.6	-0.393	0.6	95.2
		5	0.815	1.0	1.105	1.1	-0.379	1.2	-0.137	1.5	95.2
		6	0.163	1.4	0.972	1.9	-0.080	1.9	-0.051	1.5	93.3
		7	0.747	0.5	1.251	0.5	-0.162	0.8	-0.324	1.9	96.3
		8	0.362	0.7	0.524	2.0	-0.333	1.6	-0.291	0.9	94.8
	3	1	0.102	1.3	0.092	0.6	-0.350	0.8	-0.321	1.8	95.5
		2	0.517	0.7	0.806	1.9	-0.098	1.8	-0.493	1.3	94.3
		3	0.437	0.8	0.548	1.9	-0.291	1.7	-0.282	0.9	94.7
		4	0.646	1.0	0.171	1.8	-0.236	1.5	-0.218	1.7	94.0
		5	0.351	1.1	0.784	0.9	-0.350	0.6	-0.209	0.5	96.9
		6	0.325	1.7	1.255	1.2	-0.109	1.3	-0.306	1.0	94.8
		7	0.105	0.9	0.303	1.8	-0.009	0.8	-0.066	1.0	95.5
		8	0.004	2.0	0.598	0.9	-0.212	2.0	-0.161	1.4	93.7
	4	1	0.128	1.9	1.248	1.9	-0.469	0.9	-0.109	1.9	93.4
		2	0.274	0.7	0.779	1.5	-0.180	1.4	-0.425	1.4	94.5
		3	0.578	1.0	0.856	0.9	-0.298	1.7	-0.141	1.7	94.9
		4	0.837	1.9	1.074	0.5	-0.096	0.7	-0.300	0.7	95.0
		5	0.770	0.8	0.945	1.5	-0.266	1.5	-0.394	1.5	94.9
		6	0.000	1.5	0.560	1.8	-0.216	1.3	-0.154	1.3	94.2
		7	0.315	1.4	1.289	0.5	-0.479	1.0	-0.293	1.0	96.4
		8	0.226	0.8	0.286	1.8	-0.465	0.9	-0.359	0.9	95.7
2	1	1	0.113	0.6	1.223	0.8	-0.271	0.6	-0.420	0.7	97.3
		2	0.366	0.6	0.860	2.0	-0.309	0.6	-0.353	0.6	96.2
		3	0.363	1.8	1.077	1.6	-0.192	1.5	-0.314	0.9	94.2
		4	0.088	1.2	1.060	1.8	-0.165	0.6	-0.458	1.0	95.4
		5	0.172	0.9	0.045	2.0	-0.110	1.7	-0.260	1.6	93.8
		6	0.580	1.4	0.951	1.9	-0.482	1.9	-0.053	1.6	93.2
	2	1	0.543	1.7	1.116	1.5	-0.217	1.6	-0.293	1.0	94.2
		2	0.200	1.8	1.111	0.9	-0.191	1.5	-0.383	0.9	94.9
		3	0.119	0.6	0.480	2.0	-0.006	0.6	-0.342	1.0	95.8
		4	0.129	1.2	0.759	1.7	-0.397	1.1	-0.453	1.8	94.2
		5	0.230	1.2	0.116	0.5	-0.082	1.5	-0.417	1.1	95.7
		6	0.410	1.6	1.074	1.6	-0.197	1.3	-0.304	1.6	93.9
	3	1	0.605	1.6	0.505	1.5	-0.185	1.4	-0.098	1.6	93.9
		2	0.227	1.7	1.174	0.6	-0.180	1.3	-0.422	2.0	94.4
		3	0.300	1.7	1.122	0.9	-0.197	0.9	-0.420	0.8	95.7
		4	0.703	0.7	1.123	1.2	-0.088	1.4	-0.318	0.8	95.9
		5	0.133	1.2	1.083	1.7	-0.213	0.7	-0.415	1.0	95.4
		6	1.159	1.5	0.887	1.0	-0.023	2.0	-0.275	1.0	94.5
	4	1	0.159	1.1	1.022	1.4	-0.171	1.0	-0.461	1.0	95.5
		2	0.617	1.5	1.291	1.2	-0.327	1.0	-0.019	1.8	94.5
		3	0.271	1.7	1.286	1.3	-0.343	1.9	-0.300	0.6	94.5
		4	0.572	1.7	0.713	0.6	-.412	0.7	-0.242	0.8	96.2
		5	0.655	1.8	1.074	1.3	-0.366	1.1	-0.410	1.0	94.8
		6	0.509	0.9	0.914	1.4	-0.224	1.3	-0.257	1.4	95.0

Table S5.3. Optimization metric values for all strings and runs of Bayesian optimization. Values with an asterisk (*) were excluded due to sample failure. Values with a dash (-) were not calculated for that waveform.

Run	*String*	*Waveform*	*Test set accuracy (nM)*		*pH robustness (nM)*		*Ion robustness (nM)*		*LOD (nM)*	
			DA	5-HT	DA	5-HT	DA	5-HT	DA	5-HT
1	1	1	117	24	213	25	200	28	12	15
		2	73	24	213	25	159	76	16	15
		3	153	39	213	56	200	43	41	8
		4	81	31	213	26	188	89	5	15
		5	164	97	154	100	137	100	26	41
		6	82	28	208	32	91	76	42	20
	2	1	159	92	213	93	200	100	15	21
		2	134	41	371	156	216	185	69	46
		3	57	32	166	70	193	43	26	24
		4	295	73	393	88	200	100	138	3
		5	61	41	186	45	200	100	34	12
		6	72	24	185	24	200	72	19	13
		7	38	65	142	54	66	272	37	17
		8	108	21	213	17	200	79	5	13
	3	1	191	111	226	76	200	100	0	0
		2	85	21	43	36	14	29	15	21
		3	209	76	156	80	200	100	1	2
		4	75	26	89	29	200	42	28	14
		5	92	38	188	36	200	94	38	20
		6	93	41	116	75	133	111	38	18
		7	113	69	160	81	200	100	19	18
		8	168	16	212	31	200	45	0	16
	4	1	148	47	204	83	200	212	40	0
		2	98	19	190	22	200	6	68	4
		3	98	51	151	79	155	141	0	17
		4	100	47	124	66	354	126	46	16
		5	60	29	203	23	292	12	61	13
		6	80	29	141	37	267	71	26	7
		7	59	37	67	20	160	71	16	18
		8	99	71	213	75	200	100	21	31
2	1	1	91	61	21	218	181	188	-	-
		2	40	68	122	69	720	100	-	-
		3	37	34	218	52	947	83	-	-
		4	65	52	93	74	44	192	-	-
		5	244	66	213	113	309	100	-	-
		6	18	16	51	59	79	51	-	-
	2	1	86	19	161	20	14	78	-	-
		2	39	13	94	9	9	78	-	-
		3	234	65	294	72	199	100	-	-
		4	103	58	157	25	189	39	-	-
		5	261	70	213	35	200	1160	-	-
		6	41	24	72	10	296	35	-	-
	3	1	56	15	120	28	143	18	-	-
		2	59	16	122	11	*	*	-	-
		3	53	29	77	15	171	46	-	-
		4	80	40	73	13	38	17	-	-
		5	181	20	213	35	200	75	-	-
		6	136	32	210	30	200	9	-	-
	4	1	255	36	213	62	200	72	-	-
		2	91	24	119	29	305	44	-	-
		3	245	78	213	113	200	248	-	-
		4	216	114	274	115	200	100	-	-
		5	45	213	148	756	132	875	-	-
		6	83	32	125	24	122	56	-	-

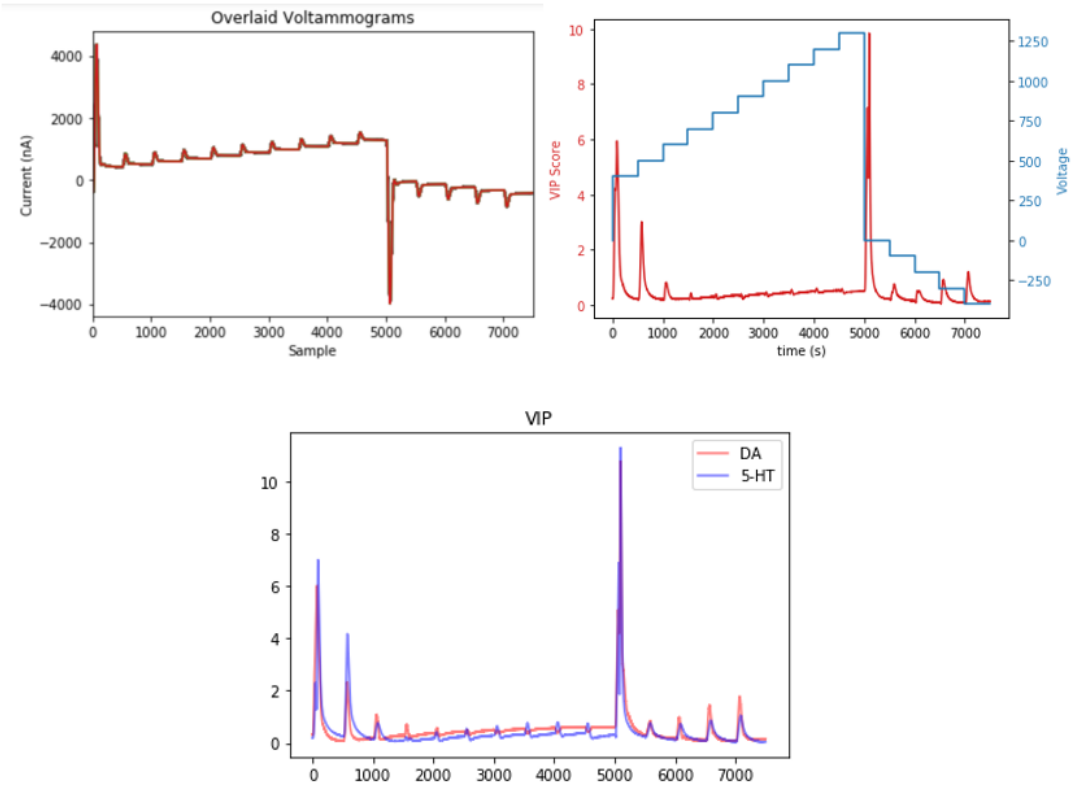

Figure S5.1. a) Representative raw current traces for staircase voltammetry of samples containing serotonin and dopamine. **b**) total variable importance in projection (VIP) scores (red) overlaid with staircase waveform (blue). **c)** individual VIP scores by analyte.

In our initial attempts to optimize RPV waveform pulse steps we tried using other pulse techniques (chronoamperometry, differential pulse voltammetry (DPV), normal pulse voltammetry (NPV), *etc*.) to gain insight into which step potentials may be better for particular analytes. For example, by running a calibration curve and examining the feature importance of the current generated at each pulse step (*i.e.,* variable important in projection (VIP) scores). However, we could not guarantee that the utility of a single pulse potential or step length (τ) extracted from the pre-patterned pulse experiment would retain its feature importance outside of that specific pulse train (*i.e*., the feature importance of a pulse may be dependent on the pulses that come before/after it). This behavior can be attributed to the complex redox mechanisms,

physiochemical properties of analytes, electrolytes, and the electrode surface that are all affected by the potentials applied in a waveform.

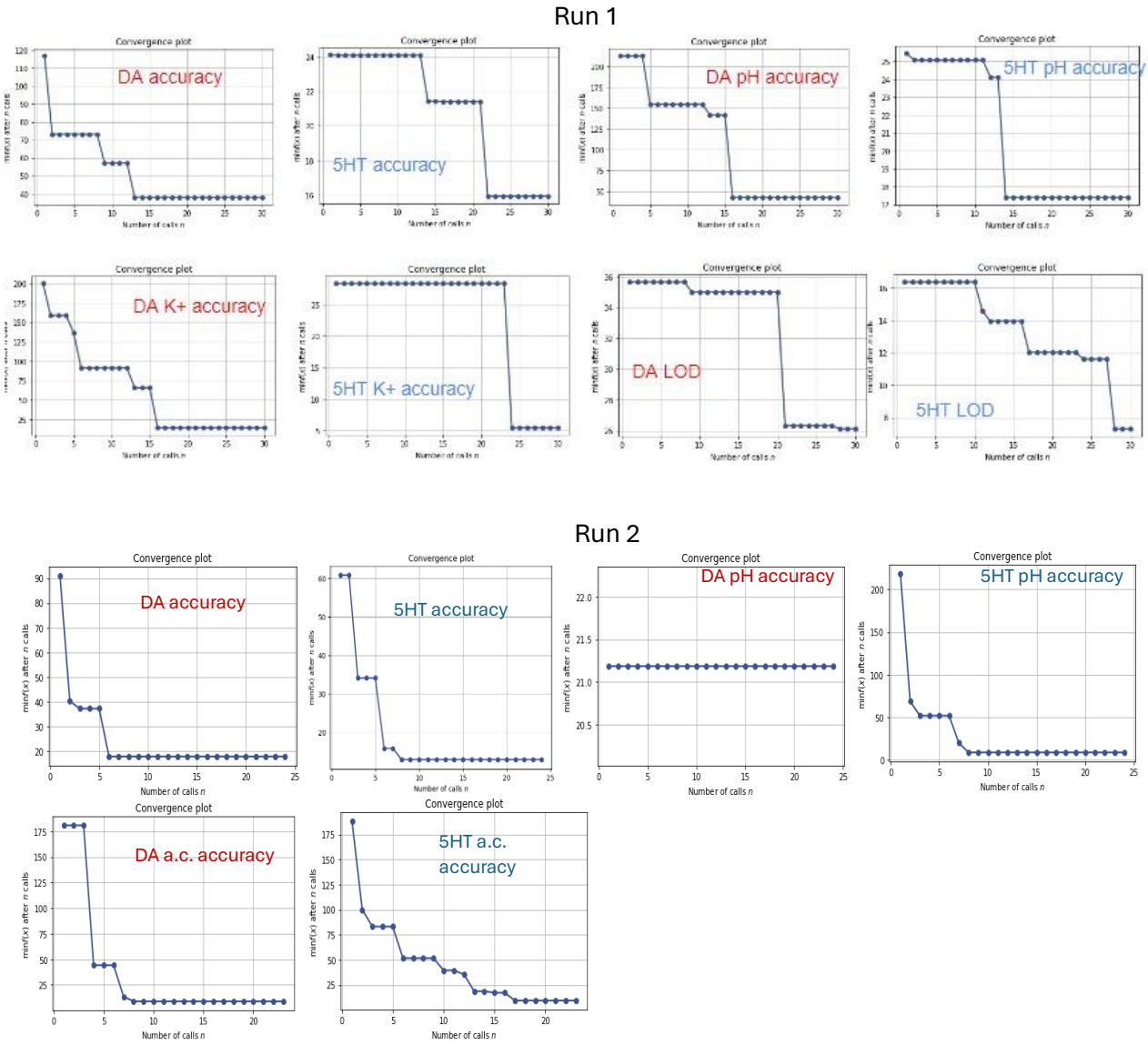

Figure S5.2. Convergence plots for each metric in run 1 and 2.

While some convergence plots failed to improve in each string or at all (DA pH accuracy), this behavior is not unexpected. Bayesian optimization, especially when used with expected improvement acquisition function as done here, favors exploration. Exploring the search space, especially where uncertainty is high, uncovers information about the location of

optima, even if the point evaluated performs poorly. It is also possible the first randomly generated waveform was the best of those generated for a given metric.

We note that though metrics for challenge samples (*i.e.,* interferent agnostic waveforms) improved accuracy against pH and a.c. for one analyte, this benefit was often at the cost of test set accuracy of the other analyte (i.e., a pH agnostic waveform for serotonin often provided poor dopamine accuracy and vice versa). Thus, multi-objective optimization should provide more promising results to balance this trade-off. Indeed, waveforms that are optimal for multiple objectives and analytes can be found (see below).

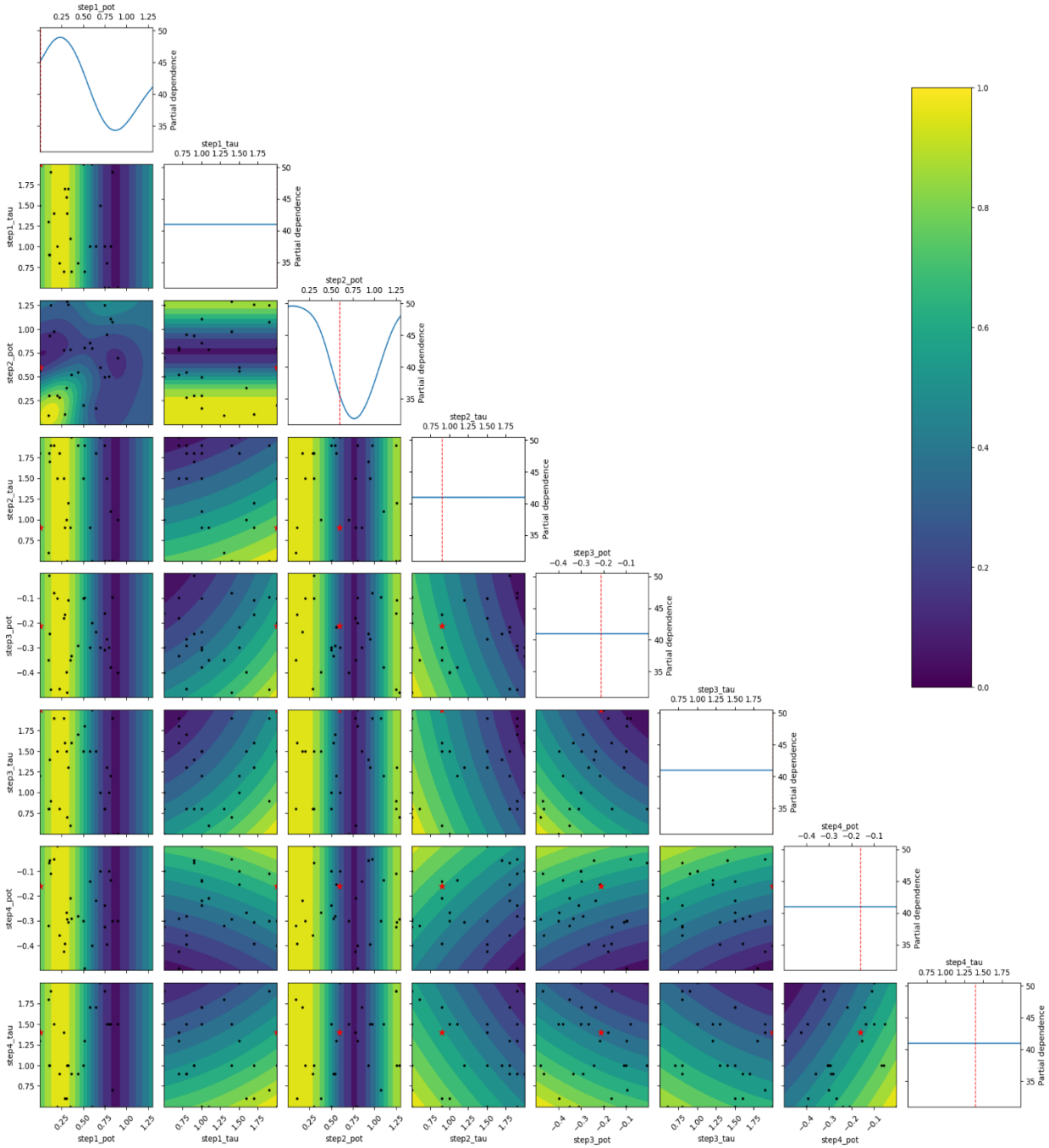

Figure S5.3. 5-HT test set accuracy PDP, run 1.

For R1 (**Fig. S5.3**), E_1 and E_2 appear to be the most important features. While E_1 appears optimal at ~0.9 V, E_2 appears optimal at ~0.8 V. However, these features also have interaction

effects as shown in the contour plot (far left column, third box down from top). Having both E_1 and E_2 at low amplitudes (*i.e.,* <0.25 V) results in the poorest accuracy (greatest error), perhaps as expected, shown by the deep purple color. Meanwhile, having a low amplitude E_1 with a high amplitude E_2 (*i.e.,* 0.75 V) results in the most optimal interaction. This finding is in agreement with the intermediate-pulse concept from VET theory. However, in the same contour plot, we see that having two, similarly high amplitude pulses may also result in a good waveform. We also note that little relationship is learned on the far right (where $E_1 > \sim 1.0$ V), as this was not experimentally possible to sample due to signal saturation. Interestingly, all other parameters have flat PDP plots. Alternative techniques below can help decipher if this is due to non-importance or averaging.

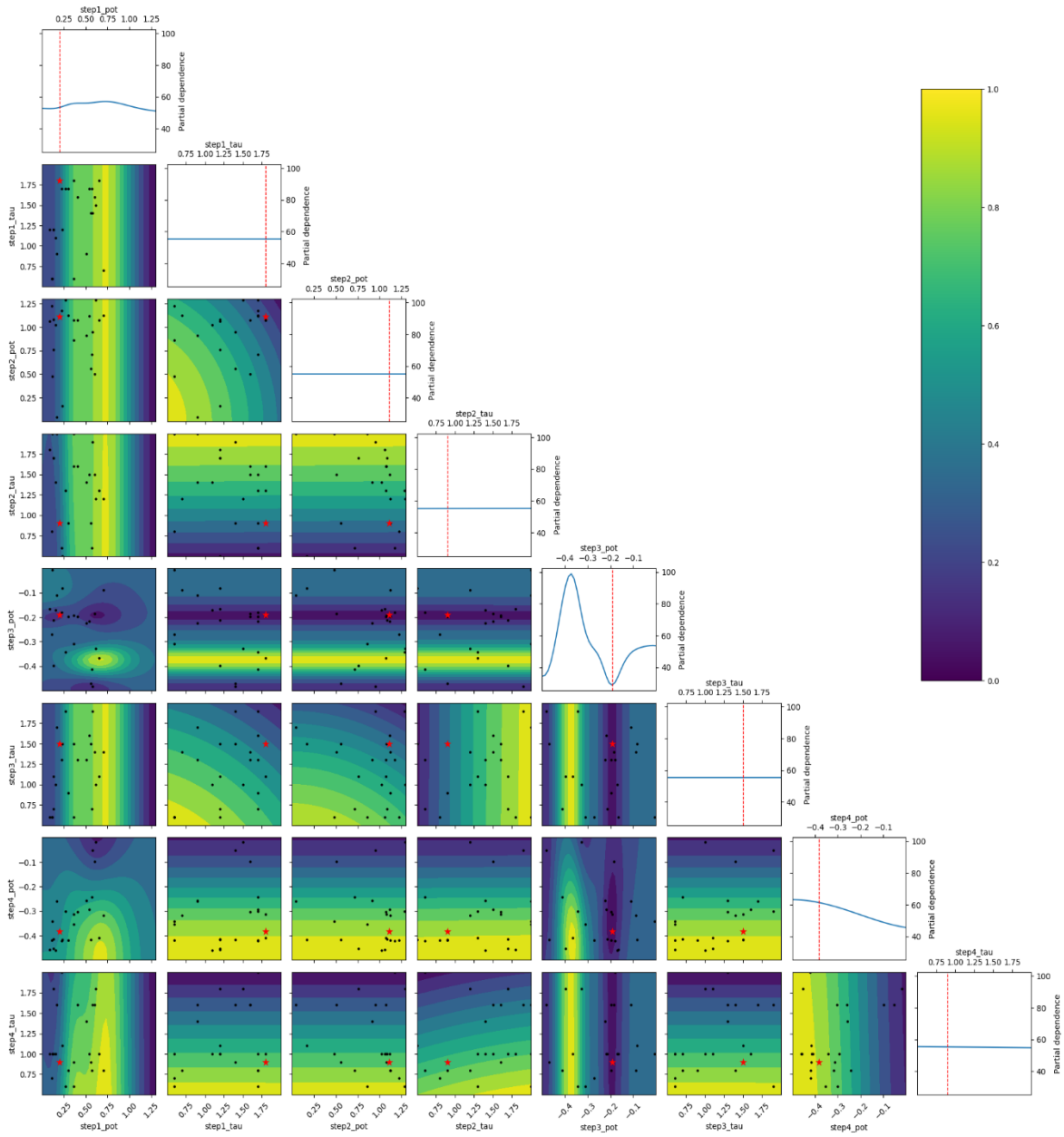

Figure S5.4. 5-HT test set accuracy PDP, run 2.

For R2 (**Fig. S5.4**), we see the most important effects appear to be coming from E_3, E_4 and E_1. A near linear relationship exists with E_4, in which more positive holding potentials results in better performance (perhaps expected for serotonin). However, the contour plots indicate more complex interactions in which E_1 and E_3 may dictate under what conditions this holds. E_3 appears

to be optimal at -0.2 V, close to the original and recently optimized equivalent cathodic sweep to -0.1 V in the N-shape waveforms. Indeed, changes to one waveform parameter are not mutually exclusive. Interestingly, E_2 has little change while E_3 has the most, which is contrary to run 1 (**Fig. S5.3**), in which E_3 has no change and E_2 has the most. This could again be due to the different training sets, or potentially a dependence between E_3 and E_2 that can manifest in either parameter.

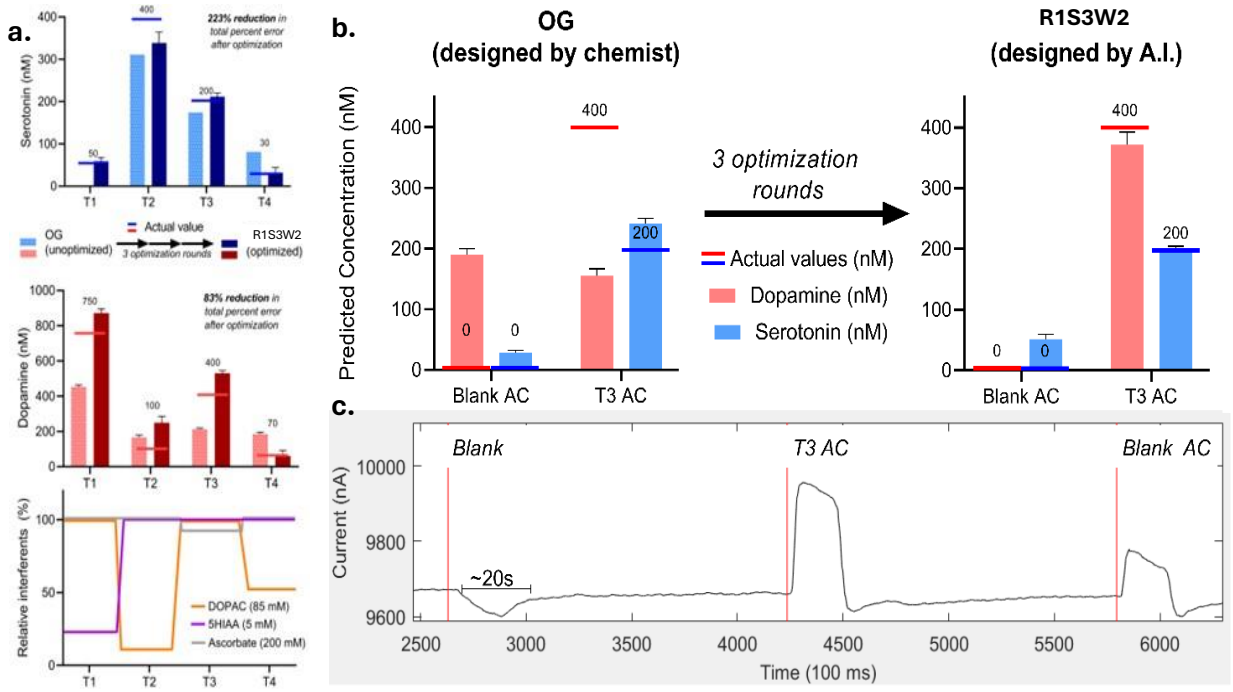

Figure S5.5. a) OG versus R1S3W2 waveform test set performance for serotonin and dopamine co-detection. **b)** Comparison of altered cation (a.c.) challenge set performance for OG and R1S3W2. **c)** Representative raw signal for challenge set samples.

Serendipitous finding of multi-objective optimized waveform: The R1S3W2 waveform resulted in 220% and 80% reductions in prediction error for T1-4 for serotonin and dopamine, respectively, in the presence of varying interferents. While we hypothesized that an improved serotonin waveform would result from the optimizer for serotonin accuracy, we did not expect this result after only three optimization rounds. Even though the output metric for W2 was serotonin accuracy, R1S3W2 improved dopamine predictions compared to the OG waveform. This result was somewhat surprising, as we are first pursuing single-objective optimization in a parallel manner. That is, our algorithm searches only for one optimal metric per waveform. Even so, we identified a waveform that improved both serotonin and dopamine accuracy (R1S3W2).

This result increases confidence that improved RPV waveforms for co-detection are in our existing search space and can be identified when using multi-objective optimization in the future.

We also noted that R1S3W2 was robust to ionic fluxes of NaCl/KCl, even though these concentrations were held constant in the training set. In a first ion robustness challenge, an aliquot of T3 was prepared at pH 7.3, but using a.c. aCSF (120 mM KCl and 30.5 mM NaCl, rather than 3.5 mM KCl and 147 mM NaCl in 'normal' aCSF) to mimic changes in the extracellular fluid just after an action potential. This separate, isotonic solution, called 'a.c.' for altered cations, was injected separately from the normal aCSF blank and T3 to gauge cation effects. Our OG waveform confounded K^+/Na^+ changes for serotonin/dopamine (**Fig. S5.5a,b**). Through Bayesian optimization, however, we identified K^+/Na^+ agnostic waveforms. For example, the R1S3W2 waveform with improved serotonin and dopamine prediction accuracies retained near-perfect predictive accuracy for serotonin and dopamine across challenge samples varying by an order of magnitude in K^+/Na^+ concentrations (**Fig. S5.5a,b**). Notably, the trained PLSR model making these predictions had never seen changes in cations prior to testing–the aCSF composition was constant during training.

In comparison, a recent background-subtracted FSCV-PCR method confused a 120 mM change in K^+ as a 2-μM change in dopamine (~1.5 μM dopamine prediction error). Only when the FSCV-PCR model was trained across [K^+] did accuracy improve. For the same change in K^+ (3.5 mM to 120 mM), our non-background subtracted R1S3W2-PLSR model was simultaneously more accurate not only at predicting dopamine (~29 nM prediction error for 400 nM dopamine), but also serotonin (~3 nM prediction error for 200 nM serotonin) (**Fig. S5.5a**). Moreso, this was without requiring explicit training across [K^+] and while maintaining accuracy, as shown for T1-4, in normal aCSF with varying 5-HIAA, DOPAC, and ascorbate concentrations. However, these results

were not reproducible across electrodes and act only as proof of concept that such waveforms may exist. Further, we were not able to identify a waveform optimal for both serotonin and dopamine that maintained pH and altered cation robustness. The R1S3W2 waveform was not agnostic to pH. Multi-objective optimization may help achieve such a waveform, as waveforms with these individual properties do exist in our current search space.

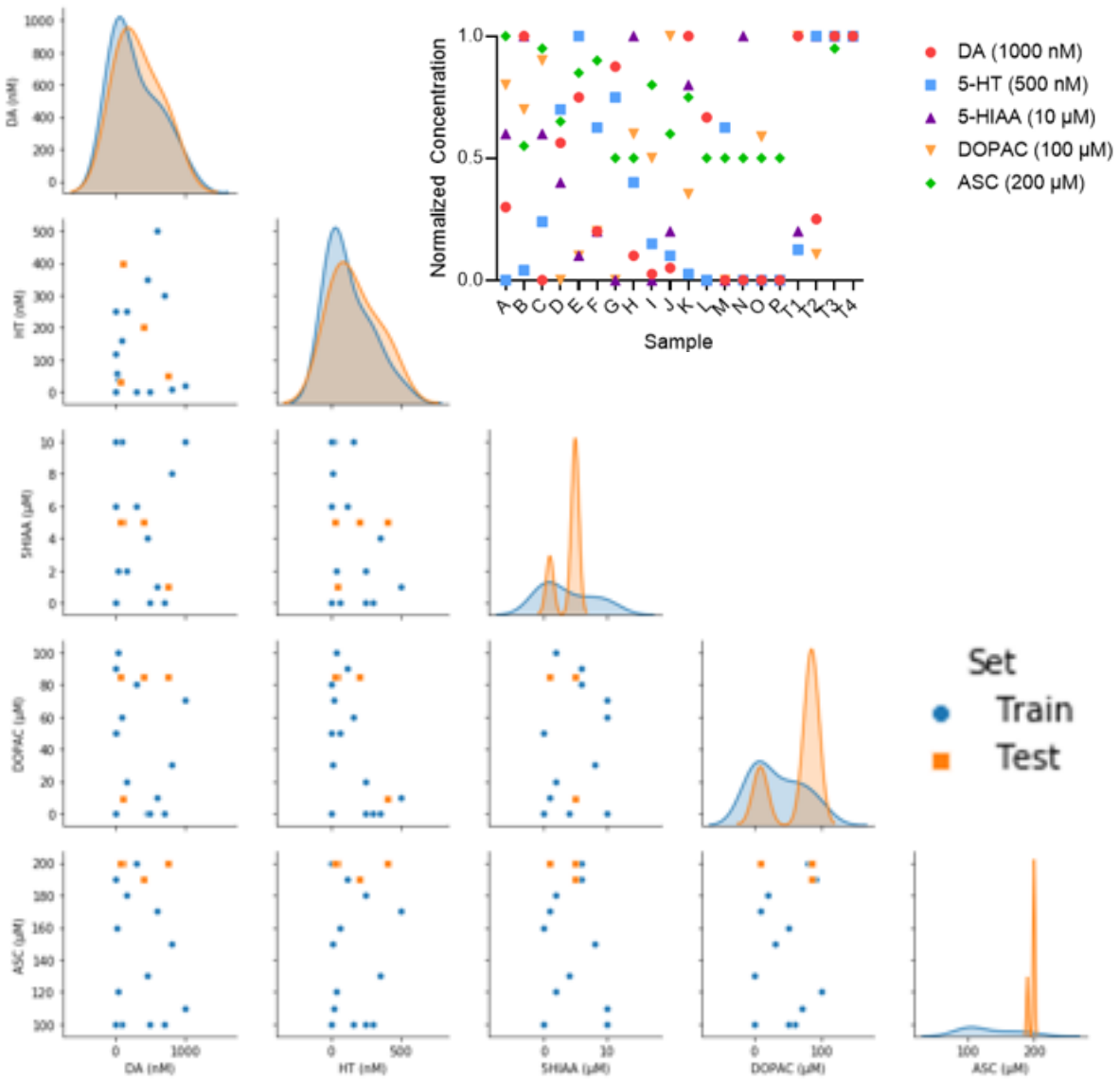

Figure S5.6. Correlation plot of train and test set concentrations. **(inset)** Normalized concentrations of each calibration sample.

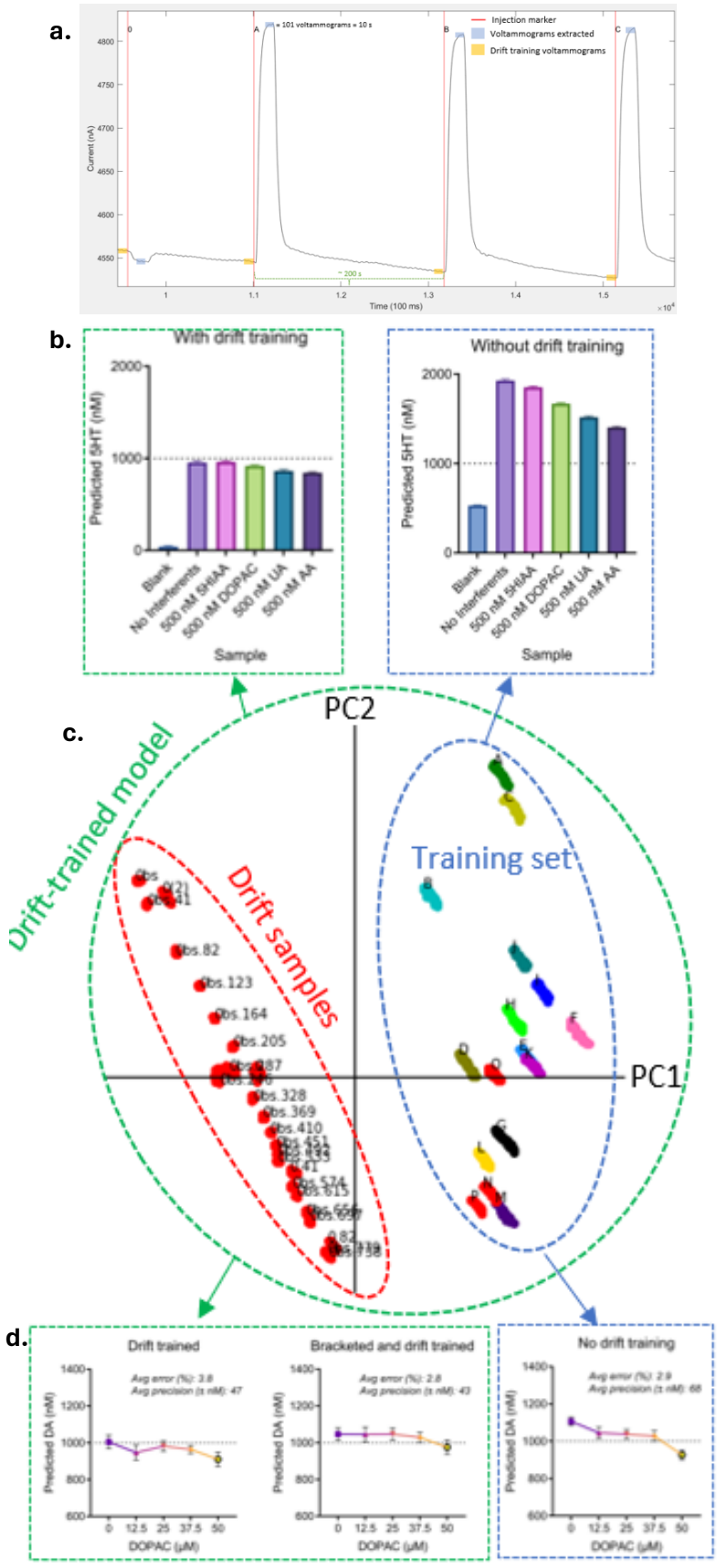
a.
Injection marker
Voltammograms extracted
Drift training voltammograms
Current (nA)
Time (100 ms)
b.
With drift training
Without drift training
Predicted 5HT (nM)
Blank
No interferents
500 nM 5HIAA
500 nM DOPAC
500 nM UA
500 nM AA
Sample
c.
Drift-trained model
Drift samples
Training set
PC1
PC2
d.
Drift trained
Bracketed and drift trained
No drift training
Predicted DA (nM)
DOPAC (μM)

Figure S5.7. Drift training and bracketing enhances PLSR model performance in the presence of interferents. **A)** Representative raw current trace indicating where voltammograms were extracted. **B)** Effect of drift training on serotonin sample predictions with varying interferents. **C)** Principal component scores plot of training set and drift-training set. **D)** Effect of using drift training, drift training and bracketing, and no drift training on dopamine samples with varying DOPAC.

We also developed a novel drift training and data processing method *in vitro*. Here, the PLSR model was trained to account for drift using voltammograms collected throughout the experiment while aCSF containing interferents was delivered and injections were not occurring (analogous to interstimulus intervals *in vivo*) (**Fig. S5.7a**). Data, in which drift was evident, were extracted from these background epochs and labeled as 'zero' analyte concentrations to teach the model what drifting, as opposed to analyte-containing, voltammograms look like. Our novel 'drift training' reduced test set prediction errors for serotonin by 93% to 4.5% error and by 23% to 6.7% error for dopamine (**Fig. S5.7b**). The drift voltammograms were taken only from the training data yet they were able to correct the drift present in the test data obtained later in the day suggesting that this procedure is generalizable. Generalizable PLSR models of drift have been reported for FSCV. Indeed, we noticed a low-dimensional clustering of drift samples in quadrants II and III of the principal components scores plot (**Fig. S5.7c**).

Metabolites with structures similar to dopamine and serotonin pose the greatest challenge for voltammetry because of highly overlapping electrochemical characteristics. In preliminary experiments, we used our lead RPV waveform and PLSR to predict test samples containing 1000 nM serotonin and dopamine in the presence of 500 nM additions of 5-HIAA, DOPAC, ascorbic acid (AA), or uric acid (UA) (**Fig. S5.7b**). The calibration set contained concentrations of serotonin and dopamine that varied; metabolite and interferent levels were held constant at a relevant background level (100 μM DOPAC, 20 μM 5-HIAA, 200 μM AA, and 100 μM UA),

unless denoted by 500 nM additions, to simulate metabolite concentration changes, as expected *in vivo*.

We further improved analyte prediction accuracy using calibration set "bracketing". That is, we injected the calibration set before *and* after the test set to account for calibration changes occurring over the course of the experiment (*i.e.,* drift, fouling). This is essentially the concept of using both 'pre-fouled' *vs.* 'post-fouled' electrodes to obtain training data. When using calibration bracketing combined with drift training, precision and accuracy of dopamine predictions improved (**Fig. S5.7d**).

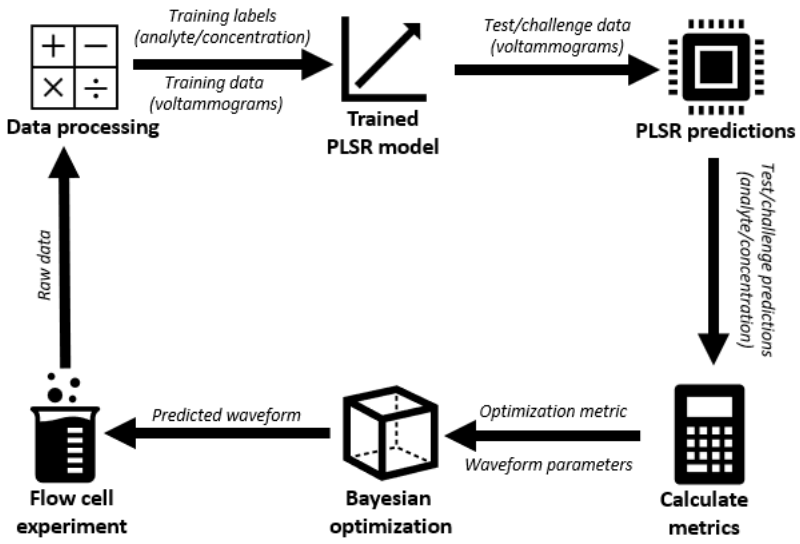

Figure S5.8. Simplified SeroOpt workflow.

5.7 REFERENCES

1. Pang, Q.; Meng, J.; Gupta, S.; Hong, X.; Kwok, C. Y.; Zhao, J.; Jin, Y.; Xu, L.; Karahan, O.; Wang, Z.; Toll, S.; Mai, L.; Nazar, L. F.; Balasubramanian, M.; Narayanan, B.; Sadoway, D. R., Fast-charging aluminium–chalcogen batteries resistant to dendritic shorting. *Nature* **2022,** *608* (7924), 704-711. https://doi.org/10.1038/s41586-022-04983-9
2. Dinh Khac, H.; Whang, G.; Iadecola, A.; Makhlouf, H.; Barnabé, A.; Teurtrie, A.; Marinova, M.; Huvé, M.; Roch-Jeune, I.; Douard, C.; Brousse, T.; Dunn, B.; Roussel, P.; Lethien, C., Nanofeather ruthenium nitride electrodes for electrochemical capacitors. *Nat. Mater.* **2024**. https://doi.org/10.1038/s41563-024-01816-0
3. Garrido-Barros, P.; Derosa, J.; Chalkley, M. J.; Peters, J. C., Tandem electrocatalytic n2 fixation via proton-coupled electron transfer. *Nature* **2022,** *609* (7925), 71-76. https://doi.org/10.1038/s41586-022-05011-6
4. Zhang, W.; Lu, L.; Zhang, W.; Wang, Y.; Ware, S. D.; Mondragon, J.; Rein, J.; Strotman, N.; Lehnherr, D.; See, K. A.; Lin, S., Electrochemically driven cross-electrophile coupling of alkyl halides. *Nature* **2022,** *604* (7905), 292-297. https://doi.org/10.1038/s41586-022-04540-4
5. Li, J.; Liu, Y.; Yuan, L.; Zhang, B.; Bishop, E. S.; Wang, K.; Tang, J.; Zheng, Y.-Q.; Xu, W.; Niu, S.; Beker, L.; Li, T. L.; Chen, G.; Diyaolu, M.; Thomas, A.-L.; Mottini, V.; Tok, J. B. H.; Dunn, J. C. Y.; Cui, B.; Pașca, S. P.; Cui, Y.; Habtezion, A.; Chen, X.; Bao, Z., A tissue-like neurotransmitter sensor for the brain and gut. *Nature* **2022,** *606* (7912), 94-101. https://doi.org/10.1038/s41586-022-04615-2

6. Willmore, L.; Cameron, C.; Yang, J.; Witten, I. B.; Falkner, A. L., Behavioural and dopaminergic signatures of resilience. *Nature* **2022,** *611* (7934), 124-132. https://doi.org/10.1038/s41586-022-05328-2

7. Batten, S. R.; Bang, D.; Kopell, B. H.; Davis, A. N.; Heflin, M.; Fu, Q.; Perl, O.; Ziafat, K.; Hashemi, A.; Saez, I.; Barbosa, L. S.; Twomey, T.; Lohrenz, T.; White, J. P.; Dayan, P.; Charney, A. W.; Figee, M.; Mayberg, H. S.; Kishida, K. T.; Gu, X.; Montague, P. R., Dopamine and serotonin in human substantia nigra track social context and value signals during economic exchange. *Nat. Hum. Behav.* **2024**. https://doi.org/10.1038/s41562-024-01831-w

8. Pipita, M. E.; Santonico, M.; Pennazza, G.; Zompanti, A.; Fazzina, S.; Cavalieri, D.; Bruno, F.; Angeletti, S.; Pedone, C.; Incalzi, R. A., Integration of voltammetric analysis, protein electrophoresis and pH measurement for diagnosis of pleural effusions: A non-conventional diagnostic approach. *Sci. Rep.* **2020,** *10* (1), 15222. https://doi.org/10.1038/s41598-020-71542-5

9. Zhao, S.; Li, H.; Dai, J.; Jiang, Y.; Zhan, G.; Liao, M.; Sun, H.; Shi, Y.; Ling, C.; Yao, Y.; Zhang, L., Selective electrosynthesis of chlorine disinfectants from seawater. *Nat. Sustain.* **2024,** *7* (2), 148-157. https://doi.org/10.1038/s41893-023-01265-8

10. Mutz, Y. S.; do Rosario, D.; Silva, L. R. G.; Galvan, D.; Janegitz, B. C.; de Q. Ferreira, R.; Conte-Junior, C. A., A single screen-printed electrode in tandem with chemometric tools for the forensic differentiation of Brazilian beers. *Sci. Rep.* **2022,** *12* (1), 5630. https://doi.org/10.1038/s41598-022-09632-9

11. Puthongkham, P.; Venton, B. J., Recent advances in fast-scan cyclic voltammetry. *Analyst* **2020,** *145* (4), 1087-1102. https://doi.org/10.1039/c9an01925a

12. Rodeberg, N. T.; Sandberg, S. G.; Johnson, J. A.; Phillips, P. E. M.; Wightman, R. M., Hitchhiker's guide to voltammetry: Acute and chronic electrodes for in vivo fast-scan cyclic voltammetry. *ACS Chem. Neurosci.* **2017,** *8* (2), 221-234. https://doi.org/10.1021/acschemneuro.6b00393

13. Daws, L.; Andrews, A.; Gerhardt, G., Electrochemical techniques and advances in psychopharmacology. In *Encyclopedia of psychopharmacology*, IP, S.; LH, P., Eds. Springer Berlin Heidelberg: Berlin, Heidelberg, 2013; pp 1-6.

14. Vreeland, R. F.; Atcherley, C. W.; Russell, W. S.; Xie, J. Y.; Lu, D.; Laude, N. D.; Porreca, F.; Heien, M. L., Biocompatible PEDOT:Nafion composite electrode coatings for selective detection of neurotransmitters in vivo. *Anal. Chem.* **2015,** *87* (5), 2600-2607. https://doi.org/10.1021/ac502165f

15. Shao, Z.; Chang, Y.; Venton, B. J., Carbon microelectrodes with customized shapes for neurotransmitter detection: A review. *Anal. Chim. Acta* **2022,** *1223*, 340165. https://doi.org/10.1016/j.aca.2022.340165

16. Castagnola, E.; Robbins, E. M.; Krahe, D. D.; Wu, B.; Pwint, M. Y.; Cao, Q.; Cui, X. T., Stable in-vivo electrochemical sensing of tonic serotonin levels using PEDOT/CNT-coated glassy carbon flexible microelectrode arrays. *Biosens. Bioelectron.* **2023,** *230*, 115242. https://doi.org/10.1016/j.bios.2023.115242

17. Rafi, H.; Zestos, A. G., Multiplexing neurochemical detection with carbon fiber multielectrode arrays using fast-scan cyclic voltammetry. *Anal. Bioanal. Chem.* **2021,** *413* (27), 6715-6726.

18. Swamy, B. E. K.; Venton, B. J., Carbon nanotube-modified microelectrodes for simultaneous detection of dopamine and serotoninin vivo. *Analyst* **2007,** *132* (9), 876-884. https://doi.org/10.1039/B705552H

19. Mena, S.; Visentin, M.; Witt, C. E.; Honan, L. E.; Robins, N.; Hashemi, P., Novel, user-friendly experimental and analysis strategies for fast voltammetry: Next generation FSCAV with artificial neural networks. *ACS Meas. Sci. Au* **2022,** *2* (3), 241-250. https://doi.org/10.1021/acsmeasuresciau.1c00060

20. Twomey, T.; Barbosa, L.; Lohrenz, T.; Montague, P. R., Deep learning architectures for FSCV, a comparison. *arXiv (Medical Physics)* **2022,** (posted 2022-12-05). https://doi.org/10.48550/arXiv.2212.01960 (accessed 2023-12-12)

21. Montague, P. R.; Kishida, K. T., Computational underpinnings of neuromodulation in humans. *Cold Spring Harbor Symp. Quant. Biol.* **2018,** *83*, 71-82. https://doi.org/10.1101/sqb.2018.83.038166

22. Dunham, K. E.; Venton, B. J., Improving serotonin fast-scan cyclic voltammetry detection: New waveforms to reduce electrode fouling. *Analyst* **2020,** *145* (22), 7437-7446. https://doi.org/10.1039/D0AN01406K

23. Rafi, H.; Zestos, A. G., Recent advances in FSCV detection of neurochemicals via waveform and carbon microelectrode modification. *J. Electrochem. Soc.* **2021,** *168* (5), 057520.

24. Phillips, P. E. M.; Stuber, G. D.; Heien, M. L. A. V.; Wightman, R. M.; Carelli, R. M., Subsecond dopamine release promotes cocaine seeking. *Nature* **2003,** *422* (6932), 614-618. https://doi.org/10.1038/nature01476

25. Hashemi, P.; Dankoski, E. C.; Petrovic, J.; Keithley, R. B.; Wightman, R. M., Voltammetric detection of 5-hydroxytryptamine release in the rat brain. *Anal. Chem.* **2009,** *81* (22), 9462-71. https://doi.org/10.1021/ac9018846

26. Venton, B. J.; Cao, Q., Fundamentals of fast-scan cyclic voltammetry for dopamine detection. *Analyst* **2020,** *145* (4), 1158-1168. https://doi.org/10.1039/C9AN01586H

27. Heien, M. L. A. V.; Phillips, P. E. M.; Stuber, G. D.; Seipel, A. T.; Wightman, R. M., Overoxidation of carbon-fiber microelectrodes enhances dopamine adsorption and increases sensitivity. *Analyst* **2003,** *128* (12), 1413-1419. https://doi.org/10.1039/B307024G

28. Kim, S. Y.; Oh, Y. B.; Shin, H. J.; Kim, D. H.; Kim, I. Y.; Bennet, K.; Lee, K. H.; Jang, D. P., 5-hydroxytryptamine measurement using paired pulse voltammetry. *Biomed. Eng. Lett* **2013,** *3* (2), 102-108. https://doi.org/10.1007/s13534-013-0093-z

29. Park, C.; Oh, Y.; Shin, H.; Kim, J.; Kang, Y.; Sim, J.; Cho, H. U.; Lee, H. K.; Jung, S. J.; Blaha, C. D.; Bennet, K. E.; Heien, M. L.; Lee, K. H.; Kim, I. Y.; Jang, D. P., Fast cyclic square-wave voltammetry to enhance neurotransmitter selectivity and sensitivity. *Anal. Chem.* **2018,** *90* (22), 13348-13355. https://doi.org/10.1021/acs.analchem.8b02920

30. Shin, H.; Oh, Y.; Park, C.; Kang, Y.; Cho, H. U.; Blaha, C. D.; Bennet, K. E.; Heien, M. L.; Kim, I. Y.; Lee, K. H.; Jang, D. P., Sensitive and selective measurement of serotonin in vivo using fast cyclic square-wave voltammetry. *Anal. Chem.* **2020,** *92* (1), 774-781. https://doi.org/10.1021/acs.analchem.9b03164

31. Oh, Y.; Heien, M. L.; Park, C.; Kang, Y. M.; Kim, J.; Boschen, S. L.; Shin, H.; Cho, H. U.; Blaha, C. D.; Bennet, K. E.; Lee, H. K.; Jung, S. J.; Kim, I. Y.; Lee, K. H.; Jang, D. P., Tracking tonic dopamine levels in vivo using multiple cyclic square wave

voltammetry. *Biosens. Bioelectron.* **2018,** *121*, 174-182. https://doi.org/10.1016/j.bios.2018.08.034

32. Shin, H.; Goyal, A.; Barnett, J. H.; Rusheen, A. E.; Yuen, J.; Jha, R.; Hwang, S. M.; Kang, Y.; Park, C.; Cho, H.-U.; Blaha, C. D.; Bennet, K. E.; Oh, Y.; Heien, M. L.; Jang, D. P.; Lee, K. H., Tonic serotonin measurements in vivo using N-shaped multiple cyclic square wave voltammetry. *Anal. Chem.* **2021,** *93* (51), 16987-16994. https://doi.org/10.1021/acs.analchem.1c02131

33. Abdalla, A.; Atcherley, C. W.; Pathirathna, P.; Samaranayake, S.; Qiang, B.; Peña, E.; Morgan, S. L.; Heien, M. L.; Hashemi, P., In vivo ambient serotonin measurements at carbon-fiber microelectrodes. *Anal. Chem.* **2017,** *89* (18), 9703-9711. https://doi.org/10.1021/acs.analchem.7b01257

34. Movassaghi, C. S.; Perrotta, K. A.; Yang, H.; Iyer, R.; Cheng, X.; Dagher, M.; Fillol, M. A.; Andrews, A. M., Simultaneous serotonin and dopamine monitoring across timescales by rapid pulse voltammetry with partial least squares regression. *Anal. Bioanal. Chem.* **2021,** *413* (27), 6747-6767. https://doi.org/10.1007/s00216-021-03665-1

35. Movassaghi, C. S.; Alcañiz Fillol, M.; Kishida, K. T.; McCarty, G.; Sombers, L. A.; Wassum, K. M.; Andrews, A. M., Maximizing electrochemical information: A perspective on background-inclusive fast voltammetry. *Anal. Chem.* **2024**. https://doi.org/10.1021/acs.analchem.3c04938

36. Campos, I.; Alcañiz, M.; Masot, R.; Soto, J.; Martínez-Máñez, R.; Vivancos, J.-L.; Gil, L., A method of pulse array design for voltammetric electronic tongues. *Sens. Actuators, B* **2012,** *161* (1), 556-563. https://doi.org/10.1016/j.snb.2011.10.075

37. Fuentes, E.; Alcañiz, M.; Contat, L.; Baldeón, E. O.; Barat, J. M.; Grau, R., Influence of potential pulses amplitude sequence in a voltammetric electronic tongue (VET) applied to assess antioxidant capacity in aliso. *Food Chem.* **2017,** *224*, 233-241. https://doi.org/10.1016/j.foodchem.2016.12.076

38. Ivarsson, P.; Holmin, S.; Höjer, N.-E.; Krantz-Rülcker, C.; Winquist, F., Discrimination of tea by means of a voltammetric electronic tongue and different applied waveforms. *Sens. Actuators, B* **2001,** *76* (1), 449-454. https://doi.org/10.1016/S0925-4005(01)00583-4

39. Ross, A. E.; Venton, B. J., Sawhorse waveform voltammetry for selective detection of adenosine, ATP, and hydrogen peroxide. *Anal. Chem.* **2014,** *86* (15), 7486-7493. https://doi.org/10.1021/ac501229c

40. Altieri, S. C.; Yang, H.; O'Brien, H. J.; Redwine, H. M.; Senturk, D.; Hensler, J. G.; Andrews, A. M., Perinatal vs genetic programming of serotonin states associated with anxiety. *Neuropsychopharmacology* **2015,** *40* (6), 1456-70. https://doi.org/10.1038/npp.2014.331

41. Yang, H.; Thompson, A. B.; McIntosh, B. J.; Altieri, S. C.; Andrews, A. M., Physiologically relevant changes in serotonin resolved by fast microdialysis. *ACS Chem. Neurosci.* **2013,** *4* (5), 790-8. https://doi.org/10.1021/cn400072f

42. Altieri, S.; Singh, Y.; Sibille, E.; Andrews, A. M., Serotonergic pathways in depression. In *Neurobiology of Depression*, CRC Press: 2011; Vol. 20115633, pp 143-170.

43. Marcinkiewcz, C. A.; Mazzone, C. M.; D'Agostino, G.; Halladay, L. R.; Hardaway, J. A.; DiBerto, J. F.; Navarro, M.; Burnham, N.; Cristiano, C.; Dorrier, C. E.; Tipton, G. J.; Ramakrishnan, C.; Kozicz, T.; Deisseroth, K.; Thiele, T. E.; McElligott, Z. A.; Holmes, A.; Heisler, L. K.; Kash, T. L., Serotonin engages an anxiety and fear-promoting

circuit in the extended amygdala. *Nature* **2016,** *537* (7618), 97-101. https://doi.org/10.1038/nature19318

44. Tye, K. M.; Prakash, R.; Kim, S.-Y.; Fenno, L. E.; Grosenick, L.; Zarabi, H.; Thompson, K. R.; Gradinaru, V.; Ramakrishnan, C.; Deisseroth, K., Amygdala circuitry mediating reversible and bidirectional control of anxiety. *Nature* **2011,** *471* (7338), 358-362. https://doi.org/10.1038/nature09820

45. Movassaghi, C. S.; Andrews, A. M., Call me serotonin. *Nat. Chem.* **2024,** *16* (4), 670-670. https://doi.org/10.1038/s41557-024-01488-y

46. Gershon, M. D.; Margolis, K. G., The gut, its microbiome, and the brain: Connections and communications. *The Journal of Clinical Investigation* **2021,** *131* (18). https://doi.org/10.1172/JCI143768

47. Murphy, D. L.; Fox, M. A.; Timpano, K. R.; Moya, P. R.; Ren-Patterson, R.; Andrews, A. M.; Holmes, A.; Lesch, K.-P.; Wendland, J. R., How the serotonin story is being rewritten by new gene-based discoveries principally related to SLC6A4, the serotonin transporter gene, which functions to influence all cellular serotonin systems. *Neuropharmacology* **2008,** *55* (6), 932-960. https://doi.org/10.1016/j.neuropharm.2008.08.034

48. Singh, Y. S.; Altieri, S. C.; Gilman, T. L.; Michael, H. M.; Tomlinson, I. D.; Rosenthal, S. J.; Swain, G. M.; Murphey-Corb, M. A.; Ferrell, R. E.; Andrews, A. M., Differential serotonin transport is linked to the rh5-HTTLPR in peripheral blood cells. *Translational Psychiatry* **2012,** *2* (2), e77-e77. https://doi.org/10.1038/tp.2012.2

49. Wrona, M. Z.; Dryhurst, G., Electrochemical oxidation of 5-hydroxytryptamine in aqueous solution at physiological pH. *Bioorg. Chem.* **1990,** *18* (3), 291-317. https://doi.org/10.1016/0045-2068(90)90005-P

50. Eltahir, A.; White, J.; Lohrenz, T.; Montague, P. R., Low amplitude burst detection of catecholamines. *bioRxiv (Neuroscience)* **2021,** (posted 2021-08-04). https://doi.org/10.1101/2021.08.02.454747 (accessed 2023-12-12)

51. Montague, P. R.; Lohrenz, T.; White, J.; Moran, R. J.; Kishida, K. T., Random burst sensing of neurotransmitters. *bioRxiv (Neuroscience)* **2019,** (posted 2019-04-13), 607077. https://doi.org/10.1101/607077 (accessed 2023-12-12)

52. Greenhill, S.; Rana, S.; Gupta, S.; Vellanki, P.; Venkatesh, S., Bayesian optimization for adaptive experimental design: A review. *IEEE Access* **2020,** *8*, 13937-13948. https://doi.org/10.1109/ACCESS.2020.2966228

53. Shahriari, B.; Swersky, K.; Wang, Z.; Adams, R. P.; Freitas, N. d., Taking the human out of the loop: A review of Bayesian optimization. *Proc. IEEE* **2016,** *104* (1), 148-175. https://doi.org/10.1109/JPROC.2015.2494218

54. Frazier, P. I., A tutorial on Bayesian optimization. *arXiv* **2018**. https://doi.org/10.48550/arXiv.1807.02811

55. Brochu, E.; Cora, V. M.; Freitas, N. d., A tutorial on Bayesian optimization of expensive cost functions, with application to active user modeling and hierarchical reinforcement learning. *ArXiv* **2010,** *abs/1012.2599*. https://doi.org/10.48550/arXiv.1012.2599

56. Wahl, C. B.; Aykol, M.; Swisher, J. H.; Montoya, J. H.; Suram, S. K.; Mirkin, C. A., Machine learning-accelerated design and synthesis of polyelemental heterostructures. *Sci. Adv.* **2021,** *7* (52), eabj5505. https://doi.org/10.1126/sciadv.abj5505

57. Shields, B. J.; Stevens, J.; Li, J.; Parasram, M.; Damani, F.; Alvarado, J. I. M.; Janey, J. M.; Adams, R. P.; Doyle, A. G., Bayesian reaction optimization as a tool for chemical synthesis. *Nature* **2021,** *590* (7844), 89-96. https://doi.org/10.1038/s41586-021-03213-y

58. Wang, Y.; Chen, T.-Y.; Vlachos, D. G., NEXTorch: A design and Bayesian optimization toolkit for chemical sciences and engineering. *J. Chem. Inf. Model* **2021,** *61* (11), 5312-5319. https://doi.org/10.1021/acs.jcim.1c00637

59. Campos, I.; Masot, R.; Alcañiz, M.; Gil, L.; Soto, J.; Vivancos, J. L.; García-Breijo, E.; Labrador, R. H.; Barat, J. M.; Martínez-Mañez, R., Accurate concentration determination of anions nitrate, nitrite and chloride in minced meat using a voltammetric electronic tongue. *Sens. Actuators, B* **2010,** *149* (1), 71-78. https://doi.org/10.1016/j.snb.2010.06.028

60. Roijers, D. M.; Vamplew, P.; Whiteson, S.; Dazeley, R., A survey of multi-objective sequential decision-making. *J. Artif. Intell. Res.* **2013,** *48*, 67-113.

61. Dagher, M.; Perrotta, K. A.; Erwin, S. A.; Hachisuka, A.; Ayer, R.; Masmanidis, S.; Yang, H.; Andrews, A. M., Optogenetic stimulation of midbrain dopamine neurons produces striatal serotonin release. *ACS Chem. Neurosci.* **2022,** *13* (7), 946-958.

62. Meunier, C. J.; Mitchell, E. C.; Roberts, J. G.; Toups, J. V.; McCarty, G. S.; Sombers, L. A., Electrochemical selectivity achieved using a double voltammetric waveform and partial least squares regression: Differentiating endogenous hydrogen peroxide fluctuations from shifts in pH. *Anal. Chem.* **2018,** *90* (3), 1767-1776. https://doi.org/10.1021/acs.analchem.7b03717

63. Molnar, C., *Interpretable machine learning*. Leanpub: https://christophm.github.io/interpretable-ml-book/, 2020.

64. Díaz-Cruz, J. M.; Esteban, M.; Ariño, C., *Chemometrics in electroanalysis*. 1 ed.; Springer: Cham, Switzerland, 2019; p 202.

65. Torres, J. A. G.; Lau, S. H.; Anchuri, P.; Stevens, J. M.; Tabora, J. E.; Li, J.; Borovika, A.; Adams, R. P.; Doyle, A. G., A multi-objective active learning platform and web app for reaction optimization. *J. Am. Chem. Soc.* **2022**. https://doi.org/10.1021/jacs.2c08592

66. Pruksawan, S.; Lambard, G.; Samitsu, S.; Sodeyama, K.; Naito, M., Prediction and optimization of epoxy adhesive strength from a small dataset through active learning. *Sci. Technol. Adv. Mate.* **2019,** *20* (1), 1010-1021. https://doi.org/10.1080/14686996.2019.1673670

67. Chesler, M.; Kaila, K., Modulation of pH by neuronal activity. *Trends Neurosci.* **1992,** *15* (10), 396-402. https://doi.org/10.1016/0166-2236(92)90191-A

68. Johnson, J. A.; Hobbs, C. N.; Wightman, R. M., Removal of differential capacitive interferences in fast-scan cyclic voltammetry. *Anal. Chem.* **2017,** *89* (11), 6166-6174. https://doi.org/10.1021/acs.analchem.7b01005

69. Johnson, J. A.; Rodeberg, N. T.; Wightman, R. M., Measurement of basal neurotransmitter levels using convolution-based nonfaradaic current removal. *Anal. Chem.* **2018,** *90* (12), 7181-7189. https://doi.org/10.1021/acs.analchem.7b04682

70. Yoshimi, K.; Weitemier, A., Temporal differentiation of pH-dependent capacitive current from dopamine. *Anal. Chem.* **2014,** *86* (17), 8576-8584. https://doi.org/10.1021/ac500706m

71. Tian, S.-Y.; Deng, S.-P.; Chen, Z.-X., Multifrequency large amplitude pulse voltammetry: A novel electrochemical method for electronic tongue. *Sens. Actuators, B* **2007,** *123* (2), 1049-1056. https://doi.org/10.1016/j.snb.2006.11.011

72. Takmakov, P.; Zachek, M. K.; Keithley, R. B.; Bucher, E. S.; McCarty, G. S.; Wightman, R. M., Characterization of local pH changes in brain using fast-scan cyclic voltammetry with carbon microelectrodes. *Anal. Chem.* **2010,** *82* (23), 9892-9900. https://doi.org/10.1021/ac102399n

73. Jo, T.; Yoshimi, K.; Takahashi, T.; Oyama, G.; Hattori, N., Dual use of rectangular and triangular waveforms in voltammetry using a carbon fiber microelectrode to differentiate norepinephrine from dopamine. *J. Electroanal. Chem.* **2017,** *802*, 1-7. https://doi.org/10.1016/j.jelechem.2017.08.037

74. Zhu, F.; Yan, J.; Sun, C.; Zhang, X.; Mao, B., An electrochemical method for selective detection of dopamine by depleting ascorbic acid in diffusion layer. *J. Electroanal. Chem.* **2010,** *640* (1), 51-55. https://doi.org/10.1016/j.jelechem.2010.01.006

75. Kishida, K. T.; Saez, I.; Lohrenz, T.; Witcher, M. R.; Laxton, A. W.; Tatter, S. B.; White, J. P.; Ellis, T. L.; Phillips, P. E. M.; Montague, P. R., Subsecond dopamine fluctuations in human striatum encode superposed error signals about actual and counterfactual reward. *Proc. Natl. Acad. Sci. U.S.A.* **2016,** *113* (1), 200-205. https://doi.org/10.1073/pnas.1513619112

76. Meunier, C. J.; McCarty, G. S.; Sombers, L. A., Drift subtraction for fast-scan cyclic voltammetry using double-waveform partial-least-squares regression. *Anal. Chem.* **2019,** *91* (11), 7319-7327. https://doi.org/10.1021/acs.analchem.9b01083

77. Jaworski, A.; Wikiel, H.; Wikiel, K., Benefiting from information-rich multi-frequency AC voltammetry coupled with chemometrics on the example of on-line monitoring of leveler component of electroplating bath. *Electroanalysis 35* (1), e202200478. https://doi.org/10.1002/elan.202200478

78. Mitchell, E. C.; Dunaway, L. E.; McCarty, G. S.; Sombers, L. A., Spectroelectrochemical characterization of the dynamic carbon-fiber surface in response to electrochemical conditioning. *Langmuir* **2017,** *33* (32), 7838-7846. https://doi.org/10.1021/acs.langmuir.7b01443

79. Hibbert, D. B., Experimental design in chromatography: A tutorial review. *J. Chrom. B.* **2012,** *910*, 2-13. https://doi.org/10.1016/j.jchromb.2012.01.020

80. https://scikit-optimize.Github.Io/stable/index

81. Pedregosa, F.; Varoquaux, G.; Gramfort, A.; Michel, V.; Thirion, B.; Grisel, O.; Blondel, M.; Prettenhofer, P.; Weiss, R.; Dubourg, V., Scikit-learn: Machine learning in Python. *J. Mach. Learn. Res.* **2011,** *12*, 2825-2830.

Chapter 6

SeroWare: An open-source software suite for voltammetry acquisition and analysis

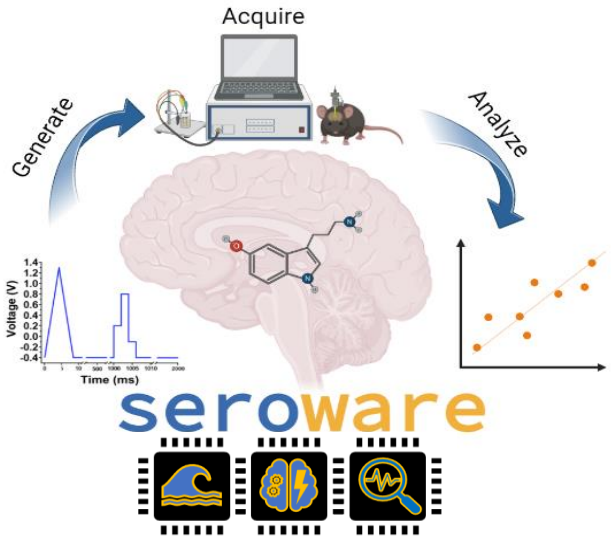

Part of the information in this chapter is in preparation for submission and has been adapted here.

Movassaghi, C.S.; Iyer, R.; Curry, M.E.; Wesely, M.E.; Alcañiz, M.; Andrews, A.M.

6.1 ABSTRACT

Voltammetry is widely used for fast, data-dense measurements of redox-active analytes in versatile environments, including monitoring brain neurotransmitters. Voltammetry requires minimal hardware beyond a potentiostat, an amplifier front-end, and a computer. However, researchers must either develop their own application-specific software or modify existing packages. Of the voltammetry software available, significant issues with source code that is inaccessible for modification, non-configurable data processing procedures, and hardware incompatibilities further complicate this landscape. These limitations coupled with recent advances in complex waveform types and increased demands for high bandwidth data acquisition and efficient data processing create a need for sophisticated, powerful, and flexible voltammetry software. We report on the development of 'SeroWare', an open-source, end-to-end, voltammetry acquisition and analysis software, custom-designed for various use cases encountered by analytical voltammetry communities. Although inspired for use in neurochemical analysis, the software is highly flexible, customizable, and compatible with other open-source toolkits. Our modular software architecture enables users to generate, acquire, and analyze voltammetry data of different types ranging from pulse and sweep waveforms to fast and slow scans *via* easily accessible and exportable file formats. Template code is provided for communicating with a variety of common external devices. We report several novel features for waveform application and data flow. In-depth documentation in the form of a User Guide and video tutorials are provided to enable the voltammetry community to use this universal platform, particularly in regard to shareability and lowering the barriers to entry for new investigators and novel research directions.

6.2 INTRODUCTION

Fast voltammetry for neurochemical analyses is in its fifth decade.[1] Advances in the field have focused on developing and implementing capabilities for faster and longer measurements,[2,3] using novel waveforms,[4-9] electrode materials and arrays,[10-12] and data processing techniques.[13-22] In the last decade alone, over 12,000 publications on fast scan cyclic voltammetry for neurotransmitter detection have been published. Underlying each of these developments is the data acquisition and analysis software that the measurements rely on. Yet only a handful of software packages have been published that provide the unique acquisition capabilities required when performing voltammetry for neurochemical analyses.[23-26]

Given the rapid increases in data acquisition speeds and storage capacities, new custom data analysis tools and voltammetry techniques are continually being developed to extract maximal chemical information from voltammograms.[9,13,14,19,22,27-39] However, there exists no single platform for the voltammetry community to integrate these tools for widespread use. As a whole, current open-source and/or commercial electroanalytical software often focuses on mechanistic simulations,[40] is amenable only to slow scan methods or other niche applications,[41] or solely aids in the analysis of data post-acquisition.[42] Many of these programs are costly, no longer maintained, poorly documented, or are not freely available forcing research labs to write time-consuming custom code solutions that are not reproducible by others. Meanwhile, fields such as neuroscience,[43] genetics,[44] bioinformatics,[45] and chemometrics[46] have benefited from a community-involved open-source approach to data acquisition and/or analysis software, including open-source data sets. Fast voltammetry would benefit similarly from readily available, easy-to-use, well-documented and maintained software with end-to-end acquisition and analysis capabilities.

To fill this need and facilitate the move towards a communal approach for fast voltammetry software, we have written and released SeroWare, an acquisition and analysis software specifically geared towards neurochemical analyses. While some of the most commonly used acquisition software is written in LabVIEW, we chose to write the initial version of SeroWare in MATLAB because it is one of the most commonly used languages for academic/scientific software development,[47] offers easy access to built-in graphical user interface (GUI) building and data acquisition/analysis tools, and is compatible with a wide array of already available open-source domain-specific signal processing and data analysis scripts.[48-52] While LabVIEW is maintained by National Instruments (NI) and therefore has facile NI card communication, MATLAB contains the built-in data acquisition (DAQ) tool box as a powerful alternative. Further, MATLAB is optimal for vectorized data analyses, lending itself naturally to electrochemical data processing.

As data analysis tool development outpaces acquisition tools, the shareability of new software is paramount. To compete with LabVIEW, which is free, we provide compiled versions of SeroWare that can run in standalone mode such that no MATLAB installation or license is required. (However, a license is required to make custom edits to the codebase. This is commonly provided to researchers at academic institutions free of charge.) The software is compatible with field-standard multifunction input/output (PCI) devices for potentiostat connections. We offer both an 'out of the box' compiled version and a developer/advanced user version for those who want to customize and/or incorporate their own scripts to the codebase. All versions of the software are publicly available with extensive documentation and tutorials on common example use cases and information for users who want to customize the software for specialized needs. We invite further testing, feature and issue requests, and code contributions through GitHub.

We named the software package SeroWare in honor of the fact that it was initially developed for brain serotonin monitoring *via* voltammetry. However, SeroWare is applicable to the analysis of any electroactive analyte or any mode of voltammetry (*e.g.*, chronoamperometry, sweep voltammetry, pulse voltammetry, *etc*.), including a wide array of applications in the voltammetric electronic tongue field (*e.g.,* wastewater, food, beverage analyses).[53-56] We introduce several new features and unique data workflows not reported in previous software publications. These include: a separate module for waveform generation that intuitively allows users to design, edit, and share waveforms of any type (FSCV, FSCAV, *etc.*), limited only by their choice of hardware; real-time waveform modification; manual and automated external event labeling; fully customizable data filtering, processing and exporting modes. We also include working code to connect and control a variety of commonly used external hardware devices (*e.g.*, injectors, stimulators, micromanipulators) over standard serial connections.

We have previously published an *in vitro* and *in vivo* validation study using the pilot version of SeroWare for all data acquistition and analysis.[29] The current paper serves as a quick-start guide for the user who is familiar with voltammetry looking for an intuitive software solution with specific yet customizable capabilities. We envision that the SeroWare package will allow the incorporation of rapidly advancing acquistion techniques and data analysis tools across the voltammetry field. Future releases will incorporate streamlined chemometric processing (*i.e.,* supervised machine learning regression for neurochemical concentration predictions) and community accessible databases for voltammetry training data.

6.3 RESULTS & DISCUSSION

SeroWare is organized into three MATLAB modules that interact in a seamless and logical manner understandable by voltammetry users of any experience level: SeroSignalGen, SeroAcq, and SeroDataProcess (**Fig. 6.1**). Together, these modules handle waveform generation, data acquisition, and initial processing of raw data, respectively, along with external event controls, filtering, analysis, and visualization tools.

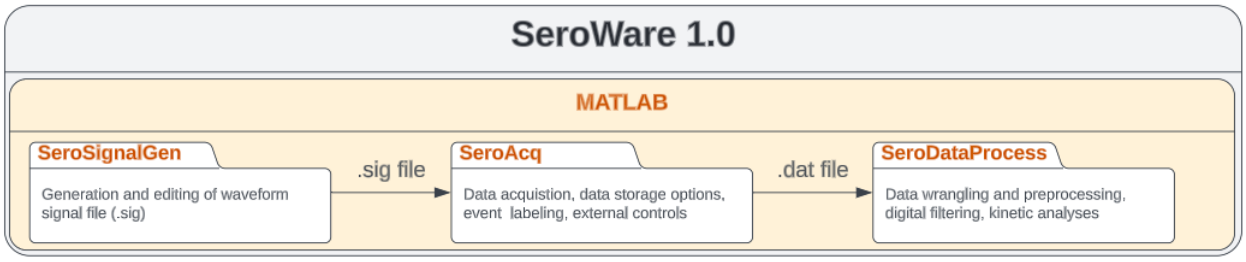

Figure 6.1. Overview of the SeroWare software suite.

6.3.1 SeroSignalGen:

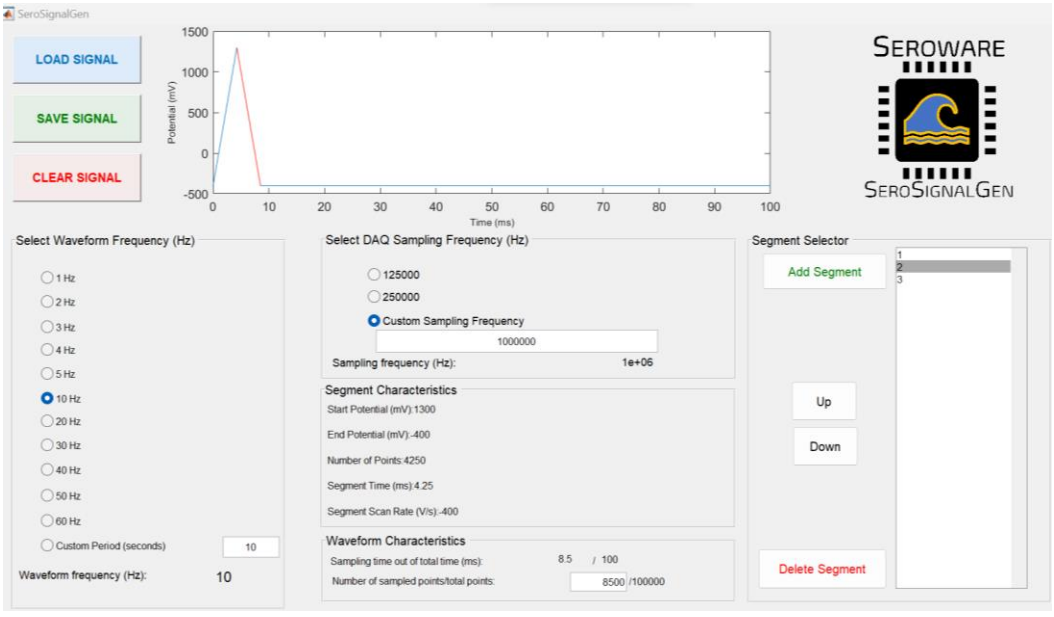

Figure 6.2. Diagram of the SeroSignalGen user interface, in which the triangle waveform has been built in a segment-wise manner.

The SeroSignalGen module enables the creation and visualization of any type of voltammetry waveform in a versatile, yet simple and user-friendly manner. The user can load a previously generated waveform in the form of a *.sig* file or generate a new waveform to be saved as a *.sig* file. An example of the ubiquitous triangle waveform for dopamine sensing in FSCV is shown in **Fig. 6.2**.[57]

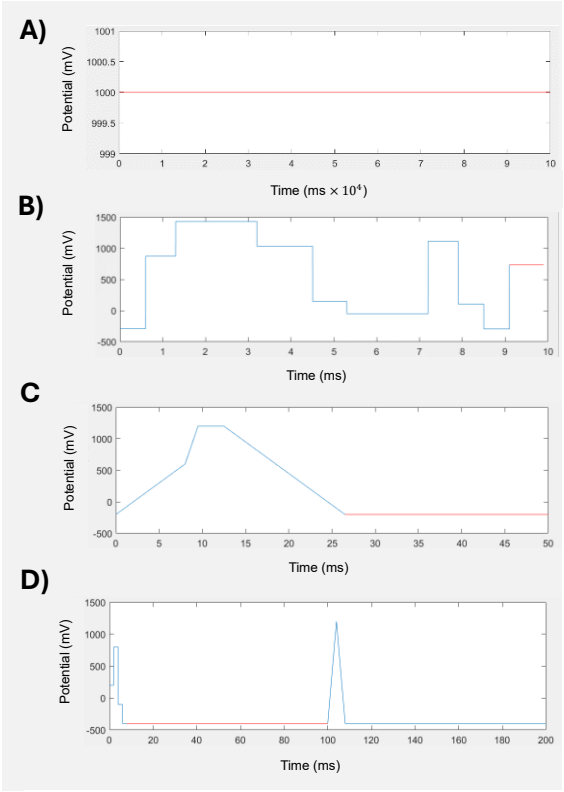

Figure 6.3. Examples of waveforms designed in SeroSignalGen. A) Continuous hold waveform for static oxidation pre-conditioning, amperometric experiments, accumulation waveforms, *etc*. B) Randomly generated pulse waveform without hold times; custom tau, step, and hold times can be implemented. C) Multiple-scan rate waveform. D) A dual alternating rapid pulse and fast scan waveform.

To generate a custom waveform, the user selects several parameters such as the waveform frequency. Some default button values are provided for ease of use (*e.g.*, 10 Hz for *in vivo* measurements,[58] 60 Hz for *in vitro* pre-conditioning[31]), but custom periods can be set by the user within the confines of the hardware. The sampling frequency (the frequency at which measured data is sampled by the data acquisition card) can be set to commonly used default values (100 kHz or 250 kHz). Other sampling frequencies can be entered using the custom text box. Faster sampling frequencies up to and exceeding 1 MHz are becoming more commonplace and can be used with SeroSignalGen provided the hardware, including the acquisition card, connected during software installation support these high frequencies. The user sets how many sampled points they want to

retain in the data files that will be acquired with the waveform in SeroAcq (*i.e.,* data need not be retained during the hold times, *i.e.,* non-sampled points, for smaller data file sizes).

SeroWare can build completely customizable waveforms in a user-friendly manner. The waveform file is built by vectorizing user-defined waveform 'segments'. These segments can be cathodic/anodic scans at user defined scan rates, constant potentials, or pulse steps defined by customized holding times/sampled points. **Figure 6.3** shows four different waveforms used in previous studies,[7,29,59] all of which can be easily built, shared, and edited in the *.sig* file format using SeroSignalGen.

For each waveform segment, various characteristics are displayed and automatically calculated. This segmented approach has several benefits: 1) the segments can be reordered easily using the up/down/delete/add buttons in the segment table, and 2) the user can build segments across any potential range by entering the desired amount of time or points to sample (for example, if a certain scan rate is desired or a minimum number of sampled points is desired). The parameters are automatically updated as needed and each segment is visualized in a real-time plot. Once the user is ready, the waveform is named and saved. Alternatively, at any time a user can load/edit a previously generated *.sig* file using the load signal button. This feature allows easy sharing and editing of waveforms across users, which we foresee as useful given the increasing numbers and complexity of recently published custom waveforms.[4,5,7,8,19,20,60] Multiple waveforms can be concatenated for intra-sample comparison studies of waveform performance.[29] Unique data handling procedures for such waveforms are also available (see *Methods*).

6.3.2 SeroAcq

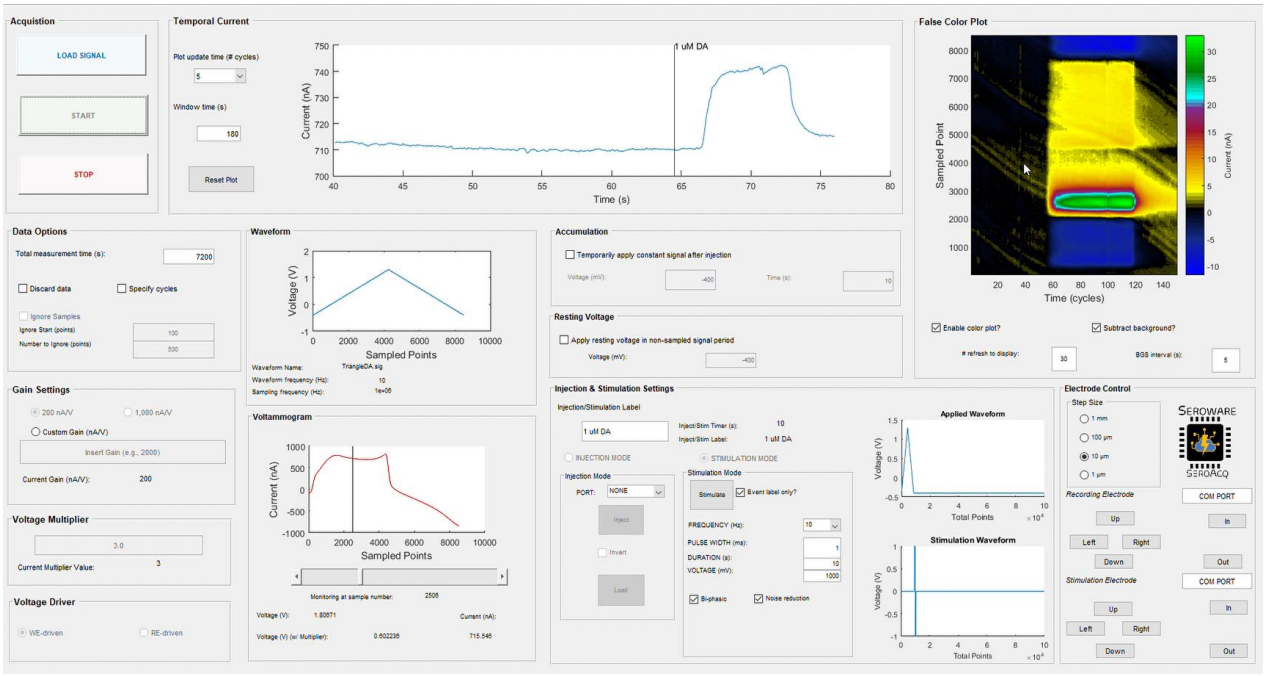

Figure 6.4. The SeroAcq graphical user interface.

Once satisfied with the waveform, the user can acquire voltammetry data by launching the SeroAcq module. The user first loads the *.sig* file corresponding to the waveform they want to apply (*e.g.,* from SeroSignalGen). They then set various global experiment parameters including the gain and data storage options. (See the User Guide in the *Supplemental Information* for more information on establishing hardware communication).

Once acquisition has started, real-time data is visualized in a temporal plot of current for a user defined point in the waveform (*e.g.,* the oxidation potential of dopamine; **Fig. 6.4**, top plot). Noise, drift, and other experimental factors at specific regions of interest can be easily monitored. Experimental events such as stimulations and injections can be labeled and time-stamped through the GUI. This visualization strategy is in addition to the usual cyclic voltammogram and false color

plots (**Fig. 6.4**). Additional data visualization options are available in a separate post-acquisition module (*vide infra* SeroDataProcess).

6.3.2.1 Acquisition modes: SeroAcq offers several unique features not previously reported in other software. These include 'Accumulation mode' and 'Resting voltage mode', which can apply impromptu changes to the waveform during acquisition in real-time without requiring the experiment to be stopped or a new waveform to be loaded. For example, accumulation mode interrupts the analytical waveform being applied and instead holds the electrode at a constant potential to accumulate charged analytes at the surface for sensitivity enhancements. Similarly, resting voltage mode allows modulation of the holding potential or 'non-sampled' region of the analytical waveform in real-time. The software applies these changes in real-time through a combination of design patterns such as event listeners, callback functions, and refresh cycles discussed in the *Methods* and *SI*. These modes are of particular interest for advanced users developing new waveforms that quickly wish to test multiple waveforms and different hold potentials/times, or are otherwise performing adsorption-based experiments.[4,6-8,29,60] More information, tutorial videos, and example data can be found in the *Supplemental Information*. For versatile data storage, experiments can be run in 'Discard mode' if the data does not need to be saved (*e.g.,* conditioning or equilibration experiments).[61] Further, using 'Ignore mode', any range of points can be ignored (not saved) to reduce file size considerably or otherwise reduce data complexity. Note that points refers to sampled points, which are dictated by the sampling frequency and used to convert sampled points to time. For example, at 125 MHz, a sampled point is acquired every 8 μs. Thus, an 8 ms waveform contains 1,000 points For example, using dual alternating rapid pulse and fast scan waveforms (**Fig. 6.3d**), points 1,001-11,500 are

not needed (this is the region of constant holding voltage, which is not needed for analysis).[29] Thus, data acquisition was run in Ignore mode, with the ignore start point at 1,001 and number of samples to ignore as 10,500. This considerably reduces file size and data overhead, especially for long (hours) *in vivo* experiments.

Other modes include 'Stimulation mode' and 'Injection mode'. Injection mode refers most often to a common *in vitro* experiment involving collecting calibration/training data using a six-port valve and flow cell, while Stimulation mode refers most commonly to an *in vivo* experiment involving evoked release (*e.g.,* pharmacological, optogenetic, electrical). For electrical stimulation, SeroWare offers several controls to administer a pulse train should users want to configure the device. Stimulation waveforms can be built in real-time during data acquisition (**Fig. 6.4**). However, some users may not have the ability or the need to configure such devices using their current set-up. To enable maximal flexibility, users can run Stimulation mode to apply generic event markers manually for devices that do not communicate directly with SeroWare. We refer to event markers as time stamps automatically generated by the software to indicate when an experimental event of interest occurs. This feature is especially useful given the wide array of experimental stimulation paradigms used with voltammetry—behavioral, light, electrical, pharmacological, *etc*. In this manner, SeroWare includes exemplary code and tutorials for those wishing to establish communication to external devices for direct control, such as injectors and stimulating electrodes. Conversely, manual event marking allows for an 'out of the box' work around for users wishing to immediately use the acquisition and analysis capabilities of SeroWare, while still being able to timestamp external events without having to force communication

between auxiliary hardware/software they may already be using. These timestamps are automatically labeled and preserved when the data is analyzed and exported (*vide infra*).

6.3.2.2 *External event control:* SeroAcq offers optional external control of the positioning of recording electrodes. For users that have COM port communication with a micromanipulator controller, the device will automatically be recognized and listed as a configuration option. Users simply select the step size at which to reposition the electrode(s) and the direction(s) in which to move. For example, we tested the software control with a Sutter Instruments MPC/ROE 200 micromanipulator controller and provide the control code within the source code (see User Guide in *Supplemental Information*). SeroAcq also offers external control of injectors for flow cell experiments, and control of stimulation electrodes for *in vivo* experiments. Due to the various instrumentation that can be used in combination with potentiostats, users may want to configure these additional devices as desired (see User Guide in *Supplemental Information*). Requests or issues for connecting additional devices can be submitted *via* GitHub for community feedback.

6.3.3 SeroDataProcess

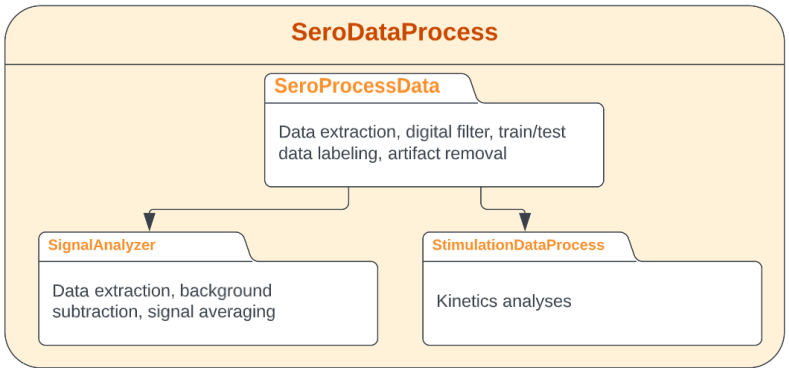

Figure 6.5. The SeroDataProcess module and submodules.

Once acquisition is complete, the saved *.dat* file can be visualized and analyzed in the SeroDataProcess module. SeroDataProcess has one main module and two sub-modules (**Fig. 6.5**). The main module is SeroProcessData. Here, data are automatically plotted at the same sampled point frequency specified during acquisition under the 'Quantification' panel, with events (*i.e.,* injections, stimulations) automatically labeled and time-stamped (**Fig. 6.6**). Users can then define areas of the data to extract automatically based on event markers or, alternatively, add and label such areas manually. We define such areas of interest as 'peaks', because historically voltammetry peaks at oxidation/reduction potentials of interest are extracted for further analysis. As an alternative to a color plot, a second temporal current plot is auto-populated under the 'Confirmation' panel at a user-defined voltage. We found two current-time traces at different voltages were helpful during new waveform development, as well as during *in vivo* analyses to visualize responses side-by-side at different voltages to ensure the presence of analyte peaks across characteristic voltages (*e.g.,* anodic and cathodic peaks). Static color plots can also be

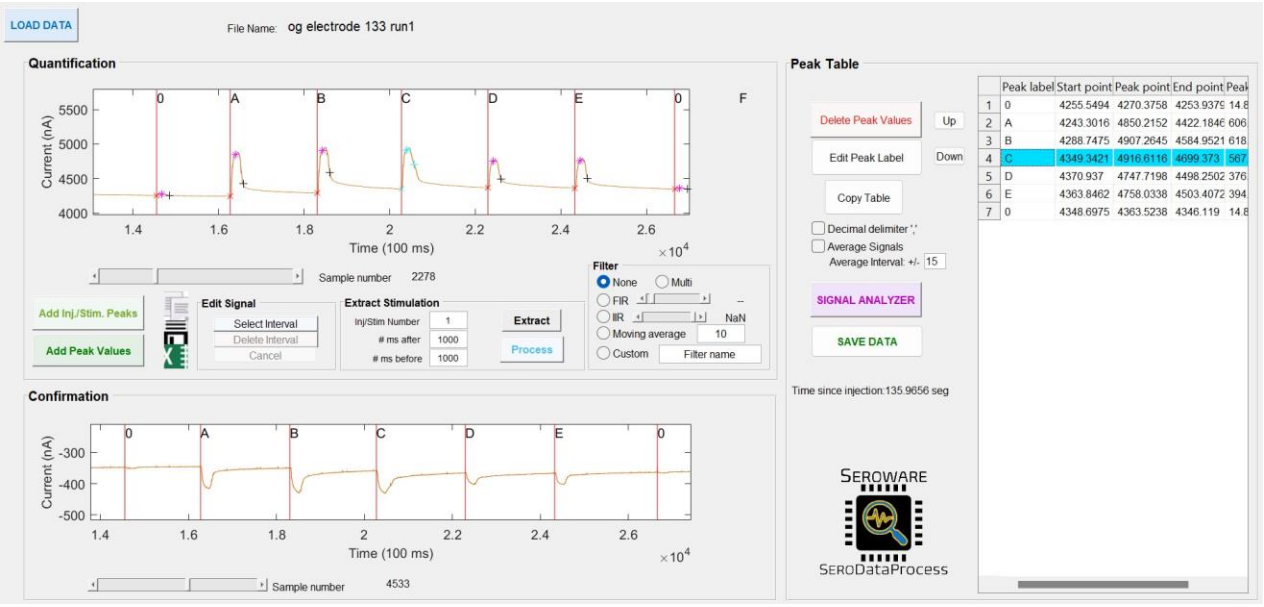

Figure 6.6. SeroDataProcess interface.

automatically generated at user-defined intervals for post-acquisition analysis (see SignalAnalyzer below). The dual current-time quantification/qualification visualization layout is similar to that used in tandem mass spectrometry software in which two separate precursor-to-product ion transitions are monitored to confirm the presence of an analyte. Here, the top panel shows an anodic current trace while the bottom shows a cathodic current trace (**Fig. 6.6**). Users can also save analysis files at any point so as not to lose progress or data on peak identification when work needs to be interrupted. For example, users analyzing long experiments (*i.e.*, hours) can stop and come back to a data file as needed. They can also save and share analyzed files with others in a reproducible and documented manner. As opposed to previous software packages, SeroWare can acquire, timestamp, and analyze the entirety of multiple hours-long experiments in a single session.[24]

Users can also individually extract identified peaks using the Peak Extraction panel. This enables users to run kinetic analyses of stimulation and uptake data (see *StimulationDataProcess*). Data can be plotted in new windows, sliced, and saved in various manners. Artifact removal can be easily performed using the select and delete interval buttons.

Several pre-set digital filtering options are available, including a moving average filter, a published infinite impulse response (IIR) filter developed for voltammetry baseline detrending,[16] and a custom finite impulse response (FIR) filter developed in-house. Further, SeroWare is fully incorporated with the MATLAB Filter Builder GUI. By selecting the custom filter option in SeroDataProcess, users can choose from over a dozen digital filter design options and specifications, and visualize the frequency responses (see *Supplemental Information*). When users are satisfied with the choice of data filter, standard or custom filters are immediately applied to the voltammetry data loaded by the user and visualized in the plots. Together with the signal

processing tools in MATLAB, SeroWare allows for easy incorporation of new, custom filters regardless of whether a user has a filter already programmed in MATLAB or not. The user can easily save and share their filters for reproducibility. The ability for seamless incorporation of powerful MATLAB analysis toolboxes with the SeroWare environment provides a key advantage over current LabVIEW software. Data can be extracted in filtered or raw formats using the SignalAnalyzer sub-module, accessible by the click of a single button.

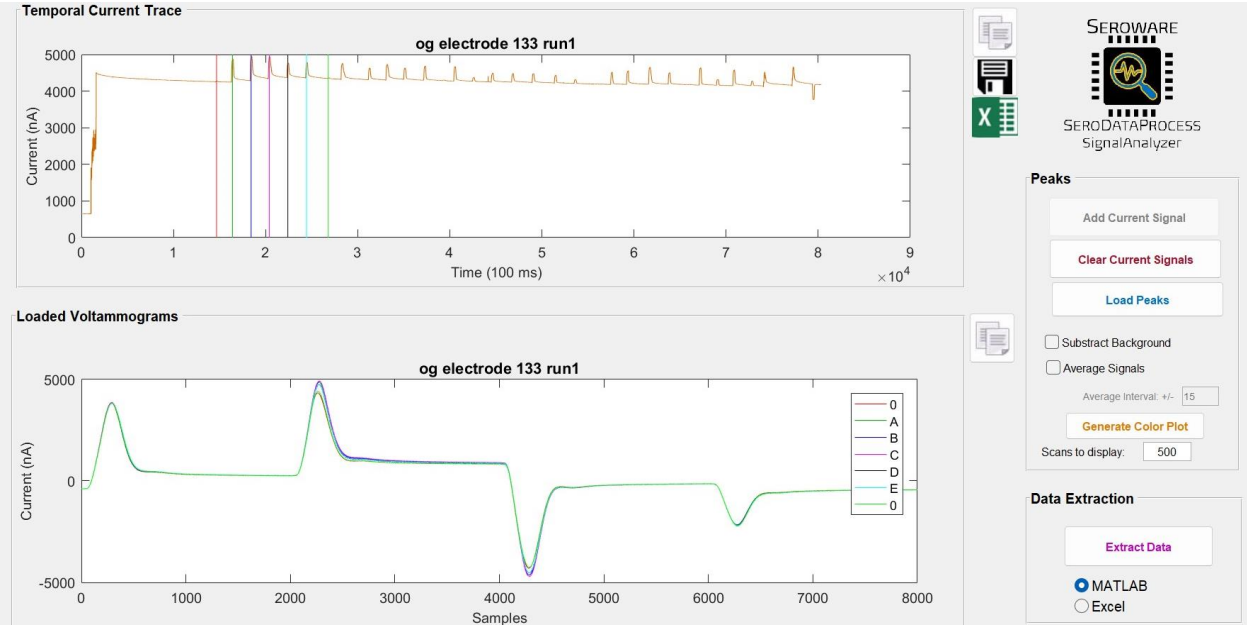

Figure 6.7. The signal analyzer GUI submodule for SeroDataProcess.

6.3.3.1 SignalAnalyzer: The ease, speed, and versatility at which SeroWare offers data extraction is a major advantage, especially as data wrangling (*i.e.,* the process of transforming data into another useful format for a specified task) into various analysis pipelines can be cumbersome.[62] To begin extracting processed data, a separate tab is opened *via* SignalAnalyzer (**Fig. 6.7**). A single button click loads the selected data from SeroDataProcess and allows users to visualize their

voltammograms, including in an unraveled, averaged, background subtracted, and/or color plotted formats. A simple click button interface instantly plots the data as desired.

Several options exist for the extraction of data to fit users' needs and data limits. The ease and versatility with which SeroWare automates data exporting is another key benefit of the software. Data can automatically be parsed and labeled as desired before exporting to a *.mat* or *.xlsx* file; each peak is referenced to a label for easy splitting into machine learning training and validation sets. Statistical learning techniques continue to be explored for voltammetry.[11,29,30,63-75] SeroWare was designed with these future directions in mind such that data can be streamlined from waveform to machine learning model.

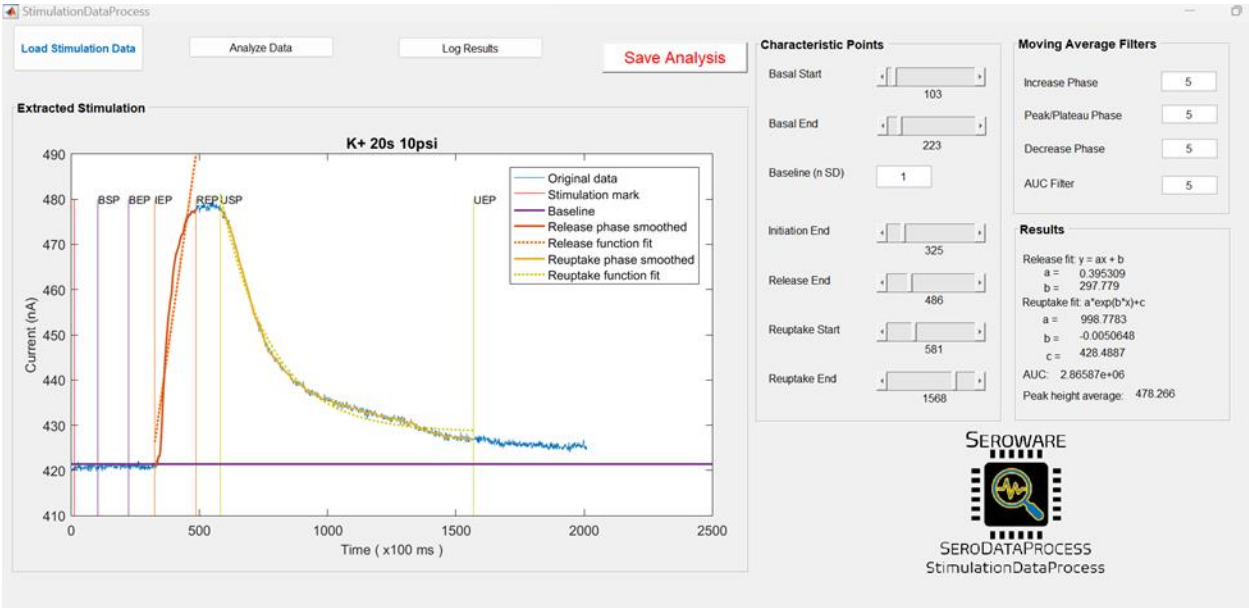

Figure 6.8. The StimulationDataProcess GUI sub-module of SeroDataProcess.

6.3.3.2 StimulationDataProcess: An important analysis strategy for *in vivo* voltammetry involving neurotransmitter monitoring is fitting data to kinetic models of release and reuptake.[76] For users who want to fit a kinetic model to an electrical stimulation event, for example, SeroWare provides

an automated extraction and analysis procedure (**Fig. 6.8**). In this initial release, SeroWare fits data to reuptake models using exponential decay rather than Michaelis-Menten models that are documented elsewhere.[27] Michaelis-Menten and other kinetic models can be incorporated into future releases by users. Nonetheless, parameters associated with exponential decay models have been shown to correlate well with Michaelis-Menten parameters and do not require transporter overflow (*i.e.,* Michaelis-Menten curve fitting may require saturated uptake conditions *via* electrical or pharmacological stimulation).[24] Data can be extracted seamlessly into a separate data file, which can be immediately opened and analyzed by StimulationDataProcess by simply hitting the Extract and Process buttons in SeroDataProcess. Data shown in **Figure 6.8** are from a potassium stimulation using an externally controlled picospritzer and the SeroWare event labeling feature.

6.4 CONCLUSIONS AND PROSPECTS

We present an open-source, thoroughly documented, customizable yet user-friendly software for the control, acquisition, and analysis of voltammetry data. The only hardware requirements are a potentiostat connected to a suitable computer with a National Instruments data acquisition card, along with a pre-amplifier and suitable electrodes. The software is compiled into a standalone version, such that users without MATLAB licenses can run SeroWare at no cost. While we have developed SeroWare for neurochemistry experiments, this software can be used for virtually any type of voltammetry experiment. Examples include the electronic tongue[55] and amperometric detection[77] fields, which measures compounds ranging from amino acids and pharmaceuticals to pollutants, explosives, food and beverages. Outside of voltammetry, the SeroDataProcess module can be used to analyze and extract other types of multi-dimensional data, provided it is formatted in MATLAB correctly. The software offers new acquisition and analysis capabilities, with an emphasis on reproducible results and community-built features.

SeroWare was purpose-built for user customization and sharing with the community at-large. It is licensed under GNU LGPL 3.0 to ensure this remains the case. We wrote SeroWare specifically to be intuitive for users with different levels of voltammetry experience. For example, we beta-tested SeroWare with novice undergraduate student researchers in our group (see *Supplemental videos*). Importantly, we also designed SeroWare for advanced users who desire customized solutions. The User Guide provides extensive information on how to edit and add to the SeroWare codebase. Users can edit the GUI using a code-free development environment (GUIDE). More in-depth documentation is provided for users desiring more extensive changes to the codebase (see *Supplemental Information*).

Currently, SeroWare only supports NI card data acquisition and a handful of external devices. SeroWare also does not currently support multichannel or array-based measurements. Depending on demand and any open-source contributions, future releases may extend support to a wider array of vendors and multiplexed hardware setups, as well as additional analysis tools. Work is underway to seamlessly incorporate additional modules to SeroWare for machine learning and data lakes. We invite the community to contribute issues and pull requests *via* GitHub.

6.5 METHODS

Software: All software was written in MATLAB R2016a (MathWorks, Inc., Natick, MA). The compiled versions of SeroWare can be run in standalone mode, such that no MATLAB installation or license is required. A MATLAB license is required to make custom edits to the code. Users can choose between stand-alone versions of each module that launch the ready-to-use program in a single click, or the raw MATLAB files, which provide straightforward access for implementing code modifications and executing changes in real-time. Each module is written in an event-driven, function-based manner, such that various functions run and accept user inputs through interaction with graphical user interfaces (GUIs) in the form of callbacks, handles, and global scope variables (see *Supporting Information*).

Data flow and storage: SeroAcq handles continuous acquisition over various lengths of time in a single file (*i.e.,* seconds to several hours), even at maximum sampling rates where data files can contain several gigabytes of data. This is facilitated by a 'batching' strategy for reading and writing data to and from the DAQ card and computer (**Fig. 6.9**). In brief, SeroWare utilizes an object-

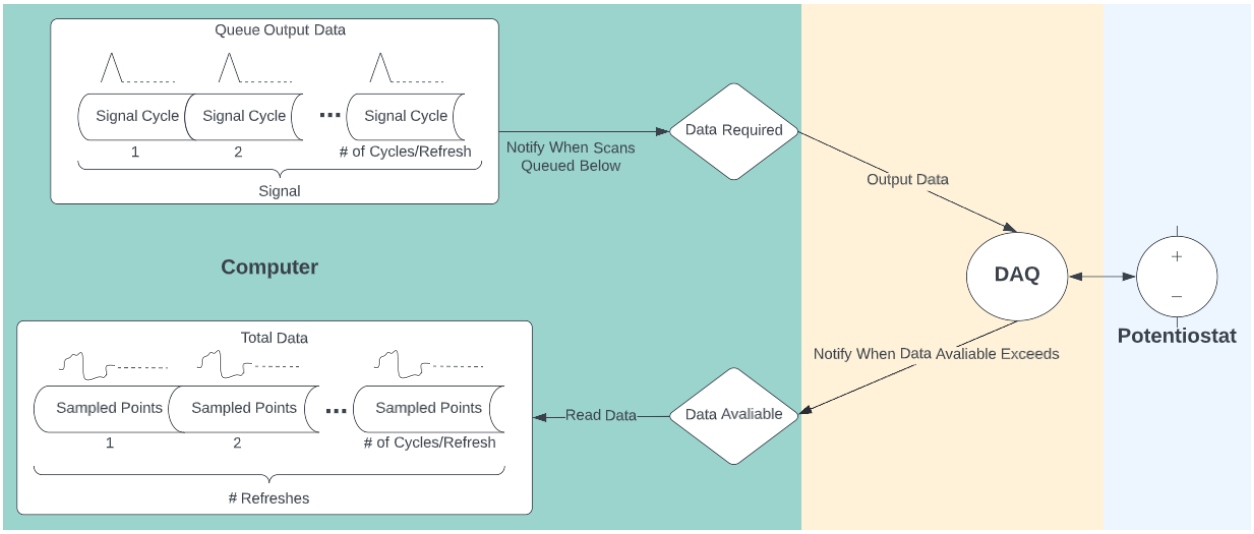

Figure 6.9. The SeroAcq data flow.

oriented approach to events and listeners, in combination with the built-in Data Acquisition Toolbox. Once an acquisition session is started, the software prepares a 'batch' of waveform cycles (*i.e.,* the repeating voltage train to apply) and initializes a matrix of the expected size of the voltammogram data that will be collected during a batch. As the DAQ card nears the end of a batch of waveform cycles and the data matrix is populated, the software then sends the next round of waveform cycles to the card and reads the data from the DAQ card to computer memory. The user can also configure how often the data is read to/from the data acquisition card from/to the computer memory based on computer performance. This feature allows users to conserve computer processing power as needed by selecting higher values of plot update times. Users can then define desired measurement times for continual data acquisition before stopping automatically or can stop the acquisition manually at any point. Data are saved in *.dat* format. The data batching procedure allows the software to employ versatile error-handling routines to ensure data are saved even if acquisition errors occur. This waveform batching and queuing procedure also enables *ad hoc* modification of waveforms in the accumulation/resting voltage modes described above.

Hardware: A Pine WaveNeuro Single Channel potentiostat with 200 nA/V or 1,000 nA/V headstages were used for data acquisition (Pine Research, Durham, NC) with a NI PCIe-6363 card (National Instruments (NI), Austin, TX). A 64-bit Dell Precision 3650 Tower with 32 GB RAM and Intel i7-11700 processer were used to run software and for data acquisition and processing. SeroWare was also tested using an EI-400 potentiostat (Cypress System, USA), a custom headstage, and a PCI-6221 card. Because SeroWare was not written to be compatible with specific hardware, only a few configuration steps were needed to switch between hardware configurations. A DS4 Bi-phasic Stimulus Isolator (Digitimer, Letchworth Garden City, UK) was used to test

electrical stimulation capabilities of the hardware. An MPC 200 controller and ROE-200 system (Sutter Instruments, Novato, CA) was used to test the external control of a micromanipulator. Two E60 and A60 6-port valves (VICI Valco Instruments, Houston, TX) and a flow cell (Pine Research) were used to test the control of external *in vitro* injections.

We have written the software to be straightforwardly compatible with common hardware and other external devices used during voltammetry experiments. For each, we provide working and/or example code that can be modified for user needs, regardless of specific hardware or connections. The hardware used above can be used as a starting point for new users. However, SeroWare can be modified to be compatible with other hardware as dictated by users depending on the density of data being acquired and other tasks that need to be run by (a) computer(s). Working or reference electrodes can be used with SeroWare if specified prior to data acquisition.

6.6 SUPPLEMENTAL INFORMATION:

The User Guide and tutorial videos are hosted at www.github.com/csmova/SeroWare.

	Demon	HDCV	SeroWare
Open source	✘	✘	✓
User Guide, tutorials, and videos freely available	✘	✘	✓
Waveform generation interface with shareable file format	✘	✓	✓
Real time data visualization	✓	✓	✓
Event labeling ***(e.g., timestamps)***			
Manual (user editable)	✘	✘	✓
Automated (device-controlled)	✓	✓	✓
Digital filters			
Pre-set filters	✓	✓	✓
Custom digital filter builder interface	✘	✘	✓
Kinetic analyses	✓	✘	✓
External control(s)			
Electrical stimulation	✓	✓	✓
Micromanipulator control	✘	✘	✓
Injector valve control	✘	✘	✓
Real-time waveform modification	✘	✘	✓
Single file format *(i.e., events and voltammograms stored together)*	✘	✘	✓
Figure generation & data reporting	✓	✓	✓
Optimized data and error handling	✘	✓	✓
Artifact removal	✓	✓	✓
Chemometric analyses	✓	✓	✓*
Automated peak finding	✓	✘	✓*
Multi-channel electrodes/electrophysiology	✘	✓	✓*

Table S6.1. Comparison of published fast voltammetry software for neurochemical analyses. The asterisk (*) denotes partial functionality, and/or upcoming or future release. Note that due to multiple releases and/or unavailability of other listed software, information for Demon, HDCV, or SeroWare may be out of date and relies only on reports at the time of writing and/or correspondence with the maintainers of the packages.

Acknowledgements & Author Contributions: CSM was supported by the National Science Foundation Graduate Research Fellowship Program (DGE-1650604 and DGE-2034835). The authors would also like to acknowledge support from the National Institute on Drug Abuse (DA045550). Any opinions, findings, and conclusions or recommendations expressed in this material are those of the authors and do not necessarily reflect the views of the National Science Foundation or the National Institutes of Health. The Authors acknowledge Katie Perrotta and Hongyan Yang for assistance with data collection and helpful discussions regarding features of the software. The Authors acknowledge BioRender and LucidChart for figure generation.

MAF designed and wrote the initial software. RI and CSM wrote additional code and added features to each module. MEC and MEW assisted with testing the software and making tutorial videos. AMA and MAF guided the project. CSM wrote the initial draft of the manuscript.

6.7 REFERENCES

1. Adams, R. N., Probing brain chemistry with electroanalytical techniques. *Anal. Chem.* **1976,** *48* (14), 1126A-1138A. https://doi.org/10.1021/ac50008a001
2. Rodeberg, N. T.; Sandberg, S. G.; Johnson, J. A.; Phillips, P. E. M.; Wightman, R. M., Hitchhiker's guide to voltammetry: Acute and chronic electrodes for in vivo fast-scan cyclic voltammetry. *ACS Chem. Neurosci.* **2017,** *8* (2), 221-234. https://doi.org/10.1021/acschemneuro.6b00393
3. Robinson, D. L.; Venton, B. J.; Heien, M. L.; Wightman, R. M., Detecting subsecond dopamine release with fast-scan cyclic voltammetry in vivo. *Clin. Chem* **2003,** *49* (10), 1763-73. https://doi.org/10.1373/49.10.1763
4. Oh, Y.; Heien, M. L.; Park, C.; Kang, Y. M.; Kim, J.; Boschen, S. L.; Shin, H.; Cho, H. U.; Blaha, C. D.; Bennet, K. E.; Lee, H. K.; Jung, S. J.; Kim, I. Y.; Lee, K. H.; Jang, D. P., Tracking tonic dopamine levels in vivo using multiple cyclic square wave voltammetry. *Biosens. Bioelectron.* **2018,** *121*, 174-182. https://doi.org/10.1016/j.bios.2018.08.034
5. Park, C.; Oh, Y.; Shin, H.; Kim, J.; Kang, Y.; Sim, J.; Cho, H. U.; Lee, H. K.; Jung, S. J.; Blaha, C. D.; Bennet, K. E.; Heien, M. L.; Lee, K. H.; Kim, I. Y.; Jang, D. P., Fast cyclic square-wave voltammetry to enhance neurotransmitter selectivity and sensitivity. *Anal. Chem.* **2018,** *90* (22), 13348-13355. https://doi.org/10.1021/acs.analchem.8b02920
6. Atcherley, C. W.; Laude, N. D.; Parent, K. L.; Heien, M. L., Fast-scan controlled-adsorption voltammetry for the quantification of absolute concentrations and adsorption dynamics. *Langmuir* **2013,** *29* (48), 14885-92. https://doi.org/10.1021/la402686s

7. Calhoun, S. E.; Meunier, C. J.; Lee, C. A.; McCarty, G. S.; Sombers, L. A., Characterization of a multiple-scan-rate voltammetric waveform for real-time detection of met-enkephalin. *ACS Chem. Neurosci.* **2019,** *10* (4), 2022-2032. https://doi.org/10.1021/acschemneuro.8b00351

8. Dunham, K. E.; Venton, B. J., Improving serotonin fast-scan cyclic voltammetry detection: New waveforms to reduce electrode fouling. *Analyst* **2020,** *145* (22), 7437-7446. https://doi.org/10.1039/D0AN01406K

9. Shin, H.; Goyal, A.; Barnett, J. H.; Rusheen, A. E.; Yuen, J.; Jha, R.; Hwang, S. M.; Kang, Y.; Park, C.; Cho, H.-U.; Blaha, C. D.; Bennet, K. E.; Oh, Y.; Heien, M. L.; Jang, D. P.; Lee, K. H., Tonic serotonin measurements in vivo using N-shaped multiple cyclic square wave voltammetry. *Anal. Chem.* **2021,** *93* (51), 16987-16994. https://doi.org/10.1021/acs.analchem.1c02131

10. Rafi, H.; Zestos, A. G., Multiplexing neurochemical detection with carbon fiber multielectrode arrays using fast-scan cyclic voltammetry. *Anal. Bioanal. Chem.* **2021,** *413* (27), 6715-6726.

11. Puthongkham, P.; Venton, B. J., Recent advances in fast-scan cyclic voltammetry. *Analyst* **2020,** *145* (4), 1087-1102. https://doi.org/10.1039/c9an01925a

12. Castagnola, E.; Garg, R.; Rastogi, S. K.; Cohen-Karni, T.; Cui, X. T., 3D fuzzy graphene microelectrode array for dopamine sensing at sub-cellular spatial resolution. *Biosens. Bioelectron.* **2021,** *191*, 113440. https://doi.org/10.1016/j.bios.2021.113440

13. Choi, H.; Shin, H.; Cho, H. U.; Blaha, C. D.; Heien, M. L.; Oh, Y.; Lee, K. H.; Jang, D. P., Neurochemical concentration prediction using deep learning vs principal

component regression in fast scan cyclic voltammetry: A comparison study. *ACS Chem. Neurosci.* **2022**.

14. Puthongkham, P.; Rocha, J.; Borgus, J. R.; Ganesana, M.; Wang, Y.; Chang, Y.; Gahlmann, A.; Venton, B. J., Structural similarity image analysis for detection of adenosine and dopamine in fast-scan cyclic voltammetry color plots. *Anal. Chem.* **2020,** *92* (15), 10485-10494. https://doi.org/10.1021/acs.analchem.0c01214
15. Johnson, J. A.; Gray, J. H.; Rodeberg, N. T.; Wightman, R. M., Multivariate curve resolution for signal isolation from fast-scan cyclic voltammetric data. *Anal. Chem.* **2017,** *89* (19), 10547-10555.
16. DeWaele, M.; Oh, Y.; Park, C.; Kang, Y. M.; Shin, H.; Blaha, C. D.; Bennet, K. E.; Kim, I. Y.; Lee, K. H.; Jang, D. P., A baseline drift detrending technique for fast scan cyclic voltammetry. *Analyst* **2017,** *142* (22), 4317-4321.
17. Laude, N. D.; Atcherley, C. W.; Heien, M. L., Rethinking data collection and signal processing. 1. Real-time oversampling filter for chemical measurements. *Anal. Chem.* **2012,** *84* (19), 8422-8426. https://doi.org/10.1021/ac302169y
18. Atcherley, C. W.; Vreeland, R. F.; Monroe, E. B.; Sanchez-Gomez, E.; Heien, M. L., Rethinking data collection and signal processing. 2. Preserving the temporal fidelity of electrochemical measurements. *Anal. Chem.* **2013,** *85* (16), 7654-7658. https://doi.org/10.1021/ac402037k
19. Meunier, C. J.; McCarty, G. S.; Sombers, L. A., Drift subtraction for fast-scan cyclic voltammetry using double-waveform partial-least-squares regression. *Anal. Chem.* **2019,** *91* (11), 7319-7327. https://doi.org/10.1021/acs.analchem.9b01083

20. Jang, D. P.; Kim, I.; Chang, S.-Y.; Min, H.-K.; Arora, K.; Marsh, M. P.; Hwang, S.-C.; Kimble, C. J.; Bennet, K. E.; Lee, K. H., Paired pulse voltammetry for differentiating complex analytes. *Analyst* **2012,** *137* (6), 1428-1435. https://doi.org/10.1039/C2AN15912K

21. Loewinger, G.; Patil, P.; Kishida, K. T.; Parmigiani, G., Multi-study learning for real-time neurochemical sensing in humans using the "study strap ensemble". *bioRxiv* **2021**, 856385. https://doi.org/10.1101/856385

22. Montague, P. R.; Kishida, K. T., Computational underpinnings of neuromodulation in humans. *Cold Spring Harbor Symp. Quant. Biol.* **2018,** *83*, 71-82. https://doi.org/10.1101/sqb.2018.83.038166

23. Bucher, E. S.; Brooks, K.; Verber, M. D.; Keithley, R. B.; Owesson-White, C.; Carroll, S.; Takmakov, P.; McKinney, C. J.; Wightman, R. M., Flexible software platform for fast-scan cyclic voltammetry data acquisition and analysis. *Anal. Chem.* **2013,** *85* (21), 10344-10353. https://doi.org/10.1021/ac402263x

24. Yorgason, J. T.; España, R. A.; Jones, S. R., Demon voltammetry and analysis software: Analysis of cocaine-induced alterations in dopamine signaling using multiple kinetic measures. *J. Neurosci. Methods* **2011,** *202* (2), 158-164.

25. Goyal, A.; Hwang, S.; Rusheen, A. E.; Blaha, C. D.; Bennet, K. E.; Lee, K. H.; Jang, D. P.; Oh, Y.; Shin, H., Software for near-real-time voltammetric tracking of tonic neurotransmitter levels in vivo. *Front. Neurosci.* **2022,** *16*. 10.3389/fnins.2022.899436

26. Kimble, C. J.; Boesche, J. B.; Eaker, D. R.; Kressin, K. R.; McIntosh, M. B.; Lujan, J. L.; Trevathan, J. K.; Paek, S.; Asp, A. J. In *Multifunctional system for observing, measuring and analyzing stimulation-evoked neurochemical signaling*, 2017 IEEE

International Symposium on Medical Measurements and Applications (MeMeA), 7-10 May 2017; 2017; pp 349-354.

27. Mena, S.; Dietsch, S.; Berger, S. N.; Witt, C. E.; Hashemi, P., Novel, user-friendly experimental and analysis strategies for fast voltammetry: 1. The analysis kid for FSCV. *ACS Meas. Sci. Au* **2021,** *1* (1), 11-19.

28. Mena, S.; Visentin, M.; Witt, C. E.; Honan, L. E.; Robins, N.; Hashemi, P., Novel, user-friendly experimental and analysis strategies for fast voltammetry: Next generation FSCAV with artificial neural networks. *ACS Meas. Sci. Au* **2022,** *2* (3), 241-250. https://doi.org/10.1021/acsmeasuresciau.1c00060

29. Movassaghi, C. S.; Perrotta, K. A.; Yang, H.; Iyer, R.; Cheng, X.; Dagher, M.; Fillol, M. A.; Andrews, A. M., Simultaneous serotonin and dopamine monitoring across timescales by rapid pulse voltammetry with partial least squares regression. *Anal. Bioanal. Chem.* **2021,** *413* (27), 6747-6767. https://doi.org/10.1007/s00216-021-03665-1

30. Xue, Y.; Ji, W.; Jiang, Y.; Yu, P.; Mao, L., Deep learning for voltammetric sensing in a living animal brain. *Angew. Chem. Int. Ed.* **2021,** *60* (44), 23777-23783. https://doi.org/10.1002/anie.202109170

31. Meunier, C. J.; Denison, J. D.; McCarty, G. S.; Sombers, L. A., Interpreting dynamic interfacial changes at carbon fiber microelectrodes using electrochemical impedance spectroscopy. *Langmuir* **2020,** *36* (15), 4214-4223. https://doi.org/10.1021/acs.langmuir.9b03941

32. Roberts, J. G.; Toups, J. V.; Eyualem, E.; McCarty, G. S.; Sombers, L. A., In situ electrode calibration strategy for voltammetric measurements in vivo. *Anal. Chem.* **2013,** *85* (23), 11568-11575. https://doi.org/10.1021/ac402884n

33. Meunier, C. J.; Mitchell, E. C.; Roberts, J. G.; Toups, J. V.; McCarty, G. S.; Sombers, L. A., Electrochemical selectivity achieved using a double voltammetric waveform and partial least squares regression: Differentiating endogenous hydrogen peroxide fluctuations from shifts in pH. *Anal. Chem.* **2018,** *90* (3), 1767-1776. https://doi.org/10.1021/acs.analchem.7b03717

34. Park, C.; Hwang, S.; Kang, Y.; Sim, J.; Cho, H. U.; Oh, Y.; Shin, H.; Kim, D. H.; Blaha, C. D.; Bennet, K. E., Feasibility of applying Fourier transform electrochemical impedance spectroscopy in fast cyclic square wave voltammetry for the in vivo measurement of neurotransmitters. *Anal. Chem.* **2021,** *93* (48), 15861-15869. https://doi.org/10.1021/acs.analchem.1c02308

35. Van Echelpoel, R.; de Jong, M.; Daems, D.; Van Espen, P.; De Wael, K., Unlocking the full potential of voltammetric data analysis: A novel peak recognition approach for (bio)analytical applications. *Talanta* **2021,** *233*, 122605. https://doi.org/10.1016/j.talanta.2021.122605

36. Cobb, S. J.; Macpherson, J. V., Enhancing square wave voltammetry measurements via electrochemical analysis of the non-faradaic potential window. *Anal. Chem.* **2019,** *91* (12), 7935-7942. https://doi.org/10.1021/acs.analchem.9b01857

37. Jaworski, A.; Wikiel, H.; Wikiel, K., Benefiting from information-rich multi-frequency AC voltammetry coupled with chemometrics on the example of on-line monitoring of leveler component of electroplating bath. *Electroanalysis 35* (1), e202200478. https://doi.org/10.1002/elan.202200478

38. Abeykoon, S. W.; White, R. J., Continuous square wave voltammetry for high information content interrogation of conformation switching sensors. *ACS Meas. Sci. Au* **2023,** *3* (1), 1-9. 10.1021/acsmeasuresciau.2c00044

39. Movassaghi, C. S.; Alcañiz Fillol, M.; Kishida, K. T.; McCarty, G.; Sombers, L. A.; Wassum, K. M.; Andrews, A. M., Maximizing electrochemical information: A perspective on background-inclusive fast voltammetry. *Anal. Chem.* **2024**. https://doi.org/10.1021/acs.analchem.3c04938

40. DeCaluwe, S. C., Open software for chemical and electrochemical modeling: Opportunities and challenges. *Electrochem. Soc. Interface* **2019,** *28* (1), 47-50. https://doi.org/10.1149/2.f04191if

41. Rowe, A. A.; Bonham, A. J.; White, R. J.; Zimmer, M. P.; Yadgar, R. J.; Hobza, T. M.; Honea, J. W.; Ben-Yaacov, I.; Plaxco, K. W., CheapStat: An open-source, "do-it-yourself" potentiostat for analytical and educational applications. *PLOS ONE* **2011,** *6* (9), e23783. https://doi.org/10.1371/journal.pone.0023783

42. Curtis, S. D.; Ploense, K. L.; Kurnik, M.; Ortega, G.; Parolo, C.; Kippin, T. E.; Plaxco, K. W.; Arroyo-Currás, N., Open source software for the real-time control, processing, and visualization of high-volume electrochemical data. *Anal. Chem.* **2019,** *91* (19), 12321-12328. https://doi.org/10.1021/acs.analchem.9b02553

43. Markiewicz, C. J.; Gorgolewski, K. J.; Feingold, F.; Blair, R.; Halchenko, Y. O.; Miller, E.; Hardcastle, N.; Wexler, J.; Esteban, O.; Goncavles, M.; Jwa, A.; Poldrack, R., The OpenNeuro resource for sharing of neuroscience data. *eLife* **2021,** *10,* e71774. https://doi.org/10.7554/eLife.71774

44. Stark, C.; Breitkreutz, B.-J.; Reguly, T.; Boucher, L.; Breitkreutz, A.; Tyers, M., BioGRID: A general repository for interaction datasets. *Nucleic Acids Res.* **2006,** *34*, D535-D539. https://doi.org/10.1093/nar/gkj109

45. Holland, R. C.; Down, T. A.; Pocock, M.; Prlić, A.; Huen, D.; James, K.; Foisy, S.; Dräger, A.; Yates, A.; Heuer, M., BioJava: An open-source framework for bioinformatics. *Bioinformatics* **2008,** *24* (18), 2096-2097.

46. Steinbeck, C.; Han, Y.; Kuhn, S.; Horlacher, O.; Luttmann, E.; Willighagen, E., The chemistry development kit (CDK): An open-source Java library for chemo- and bioinformatics. *J. Chem. Inf. Comput. Sci.* **2003,** *43* (2), 493-500. https://doi.org/10.1021/ci025584y

47. Farhoodi, R.; Garousi, V.; Pfahl, D.; Sillito, J., Development of scientific software: A systematic mapping, a bibliometrics study, and a paper repository. *Int. J. Softw. Eng. Knowl. Eng.* **2013,** *23* (04), 463-506.

48. Delorme, A.; Makeig, S., EEGLAB: An open source toolbox for analysis of single-trial EEG dynamics including independent component analysis. *J. Neurosci. Methods* **2004,** *134* (1), 9-21.

49. Egert, U.; Knott, T.; Schwarz, C.; Nawrot, M.; Brandt, A.; Rotter, S.; Diesmann, M., MEA-Tools: An open source toolbox for the analysis of multi-electrode data with MATLAB. *J. Neurosci. Methods* **2002,** *117* (1), 33-42.

50. He, B.; Dai, Y.; Astolfi, L.; Babiloni, F.; Yuan, H.; Yang, L., Econnectome: A MATLAB toolbox for mapping and imaging of brain functional connectivity. *J. Neurosci. Methods* **2011,** *195* (2), 261-269.

51. Lopez-Calderon, J.; Luck, S. J., ERPLAB: An open-source toolbox for the analysis of event-related potentials. *Front. Hum. Neurosci.* **2014,** *8*, 213.

52. de Cheveigné, A.; Arzounian, D., Robust detrending, rereferencing, outlier detection, and inpainting for multichannel data. *NeuroImage* **2018,** *172*, 903-912.

53. Campos, I.; Masot, R.; Alcañiz, M.; Gil, L.; Soto, J.; Vivancos, J. L.; García-Breijo, E.; Labrador, R. H.; Barat, J. M.; Martínez-Mañez, R., Accurate concentration determination of anions nitrate, nitrite and chloride in minced meat using a voltammetric electronic tongue. *Sens. Actuators, B* **2010,** *149* (1), 71-78. https://doi.org/10.1016/j.snb.2010.06.028

54. Fuentes, E.; Alcañiz, M.; Contat, L.; Baldeón, E. O.; Barat, J. M.; Grau, R., Influence of potential pulses amplitude sequence in a voltammetric electronic tongue (VET) applied to assess antioxidant capacity in aliso. *Food Chem.* **2017,** *224*, 233-241. https://doi.org/10.1016/j.foodchem.2016.12.076

55. Winquist, F., Voltammetric electronic tongues – basic principles and applications. *Microchim. Acta* **2008,** *163* (1), 3-10. https://doi.org/10.1007/s00604-007-0929-2

56. Winquist, F.; Wide, P.; Lundström, I., An electronic tongue based on voltammetry. *Anal. Chim. Acta* **1997,** *357* (1), 21-31. https://doi.org/10.1016/S0003-2670(97)00498-4

57. Heien, M. L. A. V.; Phillips, P. E. M.; Stuber, G. D.; Seipel, A. T.; Wightman, R. M., Overoxidation of carbon-fiber microelectrodes enhances dopamine adsorption and increases sensitivity. *Analyst* **2003,** *128* (12), 1413-1419. https://doi.org/10.1039/B307024G

58. Bath, B. D.; Michael, D. J.; Trafton, B. J.; Joseph, J. D.; Runnels, P. L.; Wightman, R. M., Subsecond adsorption and desorption of dopamine at carbon-fiber microelectrodes. *Anal. Chem.* **2000,** *72* (24), 5994-6002. https://doi.org/10.1021/ac000849y

59. Montague, P. R.; Lohrenz, T.; White, J.; Moran, R. J.; Kishida, K. T., Random burst sensing of neurotransmitters. *bioRxiv (Neuroscience)* **2019,** (posted 2019-04-13), 607077. https://doi.org/10.1101/607077 (accessed 2023-12-12)

60. Oh, Y.; Park, C.; Kim, D. H.; Shin, H.; Kang, Y. M.; DeWaele, M.; Lee, J.; Min, H.-K.; Blaha, C. D.; Bennet, K. E.; Kim, I. Y.; Lee, K. H.; Jang, D. P., Monitoring in vivo changes in tonic extracellular dopamine level by charge-balancing multiple waveform fast-scan cyclic voltammetry. *Anal. Chem.* **2016,** *88* (22), 10962-10970. https://doi.org/10.1021/acs.analchem.6b02605

61. Mitchell, E. C.; Dunaway, L. E.; McCarty, G. S.; Sombers, L. A., Spectroelectrochemical characterization of the dynamic carbon-fiber surface in response to electrochemical conditioning. *Langmuir* **2017,** *33* (32), 7838-7846. https://doi.org/10.1021/acs.langmuir.7b01443

62. Furche, T.; Gottlob, G.; Libkin, L.; Orsi, G.; Paton, N. W. In *Data wrangling for big data: Challenges and opportunities*, EDBT, 2016; pp 473-478.

63. Gundry, L.; Guo, S.-X.; Kennedy, G.; Keith, J.; Robinson, M.; Gavaghan, D.; Bond, A. M.; Zhang, J., Recent advances and future perspectives for automated parameterisation, Bayesian inference and machine learning in voltammetry. *Chem. Comm.* **2021,** *57* (15), 1855-1870. https://doi.org/10.1039/D0CC07549C

64. Matsushita, G. H. G.; Sugi, A. H.; Costa, Y. M. G.; Gomez-A, A.; Da Cunha, C.; Oliveira, L. S., Phasic dopamine release identification using convolutional neural

network. *Comput. Biol. Med.* **2019,** *114*, 103466. https://doi.org/10.1016/j.compbiomed.2019.103466

65. Chen, Y.; Wang, J.; Hoar, B. B.; Lu, S.; Liu, C., Machine learning-based inverse design for electrochemically controlled microscopic gradients of O2 and H2O2. *Proc. Natl. Acad. Sci. U.S.A.* **2022,** *119* (32), e2206321119. https://doi.org/10.1073/pnas.2206321119

66. Puthongkham, P.; Wirojsaengthong, S.; Suea-Ngam, A., Machine learning and chemometrics for electrochemical sensors: Moving forward to the future of analytical chemistry. *Analyst* **2021,** *146* (21), 6351-6364. https://doi.org/10.1039/D1AN01148K

67. Cui, F.; Yue, Y.; Zhang, Y.; Zhang, Z.; Zhou, H. S., Advancing biosensors with machine learning. *ACS Sens.* **2020,** *5* (11), 3346-3364. https://doi.org/10.1021/acssensors.0c01424

68. Fenton Jr, A. M.; Brushett, F. R., Leveraging graphical models to enhance in situ analyte identification via multiple voltammetric techniques. *J. Electroanal. Chem.* **2023,** *936*, 117299. https://doi.org/10.1016/j.jelechem.2023.117299

69. Desagani, D.; Ben-Yoav, H., Chemometrics meets electrochemical sensors for intelligent in vivo bioanalysis. *TrAC, Trends Anal. Chem.* **2023,** *164*, 117089. https://doi.org/10.1016/j.trac.2023.117089

70. Loewinger, G.; Patil, P.; Kishida, K. T.; Parmigiani, G., Hierarchical resampling for bagging in multistudy prediction with applications to human neurochemical sensing. *Ann. Appl. Stat.* **2022,** *16* (4), 2145-2165, 21. https://doi.org/10.1214/21-aoas1574

71. Chen, H.; Kätelhön, E.; Compton, R. G., Machine learning in fundamental electrochemistry: Recent advances and future opportunities. *Curr. Opin. Electrochem.* **2023,** *38*, 101214. https://doi.org/10.1016/j.coelec.2023.101214

72. Giordano, G. F.; Ferreira, L. F.; Bezerra, Í. R. S.; Barbosa, J. A.; Costa, J. N. Y.; Pimentel, G. J. C.; Lima, R. S., Machine learning toward high-performance electrochemical sensors. *Anal. Bioanal. Chem.* **2023**. https://doi.org/10.1007/s00216-023-04514-z

73. Kammarchedu, V.; Ebrahimi, A., Advancing electrochemical screening of neurotransmitters using a customizable machine learning-based multimodal system. *IEEE Sens. Lett.* **2023,** *7* (3), 1-4. https://doi.org/10.1109/LSENS.2023.3247002

74. Twomey, T.; Barbosa, L.; Lohrenz, T.; Montague, P. R., Deep learning architectures for FSCV, a comparison. *arXiv (Medical Physics)* **2022,** (posted 2022-12-05). https://doi.org/10.48550/arXiv.2212.01960 (accessed 2023-12-12)

75. Choi, H.; Shin, H.; Cho, H. U.; Blaha, C. D.; Heien, M. L.; Oh, Y.; Lee, K. H.; Jang, D. P., Neurochemical concentration prediction using deep learning vs principal component regression in fast scan cyclic voltammetry: A comparison study. *ACS Chem. Neurosci.* **2022,** *13* (15), 2288-2297. https://doi.org/10.1021/acschemneuro.2c00069

76. Bunin, M. A.; Prioleau, C.; Mailman, R. B.; Wightman, R. M., Release and uptake rates of 5-hydroxytryptamine in the dorsal raphe and substantia nigra reticulata of the rat brain. *J. Neurochem.* **1998,** *70* (3), 1077-1087. https://doi.org/10.1046/j.1471-4159.1998.70031077.x

77. Islam, M. A.; Mahbub, P.; Nesterenko, P. N.; Paull, B.; Macka, M., Prospects of pulsed amperometric detection in flow-based analytical systems - a review. *Anal. Chim. Acta* **2019,** *1052*, 10-26. https://doi.org/10.1016/j.aca.2018.10.066

Chapter 7

Conclusions & Prospects

My dissertation work focused on developing methods and software for rapid pulse voltammetry (RPV). Here, I detail additional ongoing efforts and future directions for extending the accuracy and applicability of RPV through *in vitro* and *in vivo* experiments, computational approaches, and software.

7.1 Additional method development and validation of RPV-PLSR

7.1.1 Head-to-head model comparisons: Chapters 1, 3, 4, and 5 detailed and discussed comparisons of various voltammetry waveforms and models, such as background-subtracted *vs.* background-inclusive and principal component regression (PCR) *vs.* partial least squares regression (PLSR) models. As noted in Chapter 1, head-to-head comparisons of new models and waveforms are needed to evaluate their applicability, particularly under specific circumstances. While we compared background-subtracted *vs.* -inclusive PCR and PLSR models in Chapter 3, additional *in vitro* comparisons are shown here. All experiments were performed with similar *in vitro* experimental conditions and materials as outlined in Chapters 3 and 5.

To monitor model performance as training data are added, I tracked bootstrapped R^2Y and Q^2Y scores to create model learning curves (**Fig. 7.1a**).[1] When these curves converge, (for example, extrapolation shown by dashed lines), the model has stopped 'learning', indicating that maximum information has been gleaned from the current training paradigm. Plateaus without convergence indicate that better calibration sets, waveforms, or more sophisticated machine-learning models are needed.

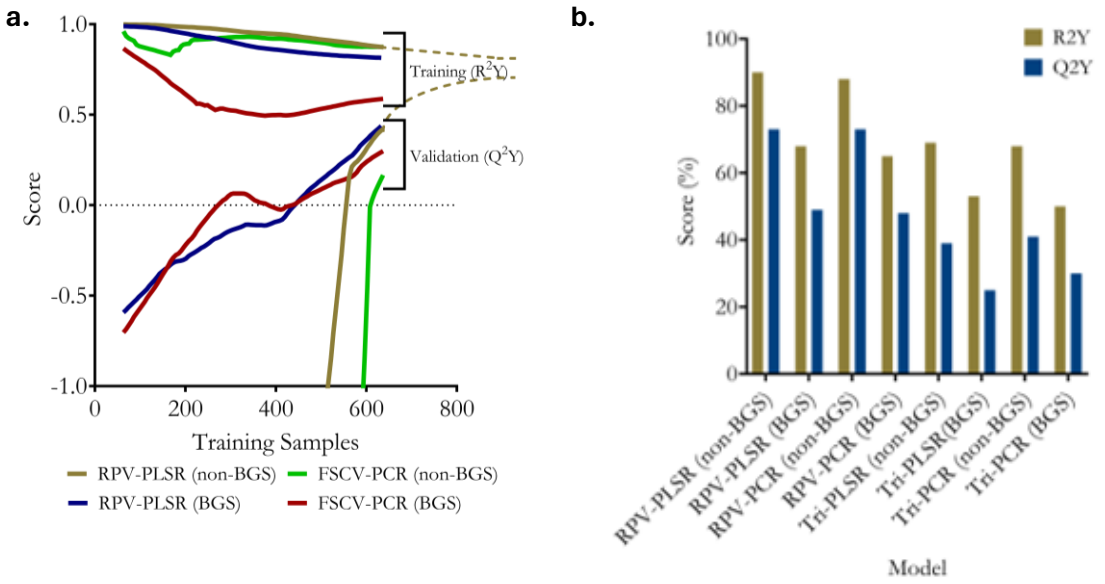

Figure 7.1: (a) Learning curves and (**b)** training and validation scores, by model-waveform combination. Tri = triangle waveform from FSCV.

I compared learning curves for RPV-PLSR (*i.e.,* pulse waveform detailed in Chapter 3) *vs.* FSCV-PCR (*i.e.,* triangle 'tri' waveform detailed in Chapter 3) under background[2] vs. non-background[3] subtracted conditions (BGS and non-BGS, respectively; **Fig. 7.1a**). Avoiding background subtraction resulted in delayed but rapid increases in bootstrapped Q^2Y, suggesting that non-BGS models learn from non-faradaic information when provided sufficient training data (*i.e.,* more evidence for the generalizability of larger training sets[3]). Notably, RPV-PLSR (non-BGS) had the most rapid Q^2Y learning curve, requiring less training data, and had the highest R^2Y, indicating it may converge first.

I combined flow cell training data from three electrodes as proof-of-concept for training across multiple electrodes. Voltammograms were obtained using RPV[4] or FSCV[5] waveforms and analyzed by PLSR or PCR. Non-BGS and RPV-PLSR models outperformed all other combinations (**Fig. 7.1b**; highest R^2Y and Q^2Y scores), including the historically used FSCV-PCR (BGS)[2] and recent FSCV-PCR (non-BGS)[3] approaches. All non-BGS and PLSR models

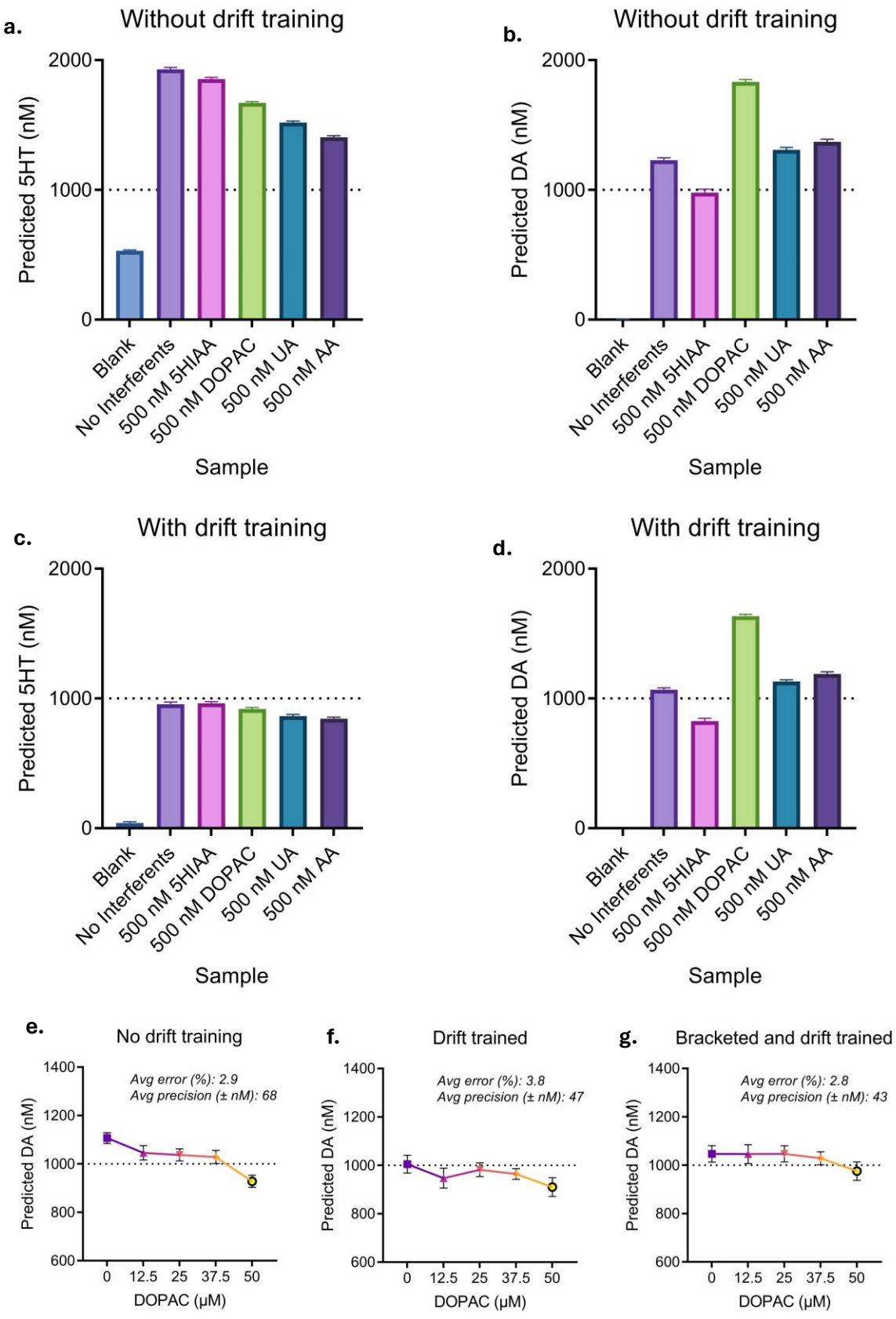
a.
Without drift training
Predicted 5HT (nM)
2000
1000
0
Blank
No Interferents
500 nM 5HIAA
500 nM DOPAC
500 nM UA
500 nM AA
Sample
b.
Without drift training
Predicted DA (nM)
2000
1000
0
Blank
No Interferents
500 nM 5HIAA
500 nM DOPAC
500 nM UA
500 nM AA
Sample
c.
With drift training
Predicted 5HT (nM)
2000
1000
0
Blank
No Interferents
500 nM 5HIAA
500 nM DOPAC
500 nM UA
500 nM AA
Sample
d.
With drift training
Predicted DA (nM)
2000
1000
0
Blank
No Interferents
500 nM 5HIAA
500 nM DOPAC
500 nM UA
500 nM AA
Sample
e.
No drift training
Avg error (%): 2.9
Avg precision (± nM): 68
Predicted DA (nM)
1400
1200
1000
800
600
0
12.5
25
37.5
50
DOPAC (μM)
f.
Drift trained
Avg error (%): 3.8
Avg precision (± nM): 47
Predicted DA (nM)
1400
1200
1000
800
600
0
12.5
25
37.5
50
DOPAC (μM)
g.
Bracketed and drift trained
Avg error (%): 2.8
Avg precision (± nM): 43
Predicted DA (nM)
1400
1200
1000
800
600
0
12.5
25
37.5
50
DOPAC (μM)

Figure 7.2: RPV-PLSR training for interferents and drift. Non-drift-trained serotonin **(a)** and dopamine **(b)** predictions. Drift-trained serotonin (5-HT) **(c)** and dopamine (DA) **(d)** predictions. Non-drift- **(e)**, drift- **(f)**, and drift-trained with bracketing **(g)** dopamine test set predictions in the presence of varying DOPAC. All samples trained in a background level of interferents (100 μM DOPAC, 20 μM 5-HIAA, 200 μM ascorbate (AA), and 100 μM urate (UA)) unless otherwise noted; x-axis in **(a-d)** refers to amount added in addition to background levels. (**a-g)** Data points per panel were acquired sequentially in time, as labeled on the x-axis, to illustrate temporal drift.

required the fewest components (7 *vs.* 8-10), supporting the parsimony of PLSR (*i.e.*, as a "quicker learner")[6], the usefulness of covariate information in the background, and the ability for RPV-PLSR to generalize across electrodes.

While new methods combine datasets across dozens to hundreds of electrodes and use various subset selection techniques (Chapter 1), these methods often compare performance benchmarks of new models to metrics from previous reports in different laboratories, using different equipment, electrodes, waveforms, *etc*. At the expense of additional computations, head-to-head comparisons (*i.e.,* in the same lab) across models, waveforms, and background subtraction techniques can provide valuable information on the true performance gains of new techniques. Community-driven open datasets and software can aid this effort (*vide infra*).

7.1.2 Structurally similar interferents and electrode drift: Metabolites with structures similar to dopamine and serotonin pose a challenge for voltammetry because of highly overlapping electrochemical characteristics.[7] In preliminary experiments, I used our lead RPV waveform and PLSR to predict test samples containing 1000 nM serotonin (5-HT) and dopamine (DA) in the presence of 5-hydroxyindole acetic acid (5-HIAA), 3,4-dihydroxyphenylacetic acid (DOPAC), ascorbic acid (AA), or uric acid (UA) (**Fig. 7.2a,b**). The calibration set contained concentrations of serotonin and dopamine that varied; metabolite and interferent levels were held constant at a

relevant background level (100 μM DOPAC, 20 μM 5-HIAA, 200 μM AA, and 100 μM UA), unless otherwise denoted, by 500 nM additions, to simulate metabolite concentration changes, as expected *in vivo*.[8-10]

I also used these experiments to test different data processing and drift training methods. The PLSR model was trained to account for drift using voltammograms collected throughout the experiment while artificial cerebrospinal fluid (aCSF) containing interferents was flowed and injections were not occurring (~2 h). Data in which drift was evident were extracted from these background epochs and labeled as 'zero' analyte concentrations to teach the model what drifting, as opposed to analyte-containing voltammograms, looked like. These 'drift zeroes' were in addition to data from injections of aCSF alone (*i.e.,* blanks) to account for flow cell injection valve and solvent pump artifacts. Our novel 'drift training' reduced test set prediction errors from as much as 93% to 4.5% for serotonin and 23% to 6.7% for dopamine (**Fig. 7.2c,d**). The drift voltammograms were taken only from the training data yet were able to correct the drift present in the test data obtained much later in the day, suggesting this procedure is generalizable. However, this claim should be investigated by applying *in vitro* drift training to *in vivo* data. Generalizable PLSR models of drift have been reported for FSCV.[11] This drift training approach was also used for serotonin prediction in Chapter 5.

Dopamine predictions were confounded by the presence of DOPAC when not trained on varying concentrations of DOPAC (**Fig. 7.2d**). To improve dopamine/DOPAC differentiation, we calibrated the model using different concentrations of dopamine and DOPAC. This greatly improved dopamine test set prediction accuracy (2.9% error), suggesting that metabolites should be included in calibration sets as needed (**Fig. 7.2e**). The more complex calibration curves used in Chapter 5 were successful in training across DOPAC, 5-HIAA, and AA (UA was not included due

to solubility constraints). However, training across every interferent a model might encounter in the brain is impractical, which motivated the interferent-agnostic waveform design paradigm in Chapter 5.

I further improved analyte prediction accuracy using calibration set "bracketing". I injected the calibration set before and after the test set to account for calibration changes occurring over the course of the experiment (*i.e.,* electrode drift, fouling). This is essentially the concept of using both 'pre-fouled' *vs.* 'post-fouled' electrodes to obtain training data, discussed below and in Chapter 1. When using calibration bracketing combined with drift training, the precision and accuracy of dopamine predictions improved (**Fig. 7.2e-g**).

7.1.3 Multi-electrode training: Electrodes are often calibrated/trained before or after brain implantation, but not both. We observed empirically that electrode responses change in minutes to ~1 h after *in vivo* implantation, making pre-fouling data most different from *in vivo* and post-fouling data (**Fig. 7.3a**).[12] This observation highlighted challenges for generalizing *in vitro* training data to *in vivo* analysis (*i.e.*, effects of biofouling). *In vitro* test sets obtained before and after electrode implantation *in vivo* were used to investigate combining pre- and post-fouled calibration data into a PLSR single model (**Fig. 7.3b**). When the PLSR model contained only pre-fouled calibration data, it could only accurately predict test data obtained using

Figure 7.3:(a) Voltammograms obtained with a pre-fouled (prior to implantation, in aCSF), *in vivo* (striatum of anesthetized mouse), and post-fouled electrode (in aCSF after implantation ~6 h). **(b)** Predicted test set concentrations for serotonin (blue) and dopamine (red) obtained on the same electrode pre-biofouling ('pre-bf'; filled symbol) and post-biofouling ('post-bf'; hollow symbol). Actual test set concentrations denoted by blue (serotonin) or red (dopamine) horizontal lines. All points are the average of 41 data points. **(c)** Comparison of *in vivo* drift experimental time course (defined as average aggregate difference in current between voltammograms at successive time points; t=0 is probe insertion into brain). Data were obtained at 2 min intervals for the first hour, then every 30 min for the remaining 4 h. **(d)** Comparison of *in vivo* voltammograms post 1-h. Inset shows greatest differences in the region of capacitive decay.

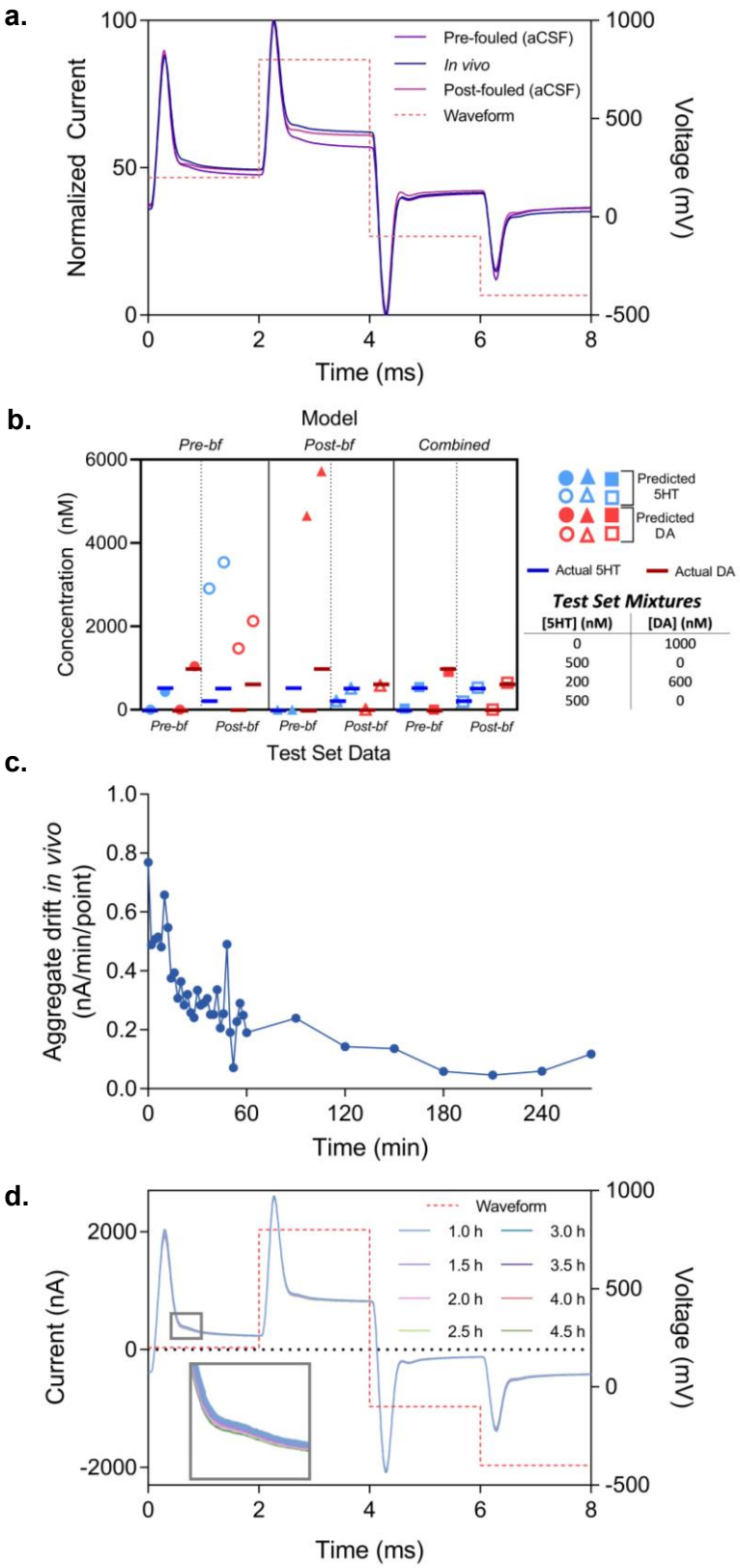

an electrode that had not been implanted in tissue, not test data obtained on the same electrode after *in vivo* implantation for ~6 h. Similarly, when the model was trained on post-fouled calibration data, it could only accurately predict test data acquired from an electrode placed in brain tissue. However, when we combined pre- and post-fouled calibration data into a single PLSR model, the model predicted pre- and post-test data with high accuracy, supporting the combined use of pre- and post-training data for *in vivo* quantification and translating background-inclusive data *in vitro* to *in vivo* (**Fig. 7.3b**). Future *in vivo* studies may benefit from 'bracketing' training data by calibrating the pre-fouled electrode *in vitro*, performing the

in vivo experiment, and training the post-fouled electrode *in vitro*. Training the model across pre- and post-fouled conditions may result in a more generalizable model rather than training only a single fouling condition. This is supported by the success of transfer learning (see below and in Chapter 1) to train models using labeled *in vitro* data and unlabeled *in vivo* data. However, more data on the timescale of fouling and resulting changes to the model parameters is needed across pre- and post-fouled conditions. A potential advantage of RPV is that pulses are less likely to induce electrode fouling/drift due to the effect that rapid changes in potential have on the electrode surface (**Fig 7.3c,d**).

7.1.4 Simulation of phasic and tonic detection: In Chapter 3, we used RPV-PLSR to predict stimulated and basal dopamine and serotonin, simultaneously, *in vivo*.[4] Our approach avoids background subtraction, enabling basal neurotransmitter predictions. However, our initial prediction accuracies for basal levels were not very accurate.[4] Using an expanded calibration set, I collected preliminary data using our lead RPV waveform to predict small increases in dopamine and serotonin (simulated phasic release *via* flow cell injections), as well as background dopamine and serotonin levels (simulated tonic levels *via* mobile phase containing 110 nM and 60 nM dopamine and serotonin, respectively, through the flow cell) (**Fig. 7.4**).[13,14] Predicted

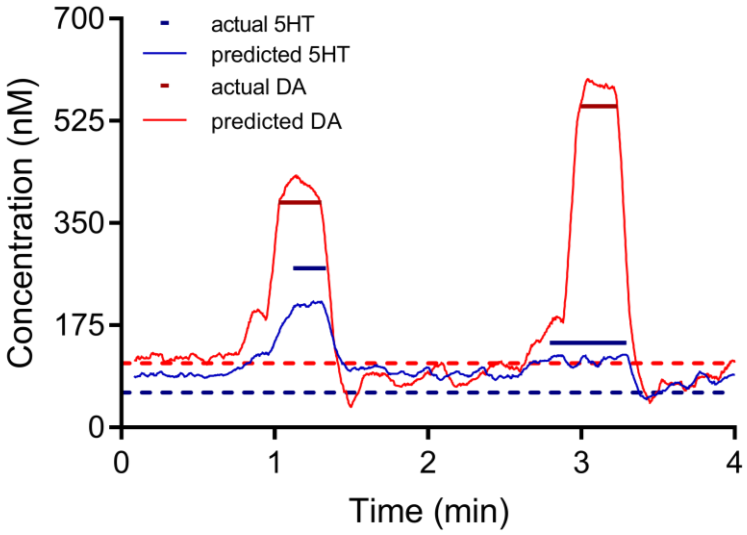

Figure 7.4: Simulated phasic release in the presence of 110 nM dopamine (DA) and 60 nM serotonin (5-HT) in aCSF with 100 µM DOPAC, 20 µM 5-HIAA, 200 µM AA, and 100 µM UA to mimic basal levels.

"basal" and "stimulated" dopamine levels showed <10% prediction errors. Nonetheless, predicted "basal" and "stimulated" serotonin levels had >10% errors. These data illustrate an approach for testing subsequent models for their ability to predict low basal levels and small stimulated increases in dopamine and serotonin, as well as how to identify model weaknesses that can be ameliorated by improving our calibration sets at the level of training, during optimization of waveforms, or both. The use of a flow cell with gradient pumps could also simulate slow-changing basal concentrations for additional train and test data to simulate *in vivo* conditions.

In vitro and/or *in vivo* method validation remains challenging for fast voltammetry in the brain (Chapter 1). New approaches simulating or mimicking brain-like conditions are needed to obtain more reliable training data. For example, picospritzing for *in vivo* standard addition training sets in genetically modified mouse lines can be used to train models with known amounts of neurotransmitter simulated release,[15] while approaches in transfer learning can be used to adapt the model to unknown domains (Chapter 1).

7.2 SeroML & SeroOpt: Open-source code notebooks for fast voltammetry data analyses

Chapter 6 detailed the development of SeroWare, a MATLAB-based analysis and acquisition software for fast voltammetry. Many state-of-the-art machine learning packages are freely available as open-source Python code.[1,16] The fast voltammetry community appears to be trending towards utilizing such packages, as surveyed in Chapter 1. Other fields have benefitted from community-led open-source and open-data instruments. The neurochemical voltammetry community may benefit from cultivating a similar open-source 'ecosystem'.

To facilitate the direct transfer of data from SeroWare to Python for advanced analyses and encourage the use of RPV-PLSR, I wrote several tutorial scripts on and functions for RPV-PLSR analyses using Python with Jupyter notebooks and other open-source Python packages. The latest version of these tutorials can be found at https://github.com/csmova/SeroML. These tutorials include pre-written functions that automate the import and labeling of voltammetry training and testing data and other common steps such as pre-processing, plotting, outlier removal, model training, cross-validation, and feature selection.

Chapter 5 detailed the development of a Bayesian optimization paradigm for rapid pulse voltammetry waveforms. I also wrote tutorial notebooks on Bayesian optimization for this voltammetry application at https://github.com/csmova/SeroOpt. The notebooks include a walkthrough of two different Bayesian optimization packages that vary in usability *vs.* customizability (Scikit-Optimize and Ax). Continued development of these notebooks is needed to encourage wide adoption by voltammetry users to optimize their waveforms using this approach. Incorporation of a graphical user interface customized for the needs of fast voltammetry users performing common machine learning tasks would extend the reach of these open-source tools to a code-free environment. This would encourage broad adoption by non-

expert users or those without coding knowledge. The applicability of these tools remains to be seen, as a community of users, maintainers, and contributors is needed.

Disclaimer: we make no guarantees on the accuracy or functionality of any software or code presented in or referenced in this dissertation.

7.3 SeroDB: Towards an open database for voltammetry

Chapter 1 detailed the progress on machine learning in fast voltammetry. A key need that was identified to push the fast voltammetry field forward was community-driven software and a database. Accordingly, we have been sponsored by the Amazon Web Services (AWS) Open Data registry to cover storage costs and provide expert resources to build a database (SeroDB) in a highly visible manner. We chose AWS because of its extensive resources. Other high-profile datasets are hosted on this platform (*e.g.,* for materials chemistry, imaging, spectroscopy, neuroscience; see https://aws.amazon.com/opendata/open-data-sponsorship-program/). The SeroDB database remains under development at the time of writing, and will require community input and participation to be successful, but our vision is outlined below.

Transfer learning has shown the utility of large training sets across domains (laboratories, experiments, animals, electrodes). A central repository where researchers can perform meta-analyses and curate custom datasets would aid these efforts. A data repository such as SeroDB can enable the discovery of embeddings and generalization strategies across various voltammetry applications. Modern voltammetry training sets easily contain tens to hundreds of thousands of voltammograms, resulting in data sets with millions of data points (gigabytes of data even for a single-day experiment). Thus, efficient storage solutions are increasingly necessary. By ensuring streamlined communication with our open-source voltammetry data acquisition and analysis

software suite (SeroWare), users can interact with SeroDB seamlessly. For example, we provide a tutorial to import results/data from SeroML into SeroDB. We hope to release and host all our voltammetry datasets for freely available community-wide use and encourage the submission of datasets from the community.

Such a database will also allow for fair benchmarking of electrodes, waveforms, and models. For example, the community could agree upon a 'baseline' dataset and task for comparing fast voltammetry models. In addition to datasets, a database that can support versatile file types, such as SeroDB, will allow the community to contribute pre-trained models (*i.e.*, neural network architectures with weights and biases that users have already trained on voltammetry data) to accompany data and be hosted on SeroDB compatible with plug-and-play analysis or finetuning on SeroML through interactive Jupyter notebooks (**Fig 7.4a**).

Voltammetry has recently seen an increase in the use of deep learning, which, in addition to requiring large data sets, requires compute-intensive resources to train neural architectures (up to hours or days, even with high-performance computing).[17-20] This is a prohibitively expensive process and a barrier to entry for non-expert voltammetry users. Having a centralized repository to store and share the optimized parameters of pre-trained voltammetry models on our database will lessen this burden and encourage broader adoption of modern machine learning in voltammetry by non-experts. In addition, it will facilitate open-source collaboration and help address the reproducibility crisis in machine learning.[21]

a.

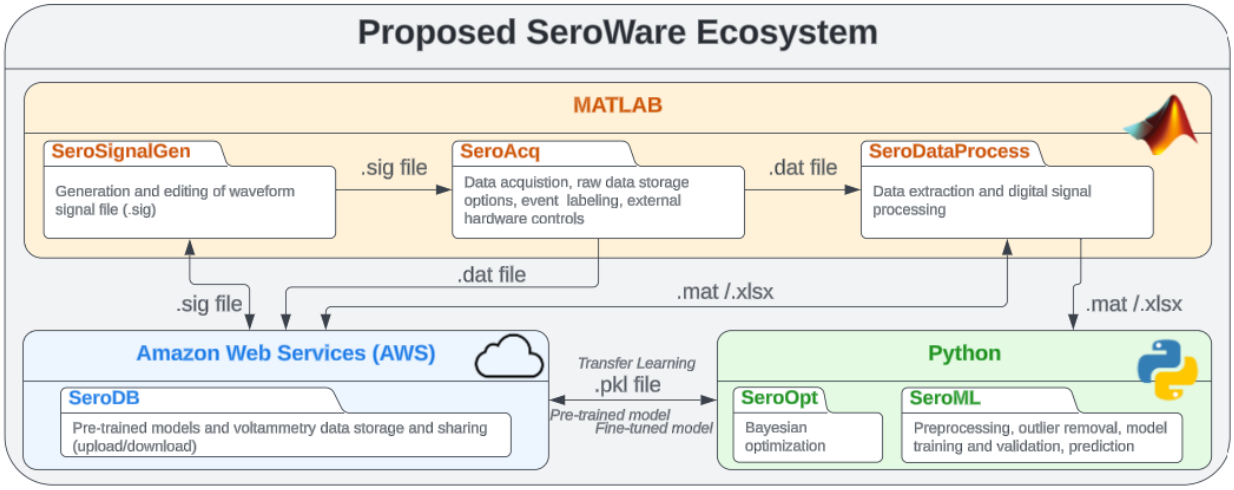

b.

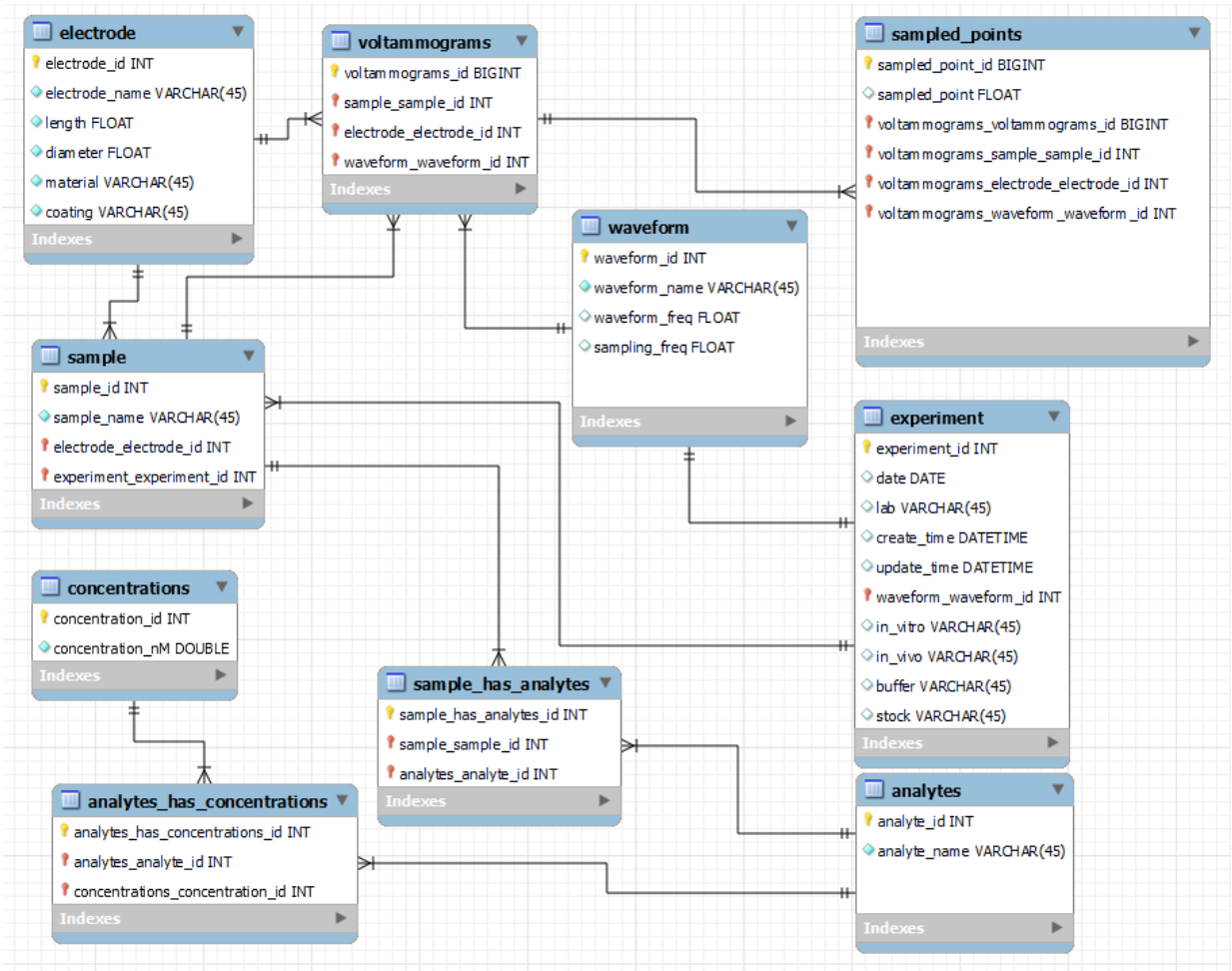

Figure 7.5: a) Proposed interacting modules of SeroWare, SeroML, SeroOpt, and SeroDB. **b)** Proposed relational database schema for SeroDB.

Curating large, diverse datasets will require careful database management. Specifically, the requirements for submission, including data quality checks and metadata about the experimental parameters, will be crucial for success. To this end, I designed a potential database schema to help organize voltammetry data logically and effectively (**Fig 7.5b**). Information regarding this effort can be found at https://github.com/csmova/SeroDB.

7.4 Recommendations for future work on electroanalytical method development and Bayesian optimization for fast voltammetry.

Future work on Bayesian optimization for voltammetry should include multi-objective Bayesian optimization to continue to optimize for challenging multi-analyte combinations. Examples of multi-objective neurotransmitter combinations include norepinephrine and dopamine (differing single by hydroxyl group). These analytes are electrochemically active yet problematic to differentiate by traditional voltammetry waveforms. Notably, more than two objectives can be optimized, and the objectives can be defined in various ways (*i.e.*, selectivity *vs.* sensitivity). With multi-objective optimization, tradeoffs can be weighted differently to achieve custom or tunable figures of merit (*e.g.,* yield *vs.* enantioselectivity when optimizing synthetic routes).[22]

Laboratory automation should also be explored to streamline optimization campaigns. The physical experiments for Bayesian optimization remain time-consuming and conducive to automation. By incorporating microfluidic flow cells, multichannel potentiostats and/or electrode arrays, open-source controlled autosamplers/gradient pumps, and automated data analysis, our RPV waveform optimization approach could be extended to a high throughput and autonomous method development paradigm for voltammetry. Such a system would allow various

experimental conditions, electrode materials, coatings, and waveforms to be optimized in a closed-loop fashion.

An interesting route to explore is if rapid pulse voltammetry allows for detecting non-electroactive analytes. Throughout Chapters 1, 3, 4, and 5, we showed that models can be trained on capacitive or non-faradic regions of voltammograms. This suggests that we may not need faradaic electron transfer to detect analytes electrochemically and can instead detect these compounds through tensammetry (*e.g.,* measuring non-faradaic currents caused by adsorption/desorption in response to waveforms).[23] Tensammetry involves a similar working principle to RPV. Tensammetry on surface-active but non-electrochemically active analytes has been reported as theoretically[24] and experimentally[25] possible, having been used to detect trace surfactants.[26] While various pre-patterned sweeps and pulse sequences have been combined with tensammetry, custom pulses that could infer never-before-seen sensitivity and selectivity have not been tested. Given the importance of non-faradaic currents to detect serotonin and dopamine, which also have specific adsorption and desorption properties,[27] RPV could be extended to non-electroactive analyte detection, especially if tensammetry is paired with modern data analysis. Few fast voltammetry techniques take advantage of the temporal dimension of data over which adsorption and desorption occur. Extending PLSR to tensor (multi-way) data (*i.e.,* 3-dimensional arrays of voltammograms encoding longer-range time-dependent adsorption and desorption that are of importance to tensammetry) could enable such an approach for suitable surface-active analytes and could be a future avenue of research to extend fast voltammetry beyond the brain.

More advanced applications of Bayesian optimization campaigns should also be explored, including physics-informed priors, electrochemistry-informed machine learning,[28] and multi-fidelity optimization by incorporating simulations. Off-the-shelf (domain agnostic) deep

learning approaches still offer only small percent increases in accuracy from less complex and computationally expensive PLSR-like approaches–deep learning and Bayesianity will truly revolutionize analytical chemistry when domain knowledge is incorporated.[29] A long-term, ambitious goal may be to leverage complementary advances in graphical neural networks for chemical property prediction,[30,31] electrochemistry-informed machine learning, and Bayesian optimization. With large, diverse, aggregated data sets of experimental and simulation data, full inverse design of waveforms solely from the molecular structures of a given analyte panel could become possible to perform fully *in silico* electroanalytical method development.

7.5 REFERENCES

1. Raschka, S.; Mirjalili, V., *Python machine learning: Machine learning and deep learning with Python, scikit-learn, and TensorFlow 2*. 3rd ed.; Packt Publishing Ltd.: Birmingham, UK, 2019.
2. Keithley, R. B.; Mark Wightman, R.; Heien, M. L., Multivariate concentration determination using principal component regression with residual analysis. *TrAC, Trends Anal. Chem.* **2009,** *28* (9), 1127-1136. https://doi.org/10.1016/j.trac.2009.07.002
3. Loewinger, G.; Patil, P.; Kishida, K. T.; Parmigiani, G., Multi-study learning for real-time neurochemical sensing in humans using the "study strap ensemble". *bioRxiv* **2021**, 856385. https://doi.org/10.1101/856385
4. Movassaghi, C. S.; Perrotta, K. A.; Yang, H.; Iyer, R.; Cheng, X.; Dagher, M.; Fillol, M. A.; Andrews, A. M., Simultaneous serotonin and dopamine monitoring across timescales by rapid pulse voltammetry with partial least squares regression. *Anal. Bioanal. Chem.* **2021,** *413* (27), 6747-6767. https://doi.org/10.1007/s00216-021-03665-1
5. Heien, M. L. A. V.; Phillips, P. E. M.; Stuber, G. D.; Seipel, A. T.; Wightman, R. M., Overoxidation of carbon-fiber microelectrodes enhances dopamine adsorption and increases sensitivity. *Analyst* **2003,** *128* (12), 1413-1419. https://doi.org/10.1039/B307024G
6. Fu, G.-H.; Xu, Q.-S.; Li, H.-D.; Cao, D.-S.; Liang, Y.-Z., Elastic net grouping variable selection combined with partial least squares regression (EN-PLSR) for the analysis of strongly multi-collinear spectroscopic data. *Appl. Spectrosc.* **2011,** *65* (4), 402-408. https://doi.org/10.1366/10-06069

7. Nakatsuka, N.; Andrews, A. M., Differentiating siblings: The case of dopamine and norepinephrine. *ACS Chem. Neurosci.* **2017,** *8* (2), 218-220. https://doi.org/10.1021/acschemneuro.7b00056

8. Meiser, J.; Weindl, D.; Hiller, K., Complexity of dopamine metabolism. *Cell Commun. Signal* **2013,** *11* (1), 34. https://doi.org/10.1186/1478-811X-11-34

9. Mohammad-Zadeh, L. F.; Moses, L.; Gwaltney-Brant, S. M., Serotonin: A review. *J. Vet. Pharmacol. Ther.* **2008,** *31* (3), 187-199. https://doi.org/10.1111/j.1365-2885.2008.00944.x

10. Qi, Z.; Miller, G. W.; Voit, E. O., Mathematical models of dopamine metabolism in parkinson's disease. In *Systems biology of Parkinson's disease*, Wellstead, P.; Cloutier, M., Eds. Springer New York: New York, NY, 2012; pp 151-171.

11. Meunier, C. J.; McCarty, G. S.; Sombers, L. A., Drift subtraction for fast-scan cyclic voltammetry using double-waveform partial-least-squares regression. *Anal. Chem.* **2019,** *91* (11), 7319-7327. https://doi.org/10.1021/acs.analchem.9b01083

12. Singh, Y. S.; Sawarynski, L. E.; Dabiri, P. D.; Choi, W. R.; Andrews, A. M., Head-to-head comparisons of carbon fiber microelectrode coatings for sensitive and selective neurotransmitter detection by voltammetry. *Anal. Chem.* **2011,** *83* (17), 6658-6666. https://doi.org/10.1021/ac2011729

13. Abdalla, A.; Atcherley, C. W.; Pathirathna, P.; Samaranayake, S.; Qiang, B.; Peña, E.; Morgan, S. L.; Heien, M. L.; Hashemi, P., In vivo ambient serotonin measurements at carbon-fiber microelectrodes. *Anal. Chem.* **2017,** *89* (18), 9703-9711. https://doi.org/10.1021/acs.analchem.7b01257

14. Oh, Y.; Heien, M. L.; Park, C.; Kang, Y. M.; Kim, J.; Boschen, S. L.; Shin, H.; Cho, H. U.; Blaha, C. D.; Bennet, K. E.; Lee, H. K.; Jung, S. J.; Kim, I. Y.; Lee, K. H.; Jang, D. P., Tracking tonic dopamine levels in vivo using multiple cyclic square wave voltammetry. *Biosens. Bioelectron.* **2018,** *121*, 174-182. https://doi.org/10.1016/j.bios.2018.08.034

15. Perrotta, K. Analytical techniques to investigate the neurochemical basis of behavior. PhD Thesis, University of California, Los Angeles, 2022.

16. Pedregosa, F.; Varoquaux, G.; Gramfort, A.; Michel, V.; Thirion, B.; Grisel, O.; Blondel, M.; Prettenhofer, P.; Weiss, R.; Dubourg, V., Scikit-learn: Machine learning in Python. *J. Mach. Learn. Res.* **2011,** *12*, 2825-2830.

17. Choi, H.; Shin, H.; Cho, H. U.; Blaha, C. D.; Heien, M. L.; Oh, Y.; Lee, K. H.; Jang, D. P., Neurochemical concentration prediction using deep learning vs principal component regression in fast scan cyclic voltammetry: A comparison study. *ACS Chem. Neurosci.* **2022,** *13* (15), 2288-2297. https://doi.org/10.1021/acschemneuro.2c00069

18. Hoar, B. B.; Zhang, W.; Xu, S.; Deeba, R.; Costentin, C.; Gu, Q.; Liu, C., Electrochemical mechanistic analysis from cyclic voltammograms based on deep learning. *ACS Meas. Sci. Au* **2022,** *2* (6), 595-604. https://doi.org/10.1021/acsmeasuresciau.2c00045

19. Twomey, T.; Barbosa, L.; Lohrenz, T.; Montague, P. R., Deep learning architectures for FSCV, a comparison. *arXiv (Medical Physics)* **2022,** (posted 2022-12-05). https://doi.org/10.48550/arXiv.2212.01960 (accessed 2023-12-12)

20. Xue, Y.; Ji, W.; Jiang, Y.; Yu, P.; Mao, L., Deep learning for voltammetric sensing in a living animal brain. *Angew. Chem. Int. Ed.* **2021,** *60* (44), 23777-23783. https://doi.org/10.1002/anie.202109170

21. Artrith, N.; Butler, K. T.; Coudert, F.-X.; Han, S.; Isayev, O.; Jain, A.; Walsh, A., Best practices in machine learning for chemistry. *Nat. Chem.* **2021,** *13* (6), 505-508. https://doi.org/10.1038/s41557-021-00716-z

22. Torres, J. A. G.; Lau, S. H.; Anchuri, P.; Stevens, J. M.; Tabora, J. E.; Li, J.; Borovika, A.; Adams, R. P.; Doyle, A. G., A multi-objective active learning platform and web app for reaction optimization. *J. Am. Chem. Soc.* **2022**. https://doi.org/10.1021/jacs.2c08592

23. Lukaszewski, Z., Tensammetric techniques for electroanalysis. *Electroanalysis* **1993,** *5* (5-6), 375-384. https://doi.org/10.1002/elan.1140050503

24. Jadreško, D.; Lovrić, M., A theory of square-wave voltammetry of surface-active, electroinactive compounds. *Electrochim. Acta* **2008,** *53* (27), 8045-8050. https://doi.org/10.1016/j.electacta.2008.06.010

25. Jadreško, D.; Zelić, M., Square-wave voltammetry of electroinactive surfactants. *Electroanalysis* **2015,** *27* (7), 1669-1675. https://doi.org/10.1002/elan.201400692

26. Canterford, D. R.; Taylor, R. J., Surfactant analysis with differential pulse tensammetry. *J. Electroanal. Chem. Interfacial Electrochem.* **1979,** *98* (1), 25-36. https://doi.org/10.1016/S0022-0728(79)80281-8

27. Kim, D. H.; Oh, Y.; Shin, H.; Park, C.; Blaha, C. D.; Bennet, K. E.; Kim, I. Y.; Lee, K. H.; Jang, D. P., Multi-waveform fast-scan cyclic voltammetry mapping of adsorption/desorption kinetics of biogenic amines and their metabolites. *Anal. Methods* **2018,** *10* (24), 2834-2843. https://doi.org/10.1039/C8AY00352A

28. Chen, H.; Yang, M.; Smetana, B.; Novák, V.; Matějka, V.; Compton, R. G., Discovering electrochemistry with an electrochemistry-informed neural network (ECINN). *Angew. Chem. Int. Ed.* **2024,** *63* (13), e202315937. https://doi.org/10.1002/anie.202315937

29. Vasudevan, R. K.; Ziatdinov, M.; Vlcek, L.; Kalinin, S. V., Off-the-shelf deep learning is not enough, and requires parsimony, Bayesianity, and causality. *Npj Comput. Mater.* **2021,** *7* (1), 16. https://doi.org/10.1038/s41524-020-00487-0

30. Reiser, P.; Neubert, M.; Eberhard, A.; Torresi, L.; Zhou, C.; Shao, C.; Metni, H.; van Hoesel, C.; Schopmans, H.; Sommer, T.; Friederich, P., Graph neural networks for materials science and chemistry. *Commun. Mater.* **2022,** *3* (1), 93. https://doi.org/10.1038/s43246-022-00315-6

31. Ahmad, Z.; Xie, T.; Maheshwari, C.; Grossman, J. C.; Viswanathan, V., Machine learning enabled computational screening of inorganic solid electrolytes for suppression of dendrite formation in lithium metal anodes. *ACS Cent. Sci.* **2018,** *4* (8), 996-1006. https://doi.org/10.1021/acscentsci.8b00229